

X-RAY PROPERTIES OF EARLY-TYPE GALAXIES

by

EWAN O'SULLIVAN

A thesis submitted to
The University of Birmingham
for the degree of
DOCTOR OF PHILOSOPHY

Astrophysics and Space Research Group
School of Physics and Astronomy
The University of Birmingham
July 2002

UNIVERSITY OF
BIRMINGHAM

University of Birmingham Research Archive

e-theses repository

This unpublished thesis/dissertation is copyright of the author and/or third parties. The intellectual property rights of the author or third parties in respect of this work are as defined by The Copyright Designs and Patents Act 1988 or as modified by any successor legislation.

Any use made of information contained in this thesis/dissertation must be in accordance with that legislation and must be properly acknowledged. Further distribution or reproduction in any format is prohibited without the permission of the copyright holder.

Synopsis

It has been known for some time that many early-type galaxies possess halos of X-ray emitting gas. However, the properties of these halos and the processes by which they form are as yet not well understood. We have compiled the largest catalogue of X-ray luminosities to date, and use it to examine the relationships between X-ray luminosity and galaxy age, environment and optical luminosity. It is shown that the mass of the X-ray halo increases with galaxy age, and that there is no trend in L_X/L_B with environment. Group dominant galaxies are shown to be more X-ray luminous than galaxies in other environments, and the effect of this on the $L_X:L_B$ relation is explored. A smaller sample of highly X-ray luminous galaxies is studied in more detail, and their properties compared to those of galaxy groups and clusters. It is shown that while galaxy halos are similar to those of larger structures they differ in that their surface brightness profiles do not vary with system temperature. It is also shown that early-type galaxies have lower gas fractions than groups and clusters, probably owing to gas loss from the system through galaxy winds.

To my parents,
who have done more towards it than they realise.

Acknowledgements

Many people deserve thanks for the help they have given me over the course of my Ph.D. First and foremost I'd like to thank my supervisor, Trevor Ponman, for his unfailing enthusiasm and encouragement. His support made this thesis possible and has made working at Birmingham a pleasure. I would also like to thank my original supervisor, Duncan Forbes, who got me started on the whole process, provided much of the impetus behind the first two papers contained in this thesis and helped lay the groundwork which allowed me to write the rest of it. I am also happy to be able to thank Steve Helsdon and Alastair Sanderson for their help with numerous aspects of my Ph.D. and in particular for the benefit of their extensive software expertise.

During my time at Birmingham numerous people have provided me with suggestions, advice and discussions, as well as helping to make it a great place to work. These include (in alphabetical order) David Acreman, Robin Barnard, Richard Brown, Simon Ellis, Bruce Fairley, Antonis Georgakakis, Jo Hartwell, David Henley, Fill Humphrey, Laurence Jones, Ed Lloyd-Davies, Ben Maughan, John Osmond, Julian Pittard, Ian Stevens and Ale Terlevich. Special thanks are owed to Rich Brown, Jo Hartwell, John Osmond and Ross Collins, all of whom worked on preliminary studies of the subjects covered in this thesis. The work presented here was carried out on the computers of the Birmingham Starlink Node and Bob Valance, Billy Wilson and David Geddes deserve thanks for maintaining both hardware and software.

Finally I would like to thank all my family and friends for their support during the last few years, and for putting up with my moaning.

Contents

Preface	1
1 Introduction	3
1.1 Basic properties of Early-type Galaxies	4
1.1.1 Dark Matter	7
1.1.2 The Interstellar Medium	8
1.1.3 X-ray Sources	10
1.1.4 Scaling Relations	15
1.2 Basic Properties of Late-type Galaxies	21
1.2.1 The Interstellar Medium	22
1.2.2 X-ray Sources	23
1.2.3 Scaling Relations	23
1.3 Galaxy Systems	24
1.3.1 Environmental classes	24
1.3.2 Identification and classification	26
1.3.3 Constitution and Properties	27
1.3.4 Scaling Relations	28
1.3.5 Unusual Objects	32
1.3.6 Environmental effects on galaxies	33
1.4 Galaxy Formation and Evolution	37
1.4.1 Halo Formation and Galaxy Winds	38
1.5 Measurement of Galaxy Age	42
1.6 Thesis Aims	45
2 X-ray Emission in Post-Merger Ellipticals	47
2.1 Introduction	47

2.2	Results	49
2.2.1	L_X/L_B versus Spectroscopic Age	50
2.2.2	L_X/L_B versus Fundamental Plane Residual	54
2.3	Discussion	55
2.3.1	Gas infall	57
2.3.2	Ongoing stellar mass-loss and galaxy winds	58
2.4	Concluding Remarks	60
3	A Catalogue and Analysis of X-ray luminosities of Early-type galaxies	61
3.1	Introduction	61
3.2	Sample selection	63
3.3	Data Reduction and Spectral Fitting	63
3.4	A Master Catalogue	66
3.5	Statistical Analysis	69
3.6	Tests of fitting accuracy	71
3.7	Results	74
3.7.1	The $L_X:L_B$ Relation for Early Type Galaxies	74
3.7.2	Potential sources of bias	78
3.7.3	The Discrete Source Contribution	82
3.7.4	Environmental Dependence of L_X/L_B	94
3.7.5	The $L_X:L_B$ relation in different Environments	97
3.8	Discussion and Conclusions	101
3.8.1	The $L_X:L_B$ Relation for Early-type Galaxies	101
3.8.2	Environmental Dependence of $L_X:L_B$	102
3.8.3	The Discrete Source Contribution	106
4	The X-ray halos of luminous Early-type galaxies	107
4.1	Introduction	107
4.2	Sample Selection	109
4.3	Data Reduction	110
4.4	Spectral and Spatial Analysis	113

4.5	Results	117
4.5.1	Spectral and spatial fits	117
4.5.2	The $L_X:T_X$ relation	124
4.5.3	$L_X:L_B$ and $L_B:T_X$ relations	126
4.5.4	The $\sigma:T_X$ relation	128
4.5.5	β_{fit} and Entropy	130
4.6	Discussion	134
4.6.1	Comparison with Groups and Clusters	136
4.6.2	Cooling Flows	144
4.6.3	Stellar Mass Loss and Galaxy Winds	146
4.6.4	Environmental Effects and Formation Epoch	149
4.7	Summary and Conclusions	156
5	Summary and Future Plans	160
5.1	Summary of main results	160
5.2	Future Work	163
5.2.1	Isolated Elliptical Galaxies	163
5.2.2	X-ray Faint Early-type Galaxies	167
5.2.3	Galaxies in Clusters and Groups	169
A	Catalogue of X-ray luminosities	187

List of Figures

1.1	The giant elliptical galaxy NGC 1316, observed by VLT/ANTU with FORS1 . . .	7
1.2	X-ray/optical overlay of NGC 3923	10
2.1	Normalised X-ray luminosity versus fine structure parameter (Σ) for early-type galaxies.	50
2.2	$\text{Log}(L_X/L_B)$ plotted against spectroscopic age for early-type galaxies.	51
2.3	Optical luminosity versus spectroscopic age for early-type galaxies.	55
2.4	X-ray luminosity versus Fundamental Plane residual for early-type galaxies. . .	56
3.1	Comparisons of corrected bolometric L_X values from our PSPC pointed data with values from three other catalogues.	68
3.2	Simulated censored data used to test alternative fitting methods.	73
3.3	$\text{Log } L_X$ vs $\text{Log } L_B$ for our full catalogue of 401 early-type galaxies.	76
3.4	Our catalogued data L_X and L_B data with mean L_X values for eight bins.	79
3.5	$\text{Log } L_X$ vs $\text{Log } L_B$ for our sample of 136 early-type galaxies from <i>ROSAT</i> PSPC pointed observations.	81
3.6	Plot of $\text{Log } L_X$ vs $\text{Log } L_B$ for a sample of nearby late-type galaxies.	85
3.7	Plot of $\text{Log } L_X$ vs $\text{Log } L_B$ for morphological subsets of late-type galaxies from Fabbiano, Kim & Trinchieri (1992).	87
3.8	Plot of $\text{Log } L_X$ vs $\text{Log } L_B$ for our early-type galaxies with L_{dscr} estimates marked.	91
3.9	$\text{Log}(L_X - L_{dscr})$ against $\text{Log } L_B$ for all galaxies in our main catalogue with $\text{Log } L_X/L_B$ greater than 30.1.	93
3.10	Plot of normalised X-ray luminosity against environmental density.	96
3.11	Plot of L_X/L_B against ρ for non-BGG galaxies from the sample of Brown & Bregman (1999).	98

3.12	Plots of $\text{Log } L_X$ vs $\text{Log } L_B$ for field, group and cluster subsets drawn from our catalogue.	100
4.1	Measured temperature profiles for our sample of galaxies	120
4.2	Fitted metallicity profiles of NGC 1399 (left panel) and NGC 4636 (right panel)	122
4.3	$\text{Log } L_X$ plotted against temperature for our sample of galaxies.	124
4.4	The $L_X:T_X$ relation for our sample, with similar relations for groups and clusters.	125
4.5	L_X plotted against L_B for our sample of galaxies.	127
4.6	L_B plotted against temperature for our sample of galaxies.	129
4.7	Velocity dispersion, σ , plotted against temperature for our sample of galaxies. . .	130
4.8	Plot of β_{fit} against temperature for our sample, with galaxies colour coded by temperature profile	133
4.9	Plot of β_{fit} against temperature for our sample, with galaxies colour coded by environment	134
4.10	Mean gas entropy measured at one tenth of the virial radius plotted against mean halo temperature.	135
4.11	Scaled X-ray surface brightness profiles for our galaxies, arranged to show departures from self-similarity.	142

List of Tables

2.1	Mean L_X/L_B values for 5 age bins, calculated using the Kaplan–Meier estimator.	53
3.1	Correction factors used to convert luminosities from Beuing <i>et al.</i> , Fabbiano <i>et al.</i> and Roberts <i>et al.</i> into our pseudo–bolometric band and MEKAL model. . .	67
3.2	Comparison between galaxies from our PSPC pointed data and those from other samples.	69
3.3	Slopes and intercepts of four morphological subsamples selected from Fabbiano, Kim & Trinchieri (1992)	86
3.4	Slopes and intercepts for the high and low luminosity late-type galaxy subsets. .	88
3.5	Mean L_X/L_B values for the environmental subsamples shown in Figure 3.10. . .	97
3.6	Best fit $L_X:L_B$ lines for galaxies in field, group and cluster environments. . . .	99
3.7	Best fit intercepts to $L_X:L_B$ relations with fixed slopes of 1.63 and 1.94.	99
4.1	Basic properties of galaxies in our sample.	111
4.2	Results of the spectral fits to our sample galaxies.	118
4.3	Results of the surface brightness fits to our galaxies, for the components associated with the galaxy halo.	123
4.4	Mean masses and other derived quantities for our sample of galaxies.	154
5.1	Basic properties of our sample of isolated early–type galaxies	172
A.1	Combined catalogue of X–ray luminosities for 401 early-type galaxies.	202

Preface

The work presented in this thesis was undertaken between 1998 and 2002, at the University of Birmingham while the author was under the supervision of Professor T. J. Ponman and Dr. D. A. Forbes. All the analysis presented is that of the author, but interpretation has involved collaborations with various co-authors which are noted below. Chapter 1 provides an introduction to the thesis and presents general background information relevant to the later chapters. Chapters 2, 3 and 4 constitute the main body of the thesis, and chapter 5 contains a summary of the most important results. Chapters 2 and 3 have been published as papers in peer reviewed journals, and it is intended to submit chapter 4 to a journal in the near future. Birmingham University regulations allow for papers to be incorporated into theses as chapters without the need to be re-written, and this has been done as stated below. It should be noted that this results in a certain amount of duplication of material, since some mention of the data analysis must be made in each of the papers. The main results chapters are:

Chapter 2 *X-ray Emission in Post-Merger Ellipticals* examines the development of the X-ray properties of early-type galaxies with age, and has been published as:

O'Sullivan, E., Forbes, D. A. and Ponman, T. J., 2001, MNRAS, 324, 420

It is incorporated into the thesis essentially in its published form, and is referred to as O'Sullivan, Forbes & Ponman (2001b). T. J. Ponman and D. A. Forbes provided extensive discussions on the interpretation of the results.

Chapter 3 *A Catalogue and Analysis of X-ray luminosities of Early-type galaxies* is a study of the well known L_X/L_B relation for elliptical and lenticular galaxies and the various factors which influence it. It has been published as:

O'Sullivan, E., Forbes, D. A. and Ponman, T. J., 2001, MNRAS, 328, 461

It is incorporated into the thesis essentially in its published form, and is referred to as O'Sullivan, Forbes & Ponman (2001a). T. J. Ponman and D. A. Forbes provided extensive discussions on the interpretation of the results.

Chapter 4 *The X-ray halos of luminous Early-type galaxies* examines the X-ray characteristics of massive elliptical galaxies in more detail than the previous chapters, and compares them to galaxy groups and clusters through a number of correlations. It is to be submitted for publication in the near future. T. J. Ponman provided extensive discussion on the interpretation of the results, and R. S. Collins carried out an early analysis of the data, later repeated in greater detail by the author.

Chapter 1

Introduction

Galaxies have been considered as X-ray sources since the detection of emission in the region of M87 by rocket borne detectors (Bradt et al., 1967). The launch of the *Einstein* observatory in November 1978 (Giacconi et al., 1979) brought the first real opportunity for detailed observations of galaxies of all types, and quickly produced one of the major discoveries of X-ray astronomy; the identification of the hot interstellar medium (ISM) in early-type galaxies (Forman et al., 1979). Although the lifespan of *Einstein* was relatively short (~ 30 months), a large number of important observations were made by the observatory, and data from it are still in use today (e.g. Lewis et al., 2002).

In 1990, X-ray astronomy took another significant step forward with the launch of two observatories, *ROSAT* and *ASCA*. These satellites had complementary properties, *ASCA* having poor spatial but relatively good spectral resolution and a wide bandpass, and *ROSAT* good spatial resolution in a narrow band. *ROSAT* in particular made a very large contribution to the study of galaxies. Although narrow, its spectral range was well chosen, covering the typical mean temperature of the diffuse gas in early-type galaxies and in galaxy groups. The good spatial resolution and large field of view allowed studies of galaxies at a range of distances and in a variety of environments. It was also used to produce the *ROSAT* All-Sky Survey, a soft X-ray map covering 99.7% of the sky (for exposures longer than 50s Voges et al., 1999). Over its 8 year lifetime, *ROSAT* was used to observe a large number of galaxies, leading to catalogues such as that of Beuing et al. (1999), and the work presented in this thesis is based on *ROSAT* observations.

Galaxies are often considered to be the building blocks of the universe. They are not typically found in isolation but are usually part of a larger structure, ranging from galaxy pairs up to clusters and superclusters of galaxies. This is particularly true for early-type galaxies, which are much more common in the dense environments at the cores of galaxy groups and clusters

than in the field (Dressler, 1980). In hierarchical models of structure formation this is assumed to be a product of their formation process. Early-type galaxies, in this model, form from the merger of late-type galaxies. Galaxies are expected to congregate together under the influence of gravity, forming groups in which galaxy mergers are more likely. These groups will also merge to form clusters, currently the largest gravitationally bound objects in the universe, and these will eventually form superclusters containing many thousands or tens of thousand of galaxies.

Without the X-ray viewpoint, it might be assumed that the only effect of this hierarchical formation on galaxies was to promote mergers. However, X-ray observations have shown that groups and clusters of galaxies often possess halos of hot gas, just as some early-type galaxies do. Many possible interactions between halos on different scales have been postulated, and it now seems likely that as well as being affected by the surrounding environment, galaxies may themselves influence the development of groups and clusters in quite profound ways. Although some of the products of these interactions can be seen at other wavelengths, only the X-ray band allows us to directly observe hot halos. It is therefore vital for the study of galaxies, providing information on the extreme products of stellar evolution (massive stars, supernovae, X-ray binaries), the development of the galaxy as a whole and its co-evolution with the surrounding environment.

1.1 Basic properties of Early-type Galaxies

The class of early-type galaxies consists of a range of objects, from bulge dominated, armless disk galaxies to pure spheroids. They were originally classified as ‘early’ by Hubble (1936) in his book *The Realm of the Nebulae*. Hubble is commonly believed to have suggested that galaxies were formed as spheroids and then slowly evolved to become more disky and develop spiral arms. Elliptical galaxies were therefore less evolved ‘earlier’ types, and spiral galaxies ‘late’ types. In fact, Hubble specifically avoided the idea of an evolutionary link between the different classes of galaxies, and this model of formation is not now widely believed to be accurate, although (as discussed in a later section) some galaxy formation theories do predict the formation of spirals from ellipticals.

Early observations of elliptical galaxies showed them to have a number of broad traits. They were old objects, with red stellar populations, lacking the gaseous nebulae and star forming

regions seen in late-type galaxies. Whereas in spiral galaxies the stellar orbits form a well defined disk, ellipticals were thought to be dominated by random orbits, with little internal structure. Lenticular (or S0) disk galaxies were seen as a transitional type linking normal spirals and ellipticals, sharing most of the properties of ellipticals, but possessing a thick disk of stars. More modern observations have shown these definitions to be largely correct. Colour-magnitude plots of elliptical galaxies show them to be about 10^{10} yr old, with a stellar turnoff $< 1 M_{\odot}$. Early-type galaxies rarely contain large star forming regions, and only more recent observations and analysis techniques have proved capable of distinguishing the younger stellar populations and cool gas in some of these objects. Most ellipticals contain between 10^9 and 10^{12} stars, although dwarf elliptical and spheroidal galaxies may have as few as 10^6 . The majority of these stars travel on randomised orbits, leading to a wide variety of forms — ellipticals may be spherical, oblate, prolate or triaxial. S0 galaxies are also dominated by stars in random orbits, but possess a sizable disk population, producing 30–40% of the light of the galaxy as a whole. As the stellar population is old, type Ia supernovae are expected to be relatively common in early-type galaxies, and it is estimated that mass loss from supernovae and stellar winds returns $0.1\text{--}1 M_{\odot} \text{ yr}^{-1}$ of gas to the interstellar medium (Faber & Gallagher, 1976).

Most early-type galaxies have surface brightness profiles which reflect their homogeneous stellar population and uniform kinematics. However, a minority have been shown to contain disturbed stellar structures. In general, elliptical galaxies whose isophotes deviate from a normal ellipse can be classified into two groups; those with ‘disky’ or ‘boxy’ isophotes. These deviations from a purely elliptical profile occur because stellar orbits are not entirely random. In ‘disky’ ellipticals there is a significant disk component, sometimes producing a bulge-to-disk ratio similar to that of lenticulars. The rotational velocity component of these galaxies is often large, though still less important than stellar velocity dispersion, and is thought to contribute to their flattened morphology. In ‘boxy’ ellipticals rotation is relatively unimportant, and the galaxy is often triaxial rather than prolate, oblate or spherical. These objects are also more likely to show signs of more extreme disturbances, such as ripples in surface brightness, ‘jets’, shells or streamers of stars, so called ‘X’-structures, large dust lanes or clouds, and kinematically distinct cores. Figure 1.1 is an optical image of NGC 1316, a giant elliptical which shows several of these features. The dust lanes in the galaxy are clear from the figure, but deeper imaging reveals

loops and arcs of stars. Radio observations have shown NGC 1316 to be a powerful radio galaxy and to have a central disc of ionized gas inclined with respect to the plane of rotation of the galaxy. All of these features are believed to be caused by the infall and consumption of at least one gas rich companion galaxy $\sim 10^9$ yr ago (Schweizer, 1980). Most disturbance features are believed to be relatively short lived structures, likely to fade and be smoothed out over time. These disturbances are thought to be related to the formation of ellipticals, and this will be discussed later in the chapter.

In undisturbed galaxies, it is possible to estimate the mass within a given radius from the velocity dispersion of the stars. The virial theorem

$$2K + W = 0, \quad (1.1)$$

relates the potential energy, W , of the system to its kinetic energy, K . These two components can be rewritten as

$$K = \frac{1}{2}Mv^2 \quad (1.2)$$

and

$$W = -\alpha \frac{GM^2}{R}, \quad (1.3)$$

where M is the mass of the galaxy within a given radius, R , v is the typical velocity of an object within the galaxy, and α is a constant of order unity determined by the distribution of matter in the potential well. We can relate the line of sight velocity dispersion, σ , of the galaxy to the velocity v using

$$3\sigma^2 = v^2. \quad (1.4)$$

We can therefore rearrange the virial theorem to show that

$$M = \frac{3R\sigma^2}{G\alpha}. \quad (1.5)$$

By measuring the velocity dispersion of a galaxy in a given aperture, we can therefore estimate the mass within that radius. Such measurements have been used to show that the luminous mass in galaxies is less than their gravitational mass, providing evidence for the existence of dark matter in these systems.



Figure 1.1: The giant elliptical NGC 1316 observed with the FORS-1 instrument on the VLT/ANTU telescope (European Southern Observatories PR image 18a/00). The image is a true-colour composite of B,V and I filter exposures. NGC 1316 is a radio galaxy in the Fornax cluster and shows signs of recent interactions, including the dust features visible in this image (Schweizer, 1980).

1.1.1 Dark Matter

Early-type galaxies are thought to have a relatively large dark matter component (Loewenstein & White, 1999). This may contribute $\gtrsim 20\%$ of the galaxy by mass within one effective radius ($1 r_e$), and up to 85% at $6 r_e$. This leads to increasingly large mass to light ratios at high radii; for example in NGC 1399, the ratio increases from $33M_\odot/L_\odot$ at 14 kpc to $75 M_\odot/L_\odot$ at 85 kpc (Jones et al., 1997). These figures show a trend for increasing importance of the dark matter

contribution with radius, at least to the radius at which it can be measured. The dark matter is thought to form a massive halo within which the optical body of the galaxy resides, with the majority of the mass at large radii.

The distribution of dark matter in galaxies (and indeed in larger systems) is poorly understood. As dark matter cannot be observed directly, it can only be studied through its effects on more visible systems. The various available techniques usually lead to estimates of mass within a given radius, such as those given above, which are of limited use in determining the distribution. Instead, the structure of the dark matter halo is commonly constrained through simulations. These suggest that dark matter is distributed in the same way across a wide range of masses, from galaxies up to clusters of galaxies. One of the most common distributions used is that of Navarro et al. (1997, hereafter NFW), which has the form:

$$\rho_{DM}(r) = \bar{\rho}_{DM} \left[\frac{r}{r_s} \left(1 + \frac{r}{r_s} \right) \right]^{-2} \quad (1.6)$$

where r_s is the scale radius and $\bar{\rho}_{DM}$ is a characteristic density for the halo, related to the critical density of the universe at the time of formation. However, more recent higher resolution simulations suggest that this parameterisation may not be accurate in the central regions of halos. For example, Moore et al. (1998) find a central slope of $\rho_{DM}(r) \propto r^{-1.4}$ rather than r^{-1} as predicted by the NFW formula.

1.1.2 The Interstellar Medium

Early-type galaxies contain significantly smaller masses of cool gas than late-type galaxies (Knapp et al., 1985; Lees et al., 1991; Roberts et al., 1991). HI was detected in only 5% of ellipticals in the survey of Roberts et al. (1991), and upper limits on the gas mass in those where it was not detected were often as low as $10^7 M_\odot$, three orders of magnitude less than the detected masses in many spirals (Bregman et al., 1992). Similarly, early-type galaxies have relatively little molecular gas compared to spirals and irregulars. These low gas contents match well with the age of the stellar population and the marked lack of star formation, suggesting that the cool gas has been removed or put into a form where it cannot condense to form new stars. In low luminosity ellipticals HI is often found in the form of a disk, with central densities which could be high enough to permit star formation. In more luminous ellipticals the gas is sometimes in a disk or ring, but is usually irregular in morphology, often extending outside the

body of the galaxy (Oosterloo et al., 1999). The gas density is usually low, precluding star formation.

Dust, unlike cool gas, is a common component of the interstellar medium (ISM) of early-type galaxies. Goudfrooij et al. (1994) detected dust lanes or patches in 41% of their sample of galaxies, and HST observations have shown that 78% of early-type galaxies contain nuclear dust features (van Dokkum & Franx, 1995). Lenticular galaxies have a slightly higher incidence of dust (Ferrari et al., 1999), but the typical mass observed is fairly constant across morphological types, at 10^3 – $10^5 M_{\odot}$. As with cool gas, dust is sometimes found to form disks, particularly near the centres of galaxies, but may also be distributed in filaments or in larger structures extending beyond the stellar body of the galaxy. Where dust lanes are observed, the inferred rotation axis is often divergent from that of the stars, suggesting an external origin for the dust (van Dokkum & Franx, 1995).

The most common (and from the point of view of this thesis, the most important) component of the ISM in early-type galaxies is hot, highly ionised gas. Typically found at temperatures of 10^6 – 10^7 K, this gas is observed in almost all optically luminous ellipticals, often in sizable quantities. Masses of 10^9 – $10^{10} M_{\odot}$ are not uncommon. The gas is often found in the form of a halo centred on the galaxy but extending beyond the stellar body. Very large ellipticals may have halos up to 100 kpc in radius, but most do not exceed 50 kpc. Figure 1.2 shows *ROSAT* PSPC X-ray contours overlaid on a Digitized Sky Survey image of NGC 3923. The stellar body of the galaxy extends to ~ 20 kpc, while the halo extends to at least 30 kpc in all directions (assuming the galaxy to be at a distance of 26.8 Mpc). It should be noted that the halo is not a smooth ellipse, but has an irregular form, partly owing to confusion with point sources (one clear example is found directly to the north of the galaxy). Exact measurements of halo size are however often hampered by a surrounding hot intergalactic medium (IGM) associated with the group or cluster in which the galaxy lies. The similarity between the mass of the hot ISM in ellipticals and the cool ISM in spirals has led to the suggestion that the two are made up from the same gas, with heating or cooling being associated with processes which convert the stellar body of the galaxy from one morphology to the other. The formation and evolution of the hot ISM will be dealt with in detail in a later section, but it is worth noting that this is an as yet unanswered question in the study of early-type galaxies, and one which cannot be ignored if we

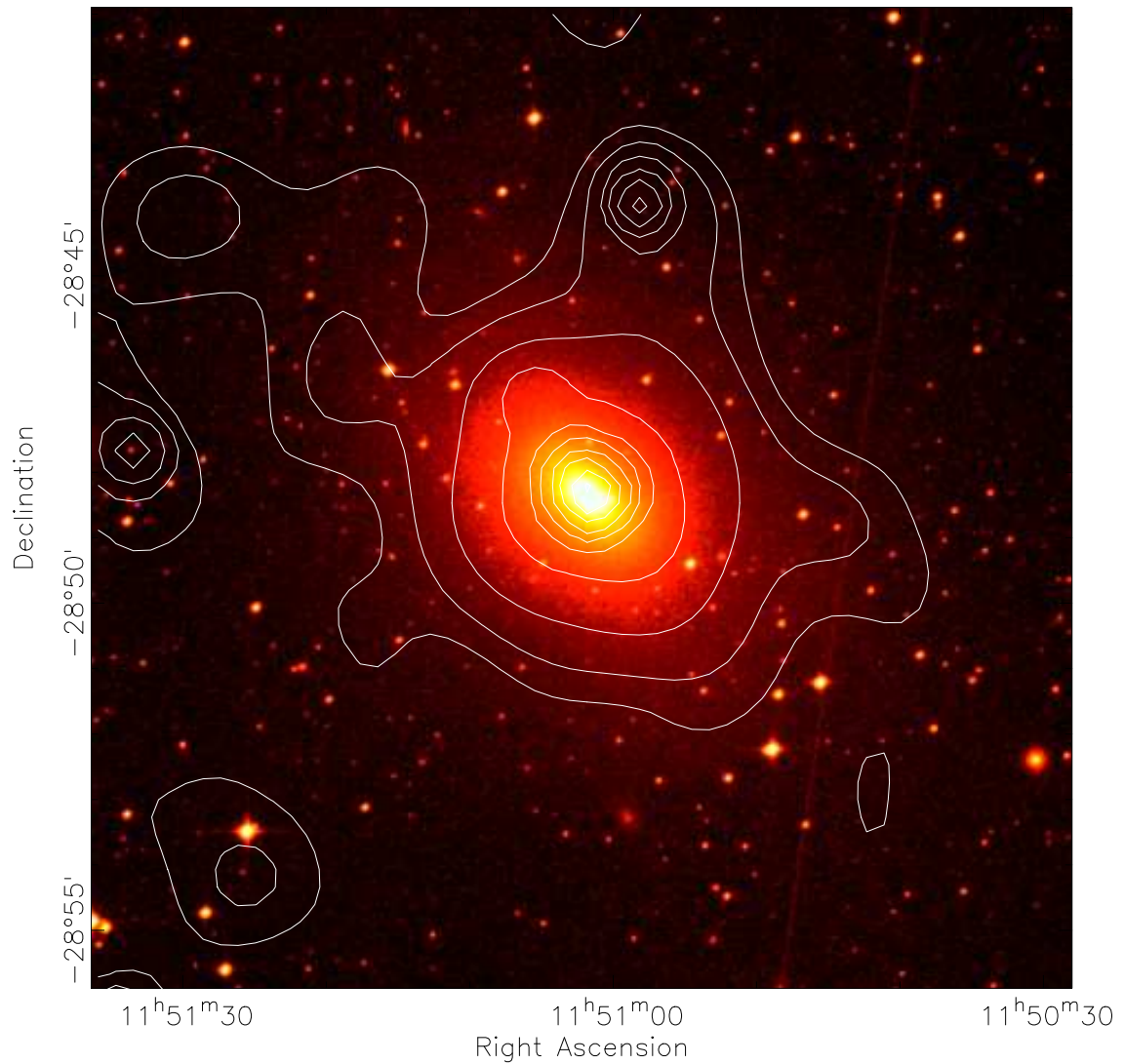


Figure 1.2: X-ray/optical overlay of NGC 3923. NGC 3923 is the dominant elliptical galaxy of the galaxy group LGG 255. This Figure shows *ROSAT* PSPC contours overlaid onto a digitized sky survey R band image of the galaxy. Assuming a distance of 26.8 Mpc, $1'$ is equivalent to ~ 8 kpc.

are to understand the origins of this class of galaxies.

1.1.3 X-ray Sources

Gaseous Halos

Early-type galaxies possess a variety of X-ray sources. In most galaxies the dominant component of their emission arises from the hot gas described above. This highly ionised material emits via thermal bremsstrahlung, recombination emission and two photon decay of metastable levels.

The gas is primarily composed of Hydrogen and Helium, with much smaller quantities of other elements, often referred to as ‘metals’. At the typical temperatures ($kT \sim 1$ keV) and electron densities (10^{-2} – 10^{-5} cm $^{-3}$) found in galaxy halos, thermal bremsstrahlung is usually the most important process. The emissivity of the bremsstrahlung component at a frequency ν can be represented as follows

$$\epsilon_\nu \propto g \frac{Z^2 n_e n_i}{\sqrt{T}} e^{-\left(\frac{h\nu}{kT}\right)}, \quad (1.7)$$

where n_e and n_i are electron and ion number densities, Z is the charge on the ion and T is the plasma temperature. g is the Gaunt factor which corrects for quantum mechanical effects and distant collisions. It is of order unity, but varies slowly with both temperature and frequency (Kellogg et al., 1975).

Integrating Equation 1.7 gives the total luminosity per unit volume

$$\int_0^\infty \epsilon_\nu d\nu \propto n_e n_i \sqrt{T} \quad (1.8)$$

and integrating over the volume therefore produces the total luminosity of the halo

$$L \propto \int_V n_e n_i \sqrt{T} dV. \quad (1.9)$$

From this it is clear that the luminosity of the halo will primarily depend on the square of the gas density (as $n_e \simeq n_i$ for a plasma mainly composed of hydrogen), and more weakly on temperature.

Although bremsstrahlung is an important emission component in galaxy halos, line emission must also be considered, in particular because it produces important features in X-ray spectra. Line emission is the signature of the highly ionised heavier elements in the plasma. In galaxies there are a number of important emission lines, mostly arising from L shell electron transitions in elements such as Fe, Mg, Si, S and O. The most important group of lines is the Fe L -shell complex at ~ 1 keV, which can contribute a significant flux in high-metallicity systems. In instruments with fairly low spectral resolution, such as the *ROSAT* PSPC, emission lines are unresolved, but produce deviations from a pure bremsstrahlung spectrum which can indicate the overall metallicity of the gas. Higher resolution instruments (such as the *XMM-Newton* RGS or *Chandra* HETG and LETG) can resolve individual lines and measure the relative abundances of different metals with remarkable accuracy (*e.g.* Xu et al., 2001), although they are not optimised for observing extended sources. Where data quality or spectral resolution is too poor for exact

measurements, it is generally assumed that the elements exist in the ratios observed in the sun or found in meteorites, and overall metal abundance is measured as a fraction of this solar abundance. Early-type galaxies are usually found to have abundances of 0.3–1 Z_{\odot} , although there is some debate over an average value, owing to differences of technique and model. The confusion of X-ray sources in early-type galaxies makes accurate measurement of metal abundance difficult. One of the best studies to date is that of Matsushita et al. (2000), in which *ASCA* spectra for a sample of X-ray bright ellipticals are fitted with two component models to allow the removal of emission from unresolved discrete sources. Fitting the remaining gas component with several different spectral models and assuming some degree of inaccuracy in these models, the authors conclude that the average metallicity is solar, but cannot constrain it more closely than to within a factor of 2.

One interesting feature associated with X-ray halo emission is the phenomenon of cooling flows. These are best known on a much larger scale in clusters of galaxies. A cooling flow can develop at the centre of a potential well which is filled with X-ray emitting gas. The gas will be densest at the centre of the potential, and will therefore cool via X-ray emission fastest at this point. As it cools and contracts the density rises, leading to runaway cooling. Gas from further out in the potential will move inwards, maintaining pressure equilibrium, and cool in turn. This simplistic model does, however, have one serious problem: what happens to the gas after it cools out of the X-ray regime? This has been a subject of great debate for a number of years, and has yet to be resolved. Suggested solutions include formation of low mass, ‘optically dark’ stars (Mathews & Brighenti, 1999), distributed mass deposition either as stars or gas (Sarazin & Ashe, 1989), and reheating of the gas (*e.g.* Pedlar et al., 1990). Recent observations of cluster cooling flows suggest that the mass deposition rate may be considerably smaller than previously thought (see Böhringer et al., 2002, and references therein), and have provided some evidence for reheating of gas by AGN (*e.g.* Blanton et al., 2001). However, spectral studies using *XMM-Newton* have raised a further potential problem, in that some cooling flows show evidence of a lower temperature limit at some intermediate temperature. It is difficult to imagine a process by which gas can cool, losing most of its energy, and then remain stable, or cool out rapidly without producing noticeable emission.

In early-type galaxies, cooling flows are likely to be small unless the galaxy lies at the centre

of a larger structure. Spatially, cooling flows can be identified through excess emission. A simple isothermal gas halo can be accurately modeled by a modified King profile (Jones & Forman, 1984), but the presence of a cooling flow will be shown by a sharp central peak in the emission. In spectral terms, the emission from a cooling flow is usually modeled as the sum of a number of plasma models spanning a range of temperatures. Mass deposition rates are unlikely to exceed a few $M_{\odot} \text{ yr}^{-1}$ in cases where the galaxy is in the core of a group or cluster, and will be considerably less for smaller scale flows. Even so, the question of the fate of the cooled gas accumulated over several 10^9 years is still problematic.

X-ray Binaries

As would be expected from old objects in which stellar evolution is advanced, X-ray binaries are common in early-type galaxies. The majority of these are probably low mass X-ray binaries (LMXBs) composed of a neutron star or possibly a black hole accreting matter from a normal companion star. Until recently, X-ray observatories were only capable of resolving the brightest binaries, and then only in nearby galaxies. This effectively limited studies of such point sources to objects within the local group, which contains no sizable early-type galaxies. Spectral studies were possible, but without resolving the sources this required high quality data and the accurate modeling of emission from other sources in the galaxy, which often dominate the integrated spectrum. However, a hard X-ray component was detected in a number of early-type galaxies using *ASCA* (Matsushita et al., 1994), and modeling of X-ray surface brightness profiles observed using *ROSAT* showed that a component with a de Vaucouleurs distribution (as expected for stellar sources) could in some cases provide a good fit (Brown & Bregman, 2001).

The launch of *XMM-Newton* and *Chandra* has vastly increased the number of galaxies in which X-ray binaries can be detected. The arcsecond resolution of the ACIS instrument on *Chandra* makes it a particularly effective tool for this task, and a number of studies of individual galaxies have already taken advantage of its capabilities (Angelini et al., 2001; Bauer et al., 2001; Blanton et al., 2001; Fabbiano et al., 2001; Irwin et al., 2002; Kraft et al., 2001; Pence et al., 2001; Sarazin et al., 2001). One of the most interesting galaxies to have been observed is NGC 4697, an E6 galaxy on the outskirts of the Virgo cluster (Sarazin et al., 2000). It is one of the closest large ellipticals to us (15.14 Mpc, assuming $H_0=75$), and was already known to be quite X-ray faint

for its optical luminosity from *ROSAT* observations (Beuing et al., 1999). An exposure of ~ 40 ks was taken using the ACIS-S3 detector, which allowed resolution of any source of luminosity $\gtrsim 4 \times 10^{37}$ erg s $^{-1}$. The approximate lower luminosity limit for X-ray binaries observed in globular clusters in our own galaxy (Hertz & Grindlay, 1983) is 10^{36} erg s $^{-1}$, so it is reasonable to expect that most X-ray binaries in the galaxy would be resolved. In practice, 82% of the emission above 2 keV was resolved into point sources, and assuming that the point source luminosity function extends unchanged down to 10^{36} erg s $^{-1}$, it is believed that $\sim 83\%$ of the total emission in the *Chandra* band (0.3–10 keV) is produced by X-ray binaries. NGC 4697 appears to be unusual amongst early-type galaxies in deriving such a high fraction of its total emission from point sources, but this result does show the importance of understanding the binary population which clearly provides a substantial contribution to galaxy X-ray properties.

X-ray binaries in our own galaxy have spectra which are fairly well characterised (in the ~ 0.1 –10 keV band) by a power law plus a black body thermal component. Spectra from binaries in external galaxies are unsurprisingly of considerably lower quality, and often contaminated by other spectral components, making accurate spectral fits more difficult. Most studies fit spectra from resolved sources using a power law (*e.g.* Sarazin et al., 2001) or high temperature bremsstrahlung (*e.g.* Blanton et al., 2001) component, and possibly a lower temperature black body if necessary. Unresolved sources may be fitted with multiple component models, but only the hard component (again usually a power law or >5 keV bremsstrahlung) is accepted as actually modeling the binary emission.

AGN

A further class of X-ray emission sometimes found in early-type galaxies is that from Active Galactic Nuclei (AGN). Most nearby galaxies show little or no sign of nuclear activity, but at high redshift giant ellipticals are known to host radio-loud QSOs and radio galaxies with luminosities in excess of 10^{46} erg s $^{-1}$ (Allen et al., 2000). There is also dynamical evidence that most early-type galaxies host supermassive black holes (*e.g.* Kormendy & Richstone, 1995; Magorrian et al., 1998; Gebhardt et al., 2000), with masses of a few 10^8 – $10^9 M_{\odot}$. It seems likely therefore that most, or possibly all, early-type galaxies are potential AGN, but that very few have central engines with mass accretion rates high enough to produce significant emission. Some

evidence for low intensity hard power-law emission from the cores of large ellipticals has been found (Allen et al., 2000), although further work on this topic (probably using *XMM-Newton*) is needed.

Where AGN are found in early-type galaxies they pose a serious problem for the analysis of the X-ray emission of the galaxy as a whole. As they are often very bright point sources, sometimes accompanied by X-ray luminous jets, they can significantly affect measurements of integrated luminosity, or spectra from low spatial resolution instruments such as *ASCA*. The solution to these problems is usually to remove galaxies harbouring AGN from consideration, or to remove contaminated regions from images before analysing the rest of the galaxy. However, contamination can sometimes be difficult to recognise, and it is likely that some part of the hard component of emission seen in many elliptical and lenticular galaxies arises from AGN emission.

1.1.4 Scaling Relations

Some of the most important discoveries about galaxies have come in the form of scaling relations. These are simple relations which hold between two or more quantities such as luminosity, mass, velocity dispersion or rotational velocity, physical size, *etc.* These relations are important primarily because they provide insights into the processes which control the structure and properties of galaxies. From a practical point of view they are also useful, as they can provide baselines to which galaxies of a given type can be compared.

X-ray Relations

X-ray emission is a tracer of mass in galaxies, both in the form of stellar sources, and in the form of hot gas. As such hot gas can only be traced by its X-ray emission, relationships between the hot gas mass and other galaxy properties are clearly of some importance. Many comparisons between the X-ray data and other variables have been made, initially using *Einstein* data and later more accurate *ROSAT* and *ASCA* observations. As distance is an important factor in determining these values, newer and more accurate calculations of distances have made some impact on the relations. Probably the best known correlation is that between X-ray and optical blue luminosity, the $L_X:L_B$ relation. This takes the form

$$\log L_X = \log L_B^\alpha + \beta. \quad (1.10)$$

For early-type galaxies, the actual value assigned to α has varied with different measurements, but recent estimations put it at about 2.2 (Beuing et al., 1999) or 2.3 (White & Davis, 1998). However, one of the most interesting features of the $L_X:L_B$ relation is the large degree of scatter found in it. X-ray luminosities may vary by two orders of magnitude for objects with the same optical luminosity, and this variation has proved difficult to explain theoretically or through modeling.

It is possible to split X-ray emission from early-type galaxies into hard and soft bands, the soft representing gaseous emission, the hard representing discrete sources. One possible explanation for the variation in the overall $L_X:L_B$ relation is that, although the levels of emission from discrete sources do scale simply with the optical luminosity, the gas emission is more weakly linked. It is therefore important to look at both components individually. Values for the hard and soft bands have been calculated using *ROSAT* (Irwin & Sarazin, 1998b), α_{hard} giving 2.48 and $\alpha_{soft} \sim 1.94$. However, a similar study using *ASCA* (whose superior spectral resolution makes it the better instrument for the task) suggests that while hard X-ray emission is well correlated with L_B , having $\alpha_{hard} \sim 1$, the soft emission does not scale with optical luminosity (Matsushita et al., 2000). The relatively small sample used to produce this result weakens it to some extent, but it is still very interesting. The slope of 1 found for discrete source emission supports the assumptions made in most studies that luminosity from these sources scales simply with galactic stellar mass. The lack of correlation in gas luminosities is quite controversial though, as most previous studies find some trend, if only a weak one.

The scatter in the $L_X:L_B$ relation has also been compared to the apparent physical size of the X-ray halo (Mathews & Brighenti, 1998b). The reasoning behind this is that the scatter could be caused by the association of excess dark matter with galaxies in the centres of groups or clusters. By looking at L_X/L_B and the ratio of optical and X-ray effective radii, a correlation can be seen, showing that these dominant galaxies really do have an excessively large halo, perhaps because they have captured both gas and dark matter from other members of their groups. Helsdon et al. (2001) studied the X-ray properties of the dominant galaxies of X-ray luminous galaxy groups in some detail, and find a similar result. Group dominant galaxies

are shown to be considerably more X-ray luminous (approximately an order of magnitude) than their neighbours. However, examination of the surface brightness and temperature profiles of these objects suggests that the excess luminosity may be caused by group scale cooling flows, rather than halo growth. In either case this extra luminosity only explains some of the scatter in L_X/L_B at the high end of the relation where $\text{Log } L_B \geq 10.5 L_\odot$.

Both diffuse X-ray emission and radio emission correlate strongly with the optical isophotal shape of elliptical galaxies. X-ray emission from galaxies with “disky”, pointed isophotes is generally weak, at the level expected from discrete sources rather than from a hot halo. Extended halo emission may in fact be almost entirely confined to those ellipticals with “boxy” isophotes (Bender et al., 1989). It has been suggested that isophote shape is related to the formation process which has produced the galaxy (*e.g.* Nieto & Bender, 1989). Boxiness or irregular isophotes would be produced by mergers, whereas disk isophotes would be a sign that no interaction had taken place, at least not since the early history of the galaxy. This idea relates mergers to a hot interstellar medium (ISM) and gaseous halo. However, modeling of mergers and examination of the remnants produced (Heyl et al., 1994) shows that the production of a galaxy whose isophotes appear boxy or disk is not simple. Modeling results instead suggest that isophotal shape will depend largely on viewing angle and therefore would not be linked to the halo properties. However, it is difficult to reconcile this with the strong observed correlation, and the issue is as yet unresolved.

A further correlation with the shape of elliptical galaxies exists: correlation with core profile. Observations of early-type galaxies with the *Hubble Space Telescope (HST)* have shown that the cores of early-type galaxies have central surface brightness profiles which can be classified as either “cuspy core” or “power law” (Faber et al., 1997). Galaxies with cores show a break in the surface brightness profile at a radius of 50 to a few 100 pc, within which the surface brightness profile is flattened. They have also been observed to have (in general) boxy isophotes, slow rotation velocities and a higher than average optical luminosity. Power law galaxies, on the other hand, are low luminosity, faster rotating, and have disk isophotes. Their inner surface brightness profiles do not break to a shallower gradient, at least down to the resolution limit of *HST*.

There is some evidence (Pellegrini, 1999b) to suggest that there is a good correlation between

these two families of galaxies and X-ray luminosity. In a sample of 59 early-type galaxies, core galaxies were shown to have L_X values over the whole range of the sample. Power law galaxies were shown to have low X-ray luminosities, below $\text{Log } L_X = 41 \text{ erg s}^{-1}$. This relation has also been shown to be stronger than the previously known correlation with isophotal shape, leading to the conclusion that the global gas properties of the galaxy are strongly tied to the nuclear stellar distribution. It is suggested that the origin of this link could be the presence and/or mass of a central super-massive black hole within the galaxy core, but the dynamics of such a link are not understood.

Another relationship is thought to exist (*e.g.* Eskridge et al., 1995) between the core radio luminosity of the galaxy in question and L_X . This suggests a link between the core radio source and the hot halo gas which is the origin of the X-ray emission, which provides a method of checking the accuracy of the modeling of these systems. As core radio sources are often thought to be related to the presence of a central black hole, this relation also bears comparison with that between core profile and L_X discussed above.

Lastly, there is the relation between L_X and environment. This has recently been dealt with by Brown & Bregman (2000), who noticed in an earlier paper (Brown & Bregman, 1998) that all the brightest galaxies in their sample of 34 were in the centres of dense groups or clusters of galaxies. Following this, they compared L_X/L_B with an environmental density parameter (Tully, 1988) and found a strong ($> 99\%$) correlation between the two. Galaxies in high density environments had L_X/L_B values over the whole range of the sample while those in low density environments were restricted to the lower end of the range. The suggested explanation for this relation is that in dense environments galaxies have the opportunity to accrete extra gas and dark matter, and are often more massive than their counterparts in less dense regions. In addition, galaxy winds in these environments may be stifled by a dense intergalactic medium or by the deeper gravitational wells of the more massive galaxies. It is hoped that with the advent of the new X-ray observatories *Chandra* and *XMM-Newton*, emission lines from cooling gas or temperature and metallicity gradients indicative of cooling and accretion around galaxies will be observable.

A previous study by White & Sarazin (1991) found a contradictory result. In their study, galaxies with lower X-ray luminosities were more likely to have neighbours, while those with

high luminosities were found in less dense environments. This could be explained if dense environments caused the removal of gas or dark matter from galaxies, perhaps through ram-pressure or viscous stripping. The most recent study of this question is that of Helsdon et al. (2001), in which it is shown that galaxies in the centres of groups are likely to have overestimated X-ray luminosities, owing to cooling flows associated with the groups they reside in. If group dominant galaxies are assumed to be biased, and removed from consideration, the trend observed by Brown & Bregman (2000) is greatly weakened, suggesting that it is driven, at least in part, by this biasing effect. The samples used by both Brown & Bregman and White & Sarazin suffer from potential biases caused by the large numbers of group and cluster dominant galaxies included, a situation which is difficult to avoid when limited to using only the brightest and best observed ellipticals.

Optical Scaling Relations

As well as relations which provide information on the X-ray properties and gas masses associated with early-type galaxies, it is also important to consider those which can tell us about the stellar populations and structure of the galaxies. The most useful of these relations are found between optical properties. Although X-ray observations can provide information about the stellar population through the properties of X-ray binaries, confusion between unresolved discrete sources and gas emission makes accuracy difficult. Optical measurements can provide information about the stellar population and its history much more directly and with less opportunity for confusion.

One example is the Faber-Jackson relation (Faber & Jackson, 1976). This relation holds between the velocity dispersion and total luminosity of the galaxy. As both properties can be considered as measures of total galaxy mass, such a relation is perhaps unsurprising. It has proved useful, in that it can be used as a redshift independent measure of the distance to a galaxy, if its velocity dispersion can be measured. It also provides another measure by which past disturbances can be identified; a galaxy lying too far off the relation has probably been dynamically disturbed, or is structurally unusual. However, there is a degree of intrinsic scatter in the relation, which must be taken into account.

The cause of this scatter is mainly the dependence of the galaxy properties on other variables. The combination of the Faber-Jackson relation with a similar relation between velocity dispersion

and isophotal radius (the D_n - σ relation) produces a more tightly constrained correlation — the Fundamental Plane (Djorgovski & Davis, 1987; Dressler et al., 1987). By plotting the three parameters as the axes of a cube, it can be shown that early-type galaxies fall in a well defined strip within the 3-dimensional space. Again, this relation can be used as an accurate redshift independent distance indicator.

Although the fundamental plane is very thin, it also has an intrinsic scatter, suggesting yet another parameter determining the properties of elliptical galaxies. One explanation for a part of this scatter is that of Forbes et al. (1998), who showed that the scatter about the Fundamental Plane, M_{g_2} line strengths and B-V colours were consistent with the effects of an aging starburst combined with an old population. In their model, galaxies which have recently undergone a starburst event lie below the plane, and move toward it with age. At an age of ~ 10 Gyr they lie on the plane, and further aging will cause them to pass through it.

As starbursts in galaxies are thought to be caused by gaseous mergers, determining the age of the starburst gives the time since the last major merger. This is an interesting parameter, giving information on merger rates for elliptical galaxies in different environments. Estimates of this age in field ellipticals (González, 1993) show that they have undergone mergers at a range of ages. On the other hand, age estimates of Fornax cluster ellipticals (Kuntschner & Davies, 1998a) are all very similar, suggesting that merging halted for most of the cluster at this point. This is good evidence in support of the hierarchical merging and clustering model of galaxy formation.

It is worth noting that it has recently been suggested (Fukugita & Peebles, 1999) that the fundamental plane might be extended to include X-ray properties. X-ray luminosity and effective radius are both measurable properties, and comparison of these with the stellar velocity dispersion might produce an interesting relation. At present this is prevented by the quality of data available for most elliptical galaxies, but the expansion of the *Chandra* and *XMM-Newton* data archives is likely to change this.

1.2 Basic Properties of Late-type Galaxies

Although this thesis is mainly concerned with early-type galaxies, it is worth taking some note of the properties of spiral and irregular galaxies. Most formation models link early- and late-type galaxies in some way, and comparisons between the properties of the two classes can be quite striking. There are also a number of areas in which the study of early-type galaxies is difficult, but where observations of spiral galaxies can provide information about properties held in common.

As discussed previously, early-type galaxies contain primarily old stars. The most obvious difference between early- and late-type galaxies is that the stellar colours of spirals are much bluer than those of ellipticals. The stars responsible for this emission are typically very massive and short lived, and only constant replenishment of the population can maintain the numbers observed. Ongoing star formation and removal of massive stars through SNI_{II} is one of the most important features of late-type galaxies.

Spiral galaxies are made up of two main components, the bulge and disk. The bulge is usually made up of older stars, and although it does rotate along with the disk, its shape is produced to some extent by stars with more random orbits. The disk is more closely constrained, often being no more than a few kpc thick. As well as containing some older stars, the disk is the site of star formation, mainly in spiral arms and in some cases in a bar. Both of these are structures formed by the conjunction of stellar orbits, which bring together gas and stars to form high density regions where gas clouds can rapidly collapse and begin the process of star formation.

The relative importance of the bulge component is the main characteristic used to classify spiral galaxies, from Sd galaxies with little or no bulge component to Sa galaxies, the most bulge dominated late-types. The succession can be seen to continue through S0 to diskly and then spheroidal elliptical galaxies, which are sometimes considered as bulges with no disk. However, spiral galaxies are typically less massive than ellipticals, particularly when compared to the largest giant ellipticals and cD galaxies. There are relatively few identified spiral galaxies with stellar masses above $10^{11} M_{\odot}$.

1.2.1 The Interstellar Medium

The ISM of late-type galaxies is also very different from that found in early-type galaxies. Very large quantities of cool atomic and molecular gas are common in spiral galaxies, as well as sizable amounts of dust. Bregman et al. (1992) give typical figures for Sa galaxies of $>10^{10} M_{\odot}$ of neutral hydrogen, $>10^6 M_{\odot}$ of dust, and $>10^9 M_{\odot}$ of molecular hydrogen. Cool gas masses also tend to increase with decreasing bulge fraction, so later-type spirals will contain even higher masses. The ISM also tends to be very complex in structure. Gas and dust tend to congregate in clouds, and stellar winds and supernovae can produce bubbles, shells and voids, as well as driving fountains of gas up out of the plane of the disk (Elmegreen & Efremov, 1997). Many bright spiral galaxies are however extremely deficient in gas within the central few kpc, producing a central “hole” through the disk (Brinks & Bajaja, 1986).

In contrast, the evidence for a hot ISM in spiral galaxies is poor, consisting mainly of upper limits on the masses of gas involved. Because of the relatively poor spatial resolutions of X-ray satellites prior to the launch of *XMM-Newton* and *Chandra*, there has been considerable difficulty in separating diffuse gas from unresolved point source emission. This throws some doubt on estimates produced with the *ROSAT* PSPC. For example, the results of Bregman et al. (1992) suggest that Sa spirals could contain 10^8 – $10^9 M_{\odot}$ of hot gas, but as they detect fewer than ten objects and have no way of separating emission from different sources, this is almost certainly an overestimate. There is no sign of large hot gas halos similar to those which surround early-type galaxies. Attempts to find low density hot gas away from the stellar body, and presumably accreting into it, have been unsuccessful (Benson et al., 1999).

A recent *Chandra* study of NGC 1291, a nearby Sa galaxy, does show some evidence for a hot ISM component (Irwin et al., 2002). In this galaxy, cool HI gas is seen to occupy a ring-like disk, leaving a central hole of ~ 7 kpc radius. A total HI mass of $1.3 \times 10^9 M_{\odot}$ is detected in the galaxy (van Driel et al., 1988). In contrast, only $\sim 6 \times 10^7 M_{\odot}$ of hot gas is detected, but it occupies the central hole, with X-ray emission from this gas detectable out to ~ 5 kpc. As Irwin *et al.* comment, the question of whether the hot gas has displaced the cool, or whether the hot gas is associated with the bulge and the cool gas with the disk, is still unresolved. It is also worth noting that as later-type spirals contain more cool gas and have smaller bulges, it is likely that hot gas masses will be smaller in these objects.

1.2.2 X-ray Sources

X-ray emission in spirals arises from the same sources as in elliptical galaxies, but in different ratios. The smaller hot gas masses observed in late-type galaxies mean that emission from this source is less important. Instead, X-ray binaries are the main source of emission. As in early-type galaxies, LMXBs are probably the most important form of discrete source, but HMXBs are far more common than in ellipticals, owing to the larger young component of the stellar population. Supernova remnants also make up a more important part of the emission than in ellipticals and S0s. The total X-ray luminosity of spiral galaxies is usually considerably lower than that of ellipticals. Most late-type galaxies have luminosities of $L_X < 10^{41}$ erg s⁻¹.

The most obvious case where this ‘rule of thumb’ does not apply is when the galaxy has an active nucleus. AGN, particularly Seyfert galaxies, are amongst the brightest X-ray sources in the local universe. As in early-type galaxies, the presence of an AGN makes study of any other part of the X-ray emission very difficult, and these galaxies are often excluded from X-ray studies. Starburst galaxies are also problematic. Starbursts occur when a significant amount (*e.g.* > 5%) of the stellar mass of the galaxy is formed rapidly in a relatively compact region. In most cases this occurs in the centre of the galaxy, when tidal interactions channel large quantities of cool gas into the core. The near simultaneous formation of very large numbers of stars produces a very rapid increase in radiation and stellar winds, forcing the remaining gas in the galaxy outwards. The formation is relatively quickly followed by supernovae among the most massive stars, producing a further increase of wind pressure. This can lead to the ejection of large quantities of cool and/or hot gas from the galaxy in a ‘superwind’, and the formation of large bubbles of hot gas within the cool ISM. The hot gas, star formation and supernovae combine to make these galaxies powerful sources of X-rays.

1.2.3 Scaling Relations

As with early-type galaxies, there are various relations which describe the properties of spiral galaxies. The wide ranging studies of Shapley et al. (2001) and Read & Ponman (2001) contain the most recent examination of the $L_X:L_B$ relation in spiral galaxies. The Shapley et al. (2001) sample contains 234 spiral and irregular galaxies (of which 114 are detected in X-rays), for which they find a strong relation of the form $L_X \propto L_B^{\sim 1.5}$. Despite the expected variation of

X-ray gas mass with morphological type, they find that the slope of the $L_X:L_B$ relation remains constant (within the errors) from Sa through Sb/Sbc to Sc/Irr. The fact that this relation is fairly stable, and has a slope >1 is important. If we assume that hot gas is playing a negligible part in the total X-ray emission, this result suggests that the relation between integrated X-ray binary luminosity and optical luminosity is not as simple as is generally assumed. This would have obvious implications for the study of early-type galaxies, as it seems likely that the relation would be similar regardless of galaxy morphology. Alternatively, if hot gas is causing the steeper than expected slope, this result suggests that it is important regardless of morphological type. Again, further study with the new X-ray observatories is probably needed to resolve this issue.

Probably the most important optical correlation for spiral galaxies is the Tully-Fisher relation (Tully & Fisher, 1977). This is analogous to the Faber-Jackson relation in early-type galaxies, as it relates the optical luminosity of the galaxy to its rotational velocity. As with the Faber-Jackson relation, this provides a redshift independent method of determining distance to the galaxy in question. However, the cool gas content of spiral galaxies means that the rotational velocity of the galaxy can be measured at radio wavelengths, allowing the inclusion of more distant targets.

1.3 Galaxy Systems

Most early-type galaxies are not found in isolation, but reside within larger structures. In groups and clusters of galaxies, individual members are brought closer together more often than in the field, and are likely to interact with each other as well as the gas and dark matter associated with the surrounding potential well. These interactions may have profound effects on galaxy formation and evolution, and need to be considered when examining the properties of early-type galaxies.

1.3.1 Environmental classes

Galaxies are usually described as being in one of three environments: clusters, groups or the field. This is something of an oversimplification, and galaxies are often misclassified or described differently in separate studies. Some authors even ignore the group category entirely, placing all galaxies outside rich clusters in the field.

Clusters are the largest collections of galaxies, generally containing 30–3000 objects. They are usually X-ray luminous objects in their own right, as the cluster potential well traps gas which is shock heated to 10^7 – 10^8 K as it falls in. Clusters often have diameters of several Mpc. They are characterized by a high velocity dispersion, with galaxies in the cluster having velocities differing by up to 2000 km s^{-1} . This means that galaxy mergers are unlikely (short of a head-on collision) to occur in clusters; encounters between galaxies at such speeds are too fast for strong interactions. However, it has been suggested that galaxies may interact with the Intra-Cluster Medium (ICM), and this will be discussed later in this section. Clusters often have one (or occasionally more than one) dominant galaxy. In relaxed clusters these are usually cD galaxies — giant ellipticals with extended envelopes of stars and high luminosity in the optical and X-ray bands. These objects are thought to be formed through multiple mergers and tidal stripping of smaller galaxies. They usually lie at the peak of the cluster X-ray emission, *i.e.* the deepest point of the cluster potential.

Collections of 3 to 30 galaxies are known as groups. However, the upper limit of this description is somewhat arbitrary, as it often ignores small galaxies below the limit of detection of the catalogue used to define the system. The group description is often applied to much larger structures, particularly “subgroups” which make up sections of clusters. Groups also cover a large range of density. Compact groups (*e.g.* Hickson, 1982) have densities equal to or greater than the cores of clusters, but with much lower velocity dispersions, as low as 62 km s^{-1} in one case (Weinberger et al., 1999). More typical groups have velocity dispersions of around 100 – 500 km s^{-1} and radii of $\sim 500 \text{ kpc}$. These densities and low velocities make groups the most favourable environment for merging.

Some groups share the X-ray properties of clusters, having their own halo in addition to those of their member galaxies. This is not always the case though — there are many examples of confirmed groups with no detected X-ray emission, particularly in groups where the fraction of spiral galaxies is high. Many groups also have a dominant galaxy, often a giant elliptical, although dominant spirals are known.

Galaxies classified as being in the field are usually thought of as completely isolated objects. The galaxy should not be associated with any group or cluster, so in principle it is either completely isolated or in a pair. However, many field galaxies are actually on the margins of

loose groups or clusters. Truly isolated galaxies are fairly rare objects. Galaxies in pairs are likely to lose energy through tidal interactions and merge in the future, although the time scale depends on the relative velocities and orbits.

1.3.2 Identification and classification

Identification and classification of groups and clusters is not a simple task. The first samples of galaxy clusters were identified by looking for overdensities in the distribution of galaxies on optical photographic plates (*e.g.* Shapley & Ames, 1932; Abell et al., 1989). This technique is adequate for identifying nearby rich clusters which have many optically luminous members. However, it takes no account of the line of sight distance to the galaxies in question. Therefore, as the number of galaxies in the system drops, the probability of misclassifying chance superpositions of galaxies as groups or clusters increases. Mistakes are most commonly made when attempting to identify loose groups, as the galaxy densities in these systems are low. Only very compact groups can be easily identified (*e.g.* Hickson, 1982; Prandoni et al., 1994).

Another disadvantage of using a simple two dimensional overdensity to identify galaxy systems is that it is unhelpful when deciding whether galaxies are bound to the system or merely happen to lie near its edge. The obvious way to improve on the technique is to add a third dimension, by taking into account either recession velocities or distances (or, preferably, both). A number of algorithms have been developed which use position and redshift to identify fairly accurately groups and their members (see *e.g.* Materne, 1978; Tully, 1980; Huchra & Geller, 1982; Slezak et al., 1990)

An alternative method is to look for the system in the X-ray band. The depth and size of the potential can be inferred from the properties and extension of the X-ray emission, and the group or cluster identified as a gravitationally bound system on this basis. Optical studies are still needed to examine the properties of the galaxies and the redshift of the system as a whole, but the difficulty of optically identifying the group or cluster is avoided. Groups are usually found to have temperatures below 2 keV, while clusters are usually hotter and can reach temperatures as high as 15 keV. However, it is again important to note that not all groups and clusters have large X-ray halos. For groups, the difficulty of determining the biases involved in the selection of targets for X-ray surveys means that the fraction of groups which are X-ray bright is not well

determined (Mulchaey, 2000). The situation for clusters is better understood, but the fraction of clusters which are X-ray faint must still be accounted for. An example of an X-ray faint cluster is the Ursa Major cluster, which lies at a similar distance to the well known X-ray bright Fornax and Virgo clusters. There is some question about the current dynamical state of this cluster, which has no major central concentration, and it has been suggested that it is in the process of formation (Tully et al., 1996), and that it will gain an X-ray halo as it develops.

1.3.3 Constitution and Properties

Groups and clusters of galaxies are made up of three main components; galaxies, an extended hot gas halo, and dark matter. Of these, the dark matter is by far the most massive component, making up 75–90% of the mass of the system (White & Fabian, 1995). As is the case in galaxies, most studies of dark matter in groups and clusters rely on measurements of velocity dispersion or the X-ray halo distribution.

Galaxies are the most visible component of groups and clusters, if the least massive. In relaxed systems with little or no substructure, their distribution is generally well described by the NFW (Navarro et al., 1997) or King (King, 1962) profiles (*e.g.* Carlberg et al., 1997; Adami et al., 1998). As mentioned above, there are some differences between galaxies found in groups and clusters, and those found in the field. The most obvious difference is the presence of cD galaxies, with their extended stellar halos, in the centres of some clusters. However, that there are more subtle differences has been known for some time (*e.g.* Oemler, 1974). The morphology-density relation (Dressler, 1980) describes the change in galaxy type with environment. In a sample of 55 rich clusters, it was found that the fraction of elliptical and lenticular galaxies rose with density, while the fraction of spiral and irregular galaxies dropped. The explanation for this is not immediately obvious. At high densities and low velocity dispersions, the conditions found in groups, we might expect to see many mergers, leading to a high fraction of early-type galaxies. However, clusters have a high velocity dispersion, making high merger rates unlikely.

The relation is usually explained as a product of the way in which clusters form. They are believed to be created by the infall and merger of small groups and individual galaxies. Therefore, the elliptical galaxies we are seeing in clusters should have been formed in groups which are now part of the cluster. If this is so, we would expect the cluster elliptical population

to be (on average) older than those elsewhere. We might also expect to observe clusters forming with groups around their edges in which the merger fraction is high. Present studies of cluster ellipticals do not definitely determine their ages, but do show that they are coeval (Kuntschner & Davies, 1998b). There is evidence in one $z = 0.83$ cluster (van Dokkum et al., 1999) that mergers are occurring at the edge of the cluster in sub-clumps which are presumably infalling groups. Others at similar redshift show significant substructure (Ebeling et al., 2000).

In addition to the morphology-density relation, strong gradients in morphological type with radius are observed in clusters (Melnick & Sargent, 1977), and it has been argued that this is the more fundamental relationship. However, as galaxy density rises monotonically with decreasing cluster radius, it is not simple to separate the two effects. It should also be noted that the luminosity function in clusters varies with morphological type, so measurements of population fraction will change for different limiting magnitudes.

The hot gas component of clusters and groups is very similar to the hot gas halos observed around early-type galaxies. It usually has a total mass several times higher than that of the galaxies, making it the dominant baryonic component in the system. The typical particle density of the IGM is $\sim 10^{-3} \text{ cm}^{-3}$. The metal content is on average lower than that of galaxy halos, with a value of 0.2–0.3 Z_{\odot} usually assumed. The gas distribution is (in undisturbed systems) well described by a modified King profile (Jones & Forman, 1984). Most clusters have profiles with similar power law slopes in their outer regions, characterised by a β parameter of ~ 0.67 , while groups show more variation, typically having values between 0.4 and 1.

1.3.4 Scaling Relations

A number of simple scaling relations have been found to apply to the X-ray halos of groups and clusters. Most of these correlations were originally found through studies of galaxy clusters, but have been extended to the group regime. The changes in the relations with mass scale allow the examination of the differences between groups and clusters, and are as yet not well understood, despite much work and a number of theories.

One simple model of galaxy systems is known as self-similar scaling. This assumes that all galaxy systems are products of their potential wells. As the dark matter profile is believed to be the same regardless of mass, any given system can be considered as simply a scaled version of

any other system. Their properties scale with mass, and so are predictable. The only parameter which does alter the dark matter profile is the formation epoch. The density of the system is expected to be related to the critical density of the universe at the epoch of formation, so that older systems are denser. This will make their dark matter profile somewhat steeper, and the systems more concentrated (Lloyd-Davies et al., 2002). However, assuming that we are observing objects which have formed recently in the local Universe, we can ignore this variation and examine the predictions of the self-similar model.

As a first step, let us take the total kinetic energy of the system

$$K.E. = \frac{1}{2}Mv^2 \propto \frac{3}{2}kTn, \quad (1.11)$$

where M is the total system mass, v is the 3D velocity dispersion of the system, T is the temperature of the gas in the system, k is Boltzmann's constant and n is the number of particles in the system. Note that this assumes a relaxed system with a fixed gas fraction, so that $M_{gas} \propto M_{tot}$ and the kinetic energy of the gas is always proportional to the kinetic energy of the system as a whole. If we assume that the gas in the system is well approximated as pure hydrogen, we can write n as M/m_H (where m_H is the atomic mass of hydrogen) and substitute Equations 1.11 and 1.3 into the virial theorem, to show

$$T \propto \frac{M}{R}, \quad (1.12)$$

where R is the characteristic radius of the system. We can therefore measure the total mass within that radius by simply measuring the X-ray temperature within that radius. We can take this further, to predict trends, if we consider that

$$M = \frac{4}{3}\pi R^3 \rho, \quad (1.13)$$

where ρ is the mean density of the system. The value of ρ is actually something of a problem, as it will be related to the mean density of the universe at the time at which the system formed.

It is known that for a Λ CDM universe ρ will vary as follows

$$\rho \propto [\Omega_\Lambda + \Omega_M(1+z)^3]\Delta_c(z), \quad (1.14)$$

where z is the redshift of formation, Ω_Λ is the vacuum energy density and Ω_M is the matter energy density of the universe, both measured at $z=0$, and $\Delta_c(z)$ is a factor dependent on the

critical density of the universe and varying with the redshift of formation. The true redshift of formation is usually unknown, and so the redshift of observation is assumed to be the approximate redshift of formation. Most models of structure formation suggest that the superclusters are the scale of object currently forming, that most clusters formed at $z \leq 1$, and that galaxies formed largely before redshift 2 (Turner, 1999). This suggests that while it may be reasonable to assume that clusters have just formed when we observe them, it is less so for groups, and not justifiable for galaxies. However, for systems of galaxies, there is no obvious way to measure the redshift of formation, so the assumption must be made. For systems at low redshift, this density term can therefore be neglected, and substituting Equation 1.13 into Equation 1.12, we produce

$$T \propto R^2. \quad (1.15)$$

Equation 1.9 shows the relation between X-ray luminosity and temperature for a plasma emitting via bremsstrahlung. We now have a relation between radius and temperature, so we can substitute into Equation 1.9 to get a relation between luminosity and temperature. As volume is proportional to R^3 ,

$$L \propto T^{\frac{1}{2}} R^3 \propto T^2 \quad (1.16)$$

where L is the X-ray luminosity. We can also produce a relationship between mass and temperature

$$M \propto T^{\frac{3}{2}} \quad (1.17)$$

and using what we know of the kinetic energy of the system (see Equation 1.11), a relationship between temperature and velocity dispersion

$$T \propto \sigma^2, \quad (1.18)$$

which then leads to a relation between X-ray luminosity and velocity dispersion

$$L \propto \sigma^4. \quad (1.19)$$

It is worth noting that another prediction of the simple self-similar scaling model is that as all gas density profiles should be governed by the potential well, they should therefore be scaled versions of one another. We would therefore expect to see all systems well modeled by a King profile with a universal slope.

In practice, studies of clusters and groups of galaxies show some departures from these relations. For example, the $L_X:T_X$ relation for clusters of galaxies is approximately $L \propto T^3$ (Fairley et al., 2000, and references therein), and for groups is even steeper; $L \propto T^{4.5}$ (Helsdon & Ponman, 2000). This suggests that the self-similar scaling model is not an accurate description of the behaviour of these systems. In order to explain the differences, a variety of processes which might alter the relations have been suggested. Cooling flows are known to be common in clusters, are observed in some groups, and can strongly affect the density and temperature structure of the halo. Allen & Fabian (1998) examined the effect of cooling flows on massive clusters, and found that by removing the effects of the cooling flow, the slope of the $L_X:T_X$ relation was reduced, bringing it into agreement with the predicted self-similar slope (within errors). A similar study by Markevitch (1998) also finds a reduction in the $L_X:T_X$ slope, but the effect is not large enough to bring the relation into agreement with predictions. It is therefore unclear whether cooling flows are indeed responsible for the slope of 3 found for massive clusters. A reduction in slope is also found in less massive clusters and groups when the cooling flow region is removed, but for these systems the change in slope is a small effect, certainly not large enough to bring them back to the predicted relation.

One method which has been used to examine the changes in the scaling relations is to look at the entropy of the gas in the system. In studies of groups and clusters entropy is usually defined, ignoring logarithms and constants, as

$$S = \frac{T}{n_e^{2/3}} \quad (1.20)$$

(*e.g.* Ponman et al., 1999). Non-gravitational processes which increase the entropy of the gas in some systems could affect the slope of the $L_X:T_X$ relation. For example, heating the gas would cause the temperature to increase and the density to decrease. Assuming the heat were injected after the collapse of the system, this would make the gas density profile shallower, and as luminosity is proportional to density squared and the square root of temperature, would decrease the luminosity significantly. Alternatively, very low entropy gas is likely to be dense and cool, ideal conditions for it to quickly cool out of the X-ray regime. This would raise the observed mean temperature and lower the density, thereby apparently raising entropy. Any extra gas entropy is most noticeable in small systems, where the entropy produced through shock heating of infalling gas is proportionately less, and goes almost unnoticed in massive clusters. A number

of models describing the method by which entropy is increased have been proposed, the most notable being heating via galaxy winds (Ponman et al., 1999), heating by AGN (Wu et al., 2000) and cooling of low entropy gas (Muanwong et al., 2001). All of these methods have problems, mainly relating to the expected efficiency of the process; for example, AGN heating must be extremely inefficient to allow the systems to form, while heating via galaxy winds must be highly efficient to produce the effects observed. It is quite possible that all three processes (and indeed others) play some part in altering the form of the scaling relations.

1.3.5 Unusual Objects

As mentioned previously, many clusters and some groups have cD galaxies at their centres, objects which share most of the properties of a giant elliptical galaxy, but have some unique features of their own. Group and cluster central galaxies as a class have some interesting features which show how their environment has affected them. As they are often assumed to be normal elliptical galaxies, these differences are important to understand so that they do not bias the study of early-type galaxies as a whole.

cD galaxies appear at first glance to be merely very large elliptical galaxies with a rather extended stellar halo. However, deep imaging studies show that this halo can be enormous; NGC 1399, the cD at the centre of the Fornax cluster, has a halo extending up to 250 kpc (Killeen & Bicknell, 1988). Studies of cluster dominant galaxies as a group have shown that they are too bright to represent the bright tail of the normal elliptical luminosity function, and are instead a separate class of objects (Bhavsar & Cohen, 1990). As they lie at the centre of clusters of galaxies, it seems likely that some part of their stellar halo is gained through tidal stripping of, or merger with, other galaxies (Ostriker & Tremaine, 1975; Richstone, 1976). Multiple mergers in the cluster core during its very early history are also a likely formation mechanism for these objects (Dubinski, 1998). Large scale cooling flows could potentially provide masses of cool gas to fuel extensive star formation, but this would need to take place over a very extended period, as little star formation is seen in cDs today (Fabian et al., 1994).

The brightest galaxies in X-ray bright groups also have some unusual properties. These galaxies are almost always giant ellipticals, and usually lie at the centre of the group X-ray halo. Although their environment is similar to that of brightest cluster galaxies, their luminosities are

consistent with them being normal (if bright) early-type galaxies (Bhavsar & Barrow, 1985). However, Helsdon et al. (2001) showed that their X-ray luminosities are exceptionally high, probably due to the influence of group scale cooling flows. They also found some evidence to suggest that non-central group galaxies in X-ray bright groups may have lower X-ray luminosities than might be expected from the $L_X:L_B$ relation for early-type galaxies. The normalised X-ray luminosity (L_X/L_B) of these galaxies was found to be constant, at ~ 3 times the expected luminosity from discrete sources alone. This deficiency may be caused by the loss of gas through stripping in the group environment.

Galaxy groups provide ideal conditions for galaxy mergers, and there are a number of compact groups where all the major galaxies show signs of interactions with one another (Weinberger et al., 1999). The probable end result of the merger process is that all the massive galaxies will merge, producing one large dominant galaxy, whose only neighbours are much less massive than itself. Such objects are known as fossil groups (Ponman & Bertram, 1993) and as yet only a small number have been found. One of the best studied was originally discovered through a *ROSAT* survey (Ponman et al., 1994), which showed that it had a high X-ray luminosity, comparable to that of a galaxy cluster. Optical observations revealed only one large galaxy, at the centre of the X-ray emission. Around 70% of the total optical emission from the group is found to come from this galaxy, and the next brightest galaxy is a factor of 10 less luminous (Jones et al., 2000). Its X-ray properties are also unusual — the halo is typical of a group in size, but highly elliptical, and it lies above the $L_X:T_X$ relation, suggesting that it is either very cool or very luminous for its mass. This may be explained by the fact that fossil groups are expected to form at early epochs, and so should have high mean densities.

1.3.6 Environmental effects on galaxies

One suggested explanation of the scatter in the $L_X:L_B$ relation is that the environment of the galaxies affects them in such a way as to raise or lower their luminosities by a significant amount. A number of methods by which large scale changes in luminosity could be effected have been proposed. Although some are expected to be strongest in particular environments, it is likely that all but the most isolated galaxies are influenced by some or all of them.

One of the processes most likely to affect galaxies is ram-pressure stripping. This occurs

when a galaxy is moving rapidly through a gaseous medium, such as the IGM of a cluster or group. The pressure of the external gas on the gas at the leading edge of the galaxy forces it backward, and Kelvin-Helmholtz instabilities form at the edge of the galaxy, stripping gas away. In simulations of early-type galaxies passing through clusters (*e.g.* Stevens et al., 1999), the fraction of gas stripped depends on parameters such as galaxy velocity, density of the IGM and the mass and gas density of the galaxy. The largest amount of gas is stripped as the galaxy passes through the core of the cluster, and at this stage the galaxy may lose almost its entire halo, if it is traveling quickly enough through a dense enough medium. Similar effects are seen in simulations of spiral galaxies (Quilis et al., 2000), although in this case the majority of the stripped gas will be cool.

Ram-pressure stripping has a number of implications, both for the galaxy and for the surrounding medium. The loss of gas in spiral galaxies would prevent or greatly reduce further star formation, and this is one method by which S0 galaxies could be formed (Gunn & Gott, 1972). As mentioned above, the scatter in X-ray luminosities of early-type galaxies could be produced by the loss of part or all of their halos through stripping. The gas lost from both early- and late-type galaxies would be much more metal-rich than the primordial gas which makes up most of the IGM in groups and clusters, so stripping provides one method by which this gas can be enriched to the levels we observe today.

In lower mass systems, the galaxy velocities and IGM densities are likely to be much lower, low enough that ram-pressure stripping is unlikely to be very effective. However, turbulent and viscous stripping is expected to be much more efficient in this regime (Nulsen, 1982), and this may still remove significant quantities of gas from the galaxy concerned. This suggests that stripping of gas is important in groups as well as clusters, and that galaxies moving more slowly through the outskirts of clusters may suffer stripping, though to a lesser degree than those which fall rapidly into the cluster core.

Simulations of the interactions which occur when two galaxies approach each other have proved quite revealing. If the galaxies are moving slowly enough, they are likely to merge. During this process, the material in the galaxies may be dragged out into tidal tails. These tails can contain very large amounts of material; it has been suggested that in some spiral-spiral mergers the tails may contain $\sim 50\%$ of the HI in the progenitors (Hibbard et al., 1994). This

gas, if left undisturbed, will fall back into the newly formed galaxy, and may be shock heated or ionised by the young stellar population in the galaxy. It is also possible that it could feed further star formation in the galaxy. On the other hand, it is possible that the gas could be blown out of the galaxy by the radiation from the newly formed stars, or possibly lost through stripping.

In cases where galaxies do not merge, such as the rapid ‘near-miss’ encounters which may happen in clusters, galaxies may still be affected by the process of tidal stripping. For the case of smaller galaxies passing by a more massive neighbour, it is likely that gas and perhaps stellar matter will be lost to the larger galaxy. It has been suggested that this mechanism could remove or weaken the disks of small spirals, converting them into spheroidal galaxies (Moore et al., 1996). It may also be one mechanism involved in producing the extended stellar halos of cD galaxies (Ostriker & Tremaine, 1975). However, the most important form of tidal stripping may involve the loss of part of the dark matter halo of the galaxy (Mathews & Brighenti, 1997). As the X-ray halo of elliptical galaxies is retained largely because of the influence of the dark matter halo, the truncation of this halo would greatly reduce the X-ray halo of the galaxy. The effect would in all likelihood be permanent, as it is difficult to imagine a process by which the dark matter could be replaced except in small amounts. The overall effect would be to increase the X-ray luminosity of large ellipticals at the expense of their less massive neighbours. Dark matter stripping might also affect spiral galaxies. It has been suggested that spirals are surrounded by a low density reservoir of gas which slowly flows inwards, fueling star formation. Loss of dark matter would make retention of this reservoir more difficult, and could potentially cause the truncation of star formation, and perhaps conversion of the galaxy to an S0.

Galaxies can also acquire extra gas, dark matter and stars through accretion. In some cases this is basically tidal stripping or a very minor merger, for example when a dwarf galaxy merges with a very large elliptical. In this case the dwarf would be quickly and completely destroyed by the interaction, simply adding its mass to the elliptical. However, galaxies can also accrete gas (and perhaps dark matter) from their surroundings, particularly in clusters and groups where there is a ready reservoir of gas to draw on (Mathews & Brighenti, 1998a). This accretion of gas could increase the X-ray halo of a large galaxy considerably, perhaps giving rise to the extreme luminosities seen in group or cluster dominant giant ellipticals.

The halos associated with groups and clusters of galaxies are also likely to have another effect on the wind flows of galaxies within them, *i.e.* stifling the wind. This would occur when the pressure of the intra-group medium was great enough to slow or stop a galactic wind before it slowed of its own accord. In this case the gas flow would begin to stagnate at its outer edge, causing a much more rapid change to late stages of wind flow than expected. Slowing the flow would increase the associated X-ray luminosity, and stalling it entirely might cause an early transition to infall, producing an even greater increase in L_X . Recent consideration of this idea (Brown & Bregman, 2000) suggests that this effect is a potentially dominant factor in the determination of halo luminosity. In this scenario, low and medium mass galaxies without a surrounding medium to hold in their halos could lose most of their gas and thus most of their X-ray luminosity would be produced by stellar sources.

Interactions between galaxies are known to cause star formation. Merging galaxies show knots of star formation and in some cases starburst regions (Hernquist & Mihos, 1995). This leads to the conclusion that interactions will increase the stellar X-ray luminosity of the galaxies involved. It seems likely, given the variation in L_X/L_B in faint elliptical galaxies, that even in quite old and passive galaxies there are variations in the numbers of stellar X-ray sources (Irwin & Sarazin, 1998a). This produces an intrinsic scatter in the baseline of the L_X/L_B relation, and makes determination of such a baseline more difficult.

Given these possible mechanisms for a relation between environmental conditions and X-ray luminosity, and the observational evidence (Brown & Bregman, 2000), it seems that the environment is a factor which cannot be ignored. The simplest way of taking its effects into account is to compile samples of galaxies which are extensive and cover all environments, so as to produce a useful average. A more difficult alternative would be to try to collect good enough data to make estimates of the effect of each of the processes given above. One final option would be to try to remove as many effects as possible, by examining galaxies which are in true isolation. Outside group and cluster halos, and away from other galaxies, only the galaxies' own histories should influence their current status.

1.4 Galaxy Formation and Evolution

The method by which early-type galaxies are formed has been the subject of debate for a number of years. Two main schools of thought dominate the debate, namely monolithic collapse (Larson, 1975) and the merger hypothesis (Toomre & Toomre, 1972). Monolithic collapse suggests that all galaxies form in the same way, from the collapse of gas clouds, with morphology determined by the strength of the velocity components of the gas. Clouds with high angular momentum form spirals, those with stronger random motions form ellipticals, and those with fairly evenly matched rotational and random components form lenticular galaxies. The alternative is the merger hypothesis, which suggests that elliptical galaxies could be formed through the merger of spirals. In this model, spiral galaxies would form through collapse of gas clouds, and elliptical and lenticular galaxies would be formed later through galaxy mergers and interactions. There would be no need to form early-type galaxies directly, although this is not ruled out.

The merger hypothesis is based on N-body simulations of the interactions of merging spiral galaxies. Although at first these objects appear highly disturbed, they eventually settle down as elliptical-like objects, and the grosser signs of recent merger, such as tidal tails and streamers, fade fairly rapidly. Support for the simulations has come from the extensive studies of ongoing mergers and recent post-merger candidates. Ongoing mergers are relatively rare (only 10 are listed in the *New General Catalogue*; Dreyer, 1888), but there is a much larger population of galaxies which show signs of having undergone mergers in the past (Toomre & Toomre, 1972), including the Milky Way (Searle & Zinn, 1978).

When galaxies merge, they are thought to undergo a process known as violent relaxation. The change from two relatively shallow potential wells to one deeper well causes a randomisation of the orbits of the stars, breaking up large structures such as disks, and causing rapid infall of gas to the centre of the new galaxy. The orbital changes give rise to the elliptical or spherical shape of early-type galaxies, although many such galaxies are observed to contain small disks (Carollo et al., 1997). These may be remnants of the disks of progenitor galaxies, or may be formed in the burst of star formation which is triggered by the collection of gas in the merger (Schweizer et al., 1990). Many interacting or merging galaxies are observed to contain such starbursts. It is important to note that violent relaxation is a product of the change of the potential well. Many standard properties of the galaxy, such as stellar velocity dispersion and

gas density profile are determined by the potential, and so any merger which significantly alters it will effectively “reset” these properties to new values.

The merger hypothesis has now been included in the larger framework of cosmology, as part of the hierarchical clustering and merging (*e.g.* Coles & Lucchin, 1995) predicted by the cold dark matter model (Blumenthal et al., 1984). In a hierarchical model of structure formation, the merger of galaxies is part of a pattern of mergers at all levels of structure. Individual galaxies form initially in isolation, then collect together to form groups. The galaxy merger rate in groups is high, but at the same time as the galaxies are merging with one another, the groups of galaxies begin to merge to form clusters and superclusters of galaxies. Observational evidence in support of these ideas is now becoming available, primarily in the form of clusters forming and accreting groups of galaxies at high redshift (van Dokkum et al., 1999). A high fraction of galaxies undergoing mergers is observed in the cluster studied by van Dokkum *et al.*, and in nearby dense groups of galaxies (*e.g.* Weinberger et al., 1999; Ponman & Bertram, 1993). Strong evidence of multiple mergers can also be seen in the class of ultra-luminous infra-red galaxies, the majority of which show physical signs of interactions and many of which have multiple nuclei (Borne et al., 1999).

Hierarchical merging models make certain predictions about the evolution of galaxies which have yet to be tested. One of these is that not only does the merger of spiral galaxies produce elliptical galaxies with appropriate stellar populations and hot gas halo, but that if left to evolve passively, the halos of these ellipticals will cool and this newly formed cool gas will be accreted to form disks, so that an elliptical will change back into a spiral galaxy. In this model the bulges of spiral galaxies would be the stellar remains of an elliptical, and observational evidence seems to lend some support to this. However, as yet there is little evidence of sizable X-ray halos associated with spiral bulges, and alternate formation methods have been proposed.

1.4.1 Halo Formation and Galaxy Winds

As mentioned earlier, X-ray imaging of early-type galaxies has shown that they often contain, or are embedded in, halos of 10^{6-7}K gas. However, it is also known that some galaxies of this type do not possess hot gas at detectable levels. It is also notable that late-type galaxies have large amounts of cool gas but at best quite small amounts of hot gas. Given the masses of gas

involved, it is important that galaxy formation models be able to explain these differences, and give means of reliably predicting the X-ray properties of galaxies.

One of the more widely accepted models of halo formation in early-type galaxies is based on the idea of galaxy winds. Galaxy wind models describe the large scale movement of gas within the galaxy and its halo. A simple example is a galaxy with no gas, with an aging stellar population. The stars will lose mass through stellar winds, supernovae, and the formation of planetary nebulae, and this gas will mix and be heated by shocks and radiation. As the temperature of the gas rises, it will begin to flow outwards, forming a wind whose speed is largely determined by the degree of heating. Such models began to be formulated and studied at around the same time as good X-ray observations of early-type galaxies became available, and although the simpler models make various assumptions which have since been shown to be erroneous, they still produce quite realistic results, comparable to the observational data available.

One example of such work is D’Ercole et al. (1989). The models used in this study are of low resolution compared to recent work, follow a King mass distribution for computing ease, and assume a fairly simple dark matter model. The method of gas heating is to have a large starting burst of type II supernovae from the initial galaxy formation, with later heating provided by type Ia supernovae. The rate of type Ia explosions is set to decline slightly faster than the rate of mass return from dying stars.

The simulations show three phases in the movements of gas in the galaxy. The first, triggered by the initial type II supernovae, is a supersonic wind, blowing gas and dust out beyond the edge of the galaxy. The gas in this wind is not a strong X-ray source, and would not be detected, except perhaps near the centre of the galaxy. As the heating of the gas drops off with time, the gas slows, becomes subsonic, and its density rises, making it more visible to us. This is the outflow phase. Lastly, as the rate of heating drops below the rate of radiative cooling, the gas temperature decreases until it begins to fall back into the galaxy. Diffuse X-ray emission is at its brightest when outflow stagnates and changes to inflow, but overall X-ray luminosity might continue to increase past this point as inflow to the centre of the galaxy allows large amounts of X-ray emission there.

The timescale of each phase depends strongly on the mass (particularly dark matter mass)

of the model galaxy. In small galaxies, the mass of the galaxy does not exert much force on the out flowing gas, so it would be possible to have, at the present time, supersonic winds and therefore low X-ray luminosity in these galaxies. Most galaxies would be in the outflow phase, slowly increasing their X-ray luminosity as their outflows slow. Only a few of the most massive galaxies would have passed into the inflow phase. This effect could possibly explain the scatter in the L_X/L_B relation, with galaxies of similar optical luminosity being at different stages of wind flow.

Unfortunately, despite these promising results, some of the conditions (*e.g.* the supernova rate and dark matter profile) assumed for this model are now thought to be inaccurate. One more recent follow up study (Pellegrini & Ciotti, 1998) uses improved models of both dark matter and stars, and has a lower supernova rate than previous work, based on more up to date estimations. *ASCA* data suggesting that type Ia supernovae may be suppressed in early-type galaxies has been incorporated. The ratio of dark to luminous matter is significantly increased.

Initially, the model galaxies are free of gas, having been swept clean by type II supernovae. As gas builds up, a wind similar to that in the previous model begins to blow out of the galaxy. As before, this does not produce much X-ray emission. However, at the centre of the galaxy, the local density of the gas very quickly becomes high enough for the gas to radiate its energy, rapidly cooling and beginning a collapse. This collapse may stay small, within ~ 100 pc, if the galaxy is not very massive, so that the majority of the gas remains supersonic and overall X-ray luminosity stays small up to the present day. However, the higher the mass of the model galaxy, the more rapidly the zone of cooling inflow will grow, and the greater the value of L_X . The inflow zone, surrounded by a zone of stagnation, may extend out to at least $10 R_e$ in the most massive X-ray luminous galaxies. The situation where the outer parts of the galaxy are in outflow while the inner regions are collapsing is referred to as a partial wind, and this is the stage at which most ellipticals are thought to be.

More detailed modeling has been carried out, centred on galaxy winds in S0 galaxies (D’Ercole & Ciotti, 1998) and the effect of galaxy-galaxy interactions on established galaxy winds (D’Ercole et al., 2000). The models of lenticular galaxies demonstrate the profound effect which rotation can have upon a galaxy wind. While the outer galactic disk is still in an outflow phase, the lack of rotational support to gas near the centre of the galaxy and above the plane of the disk

can cause an early inflow. This develops most strongly in the polar regions, and can produce filaments of cold gas at the interfaces between inflowing and outflowing winds. The overall effect is to reduce the X-ray luminosity, as compared to a more spherical galaxy. This matches well with a study comparing elliptical and S0 galaxies which suggested that lenticular galaxies are on average less X-ray luminous than ellipticals of equal L_B (Eskridge et al., 1995; Eskridge et al., 1995). In the case of galaxy-galaxy interactions, it was found that the tidal forces exerted during a close encounter can produce dense filaments of gas which will rapidly cool and fall toward the centre of the galaxy. The interaction is expected to occur over a fairly short timescale (<1 Gyr), but the increase in X-ray luminosity caused by the filaments and rapidly cooling gas which is funneled into the galaxy core may last considerably longer.

In the most massive ellipticals, galaxy winds models tend to show only a very short period of outflow, followed by inflow over most of the life of the galaxy. The models of Brighenti & Mathews (1999) consider the case where a massive elliptical lies at the centre of a group of galaxies, surrounded by the group halo. In this situation, the inflow region can extend out into the group halo, and the galaxy can gain significant amounts of high temperature gas without being part of a true group-scale cooling flow. The overall effect is to increase greatly the X-ray luminosity of the galaxy, and this is likely to be maintained over the lifetime of the galaxy, so long as it is not disturbed.

Recent X-ray observations (Beuing et al., 1999) of a large sample of galaxies in the *ROSAT* All-Sky Survey (RASS) show a split between ellipticals at different stages of development. The luminosities derived from the sample suggest that around 95% of ellipticals are in the supersonic outflow or partial wind phases. Many of these galaxies are so faint that only an upper limit on their luminosity can be calculated, but these values have been used to place restrictions on the L_X produced by discrete sources. The remaining 5% of elliptical galaxies which are thought to be in the inflow stage include several cluster central galaxies whose luminosity is extreme enough to provide evidence that they have accreted extra cluster gas and dark matter.

However, the models still retain problems which are difficult to solve. How does the gas which has flowed far beyond the range at which supernovae can heat it remain at a temperature of 10^7 K for such long periods of time? Possibly a rapidly moving dark matter halo could keep it hot through shocks and other interactions, but as so little is known about such halos, this can

only be assumed, not proved. And what happens to the infalling gas predicted by the models? Some cool gas emission can be seen in some elliptical galaxies, but infalls on the scales predicted for the most luminous galaxies are difficult to deal with.

1.5 Measurement of Galaxy Age

When considering models of galaxy formation and evolution, the typical age of a particular class of galaxies is obviously an important piece of information to have. For some time, most theories supported the idea of a single epoch of galaxy formation, during which the majority of the objects seen today were formed (Frenk et al., 1988). However, from the point of view of a hierarchical model, formation is a more gradual process, with many small, medium and possibly large late-type galaxies forming earlier in dense regions and then beginning the process of merging and collapsing to form the galaxies presently observed and the large scale structures we see in the local universe.

In the case of elliptical galaxies, we must take into account the fact that we are unsure of the process of formation. In the case of monolithic collapse, assuming the galaxy undergoes no major mergers after formation, the observed properties will be related to the galaxy potential well at the time of formation. The stellar population will have formed at this time, and the X-ray halo will presumably have begun to form. In the case of a galaxy which has undergone mergers, things are very different. Any major merger will restructure the potential well, causing changes in gas properties and stellar orbits. Mergers involving late-type galaxies are likely to produce bursts of star formation, producing a mixed stellar population and probably producing profound changes in any hot gas halo. In this case we may be more interested in how long ago the galaxy last underwent a major merger rather than when the older part of its stellar population began to form. Given this age, we can attempt to find relations between age and X-ray properties, in order to constrain halo formation models.

One method of directly determining age is to examine the optical colours and absorption line strengths of a galaxy. As the stars in a galaxy age, they evolve and their emission changes. Young stellar populations have a strong blue component, produced by hot stars with short lifespans. Older populations are predominantly red, as the blue stars are mostly reduced to compact objects such as white dwarfs, leaving the less massive members of the population as

the dominant optical sources. In principle it is therefore possible to match the colours of a population to those predicted by stellar evolution models and find an average age for the stars in a galaxy. In practice this is done using specific absorption indices, and is not an easy process.

The most important difficulty involved is that of age-metallicity degeneracy (Faber, 1972, 1973; O’Connell, 1980). The problem revolves around the fact that it is possible to change the colours of a stellar population by altering the metal content of the stars. A stellar population might be bluer than expected because of a young age, or because its stars are metal poor. Most broad band colours and metal line strengths are dominated by giant branch stars, where quite small changes in metallicity can produce larger changes in colour than huge differences in age. The solution to this degeneracy is to avoid examining the giant branch stars and instead concentrate on those at the main sequence turnoff. The Hydrogen Balmer lines are excellent tracers of main sequence turnoff temperature, and measurements of $H\beta$ are possible, although there is still some metallicity dependence. However, models of the behaviour of $H\beta$ compared to metal lines such as those of Iron or Magnesium have now become available (*e.g.* Worthey, 1994) and these have allowed the age-metallicity degeneracy to be broken.

There are however limitations to this technique. Firstly, and most importantly, it must be remembered that in the case of a galaxy which has undergone any significant merger events, the stellar population will be of mixed age, and almost certainly of mixed metallicity. The line strengths measured are likely to be dominated by the young stellar population, as this contains the more highly luminous stars, but will be affected to some extent by the older population as well. The age derived from these measurements will therefore be luminosity-weighted and cannot be considered an absolute value (or “true age”). Ages of different galaxies can only be compared relatively. There are also a number of different models which describe stellar populations (*e.g.* Buzzoni et al., 1992, 1994; Bruzual & Charlot, 1993; Fritze-von Alvensleben & Burkert, 1995; Worthey & Ottaviani, 1997), and these do not always agree. Ages calculated using different models are not generally comparable, although large differences could allow qualitative statements, such as that a particular galaxy is older than another. There is some hope that as models become more accurate this situation will improve. One promising area is the inclusion of near-UV spectra in models, which can provide accurate measurements of metallicity for some classes of stars (Nolan et al., 2001). A more exact constraint on absolute metallicity makes

measurement of age simpler, and may in future allow absolute ages to be calculated.

One way of avoiding the problem of mixed stellar populations is to only look at very specific regions of a galaxy. Typically, the burst of star formation associated with mergers is mainly confined to the core of the galaxy, as gas is funneled into this region. By only using spectra from the central regions of the galaxy, the dominance of the young stellar population is reinforced, giving a final age closer to the true age of this component. However, to truly produce the single stellar population assumed by the models, it is necessary to look at globular clusters. These are thought to form from single gas clouds, so all stars in the cluster will have essentially identical ages and metallicities.

Studies of globular clusters around early-type galaxies have shown that it is possible to calculate relatively accurate ages from these objects. However, once again there are problems. Firstly, acquiring data of sufficiently high quality from such small objects can be difficult, particularly for more distant galaxies. Secondly, it has been shown that in many early-type galaxies, there is more than one population of globular clusters (*e.g.* Lee & Geisler, 1993). The more metal-rich population has been shown to have a similar metallicity to that of the galaxy as a whole (Forbes et al., 1997). From this and from comparisons of globular cluster and galaxy colours (Forbes & Forte, 2001), it seems fairly likely that the metal-rich population formed from gas which “knew about” the galaxy and potential well we observe, while the metal-poor population formed elsewhere, probably in smaller pre-merger galaxy progenitor objects.

In order to interpret the ages calculated from globular clusters, it is necessary to have a model of how they formed in relation to the galaxy. There are currently a number of theories which suggest ways in which galaxies can form or acquire globular clusters; during galaxy mergers (Schweizer, 1987; Ashman & Zepf, 1992), two phase collapse (Forbes et al., 1997), or through tidal stripping from other galaxies (Forte et al., 1982). The evidence of a connection between the metal-rich clusters and their host galaxies suggests that two phase collapse or galaxy mergers are the more likely processes in normal ellipticals, although for the merger model to work, the progenitors must have merged at an early epoch, while largely gaseous. Acquisition of globular clusters through stripping is likely to play a part in building up the halo populations of cluster dominant galaxies. For example, NGC 1399 (the cD at the centre of the Fornax cluster), has around 10 times as many globular clusters as the nearby galaxies NGC 1404 and NGC 1380

(Kissler-Patig et al., 1999) and it is difficult to imagine any other scenario which could produce such an overabundance.

Despite the difficulties associated with measuring and interpreting spectroscopic ages, this is probably still the best method of determining an age (or age since last merger) for early-type galaxies. There are more qualitative methods which can be employed. One example is the Fine Structure parameter (Schweizer & Seitzer, 1992a). The parameter is a measurement of the disturbance of the galaxy. By looking for signs of structural disorder, such as ripples in the galaxy surface brightness, jets or plumes of stars or boxy isophotes, and judging the strength of the features, it is possible to assign a value, allowing comparisons between galaxies. If early-type galaxies are assumed to have formed through merger, then signs of disturbance suggest that a major merger has happened recently. Unfortunately, most of the structures the parameter considers fade rapidly, so this technique can only be used in the case of the most youthful galaxies. Another alternate measure of age may come from the fundamental plane of elliptical galaxies. Forbes et al. (1998) showed that the scatter about the fundamental plane is correlated with spectroscopic age, with young galaxies below the plane and old galaxies above it. As fundamental plane position can be calculated more easily than spectroscopic ages, many more galaxies can be assigned ages in this way. However, the scatter in the relation is sizable, so this is more useful for large statistical samples than for calculating accurate ages for individual galaxies.

1.6 Thesis Aims

In the following chapters the properties of two samples of early-type galaxies are studied, in order to clarify the processes by which these objects form, evolve and interact with their environment. As has already been shown, these issues are still under discussion in the literature, and are important for our understanding of galaxies and galaxy systems. The first of our samples is extensive, but only examines the integrated luminosity of the galaxies. Chapter 2 presents an examination of the variation of X-ray luminosity with galaxy age, from which we have drawn conclusions about the processes which form the X-ray halo. In Chapter 3 we examine the $L_X:L_B$ relation and consider how discrete sources and hot gas vary with galaxy optical luminosity. The influence of environment is also studied, and we attempt to resolve some of the conflicting results

produced by previous work in this area. The second sample, discussed in Chapter 4, contains fewer galaxies but uses data of considerably higher quality, allowing us to study the properties of the galaxy halo in detail. We compare galaxy halos to those of larger structures for the first time, and use these comparisons to consider the formation mechanism of the halo, its dependence on the potential well of the galaxy, and the effect of environment and galaxy winds on the present state of the gas.

Chapter 2

X-ray Emission in Post-Merger Ellipticals

Abstract

The evolution in X-ray properties of early-type galaxies is largely unconstrained. In particular, little is known about how, and if, remnants of mergers generate hot gas halos. Here we examine the relationship between X-ray luminosity and galaxy age for a sample of early-type galaxies. Comparing normalised X-ray luminosity to three different age indicators we find that L_X/L_B increases with age, suggesting an increase in X-ray halo mass with time after a galaxy's last major star-formation episode. The long-term nature of this trend, which appears to continue across the full age range of our sample, poses a challenge for many models of hot halo formation. We conclude that models involving a declining rate of type Ia supernovae, and a transition from outflow to inflow of the gas originally lost by galactic stars, offer the most promising explanation for the observed evolution in X-ray luminosity.

2.1 Introduction

A potential problem with forming ellipticals from merging spirals is how to account for the different gas properties in the two types of galaxies. In particular, spirals contain relatively high masses of cold ($T \sim 100$ K) gas, whereas ellipticals have very little. The opposite situation is true for the hot ($T \sim 10^6$ K) gas masses – normal spirals contain rather little hot gas, while ellipticals may possess extensive hot halos. Since the total gas masses per unit stellar mass are broadly comparable in early and late-type galaxies, this raises the possibility that inefficient merger-induced star formation might heat the cool interstellar gas in spirals to form the hot

halo in post-merger ellipticals. Recently, Georgakakis et al. (2000) have shown that the cold gas mass indeed decreases in an ‘evolutionary sequence’ from merging spirals to post-merger ellipticals.

However, it is not clear that gas heated in an intense starburst can be retained within the galactic potential. Read & Ponman (1998) examined the X-ray properties of eight on-going mergers placed in a chronological sequence. Their study revealed that material is ejected from merging galaxies soon after the first encounter. Massive extensions of hot gas are seen (involving up to $10^{10} M_{\odot}$) at the ultraluminous peak of the interaction, as the two nuclei coalesce. There is evidence for this in the *Antennae*, Arp 220, and NGC 2623. However, after this phase of peak activity, the X-ray luminosity actually declines. For example, NGC 7252 (a prime example for the remnant of a merger that occurred 0.7 Gyr ago) shows some evidence of a hot halo, but one that is much smaller than the halos seen in typical ellipticals.

Two post-merger ellipticals were studied in the X-ray by Fabbiano & Schweizer (1995). They found that neither galaxy had an extensive hot halo. Given the correlation between X-ray luminosity and isophotal boxiness (thought to be a signature of a past merger) demonstrated by Bender et al. (1989), this was a somewhat surprising result. If post-merger ellipticals are to resemble ‘normal’ ellipticals they need to acquire a hot gas halo. Possible mechanisms include:

- 1) The late infall (i.e. after a few Gyr) of HI gas associated with the tidal tails (Hibbard et al. 1994). This cold gas may be shocked to X-ray emitting temperatures as it falls back into the merger remnant.
- 2) A reservoir of hot gas, possibly expelled at the nuclear merger stage, might infall from large radii, where its low density makes it undetectable to current X-ray satellites.
- 3) After the initial violent starburst, the continued mass loss from stars and heating from stellar winds recreates a hot ISM.

The first study to attempt an ‘evolutionary sequence’ for post-merger ellipticals was that of Mackie & Fabbiano (1997). For 32 galaxies they showed a weak trend for L_X/L_B to increase with a decreasing Σ parameter. The Σ parameter is defined by Schweizer & Seitzer (1992b), and is a measure of a galaxy’s fine structure, *i.e.* optical disturbance. They showed that it correlates with blue colours and Balmer line strength, and is thus a rough indicator of dynamical youth.

The Mackie & Fabbiano trend therefore suggested that post-merger ellipticals became more X-ray luminous, for a given optical luminosity, as the galaxy aged. They also plotted L_X/L_B against $H\beta$ absorption line EW, which revealed a similar trend. A more recent study by Sansom et al. (2000) confirms the trend in X-ray overluminosity with Σ for 38 galaxies, and suggests that it might be explained by the build up of hot gas in post-merger galaxies. However, both Σ and $H\beta$ EW have their drawbacks – Σ is only semi-quantitative at best and the strength of $H\beta$ is affected by both stellar age and metallicity.

Here we reexamine the trend seen by Mackie & Fabbiano (1997) for a larger sample, and investigate two new measures of galaxy age: residual from the Fundamental Plane and spectroscopic age. Using these three measures we explore the X-ray luminosity evolution of post-merger ellipticals.

Throughout the paper we assume $H_0 = 75 \text{ km s}^{-1} \text{ Mpc}^{-1}$ and normalise L_B using the solar luminosity in the B band, $L_{B\odot} = 5.2 \times 10^{32} \text{ erg s}^{-1}$.

2.2 Results

We first reexamine the trend of normalised X-ray luminosity with Fine Structure parameter Σ , presented initially by Mackie & Fabbiano (1997) for 32 galaxies. Here we use a sample of 47 early-type galaxies with Σ taken from Schweizer & Seitzer (1992a), and normalised L_X values from our recent catalogue (O’Sullivan et al. 2001a) of X-ray luminosities (mostly based on *ROSAT* data). The L_X values are approximately bolometric. The L_B values are based wherever possible on B_T magnitudes taken from Prugniel & Simien (1996). If these are unavailable, values from NED are used. Fig. 2.1 shows the sample of 47 early-type galaxies plotted in order of decreasing Σ or increasing age.

As noted by Mackie & Fabbiano, the scatter at low values of Σ is large, covering around 2 orders of magnitude in L_X/L_B , while at higher Σ the scatter appears to be smaller and L_X/L_B limited to low values. A similar trend was seen by Sansom et al. (2000) for 38 galaxies. This suggests that dynamically young galaxies have low X-ray luminosities and that aging produces a range of luminosities, presumably dependent on other factors.

In order to test the strength of this relation we apply Kendall’s K test to the X-ray detections from our sample. The test does not assume any distribution in the data, and the K statistic

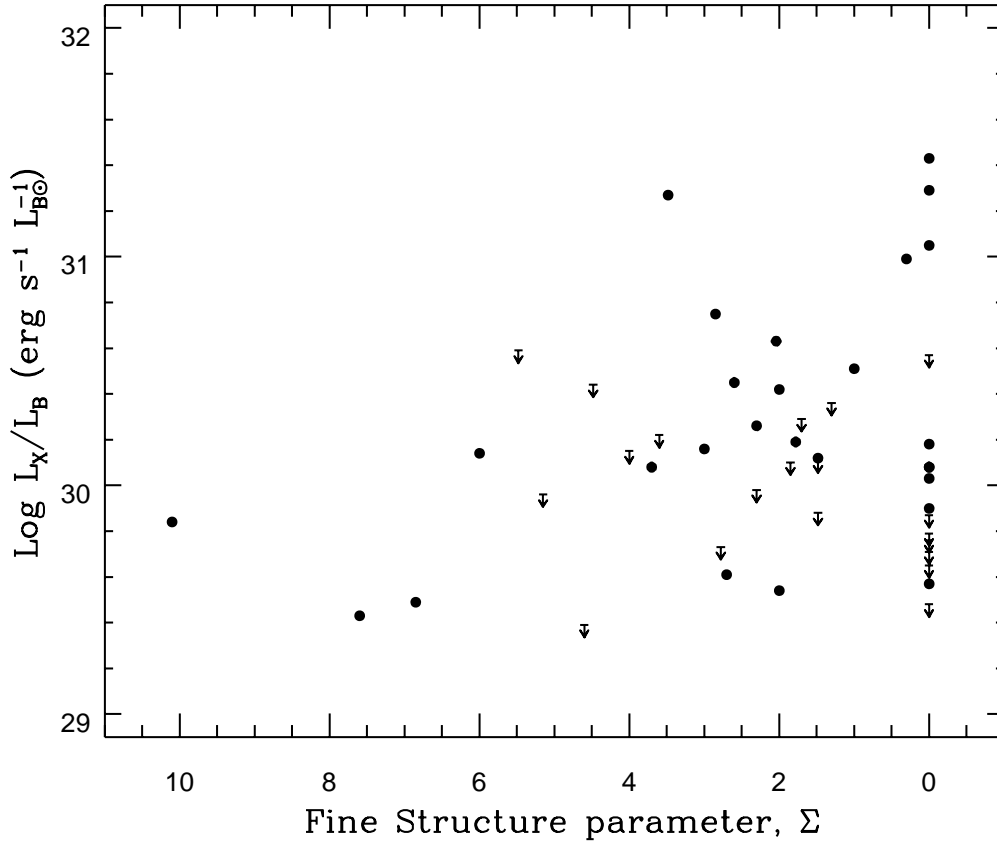


Figure 2.1: Normalised X-ray luminosity versus fine structure parameter Σ for early-type galaxies. Filled circles are detections, arrows denote upper limits. Dynamically young galaxies (high Σ) have low L_X/L_B .

is unit normal distributed when at least 10 data points are present. For our data we find $K = -2.31054$ (using 27 data points), indicating an anti correlation between $\text{Log } L_X/L_B$ and Σ of $\sim 2\text{-}\sigma$ significance. For comparison, we also apply the test to the sample of Sansom *et al.* , and find a correlation of very similar significance, $K = -2.28749$ for 30 detections.

2.2.1 L_X/L_B versus Spectroscopic Age

Fine structure only persists in dynamically young galaxies, so Fig. 2.1 provides information only on the early galaxy evolution of these objects. A more general measure of age is needed to show how X-ray properties evolve over a longer timescale. Galaxy spectroscopic ages are now available for a large number of early-type galaxies from the catalogue of Terlevich & Forbes

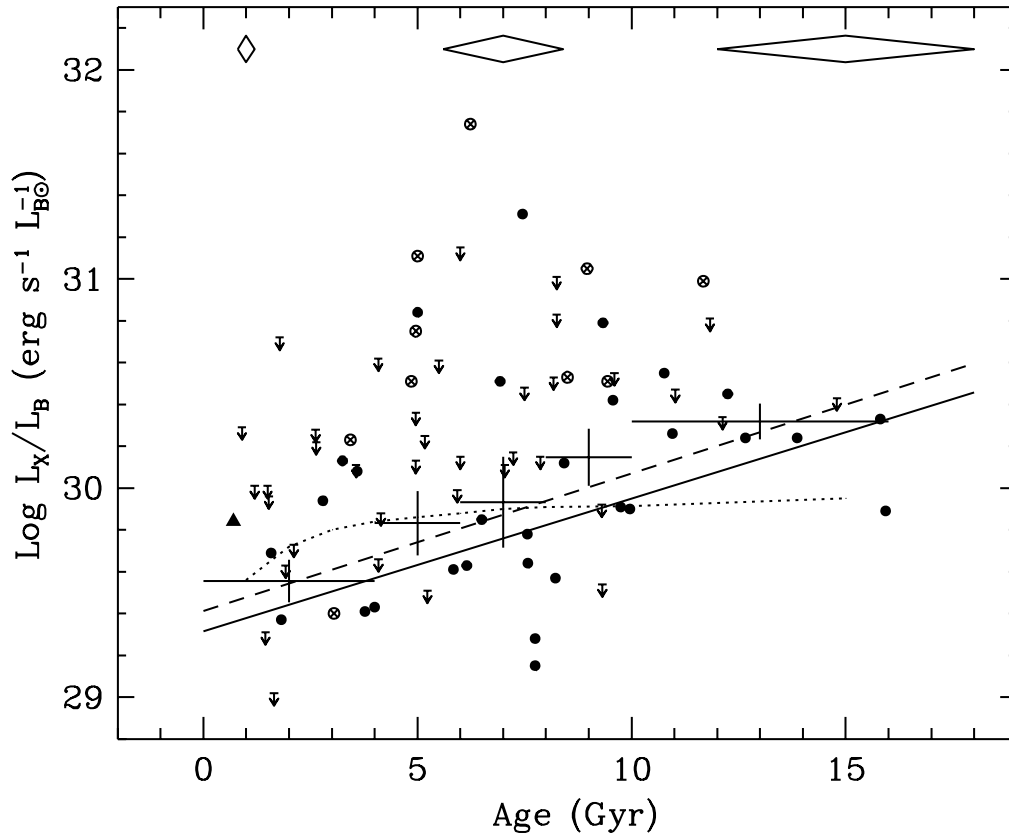


Figure 2.2: $\text{Log}(L_X/L_B)$ plotted against spectroscopic age. Crossed circles represent group or cluster dominant galaxies, filled circles all other detections. Arrows denote upper limits and the filled triangle represents NGC 7252, a young post-merger. The three diamonds at the top of the graph show typical age and L_X/L_B errors for galaxies of age 1, 7 and 15 Gys. The two lines are fits to the data, including (dashed line) or excluding (solid line) the group and cluster dominant galaxies. The large crosses represent mean L_X/L_B for the five age bins described in the text. The dotted line shows the expected increase in L_X/L_B caused by the decrease of L_B with age. Normalisation of this line is arbitrary, and the position shown can be considered to represent a “worst case” scenario.

(2002). These ages are generally based on $H\beta$ absorption line measurements and the stellar population models of Worthey (1994). The line index measurements come from the galaxies’ central regions, and are luminosity weighted. Thus they are dominated by the last major burst of star formation, which is presumably triggered by a major merger event. Although not a reliable absolute measure of the age of each galaxy, these spectroscopic ages do provide us with a much more useful estimate of their ages relative to one another. In Fig. 2.2 we show L_X/L_B plotted against spectroscopic age (from Terlevich & Forbes 2002).

The plot shows a large degree of scatter, most notably in the age range between 4 and 10 Gyrs. This is likely to be in part caused by the uncertainties in calculating ages, which we estimate lead to a typical error of $\sim 20\%$. We also expect a mean $1\text{-}\sigma$ error in X-ray luminosity of $\sim 15\%$. Typical error bounds for points at 1, 7 and 15 Gyrs are shown in Fig. 2.2 by the diamonds at the top of the plot. The graph also contains a relatively large number of upper limits, so we have used the survival analysis packages available under IRAF to assess the strength of any correlation and fit regression lines. The Cox proportional hazard, Spearman's rho and generalised Kendall's tau tests are used to determine correlation strength. Linear regression fitting is carried out using the expectation and maximization (EM) algorithm and the Buckley-James (BJ) algorithm. In all cases we found that the two fitting algorithms agreed closely.

Using the full sample of 77 early-type galaxies, we find a correlation of at least 99.6% significance between L_X/L_B and age. Line fits to the sample produce slopes of 0.066 ± 0.022 (EM) and 0.063 ± 0.025 (BJ). The former is shown as the dashed line in Fig. 2.2.

Recent work on the X-ray properties of galaxies in groups (Helsdon et al. 2001) lead us to suspect that some of the scatter seen in Fig. 2.2 might be caused by inclusion of group or cluster dominant galaxies (marked as crossed circles) in our sample. It is also important to note that there is evidence to suggest that the largest ellipticals may have non-solar abundance ratios (*e.g.* Carollo et al. 1993). This could lead to their ages being underestimated by a small amount, again adding to the scatter. We therefore removed from our sample a number of galaxies listed by Garcia (1993) as group dominant or known cDs and retested the sample. This improves the correlation slightly (to $>99.75\%$) and makes the line fit slightly shallower; 0.063 ± 0.019 (EM) and 0.061 ± 0.022 (BJ). The EM fit is plotted as a solid line in Fig. 2.2.

To confirm that the increase in L_X/L_B occurs across the range of ages, rather than just the first few Gyrs, we also binned the sample into subsets by age. The age range of each subset was chosen so as to have roughly equal numbers of detections in each bin. We then calculated a mean L_X/L_B for each bin, using the Kaplan-Meier estimator. The results are shown in Table 2.1, and as large crosses on Fig. 2.2. These show the same trend for increasing L_X/L_B with age, and indicate that the trend is continuous across the age range covered by the data.

The Kaplan-Meier estimator (Feigelson & Nelson 1985) includes upper limits by constructing a probability distribution function for the data in which the probability associated with each

Age (Gyrs)	No. of detections	No. of upper limits	Log L_X/L_B ($\text{erg s}^{-1} L_{B\odot}^{-1}$)	error
$A < 4$	9	12	29.56	± 0.11
$4 \leq A < 6$	6	11	29.83	± 0.15
$6 \leq A < 8$	9	4	29.93	± 0.22
$8 \leq A < 10$	9	6	30.15	± 0.14
$A \geq 10$	8	4	30.32	± 0.09

Table 2.1: Mean L_X/L_B values for 5 age bins, calculated using the Kaplan–Meier estimator.

upper limit is redistributed equally over detected values which lie below the upper limit. So long as there is no systematic difference between the detected and undetected systems, this should be a reasonable procedure. A problem arises when the *lowest* point in a given bin is an upper limit (since there are no lower points over which to redistribute the corresponding probability). When this occurs, the Kaplan–Meier estimator treats the limit as a detection and hence may be biased.

Of the five bins chosen, two (the youngest and second oldest) have upper limits as their lowest values. For the second oldest bin, the problem data value is only slightly lower than a detected point, so the bias will be small. However, the youngest bin has two upper limits as its lowest points, one of which is considerably below the nearest detection. To check for bias, we recalculated a mean log L_X/L_B of 29.66 for this bin excluding these points, compared to 29.56 previously. This indicates that although the youngest bin may be slightly biased, it still supports the trend observed.

As a further check of the robustness of our conclusions, we examined the L_X/L_B :Age relation using detected points only, and find a correlation significant at $\sim 2.1\text{-}\sigma$. The upper limits also show a correlation with age (at $\sim 2.3\text{-}\sigma$). These trends cannot be selection effects in the data, since neither source distance, nor X-ray exposure time are correlated with age. They therefore point to a genuine trend in the data. Galaxies with larger spectroscopic ages typically have higher L_X/L_B than younger ones.

As the merger-induced starburst fades, we would expect the blue luminosity to decline with time. This will cause an increase in L_X/L_B , even for constant L_X , which will combine with any trends in L_X which are present. With this in mind, we show in Fig. 2.2 the expected change due to a fading starburst from stellar population models (Worthey 1994). Here we have crudely

assumed that the progenitor galaxies consisted of a solar metallicity, 15 Gyr old population, and that the new stars created in the merger also have solar metallicity. The relative mass ratios are 90% progenitor stars and 10% new stars. The total B band luminosity fading of this composite stellar population is shown in Fig. 2 (we assumed that the fading of the progenitor stars after reaching 18 Gyrs old is insignificant). It can be seen that the starburst fades rapidly in the first few Gyrs, roughly matching the trend seen in L_X/L_B , but at later times there is very little change, whereas the observed mean L_X/L_B value continues to rise. So although the L_X/L_B evolution at early times could be simply driven by the fading starburst, this cannot account for the evolution at late times.

A further possibility to be checked is that our sample might contain a trend in mean optical luminosity with age. Since L_X/L_B has been widely reported (see however Helsdon et al. (2001)) to rise with L_B , this could lead to a consequent correlation between age and L_X/L_B . To test this, we show in Fig. 2.3 a plot of $\log L_B$ with measured age. An anti-correlation between L_B with age could produce the observed trend in L_X/L_B . Fig. 2.3 does not appear to show any such trend, and in order to test for a correlation, we apply Kendall's K test to the data. We find a K statistic (which is unit normal distributed) of ~ 0.44 (for 77 galaxies), and excluding group dominant galaxies reduces this to ~ 0.33 (for 65 galaxies). This result indicates that there is no trend in the data, even at the 1σ level. We therefore conclude that our sample does not show an anti-correlation of L_B with age, and that the L_X/L_B trend with age reflects an increasing X-ray luminosity.

2.2.2 L_X/L_B versus Fundamental Plane Residual

As further evidence of X-ray evolution with age we have compared L_X/L_B to residual from the Fundamental Plane (FP). Work by Forbes et al. (1998) has shown that galaxy age appears to be a ‘‘fourth parameter’’ affecting the position of a galaxy relative to the plane. Galaxies below the plane (negative residual) are generally young, while older objects lie on or above the plane (positive residual). Fig. 2.4 shows 212 galaxies with Fundamental Plane residuals taken from Prugniel & Simien (1996).

As with Figs. 2.1 and 2.2, this shows a trend of increasing L_X/L_B with age. For the complete data set, the correlation strength is $>99.98\%$. However, only a small number of points

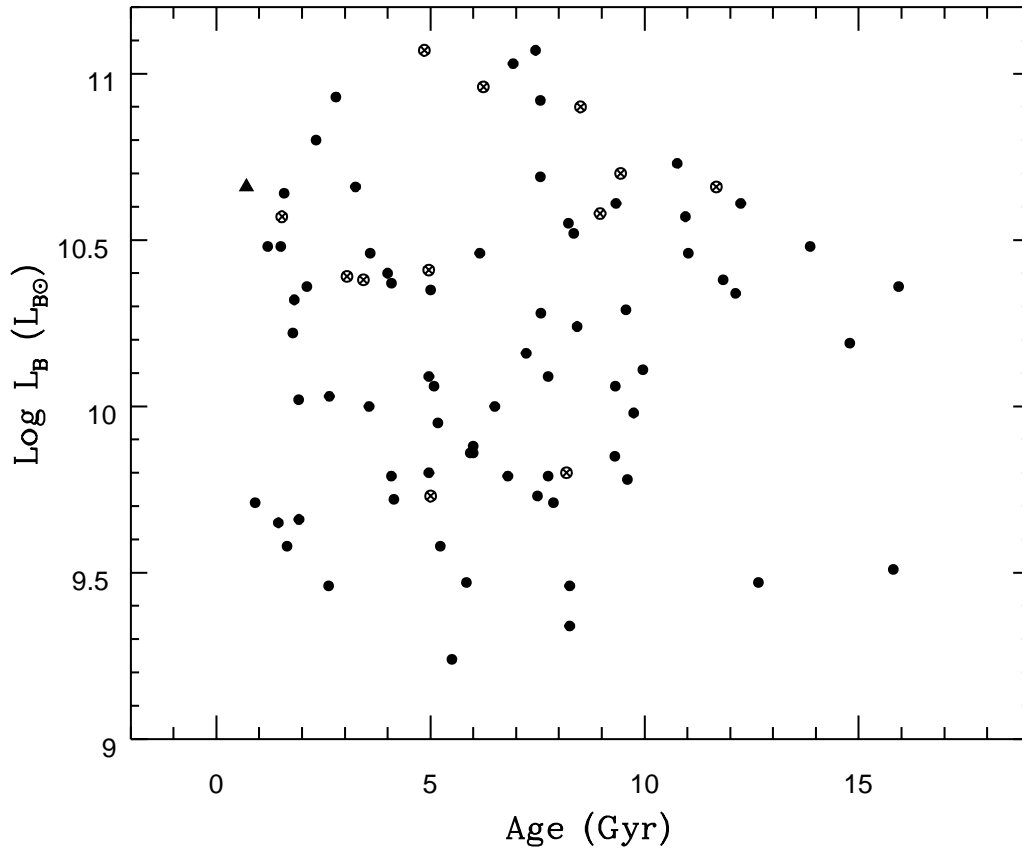


Figure 2.3: Optical luminosity versus spectroscopic age. Crossed circles represent cluster or group dominant galaxies and filled circles all other detections. The triangle is the recent merger remnant NGC 7252. The cE galaxy, M32, has been excluded from the plot and associated statistical tests.

lie outside the range $-0.5 < \text{FP residual} < 0.5$. These are unlikely to be representative of the general population, but will have a strong influence on the statistical tests. Excluding them lowers the correlation strength to $\sim 99.95\%$, with a slope of 1.39 ± 0.40 (EM). This line is shown in Fig. 2.4. Again the trend shown in Fig. 2.4 is one of increasing X-ray luminosity, relative to the optical, as a galaxy evolves.

2.3 Discussion

In the previous section we have used three age estimators to show a strong correlation between normalised X-ray luminosity and galaxy age. The X-ray emission from early-type galaxies is

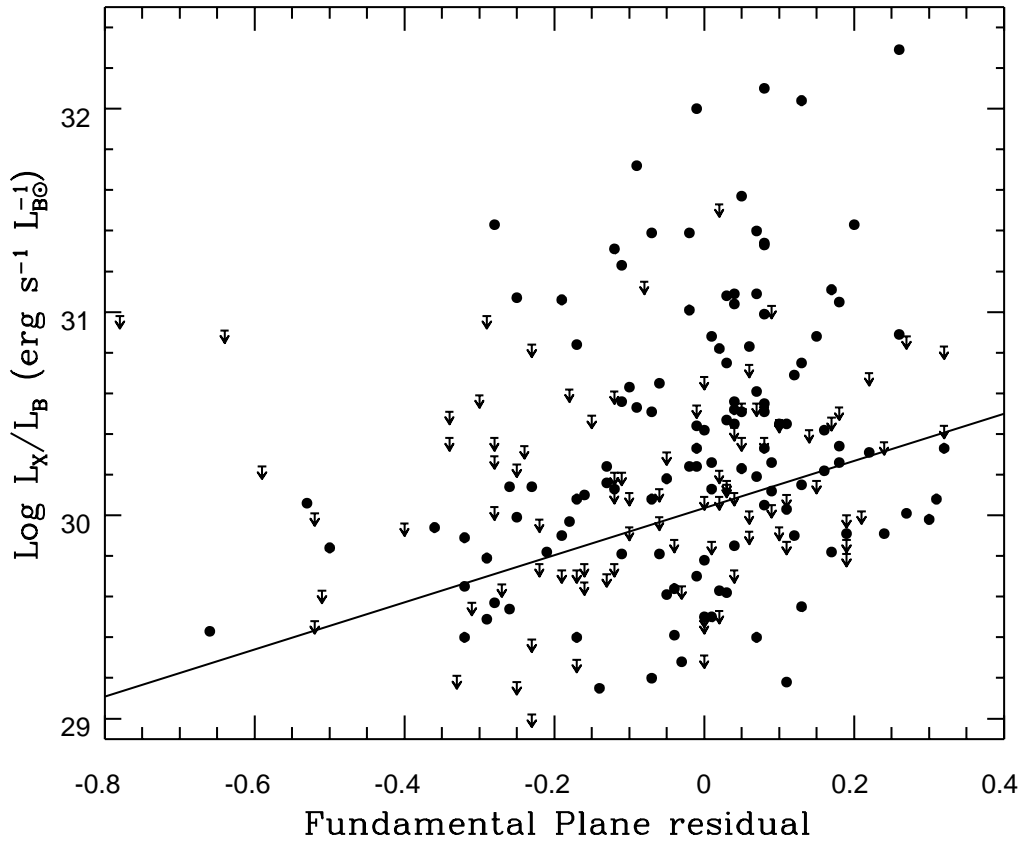


Figure 2.4: X-ray luminosity versus Fundamental Plane residual for early-type galaxies. Filled circles represent detections and arrows upper limits. The solid line is a fit to all points with $-0.5 < \text{FP residual} < 0.5$

known to be produced by sources of two main types; discrete sources such as X-ray binaries, and hot gas. The contribution of discrete sources has been shown to be important in low luminosity early-type galaxies (Fabbiano et al. 1994; Irwin & Sarazin 1998a; Sarazin et al. 2000) and in late-type galaxies, where they are generally the dominant source of X-ray emission. On the other hand, most early-type galaxies have a strong hot gas component, and massive ellipticals are certainly dominated by hot gas emission (Matsushita et al. 2000; Matsushita 2001). As the contribution of hot gas is known to vary a great deal, while the contribution from discrete sources is generally believed to scale with L_B (Matsushita et al. 2000; Fabbiano et al. 1992), it seems likely that the trend we observe in L_X/L_B is caused by changes in the hot gas content of these objects with age. We now go on to discuss possible hot halo formation mechanisms which

may be responsible for this trend of increasing X-ray gas content with age.

2.3.1 Gas infall

It has been suggested (Hibbard & van Gorkom 1996) that the hot gas in elliptical galaxies may be produced during a merger by the shock heating or photoionisation of cool gas from the progenitor galaxies. In some ongoing mergers the tidal tails are thought to contain up to half the HI gas originally present in the progenitor galaxies (Hibbard et al. 1994). When this gas falls back into the body of the galaxy, shock heating should be capable of heating it to X-ray temperatures. An alternative is that the temperature of the gas is caused by heating in the starburst phase of the merger. In this case the hot gas would be blown out to large radii, but might be contained by the dark matter halo of the galaxy (Mathews & Brighenti 1998b). At these large radii it would be too diffuse to be detected, but would eventually fall back into the galaxy, forming the observed X-ray halo.

In terms of available masses of gas, both these models appear to be viable formation processes. Bregman et al. (1992) derived X-ray and cold gas masses for a large sample of early-type galaxies, finding M_X of between $\sim 10^6$ and $10^{11} M_\odot$. The mean X-ray gas mass was a few $10^9 M_\odot$. On the other hand, very few detections of HI were made in early-type galaxies, although Sa galaxies were found to contain between 10^7 and $\sim 5 \times 10^{10} M_\odot$ of HI. Studies of HI masses in later-type galaxies (Huchtmeier & Richter 1989; Huchtmeier & Richter 1988) give an average of a few $10^9 M_\odot$, depending on the range of morphologies chosen. Given that large elliptical galaxies are likely to have been formed by the merger of many smaller spiral galaxies, these results suggest that fairly modest conversion efficiencies could produce the expected X-ray halo gas masses either from infalling HI or via starburst heating and later infall.

However, the infalling HI model fails to explain the timescale over which we observe the L_X/L_B trend. In the well known merging galaxy NGC 7252, 50% of the cold gas currently in the tidal tails is expected to fall back into the main body of the galaxy within the next 2–3 Gyr (Hibbard & van Gorkom 1996). This suggests that we should expect to see a rapid build up of X-ray emission in the first few gigayears after merger. This increase should be made even more noticeable by the fading of the stellar population, as this is the period during which L_B is dropping most quickly. Rapid generation of the X-ray halo is inconsistent with our results.

A model involving infall of hot gas is likely to have similar problems. It is difficult to see how gas falling back into the body of the galaxy can do so at the steady rate needed to produce a smooth increase in L_X/L_B . Infall may be delayed, as the hot gas reaches larger radii than the cold, but it will still occur on a galaxy dynamical timescale. Models involving cooling and infall of gas onto central dominant galaxies in groups or clusters (Brighenti & Mathews 1999) may be able to produce an inflow over a longer period, but these are unlikely to be generally applicable. Group dominant galaxies have exceptionally large dark halos, making them more able to retain (or accrete) hot gas. They also lie at the bottom of a group potential well, and may be at the centre of a group X-ray halo, providing them with an extra reservoir of hot gas. These conditions do not apply to the majority of early-type galaxies. Therefore we suggest that infall of (cold or hot) gas is unlikely to be the dominant process in the generation of X-ray halos in typical ellipticals.

2.3.2 Ongoing stellar mass-loss and galaxy winds

Since infall of either hot or cold gas seems unable to provide the sort of long term trend in L_X/L_B seen in Fig. 2.2, we now look to models involving gas generated by mass loss from the galactic stars. This source of gas is fairly well understood, and can provide the sort of gas masses required to account for the halos of many early-type galaxies (though probably not the very brightest – Brighenti & Mathews 1998), provided that the gas is retained within the galactic potential. Two main timescales are involved. One is the mass loss rate from stars, primarily giant stars. The second is the rate of type Ia supernovae (SNIa) which provide the main heat source (after the brief SNII phase). These two factors, and the interplay between them, can potentially lead to changes in the hot gas content of elliptical galaxies on timescales much longer than a dynamical time, and so have the potential to explain the slow trend we observe. The stellar mass loss rate is fairly well understood (e.g. Ciotti et al. 1991), and for a single-aged stellar population it declines approximately as $t^{-1.3}$. However, the SNIa heating rate, which dominates the effective specific energy of the injected gas, is highly uncertain. Recent estimates of the SNIa rate in old stellar populations (e.g. Cappellaro et al. 1999) have revised the classic Tammann (1982) value of the rate in old stellar populations down by a factor 3-4, and the evolution of this rate with population age is very model-dependent. Given our continuing ignorance about the precise

nature of SNIa, it must therefore be regarded as largely unknown.

The specific energy of the injected gas determines whether gas is retained in a hydrostatic hot halo, or escapes the galaxy as a wind. The way in which the specific energy evolves, depends upon the evolution of the SNIa rate relative to the stellar wind loss rate. There are therefore two fundamentally different classes of models: those in which the SNIa rate is constant, or declines more slowly than the stellar mass loss rate (e.g. Loewenstein & Mathews 1987; David et al. 1991) and those in which the supernova rate drops more quickly than the gas injection rate (Ciotti et al. 1991; Pellegrini & Ciotti 1998). Broadly speaking, when the specific energy of the injected gas is smaller than its gravitational binding energy it will be retained in a hot halo. It may subsequently cool in a luminous cooling flow. However, if the specific energy of the gas substantially exceeds its binding energy it will escape from the galaxy in a fast wind, which results in a much lower X-ray luminosity. The first class of models, in which the specific energy rises with time, therefore produces an evolution from an early inflow phase to a later wind phase, predicting a *declining* X-ray luminosity with time. Such models are clearly inconsistent with our results.

Models in which the SNIa rate drops more quickly than $t^{-1.3}$ evolve, in broad terms, from a low luminosity wind phase, toward a more luminous halo/cooling flow phase. The timescale for this evolution depends upon a variety of factors, such as the depth and shape of the potential, but it is typically ~ 10 Gyr (Ciotti et al. 1991). In fact, none of the models studied to date shows the rather simple monotonic rise in L_X with age which we observe. The models of Ciotti et al. (1991) predict an initial luminous phase, when the gas loss rate from stars is very high. The X-ray luminosity then declines as the wind loss rate drops, and then rises again during the transition to a bound hydrostatic halo, at which point the X-ray luminosity is essentially equal to the SNIa luminosity. This whole development describes a fairly symmetrical dip and rise, lasting $\sim 5 - 15$ Gyr, which is again not what we see in the data. However, this model describes a galaxy in which *all* stars are formed at $t = 0$. In contrast, the spectroscopic age of our galaxies probably denotes the time since a merger-induced starburst involving only a few percent of the stellar mass. In this case, the early stellar mass loss rate will be much lower than in the Ciotti et al models, and the X-ray luminosity correspondingly less (scaling approximately as the square of the mass loss rate). The main change in L_X will be a rise associated with the

slowing wind and transformation into a hydrostatic halo. In addition, as shown in Fig. 2.2, the decrease in optical luminosity as the starburst population fades will produce a rise in L_X/L_B over the first 1-2 Gyr.

2.4 Concluding Remarks

We have examined the evolution of the X-ray properties of early-type galaxies. For three galaxy age estimators (fine structure parameter, Fundamental Plane residuals and spectroscopic ages) we find that the normalised X-ray luminosity evolves with time. In particular, the X-ray luminosity, which reflects the mass of hot halo gas, appears to increase at a steady rate over ~ 10 Gyrs.

Comparing the long term trend in L_X/L_B which we observe with expectations from possible mechanisms for hot halo formation, we conclude that the only viable mechanism appears to be the slow evolution from an outflowing wind to hydrostatic halo phase driven by a declining SNIa rate. Infalling gas seems unlikely to be the main cause of such a long term trend. Our results suggest that some of the scatter seen in the global L_X versus L_B relation is due to the evolutionary state, and past merger history, of early-type galaxies.

Chapter 3

A Catalogue and Analysis of X-ray luminosities of Early-type galaxies

Abstract

We present a catalogue of X-ray luminosities for 401 early-type galaxies, of which 136 are based on newly analysed *ROSAT* PSPC pointed observations. The remaining luminosities are taken from the literature and converted to a common energy band, spectral model and distance scale. Using this sample we fit the $L_X:L_B$ relation for early-type galaxies and find a best fit slope for the catalogue of ~ 2.2 . We demonstrate the influence of group-dominant galaxies on the fit and present evidence that the relation is not well modeled by a single powerlaw fit. We also derive estimates of the contribution to galaxy X-ray luminosities from discrete sources and conclude that they provide $\text{Log } L_{dscr}/L_B \simeq 29.5 \text{ erg s}^{-1} L_{B\odot}^{-1}$. We compare this result to luminosities from our catalogue. Lastly, we examine the influence of environment on galaxy X-ray luminosity and on the form of the $L_X:L_B$ relation. We conclude that although environment undoubtedly affects the X-ray properties of individual galaxies, particularly those in the centres of groups and clusters, it does not change the nature of whole populations.

3.1 Introduction

One of the most surprising results from the *Einstein* observatory (launched in 1978) was the discovery of diffuse X-ray emission from early-type galaxies. Since then, many X-ray studies of galaxies have been published, ranging between detailed analyses of individual objects and large catalogues designed to shed light on their global properties. Fabbiano et al. (1992) (FKT)

produced one of the most extensive catalogues using *Einstein* data, observing 148 early-type galaxies and examining (among other things) the $L_X:L_B$ relation for these objects. Other works in a similar vein include those of Burstein et al. (1997), a somewhat larger catalogue of *Einstein* data, Davis & White (1996) and Brown & Bregman (1998) which use smaller samples based on *ROSAT* PSPC pointed observations, Beuing et al. (1999) based on the *ROSAT* All-Sky Survey, and Matsushita (2001) using *ROSAT* pointed data.

The largest of these catalogues, that of Beuing *et al.* , contains almost 300 galaxies, but most of these have exposure times of only a few hundred seconds. Catalogues based on pointed data have much longer exposures, but lack the coverage to be truly representative of the general population of early-type galaxies. The problem is exacerbated by the fact that most small and medium sized samples focus on the brightest objects, and pass over the fainter and less well studied galaxies. It can also be difficult to compare between catalogues, as each employs its own analysis procedure and presents results in its own particular format. For example, we have not used data from the sample of Burstein et al. (1997) because the method used to convert count rates to fluxes is not based on a single spectral model, making it more difficult to correct luminosities from this catalogue to our own model and waveband.

Our intention in this paper is to provide a large general catalogue of X-ray luminosities for early-type galaxies. We have therefore calculated new X-ray luminosities for 136 galaxies, based on *ROSAT* PSPC data, and added a further 265 luminosities from previously published catalogues. All of the X-ray luminosities have been converted to a common format based on a reliable distance scale (assuming $H_0 = 75 \text{ km s}^{-1} \text{ Mpc}^{-1}$) and correcting for differences in spectral fitting techniques and waveband. We use the resulting catalogue to study the X-ray properties of early-type galaxies, focusing in particular on the $L_X:L_B$ relation and on the influence of environment.

In Section 3.2 we give details of our sample, and discuss our X-ray analysis of *ROSAT* data in Section 3.3. Section 3.4 covers the methods used to add data from the literature to our own results, and Section 3.5 briefly discusses the survival analysis techniques used to fit lines to censored data. In Section 3.7 we report the results of our line fits to the $L_X:L_B$ relation, as well as giving an estimate of the contribution of discrete sources and examining the influence of galaxy environment. Section 3.8 is a discussion of some of our results and the conclusions we

draw from them. Throughout the paper we normalise L_B using the solar luminosity in the B band, $L_{B\odot} = 5.2 \times 10^{32} \text{ erg s}^{-1}$.

3.2 Sample selection

Our sample of early-type galaxies was selected from the Lyon–Meudon Extragalactic Data Archive (LEDA). This catalogue contains information on $\sim 100,000$ galaxies, of which $\sim 40,000$ have redshift and morphological data. Galaxies were selected using the following criteria:

- Morphological Type $T < -1.5$ (*i.e.* E, E–S0 and S0 galaxies)
- Virgo corrected recession velocity $V \leq 9,000 \text{ km s}^{-1}$
- Apparent Magnitude $B_T \leq 13.5$

The redshift and apparent magnitude restrictions were chosen in order to minimise the effects of incompleteness on our sample. The LEDA catalogue is known to be 90% complete at $B_T = 14.5$ (Amendola et al. 1997), so our selection should be close to statistical completeness. The selection process produced ~ 700 objects. We then cross-correlated this list with a list of public *ROSAT* PSPC pointings. Only pointings within $30'$ of the target were accepted as further off axis the PSPC point–spread function becomes large enough to make analysis problematic. This left us with 209 galaxies with X–ray data available.

3.3 Data Reduction and Spectral Fitting

Data reduction and analysis of the X–ray datasets were carried out using the ASTERIX software package. Before the datasets can be used, various sources of contamination must be removed. Possible sources include charged particles and solar X–rays scattered into the telescope from the Earth’s atmosphere. Onboard instrumentation provides information which allows periods of high background to be identified. The master veto counter records the charged particle flux, and we have excluded all time periods during which the master veto rate exceeds 170 count s^{-1} . Solar contamination causes a significant overall increase in the X–ray event rate. To remove this contamination we excluded all times during which the event rate deviated from the mean by more than 2σ . This generally removes no more than a few percent of each dataset.

After this cleaning process each dataset is binned into a 3-dimensional (x , y , energy) data cube. Spectra or images can be extracted from such a cube by collapsing it along the axes. A model of the background is generated based on an annulus taken from this cube. We used annuli of width 0.1° , and inner radius 0.4° where possible. In cases where this would place the annulus close to the source we moved the annulus, generally to $r = 0.55^\circ$. To ensure that the background model is not biased by sources within the annulus, an iterative process was used to remove point sources of $> 4.5\sigma$ significance. Occasionally the annulus lies over an area of diffuse emission, in which case we either remove that region by hand or move the annulus to an uncontaminated region. The only exception to this occurred in cases where the target galaxy was surrounded by group or cluster emission. In such cases the target is contaminated by group emission along the line of sight, increasing its apparent luminosity. To counter this we allowed the annulus to lie over the outer region of the group emission (unless prevented by large numbers of point sources), thereby removing at least a part of the contamination. The resulting background model was then used to produce a background-subtracted cube. Regions near the PSPC window support structure were removed from these images, as objects in those areas would have been partially obscured during the observation. The cube was further corrected for dead time and vignetting effects, and point sources were removed.

Examination of background subtracted images allowed us to locate each galaxy and produce a radial profile of its emission. This profile was used to determine the radius of the region from which a spectrum was extracted, with the cutoff radius taken at the point where the X-ray emission drops to the background level. We excluded 73 sources for which derived X-ray fluxes were unreliable at this stage. Many were too close to the support structure, or only had very poor quality data available. Others were found to be located close to bright X-ray sources. Galaxies in groups and clusters were only accepted if they stood out clearly above the general cluster emission. Point sources within the extraction region were not removed, as we considered these likely to be part of the galaxy emission. A spectrum of this region was then obtained by collapsing the cube along its x and y axes.

Galaxy spectra were fitted with a MEKAL hot plasma model (Kaastra & Mewe 1993; Liedahl et al. 1995). Hydrogen absorption column densities were fixed at values determined from radio surveys (Stark et al. 1992), and temperature and metal abundance were fixed at 1 keV and 1

solar respectively. Fitting in this way provides a fairly crude measure of the bolometric X-ray flux, but allows all the galaxy spectra to be fitted by the same model, regardless of the quality of the data available.

Our choice of temperature and metallicity for these fits was influenced by our intention to combine our results with those of other studies. The catalogues of Beuing et al. (1999) and Fabbiano et al. (1992) both assume these values in their fits to early-type objects, although they use a Raymond & Smith (Raymond & Smith 1977) plasma model rather than the more accurate MEKAL model. There is a strong body of evidence showing that these parameters are representative of the majority of early-type galaxies. The recent study by Matsushita et al. (2000), uses high quality *ASCA* observations to examine the gas metallicity in a number of X-ray luminous early-type galaxies. Taking into account probable errors in the modeling of the Fe-L spectral region, average metal abundances are found to be solar to within a factor of two, regardless of the plasma code used. Measured temperatures of early-type galaxies usually range between 0.2 and 1.3 keV (*e.g.* Matsushita 2001; Davis & White 1996), but finding an accurate average is hampered by the lack of high quality data.

The spectral representation we employ is clearly over-simplistic given that these objects are probably better fit by two component models (Matsumoto et al. 1997). While such multi-temperature models should give more accurate measurements of halo gas temperatures, they require higher quality data, and have been used to date on only relatively small samples of bright galaxies. Single temperature 1 keV models are most likely to be poor descriptions of X-ray faint galaxies, which are expected to be dominated by emission from X-ray binaries (Matsumoto et al. 1997). In these galaxies, emission is likely to be better represented by a high temperature bremsstrahlung model. If we assume that our lowest luminosity galaxies are actually better described by a 10 keV bremsstrahlung model, we find that we will have underestimated their bolometric luminosity by a factor of ~ 2 .

In total we fitted luminosities for 136 early-type galaxies, of which only 15 are upper limits. These form the core of our catalogue.

3.4 A Master Catalogue

Comparison of our new data with previously published catalogues was hampered by the different basic parameters used in these catalogues. The three catalogues we examined are those of Beuing et al. (1999), Fabbiano et al. (1992) and Roberts et al. (1991). These use a range of models to fit the data, different wavebands, distances and blue luminosities. We have corrected for these differences by converting the catalogues to a common set of values, as used for our own results.

Where possible, we take our distances from Prugniel & Simien (1996). These are computed using the model of Faber & Burstein (1988) which accounts for the influence of the Great Attractor and Virgocentric flow. For galaxies not listed in Prugniel & Simien we used distances from LEDA, which are corrected only for Virgocentric motion. Similarly, we have calculated L_B for each object based where possible on the B_T values given in Prugniel & Simien. Where these are unavailable we use B_T , or in some cases m_B , from NED. Galaxies for which we have used m_B to calculate L_B are marked in the final catalogue, and in order to test their effect on our results we compared their distribution on an $L_X:L_B$ graph with that of the rest of our catalogue. We found no significant difference between the two subsets. We therefore believe that these values provide us with a reasonably homogeneous and accurate set of distances and luminosities on which to base our study.

The three catalogues we wish to compare our results to each quote L_X in different wavebands. Fabbiano et al. (1992) and Roberts et al. (1991), working with the *Einstein* IPC, quote luminosities in the 0.2–4.0 keV and 0.5–4.5 keV bands. Beuing et al. (1999) choose a 0.64–2.36 keV band, as their work is based on relatively low signal to noise *ROSAT* PSPC All-Sky Survey data. To allow us to compare these with our luminosities we convert each to a pseudo-bolometric band. The spectral models available generally have limited energy range; for example, the Raymond & Smith model grid available on ASTERIX covers the 0.088–17.25 keV range. However, we have assumed a typical galaxy temperature of 1 keV, as do the three other catalogues, so contributions to any model from outside the available range should be negligible. Using XSPEC (v11.0.1) we have tested this and find that changing the lower bound to 10 eV increases L_X by $\sim 6\%$, while changing the upper bound to 100 keV produces no measurable increase.

We also need to correct for different spectral models. For our analysis we have used the

Catalogue	Correction Factor $\Delta \text{Log } L_X$
Beuing <i>et al.</i>	+0.27
Fabbiano <i>et al.</i>	+0.15
Roberts <i>et al.</i>	+0.36

Table 3.1: Correction factors used to convert luminosities from Beuing *et al.*, Fabbiano *et al.* and Roberts *et al.* into our pseudo-bolometric band and MEKAL model.

MEKAL model, as this is probably the most accurate generally available. However, both Beuing *et al.* and Fabbiano *et al.* use the Raymond & Smith model, and Roberts *et al.* use a simple bremsstrahlung model. Luckily, the choice of solar metallicity is common to all. Therefore, we calculated conversion factors between 1 keV, solar metallicity Raymond & Smith and bremsstrahlung models in the appropriate wavebands and our own MEKAL model in the pseudo-bolometric band. We then apply these corrections to the catalogues, bringing their luminosities into line with ours. The correction factors, including the effects of plasma code and conversion to bolometric luminosities, are shown in Table 3.1.

To confirm that this process acts as intended, we compare L_X values for those galaxies which are listed in more than one catalogue. Plots of these comparisons are shown in Figure 3.1.

In all three plots, a strong and fairly tight correlation is clear. In order to establish the relation between the three catalogues and our own points, we have fitted regression lines to the data. Galaxies actually detected in two catalogues should have very similar measured luminosities. However, the differences in data quality between the samples imply that upper limits may not be similar. We therefore fit the lines using detections only. We also expect a certain number of galaxies for which the measured luminosities disagree. There may be cases where the lower spatial resolution of the *Einstein* IPC or the small exposure times of the RASS observations allow confusion from nearby sources. Contamination from group or cluster emission is also likely to be dealt with differently in the different catalogues. To avoid bias from such cases we therefore exclude from our fits galaxies for which the luminosities disagree by more than a factor of ~ 3 . A search in NED revealed that all the galaxies thus excluded are either AGN (such as Cen A), surrounded by group or cluster emission (such as M86 or NGC 720) or lie near a much brighter companion galaxy (NGC 3605). Lastly, we also exclude the local group dwarf elliptical, M32, as it has a much lower luminosity than any of the other galaxies, and tends to drive the fitting

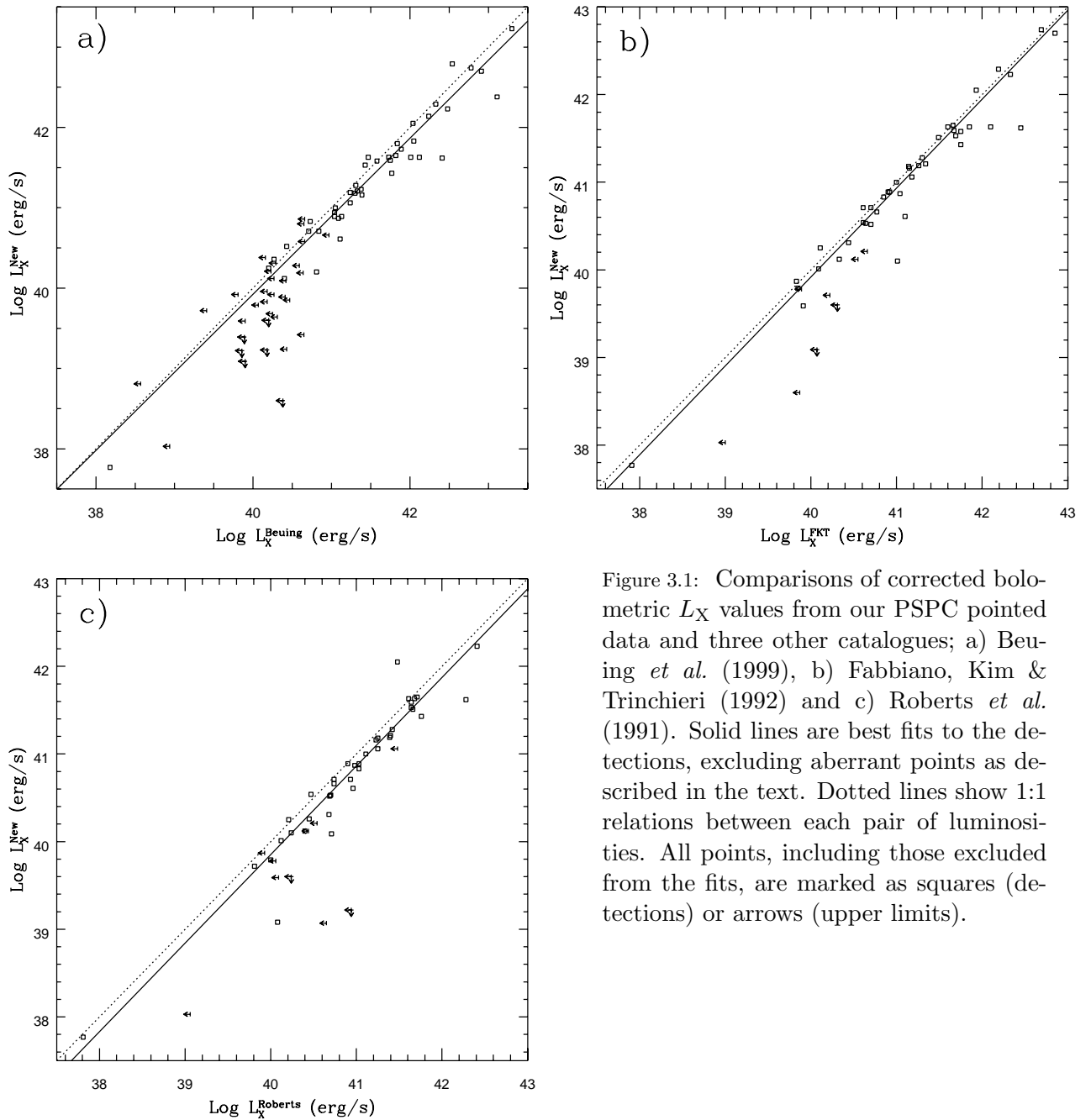


Figure 3.1: Comparisons of corrected bolometric L_X values from our PSPC pointed data and three other catalogues; a) Beuing *et al.* (1999), b) Fabbiano, Kim & Trinchieri (1992) and c) Roberts *et al.* (1991). Solid lines are best fits to the detections, excluding aberrant points as described in the text. Dotted lines show 1:1 relations between each pair of luminosities. All points, including those excluded from the fits, are marked as squares (detections) or arrows (upper limits).

process. With these galaxies excluded, we use the OLS bisector method to fit lines to the data. The slopes and intercepts are shown in Table 3.2.

The relations between the two *Einstein*-based catalogues and our own L_X values both have slopes close to unity, and small intercept values. We take this as an indication that the corrected catalogues are comparable. In the case of the Beuing *et al.* luminosities we find a slope of slightly less than unity, suggesting that their luminosities become systematically brighter than ours at

Catalogue	Best Fit	
	Slope (Error)	Intercept (Error)
Beuing <i>et al.</i>	0.971 (± 0.031)	1.057 (± 1.298)
FKT	1.014 (± 0.028)	-0.672 (± 1.160)
Roberts <i>et al.</i>	1.011 (± 0.028)	-0.593 (± 1.132)

Table 3.2: Comparison between galaxies from our PSPC pointed data and those from other samples.

high L_X . We believe this to be caused by a difference in analysis technique. Beuing *et al.* take source radii, as we do, as the radius at which the X-ray emission drops to the background level. However, when dealing with group-dominant galaxies they set the radius to include the group halo, whereas we attempt to use a radius at which the galaxy emission drops to the group level. This means that at high L_X , some of their luminosities include considerably more group emission than ours.

These relations show that our correction factors do indeed bring the catalogues into good agreement with one another. We do however recognise that there are likely to be factors we are unable to take into account, such as the use of different source extraction radii, and so we apply the relations defined in Table 3.2 as a further correction factor to the X-ray luminosities from the literature. In practice, it should be noted that the corrections are small (generally less than $\Delta \text{Log } L_X = 0.1$) and therefore have a minimal effect on the results presented in the rest of this paper.

3.5 Statistical Analysis

Before presenting the results of our new measurements, we first discuss the statistical techniques used to analyse the various correlations presented in this paper. Throughout this study we deal with data which contain both upper limits and detections. This is unavoidable when attempting to compile a large catalogue of galaxy X-ray luminosities. Many of the objects included only have serendipitous pointings available, and there are a number of faint galaxies which would require longer pointings to be detected.

To deal with data containing upper limits, we use the survival analysis tasks available in IRAF. Survival analysis assumes that the censoring of the data is random – *i.e.* that the upper

limits are unrelated to the true values of the parameter. In more detail, the assumption is made that for each upper limit, the distribution of detections below this value forms a reasonable model for the probability distribution of the true value associated with the upper limit. This assumption would be invalidated if, for example, sensitivity limits were systematically related to the true fluxes from sources – for example by observing known faint sources for longer in an attempt to detect them. In the case of our samples, we have upper limits representing galaxies over the majority of the range of L_X , and the detection limits are determined by exposure time, source distance, off axis angle and in some cases source environment. Most of the galaxies whose X-ray luminosities we have calculated based on *ROSAT* pointed data were not the target of the pointings used. This suggests that exposure time should be unrelated to the galaxy luminosity or distance. Similarly, luminosities taken from the Beuing *et al.* sample are based on exposures whose length is unrelated to any particular target. The situation is less clear in the case of the luminosities based on *Einstein* data, as more of these objects are likely to have been the target of the observation. However, for the great majority of galaxies, random censoring appears to be a fair assumption.

Three correlation tests are available in IRAF; the generalised Kendall’s tau, generalised Spearman’s rho and Cox proportional hazard tests. Both the Kendall’s tau and Cox hazard tests are known to perform poorly when the data contains large numbers of tied values, and all three tests function best on large datasets (Feigelson & Nelson 1985). Our samples are mainly large, in which case we use all three tests. We quote the least favourable result - *i.e.* the lowest significance found. In the few cases where a sample contains less than 30 objects we do not use the generalised Spearman’s rho test.

To fit lines to our samples we use two of the three linear regression tasks available. These are the expectation and maximization (EM) algorithm and the Buckley–James algorithm (BJ). The EM algorithm is a parametric test and assumes that the residuals to the fitted line follow a Gaussian distribution. The BJ method is non-parametric, using the Kaplan–Meier estimator for the residuals to calculate the regression, and therefore only requires the censoring distribution of the data about the line to be random. In almost all cases we find that these two methods agree reasonably well, and in most cases their results are nearly identical. However, in cases where the two methods are not in close agreement it should be noted that the BJ algorithm is probably

the more reliable of the two, as it makes no assumption about the underlying distribution of the data. When using these tasks or the correlation tests, we take the uncensored parameter as the independent variable and the censored parameter as the dependent variable. The EM and BJ algorithms also produce values for the standard deviation about the regression, giving an estimate of the scatter in the relation.

The third linear regression task available to us is the Schmitt binning method. This technique can deal with upper limits on both axes, which allows a bisector fit to be carried out, based on fitting both y/x (y on x) and x/y regression lines. However, the Schmitt algorithm is known to be unreliable when used with heavily censored data (Isobe et al. 1986; Schmitt 1985), a result confirmed by the simulations reported in section 3.6. We therefore do not use Schmitt binning for our analysis.

To calculate means, we use the Kaplan–Meier estimator, which produces reliable results and error estimates except in cases where the lowest point in the data is an upper limit. When this occurs, the mean value derived tends to be underestimated. The estimator can also be used to effectively fit lines of fixed slope. For example, when fitting a line of slope unity to $L_X:L_B$ relations, as the mean value of the L_X/L_B distribution is equal to the intercept of a slope unity line.

3.6 Tests of fitting accuracy

When attempting to determine the underlying relationship between two uncensored variables, an OLS bisector fit is likely to be the most reliable fitting method (Isobe et al. 1990). For our censored data we have used the EM and BJ algorithms, which perform y on x regression. An alternative to these fits is to use the Schmitt binning method to perform y/x and x/y fits and then calculate a bisector of the two. We have carried out fits using this method, as described in Shapley et al. (2001), on various subsamples of our data. The slopes of these ‘Schmitt bisector’ fits are generally somewhat steeper than the EM and BJ fits, as might be expected. However, in many cases the slopes are very different from those found by the other two algorithms, and in a few cases a shallower slope is found. In order to test how well the three algorithms measure the underlying distribution of data, we have carried out a number of comparisons using simulated data.

We simulate datasets by using a random number generator to produce a set of data points, based on a predetermined straight line relation and range of x-values. We define a level of scatter, and points are shifted up or down by a random distance uniformly distributed within this range. To censor the data, we randomly select a number of data points and calculate a new y-axis value for each, corresponding to a detection threshold. If this new value is higher than the original, the data point is declared to be an upper limit at the new, higher value. The range of scatter of these detection thresholds is defined separately from the scatter in the data values, and both have been chosen to be comparable to that seen in our real dataset. Datasets containing the initial “detected” values (i.e. without any thresholding) are also produced, and these are fitted using a standard OLS bisector, as well as by the EM, BJ and Schmitt bisector methods.

As a test of the basic fitting properties of the four techniques, we simulated a line of slope 2, intercept 0, with x ranging between 0 and 10 and a scatter in the points of ± 0.5 . We generated datasets containing 400, 200, 100 and 48 points, in which we censored 25, 50 and 75 per cent of the data. We also performed simulations involving 100 points with a larger scatter of ± 1 . In all cases, the four techniques agreed well (within errors) with each other and with the original input slope. The Schmitt bisector generally produced slopes furthest from the OLS bisector slope. We conclude that all four techniques are capable of fitting a single line, though the survival analysis techniques may have problems in cases of large scatter.

However, our data set as a whole does not follow a single linear relationship. As can be seen in Figure 3.3, it is probably better described as a broken power law, with a shallow slope below $\text{Log } L_B \simeq 10 L_{B\odot}$ and a steeper incline above. We therefore simulated a new dataset based on a broken power law similar to that indicated in our data (see Section 3.7.1), with a gradient of 1.0 over the range $x=9.0-10.2$, and gradient 2.5 over $x=10.2-11.0$. Scatter about each segment was set at ± 1 and each line was used to generate 150 data points, of which 75 were censored. The results of a variety of fits to this simulated dataset are shown in Figure 3.2.

The OLS bisector fit to this dataset gives a slope of ~ 1.8 , as does the Schmitt bisector which is offset downwards from the OLS bisector line. The EM and BJ algorithms both have slopes of ~ 1.49 . These results suggested that the Schmitt bisector does indeed behave, as expected, in a similar way to the OLS bisector fit, but that both are more influenced by the steeper line

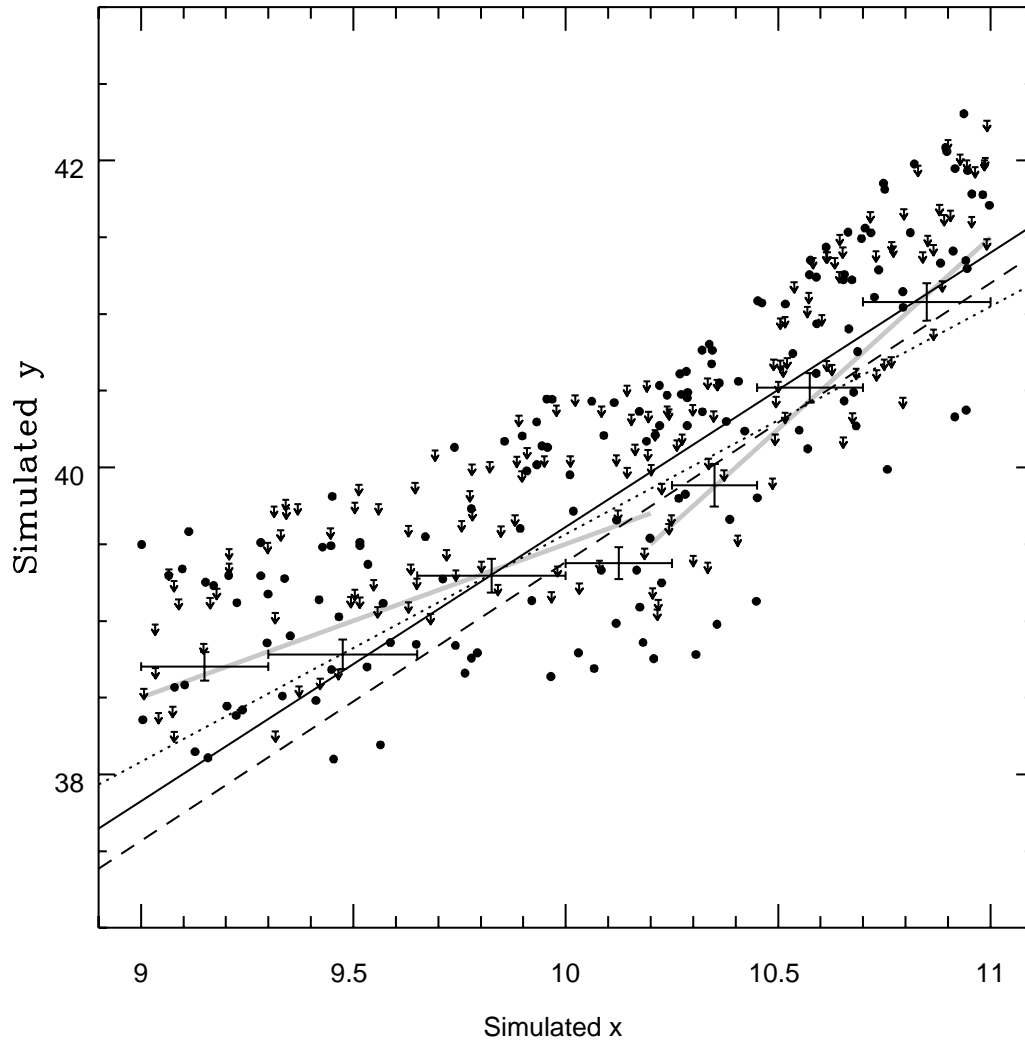


Figure 3.2: Simulated censored broken powerlaw data used to test alternative fitting methods. The solid line is an OLS bisector fit to the underlying, uncensored data, while the dashed line is a Schmitt bisector fit to the censored data. The dotted line represents the EM and BJ fits. The large crosses show the mean y value for the censored data with 1σ errors in seven x axis bins, derived using the Kaplan–Meier estimator. The two solid grey lines show the original lines used to generate the data points.

than the shallower. The y/x fits give consistently shallower slopes, but these may be more representative of the general spread of points.

To further test the quality of fit, we binned the data from the broken powerlaw simulation and used the Kaplan–Meier estimator to calculate the mean y value in each bin. The binned data are shown in Figure 3.2 and follow the original input lines fairly accurately. All four fit

lines deviate from the binned data points at some point on the graph. Both bisector fits deviate quite strongly at low x and are probably better descriptors of the steeper high x points. The EM and BJ fits also deviate at low and high x values, but do a rather better job of describing the overall trend of the binned points across the whole range of x .

This result shows clearly that fitting a single line to data which is better described as the combination of two lines of different slopes will cause difficulties. The results from the single line simulations, when considered in conjunction with these results lead us to further conclude that for our data, which has a high degree of scatter and is unlikely to be described well by a single line, the Schmitt bisector should not be used. The EM and BJ algorithms appear likely to give reasonable estimates of mean trends, but binning the data should provide the most accurate picture of the underlying distribution.

3.7 Results

Having applied the corrections described in section 3.4, we add a total of 289 early-type galaxies from the three catalogues to our own. This gives a combined catalogue of 425 galaxies, listed in Table A.1. When galaxies are listed in more than one catalogue we choose the final L_X value using the following order of preference: our results, Beuing *et al.* (1999), Fabbiano *et al.* (1992), Roberts *et al.* (1991). Detections are always preferred to upper limits, regardless of source. The T-type listed in Table A.1 is taken from LEDA. The catalogue contains 24 galaxies which are listed in previous studies as early-type, but which have LEDA T-types ≥ -1.5 . We exclude these late-type objects from further consideration.

3.7.1 The $L_X:L_B$ Relation for Early Type Galaxies

We have plotted $\text{Log } L_X$ against $\text{Log } L_B$ for the catalogue in Figure 3.3. AGN (taken from Veron-Cetty & Veron (1996)) and cluster central galaxies are likely to have anomalously high X-ray luminosities and are marked on the plot. Excluding these objects and dwarf galaxies ($\text{Log } L_B < 10^9 L_{B\odot}$), which are unlikely to be massive enough to retain a halo of X-ray gas, leaves 359 early-type galaxies of which 184 have X-ray upper limits. The tests described in Section 3.5 show a correlation of $>99.99\%$ significance. The best fit line from the expectation and maximization (EM) algorithm is:

$$\text{Log } L_X = (2.17 \pm 0.11) \text{Log } L_B + (17.98 \pm 1.12) \quad (3.1)$$

and from the Buckley–James (BJ) algorithm:

$$\text{Log } L_X = (2.28 \pm 0.12) \text{Log } L_B + 16.80 \quad (3.2)$$

where L_X is in units of erg s^{-1} and L_B is in $L_{B\odot}$. The standard deviations about the two regression lines are $\sigma_{\text{EM}}=0.69$ and $\sigma_{\text{BJ}}=0.68$ respectively.

These values are in fairly good agreement with a number of previous estimates (Beuing et al. 1999; Donnelly et al. 1990; White & Sarazin 1991), but differ from those of Brown & Bregman (1998) who found a slope of ~ 2.7 using a small sample of optically bright galaxies.

X-ray emission from discrete sources is expected to produce a lower bound to the distribution of galaxies in Figure 3.3. We discuss the question of discrete source emission in detail in Section 3.7.3, but at this stage we note that our points are reasonably consistent with the estimate of discrete source emission made by Ciotti et al. (1991).

Previous work with group galaxies (Helsdon et al. 2001) has shown that the properties of central dominant group galaxies are substantially different from those of normal group members and field galaxies. The X-ray luminosity of these dominant galaxies is in fact more closely correlated with the properties of the group as a whole than with the optical luminosity of the galaxy (Helsdon & Ponman 2002). Temperature profiles of X-ray bright groups suggest that these objects are at the centres of group cooling flows, which explains their overluminosity compared to non-central galaxies. The Brown & Bregman sample contains a large number of group-dominant galaxies (Helsdon et al. 2001), which may account for the high slope of their best fit $L_X:L_B$ relation.

Group-dominant galaxies can be identified by their position at the centre of the group X-ray halo. Unfortunately, since part of our catalogue is drawn from the literature, we are unable to carry out identifications in this way. However, group-dominant galaxies are usually the most massive and luminous object in the group. In order to remove any bias produced by these dominant galaxies, we excluded all brightest group galaxies (BGGs) and then fitted the remaining data. The majority of BGGs are selected using the catalogue of groups by Garcia (1993). However, 48 of our galaxies lie beyond the Garcia redshift limit ($5,500 \text{ km s}^{-1}$), and in

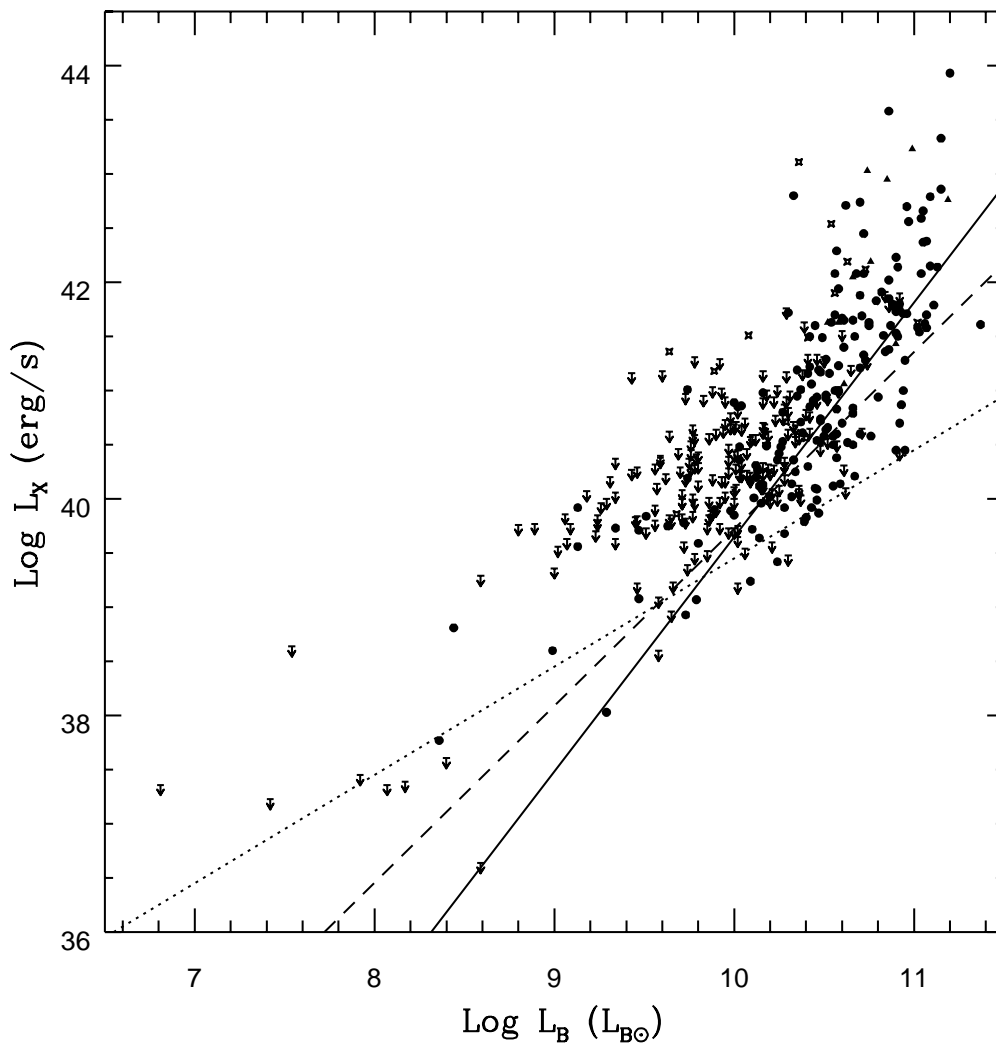


Figure 3.3: $\text{Log } L_X$ vs $\text{Log } L_B$ for our full catalogue of 401 early-type galaxies. Triangles are cluster central galaxies, stars AGN and circles all other detections. The lines shown are the best fit line to the early-type galaxies excluding AGN, BCGs and dwarfs (solid line), the best fit to the galaxies excluding all questionable objects (dashed line), and an estimate of the discrete source contribution taken from Ciotti *et al.* (1991).

these cases we are forced to identify BGGs using other catalogues. Using NED, we were able to check each galaxy for membership of the catalogues of Abell *et al.* (1989), White *et al.* (1999), Hickson (1982) and Mahtessian (1998). As White *et al.* do not list the BGG of each group, we have identified them based on the apparent magnitudes given in NED.

In order to check for other objects which might bias the fits, we also used NED to check all galaxies with $\log L_X/L_B > 31.5 \text{ erg s}^{-1} L_{B\odot}^{-1}$ for unusual properties. A surprising number of these objects show potential problems. For example, we found several probable AGN not

identified in Veron-Cetty & Veron (1996) (*e.g.* NGC 3998, NGC 4203, NGC 7465). Excluding all BCGs, BGGs, AGN and dwarf galaxies, leaves a total of 270 objects. Fitting $L_X:L_B$ for this reduced sample lowers the slope of the best fit lines significantly, to 1.98 ± 0.13 (EM) or 2.17 ± 0.15 (BJ), with $\sigma_{EM}=0.69$ and $\sigma_{BJ}=0.70$. This change demonstrates the influence of BGGs on the $L_X:L_B$ relation.

As a final precaution we also fit a very conservative subsample, from which we have removed not only all AGN, BCGs, BGGs and dwarf galaxies, but also all objects which lie at a distance >70 Mpc, to avoid including misclassified galaxies. We also remove the anomalous galaxies NGC 5102 and NGC 4782 from this conservative subsample. NGC 4782 has an unusually high L_B , and the B magnitude given for it in Prugniel & Simien (1996) disagrees with those in LEDA and NED by >1 magnitude. NGC 5102 is a relatively small E-S0 galaxy ($\text{Log } L_B = 9.29 L_{B\odot}$) with an exceptionally low X-ray luminosity ($\text{Log } L_X = 38.03 \text{ erg s}^{-1}$). It is thought to have undergone an episode of star formation a few 10^8 years ago (Bica & Alloin 1987). Although during and shortly after the starburst we might expect to observe an enhanced L_X compared to L_B (Read & Ponman 1998), galactic wind models predict that the starburst can remove all gas from the galaxy, leaving it significantly underluminous until the halo is rebuilt (Ciotti et al. 1991; Pellegrini & Ciotti 1998). The B-band luminosity will also be enhanced by the population of young stars produced by the starburst, making the position of such an object on an $L_X:L_B$ plot even more aberrant.

Removing all of these objects reduces our dataset to 246 galaxies, of which 159 have X-ray upper limits. This lowers the slope of the best fit lines considerably, to 1.63 ± 0.14 (EM) and 1.94 ± 0.17 (BJ), with $\sigma_{EM}=0.60$ and $\sigma_{BJ}=0.62$. The difference in results between the two fitting methods in this case is large, particularly as the 1σ error regions do not overlap. As mentioned in Section 3.5, the only difference between the two techniques is the assumed underlying distribution of points. As the EM method assumes the distribution to be normal, we tested the distribution of detections (87 points) for normality, using the algorithm AS 248 (Davis & Stephens 1989; Stephens 1974) which provides several measures of goodness of fit. These tests showed that the detected points were normally distributed about the best fit line at 50-60% significance. This is not a strong confirmation of the normality of the data, but is also not poor enough to rule out a normal distribution.

It is notable that the agreement between the two fitting algorithms worsens as the fraction of upper limits in the data increases. Our complete catalogue has $\sim 50\%$, and the fits are in reasonable agreement, whereas our conservative subsample has $\sim 65\%$ upper limits and shows poor agreement. Isobe et al. (1986) simulate fits to datasets containing 30 points, of which $\frac{2}{3}$ are upper limits, and produce acceptable results, but their data does not appear to have as large a degree of scatter as ours. It seems likely that our conservative subsample is rather poorly constrained, and is perhaps not well modeled by a normal distribution. This suggests that the BJ method is the more reliable in this case.

Even excluding BGGs, there is some evidence of a change in the slope of the $L_X:L_B$ relation above $\text{Log } L_B \simeq 10 L_{B\odot}$. To see how this apparent change in slope affects our fits, we binned the very conservative sample and calculated the mean L_X in each bin. These are plotted in Figure 3.4. The bins clearly follow a general trend, but at low L_B , the gradient becomes shallower. We also defined a new sample of data which excludes AGN, BGGs, BCGs, galaxies with distances >70 Mpc or $\text{Log } L_B < 10 L_{B\odot}$, NGC 5102 and NGC 4782. This sample should have had most points which are likely to bias the fit removed, and with $\text{Log } L_B > 10 L_{B\odot}$ it should model the steeper section of the relation. EM and BJ fits to this sample give slopes of 1.96 ± 0.25 and 2.28 ± 0.29 respectively, with standard deviations about the fits in both cases of $\sigma = 0.58$. Both fits seem to do a reasonably good job of matching the binned data points at $\text{Log } L_B > 10 L_{B\odot}$, with the EM fit being slightly closer to the points at high and low L_B .

3.7.2 Potential sources of bias

Our catalogue is made up of X-ray luminosities which can be split in to three main categories; those which we have calculated based on pointed *ROSAT* PSPC data, those which are based on *ROSAT* All-Sky Survey data, and those which are based on pointed *Einstein* IPC data. Clearly it is important to examine possible biases which may arise from this combination of data.

Sansom et al. (2000) have carried out a *ROSAT* study of 52 galaxies with optical fine structure. In order to check the accuracy of their own analysis of PSPC pointed data, they compare their own count rates with those of Beuing et al. (1999). For the majority of their sample both analyses are in agreement, but they note that in three cases the count rates differ by more than a factor of two. The objects concerned are NGC 7626, in the Pegasus I cluster,

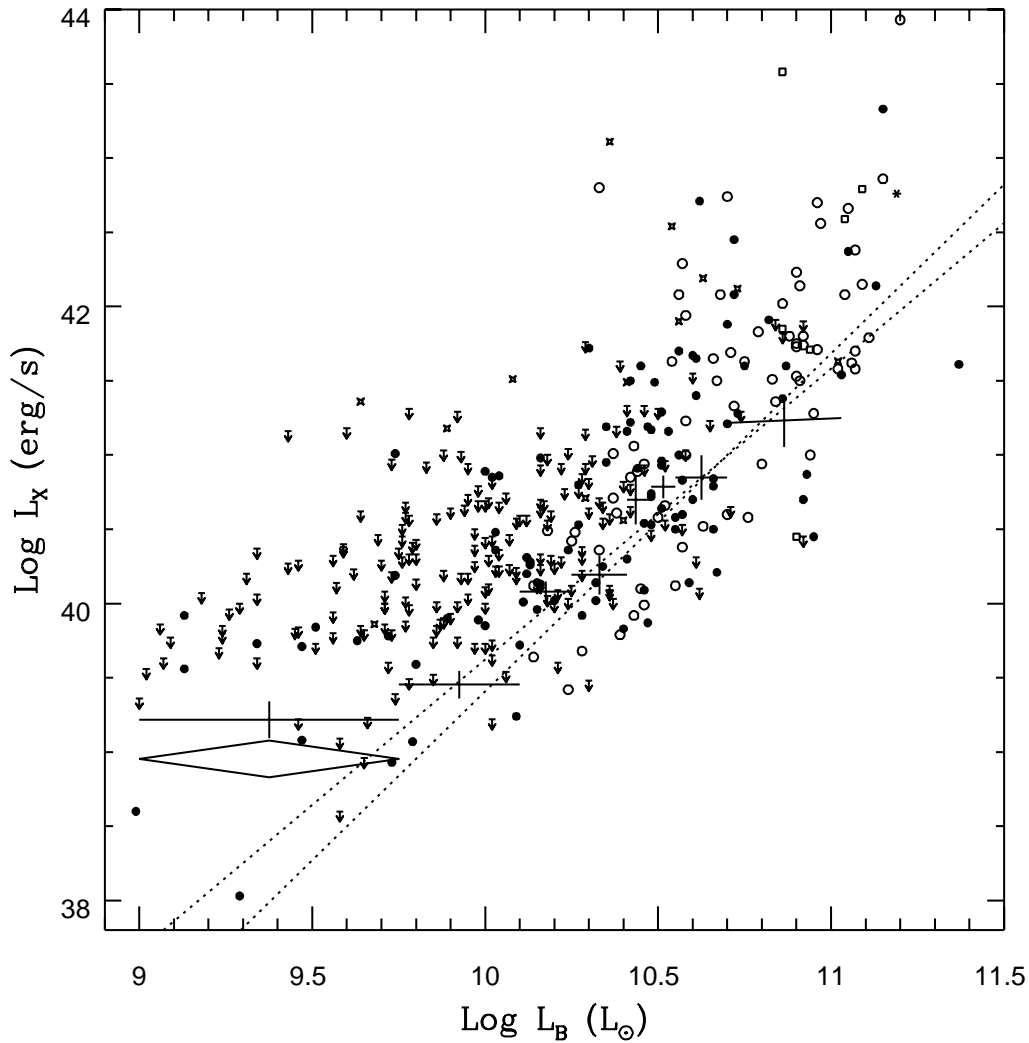


Figure 3.4: Our catalogued data L_X and L_B data with mean L_X values for eight bins. Open circles are BGGs, triangles are BCGs, stars are AGN, filled circles are detected normal galaxies and arrows are upper limits. The large crosses show the mean L_X in eight bins, calculated using the Kaplan–Meier estimator and excluding AGN, BCGs, BGGs, dwarfs, galaxies at distances >70 Mpc, NGC 5102 and NGC 4782. The diamond shows the mean L_X in the lowest bin, corrected to remove the expected contribution from discrete sources (see Section 3.7.3). The dotted lines are EM (shallower) and BJ (steeper) fits to the same data.

NGC 3226 which has an X-ray bright neighbour, and NGC 4203 which is close to an unrelated X-ray source. The inclusion of the neighbouring sources in the Beuing *et al.* analysis for the latter two cases is caused by the short exposure times (typically ~ 400 s) of RASS observations. Although extraction radii for detected galaxies were based on surface brightness profiles, low numbers of counts may cause close pairs of sources to be blurred together, appearing as a single object.

A similar but perhaps more serious problem occurs in cases where the target galaxy is surrounded by X-ray emission from a group or cluster halo. In these cases, Beuing *et al.* calculate luminosities for those galaxies which clearly stand out from the emission or are at the centre of emission which is reasonably symmetric around them. Galaxies which stand out from the background emission may have overestimated luminosities, owing to the inclusion of emission from that part of the group/cluster halo lying along the line of sight. However, this is true of most luminosity estimates for galaxies in such environments, and as the galaxy clearly stands out against its surroundings, it seems fair to assume that its own emission dominates. On the other hand, it seems likely that galaxies in the centres of groups and clusters will have seriously over-estimated luminosities, due to the inclusion of the majority of the surrounding halo emission. Beuing *et al.* exclude cluster dominant galaxies from their fitting, but not group-dominant galaxies, which may steepen the slope of their $L_X:L_B$ relation.

Despite the corrections described in Section 3.4, we are almost certainly including some data from Beuing *et al.* which are biased by inclusion of extraneous sources or group emission. However, we perform fits which exclude BGGs, and may therefore expect to remove the majority of the most biased points. It is also worth noting that Beuing *et al.* calculate upper limits on X-ray luminosity using a fixed aperture 6 optical half-light radii in diameter, and do not use upper limits for galaxies embedded in bright cluster emission.

Luminosities calculated from *Einstein* data are generally based on considerably larger numbers of counts than those taken from the RASS. They should therefore be somewhat less likely to suffer from the problems described above. Unfortunately the poorer spatial resolution of the IPC compared to the PSPC makes confusion of close sources more likely, particularly if the sources are relatively faint. Our comparisons in Section 3.4 show that there is no major systematic offset, but there are still likely to be individual galaxies which have been over-estimated.

In our own analysis of PSPC pointed data we have attempted to avoid these problems where possible. Confusion between close sources should be minimal, as we work with considerably larger numbers of counts. We have attempted to remove at least a part of any contaminating group or cluster emission where possible, reducing the degree to which group and cluster gas biases the $L_X:L_B$ relation. However, without two dimensional fitting of the surface brightness profile of the group and galaxy it is not possible to completely remove this contamination, so

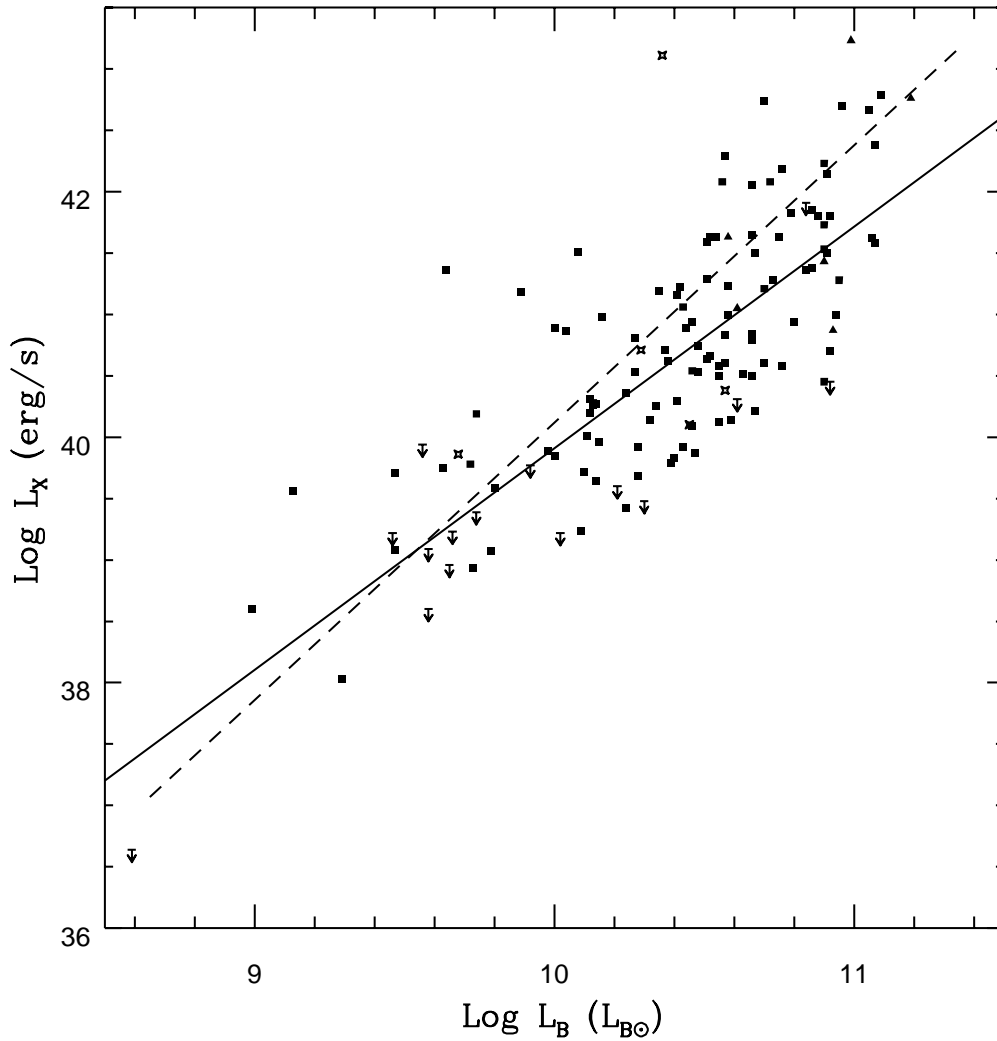


Figure 3.5: $\text{Log } L_X$ vs $\text{Log } L_B$ for our sample of 136 early-type galaxies from *ROSAT* PSPC pointed observations. Filled squares are early-type galaxies, triangles represent cluster central galaxies and stars AGN. The solid line is our best fit to the data, excluding AGN, dwarfs and cluster central galaxies. The dashed line is the Beuing *et al.* best fit relation.

we must expect to over-estimate some of the luminosities.

In order to examine our data for possible biasing effects we have fitted an $L_X:L_B$ relation for a subset of the catalogue, made up of those galaxies whose X-ray luminosities are the product of our own analysis of PSPC data. Figure 3.5 shows a plot of $\text{Log } L_X$ vs $\text{Log } L_B$ for this sample. For the complete subset, the statistical tests described in section 3.5 show a probability $>99.99\%$ that a correlation exists, and give slopes of 1.73 ± 0.12 (EM) and 1.71 ± 0.13 (BJ) respectively. The standard deviations about the two regressions are $\sigma_{EM}=0.74$ and $\sigma_{BJ}=0.69$.

As discussed in Section 3.7.1, fitting a line to the complete sample does not provide a good

estimate of the true $L_X:L_B$ relation for the sample, as there are a number of unusual objects included. Removing cluster central galaxies, AGN and dwarf galaxies steepens the slope to 1.81 ± 0.15 (EM) or 1.79 ± 0.15 (BJ), with $\sigma_{EM}=0.61$ and $\sigma_{BJ}=0.59$. The EM fit is shown as the solid line in Figure 3.5.

For comparison the $L_X:L_B$ relation of Beuing *et al.* (1999), which has a slope of 2.23 ± 0.13 , is shown. It is clear that the Beuing *et al.* line is not a particularly good fit to the data. However, our fitted slopes are similar to the slope found by Fabbiano *et al.* (1992) for their sample of elliptical galaxies observed with *Einstein*. We believe that these differences in slope are caused by the different analysis strategies adopted for the three samples, and that the steeper slope of the Beuing *et al.* data may be caused by cases of over-estimation of L_X , as discussed above.

3.7.3 The Discrete Source Contribution

The X-ray emission from early-type galaxies is thought to be produced by a combination of sources. These can be generalised into two categories; hot gas and discrete sources. Discrete sources (*e.g.* X-ray binaries, individual stars, globular clusters) are essentially stellar in origin and so the total X-ray luminosity from these sources should scale with L_B . This can be seen in the $L_X:L_B$ relation of Beuing *et al.* (1999), which at low L_B agrees well with discrete source estimates with slope unity. However, the normalisation of these discrete source estimates is not well defined – those quoted in Beuing vary over at least an order of magnitude, and only the highest is ruled out by that data set.

Most previous estimates of the discrete source contribution to L_X (hereafter L_{dscr}) are based on a small number of relatively nearby objects. For example, Trinchieri & Fabbiano (1985) base their estimates on *Einstein* observations of M31, Forman *et al.* (1985) use Centaurus A, while Irwin & Sarazin (1998b) use M31 and NGC 1291. Estimates based on early-type galaxies are rare, as it is difficult to separate a discrete source component from the overall emission. One simple method to avoid this problem is employed by Ciotti *et al.* (1991), who fit a slope unity line to the lower envelope of data from Canizares *et al.* (1987). This gives an estimate of $\log(L_{dscr}/L_B) = 29.45 \text{ erg s}^{-1} L_{B\odot}^{-1}$ (using our pseudo-bolometric bandpass and model). This value has been shown to be a good estimate of the lower bound of the Beuing *et al.* sample, and is also a reasonably good match to our data. However, this does not necessarily imply that the

value is a good estimate of the mean L_{dscr} . To produce more accurate estimates we need either a large sample of data from late-type galaxies which have little or no hot gas emission, or much more detailed spectral studies of early-type objects.

X-ray emission from late-type galaxies

Late-type galaxies are known to be sources of X-ray emission, though not of the same magnitude as elliptical and S0 galaxies (*e.g.* Fabbiano et al. 1992). Early studies (Fabbiano & Trinchieri 1985) showed that there is a strong correlation between the X-ray and optical emission, giving rise to an $L_X:L_B$ relation similar to that observed for early-type galaxies. However, in late-type galaxies this relation has a much shallower slope than in early-types. Most studies find this slope to be $\gtrsim 1$.

The most common explanation for this relation is that the X-ray emission observed is produced mainly by X-ray binaries and hot stars. As these sources are stellar in origin, their numbers should be directly related to the optical luminosity of the galaxy, and the $L_X:L_B$ relation for spirals should have a slope of $\simeq 1$. Emission from other sources, such as hot gas, may not be so directly linked to stellar populations. If spiral galaxies contain significant amounts of hot gas as well as discrete sources, we might expect to see evidence of this gas in the $L_X:L_B$ relation. Assuming the gas to have a similar source and behaviour to that found in elliptical galaxies, we could expect a relation between $\text{Log } L_X$ and $\text{Log } L_B$ with a slope greater than unity.

Detailed spectral studies of the X-ray emission from nearby spiral galaxies (*e.g.* Turner et al. 1997; Read et al. 1997; Ehle et al. 1998) have shown that such a hot gas component is present in some cases. Using a large sample of galaxies observed with *Einstein*, Kim et al. (1992) showed that this ISM component was mainly associated with early-type (Sa) spirals, and that there was a succession of spectral properties with morphology. Elliptical and E/S0 galaxies were mainly dominated by gaseous emission, S0 galaxies had a somewhat harder spectrum, Sa spirals were harder still with the hard component dominating, and late-type spirals showed little sign of a hot ISM. This points toward the hot gas being associated with the bulge of the galaxy; Sb and Sc galaxies have small bulges and little or no hot gas, whereas ellipticals are essentially all bulge, and have large gaseous halos.

More recent studies have confirmed the lack of significant halos around spiral galaxies. Benson et al. (1999) used *ROSAT* observations of three massive edge-on spiral galaxies to look for large scale extended emission predicted by galaxy formation models to arise as hot gas cools to form the galaxies' disks. They found no evidence for X-ray halos of the extent seen around early-type galaxies. Studies of diffuse emission within or near spiral galaxies suggest that hot gas does not extend far beyond the stellar body of the galaxy except in the case of starburst galaxies (Read et al. 1997). We have avoided all such galaxies, as the contribution to the X-ray emission from active star-formation and the associated galactic winds would seriously affect our results.

To define an $L_{dscr}:L_B$ relation for spirals we tried two approaches. The first was to search the literature for attempts to separate gaseous and discrete emission in spiral galaxies. The second was to obtain a large sample of spiral galaxies observed in X-rays and split this into subsamples by morphological type. The hierarchical merger scenario implies that galaxies with small bulges should have minimal X-ray emission from hot gas, so there should be a trend for a lower and less steep $L_X:L_B$ relation for later-type spirals.

Nearby spiral galaxies sample

We have collected L_X values for 13 spirals, and normalised them to bolometric luminosities. The following list gives details of these sources:

- Nine galaxies from Read et al. (1997). The objects chosen are those which are not listed as starburst galaxies in the paper, NGC 55, NGC 247, NGC 300, NGC 598, NGC 1291, NGC 3628, NGC 3628, NGC 4258 and NGC 5055. The X-ray luminosities given are for emission from the galaxies after any resolved point sources had been removed.
- M83, from Ehle et al. (1998). The L_X value given is for the harder of two diffuse emission components fitted, thought to represent unresolved discrete sources in the disk and bulge. Resolved point sources were removed before fitting.
- Centaurus A (NGC 5128), from Turner et al. (1997). The L_X value given is for the 5 keV component of a two temperature Raymond & Smith plasma model fitted to the diffuse emission from the galaxy. Regions contaminated by the nucleus and associated jet were

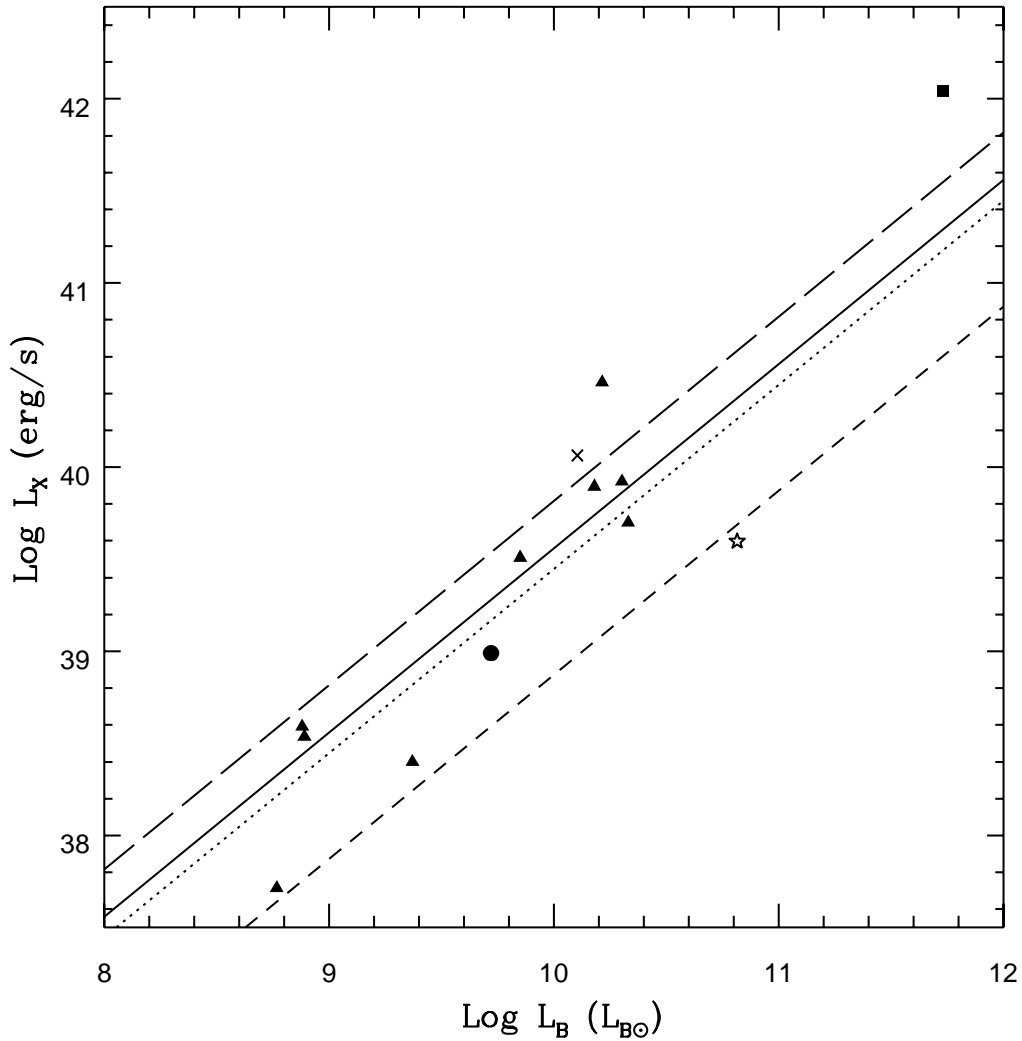


Figure 3.6: Plot of $\text{Log } L_X$ vs $\text{Log } L_B$ for a sample of nearby late-type galaxies. Solid triangles represent data from Read, Ponman & Strickland (1997), the square M83, the cross NGC 4631, the star Centaurus A, and the circle the bulge of M31. The solid line is the best fit slope unity line, with the other lines showing estimates of L_{dscr} from the literature. The dotted line is the estimate of Ciotti *et al.* (1991), the short dashed is taken from Forman *et al.* (1985) and the long dashed is from Canizares *et al.* (1987)

removed, but some point source emission was included.

- NGC 4631, from Fabbiano & Trinchieri (1987). The value used is that given for a soft (0.2-0.8 keV) component associated with the disk of this galaxy.
- The bulge of M31, from Irwin & Sarazin (1998a).

In most of the cases listed above, we have selected the component of emission which is most likely to represent the discrete sources in each galaxy, and excluded components corresponding

Group	N	Unit slope	Variable slope	
		intercept	slope	intercept
Sa	90	30.59 ± 0.11	2.14 ± 0.31	19.07 ± 3.07
Sb	74	30.22 ± 0.09	1.14 ± 0.29	28.77 ± 2.90
Sc	98	30.12 ± 0.06	1.38 ± 0.16	16.35 ± 1.60

Table 3.3: Slopes and intercepts of four morphological subsamples selected from Fabbiano, Kim & Trinchieri (1992)

to gaseous emission. However, we have also excluded a number of resolved point sources, which could be a part of the discrete source population. To be resolved by the instruments used in these studies, the point sources must be highly luminous. At worst, this suggests that they might be AGN or bright transient sources. At best they could be unusually powerful LMXBs, or possibly black hole binaries. We have decided to exclude these sources to avoid the possibility of contaminating the sample with emission from objects which are not part of the population in which we are interested.

The results are shown in Figure 3.6. IRAF survival analysis tasks were then used to fit lines to these points, both with a fixed slope of unity and with the slope allowed to vary. Using the Kaplan-Meier estimator, we found the intercept of the slope unity line to be 29.56 ± 0.13 . Fitting of a variable slope line with the EM algorithm gave a slope of 1.21 ± 0.15 and an intercept of 27.51 ± 1.44 . The fixed slope line is plotted on Figure 3.6, as well as three estimates of discrete source emission taken from Ciotti et al. (1991), Forman et al. (1985) and Canizares et al. (1987). Our line agrees within errors with that of Ciotti *et al.* .

Morphologically defined samples

Working with the large spiral sample of Fabbiano *et al.* (1992) we define three morphological subsets; Sa, Sb and Sc. Results from fits to the $L_X:L_B$ properties of these subsets with fixed (unity) and variable slopes are shown in Figure 3.7 and listed in Table 3.3. It can be seen that there is a distinct difference between the earlier-type spirals in group 1, and the later types in groups 2 and 3. Therefore, it seems that these results support the idea that X-ray gas luminosity is correlated with bulge size, though the effect is not large.

As a check of this result we have also carried out fits to samples of spiral galaxies taken from the catalogue of Burstein et al. (1997). This catalogue, although it contains a larger number

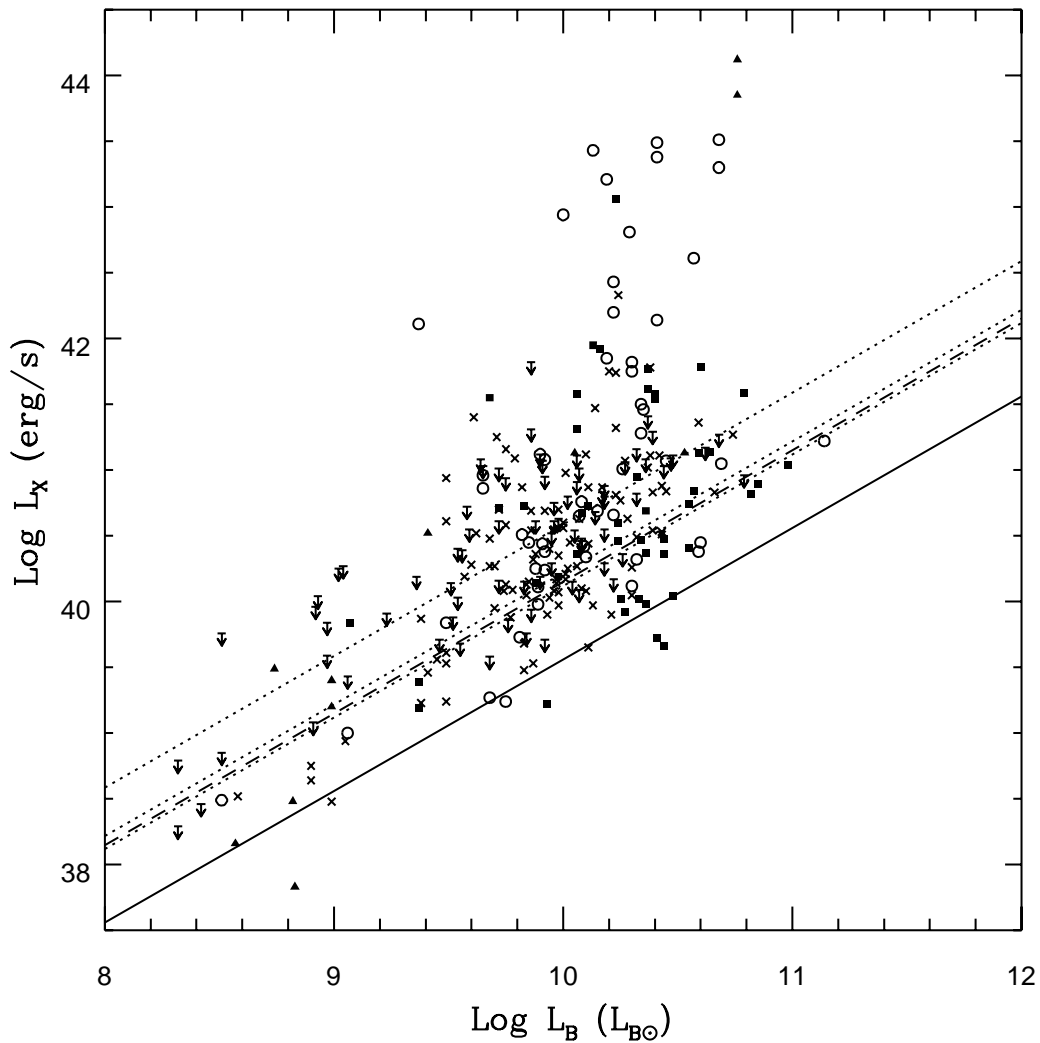


Figure 3.7: Plot of $\text{Log } L_X$ vs $\text{Log } L_B$ for morphological subsets of late-type galaxies from Fabbiano, Kim & Trinchieri (1992). Circles are Sa, squares Sb, crosses Sc, and triangles Sd and Irregular galaxies. Upper limits from all classes are shown as arrows. The solid line is the same as that shown in Figure 3.6, while the dotted lines are slope unity fits to the three subclasses discussed in the text. The dashed line corresponds to the slope unity fit to the data below $\text{Log } L_B = 9.9 L_{B\odot}$. See text for further details.

of galaxies than that of Fabbiano *et al.*, is dominated by upper limits and uses an average of three spectral models to convert count rates to fluxes. We have not therefore converted it to our waveband and model, but have instead simply compared general trends in the results with those we find using the Fabbiano *et al.* data. Fitting lines of unit slope to Sa, Sb and Sc subsamples we find a similar trend in relative normalisation; the Sa sample has an intercept significantly above either of the other subsets.

The line fits to the Fabbiano *et al.* data and the data values themselves can be seen in Figure 3.7. For comparison the fit to the nearby spiral data discussed above is also shown. It

Group	N	Unit slope	Variable slope	
		intercept	slope	intercept
Low L_B	115	30.15 ± 0.06	1.01 ± 0.13	30.34 ± 1.18
High L_B	164		2.03 ± 0.38	20.13 ± 3.93

Table 3.4: Slopes and intercepts for the high ($\text{Log } L_B > 9.9 L_{B\odot}$) and low luminosity subsets.

is clear that even the lowest of the fits to the Fabbiano et al. (1992) data is considerably higher than that to the nearby galaxies, presumably owing to the removal of point sources and (in some cases) gaseous emission from the nearby spiral data.

In Figure 3.7, it can be seen that as L_B increases, the data points for all the subclasses diverge more and more from the slope unity lines. We therefore decided to split the sample into two new subsets. These are the low luminosity ($\text{Log } L_B \leq 9.9 L_{B\odot}$) and high luminosity ($\text{Log } L_B > 9.9 L_{B\odot}$) subsets. Line fits for each are shown in Table 3.4.

These figures show clearly that there is a large difference in the $L_X:L_B$ relation for low and high luminosity spirals. The high L_B subset has a slope similar to that found for elliptical galaxies, while the low L_B sample slope is very close to 1. The slope unity fit to the low L_B sample is shown in Figure 3.7 as a dashed line.

L_{dscr} from early-type galaxies

In order to directly measure L_{dscr} from early-type galaxies, it is necessary to distinguish between emission from hot gas and the contribution of the discrete source population. Whereas X-ray bright galaxies are usually fit using a single component MEKAL or Raymond & Smith model with $kT \sim 1$ keV, X-ray faint galaxies have been shown to be better fit by two component models (Fabbiano et al. 1992; Pellegrini 1994). These consist of a high temperature ($kT \sim 10$ keV) component generally associated with X-ray binaries and a low temperature component with $kT \sim 0.2$ keV. A number of possible sources for this low temperature component have been suggested (*e.g.* Irwin & Sarazin 1998b), but LMXBs again seem to be the most likely source (Irwin & Sarazin 1998a; Irwin et al. 2000). The advent of *Chandra* has made it possible to resolve significant numbers of point sources in nearby galaxies. Observations of NGC 4697 (Sarazin et al. 2000) and NGC 1553 (Blanton et al. 2001) reveal considerable numbers of point sources with hard spectra. Blanton *et al.* show that, at least in the case of NGC 1553, the emission from

resolved point sources is best fit using a model which includes a low temperature component. From the Blanton *et al.* results we estimate that the total flux from discrete sources, excluding the AGN, is $8.58 \times 10^{-13} \text{ erg s}^{-1} \text{ cm}^{-2}$ in the 0.3-10 keV band. Using our distance and L_B for NGC 1553 gives $\text{Log } L_{dscr}/L_B = 29.44 \text{ erg s}^{-1} L_{B\odot}^{-1}$. As we do not have the exact details of the Blanton *et al.* best fit model, we cannot convert this to our own model and waveband, but any correction should be small, as the *Chandra* waveband extends to much higher energies than that of *Einstein* or *ROSAT*. Assuming a 20% conversion factor from the *Chandra* band into our own produces $\text{Log } L_{dscr}/L_B = 29.52 \text{ erg s}^{-1} L_{B\odot}^{-1}$, very similar to our other estimates. However, both NGC 1553 and NGC 4697 have low X-ray luminosities, and relying purely on the lowest luminosity galaxies for measurements of L_{dscr} may be unwise. Irwin & Sarazin (1998b) note that small fluctuations in the discrete source populations in these objects could cause a large degree of scatter in L_X , as their total X-ray luminosities are small. This is confirmed by comparison of the luminosity functions of the point source populations of four galaxies observed by *Chandra* (Kraft *et al.* 2001). These show differences in L_{dscr} of a factor ≥ 4 between the galaxies. Clearly estimates based on large samples are likely to be more reliable.

With high quality *ASCA* data, it is possible to fit high luminosity galaxies using both a 1 keV gaseous halo and a high temperature discrete component (*e.g.* Matsumoto *et al.* 1997). The most recent study of this sort (Matsushita *et al.* 2000) fits a 10 keV bremsstrahlung model to 27 galaxies, excluding those which show signs of harbouring low luminosity AGN, producing a value of $\text{Log } L_{dscr}/L_B = 29.41 \text{ erg s}^{-1} L_{B\odot}^{-1}$ (converted to our passband and model). Given the quality of the data used, this is probably the most reliable value available from studies of elliptical galaxies. Its only drawback is that it does not take into account the effects of a low temperature component in LMXB emission. Such a component is unlikely to be detected by *ASCA*, which has a relatively low collecting area and poor spectral capabilities below 1 keV. Assuming the *Chandra* observation of Sarazin *et al.* to be representative, we expect that the effects of such a component would be strongly affected by hydrogen column, but would only increase L_{dscr} by up to a factor of two (i.e. 0.3 dex).

One other interesting method of estimating the discrete contribution is that of Brown & Bregman (2001). This involves fitting the surface brightness profiles of seven elliptical galaxies, representing the hot gas component with a King profile and the discrete sources with a de

Vaucouleurs $r^{1/4}$ profile. Using the fitted normalisation of the de Vaucouleurs component, Brown and Bregman find a median best fit $\text{Log } L_{dscr}/L_B = 28.51 \text{ erg s}^{-1} L_{B\odot}^{-1}$, with a 99% upper limit of $\text{Log } L_{dscr}/L_B = 29.21 \text{ erg s}^{-1} L_{B\odot}^{-1}$. Although this method should in principle be able to produce similar results to 2-component spectral fitting, these values are somewhat lower than those found by other methods. This may be a product of the small size of the sample, or of assuming circular symmetry to allow 1-dimensional profile fitting. It also remains to be established how well the discrete X-ray source population is modeled by a de Vaucouleurs profile which fits the optical profile. The excellent spatial resolution of *Chandra* should allow this question to be answered in the near future.

Summary

Possible choices for $\text{Log } L_{dscr}$ (in units of $\text{erg s}^{-1} L_{B\odot}^{-1}$) are then as follows:

- Nearby late-type galaxies sample intercept = 29.56 ± 0.13
- Sc galaxy sample intercept = 30.12 ± 0.06
- Low L_B sample intercept = 30.15 ± 0.11
- Ciotti et al. (1991) estimate = 29.45
- Matsushita et al. (2000) hard component = 29.41
- Blanton et al. (2001) *Chandra* estimate from NGC 1553 $\simeq 29.52$
- Brown & Bregman (2001) 99% upper limit ≤ 29.21

These values are compared with our data in Figure 3.8.

As the two higher values are derived from samples in which L_X may include emission from gas and bright point sources, they do not seem reliable options. The Brown & Bregman value is considerably lower than the other estimates, particularly as it is an upper limit. The values from Ciotti *et al.*, Matsushita *et al.*, Blanton *et al.* and the nearby galaxies sample agree within errors, and would seem to be a reasonable choices. A value of $\text{Log } L_{dscr}/L_B = 29.5 \text{ erg s}^{-1} L_{B\odot}^{-1}$ lies between the four and is close to being the average. This value is marked in Figure 3.8 as a solid line. This value cannot be considered to be a “hard” lower limit; as the plot shows, a

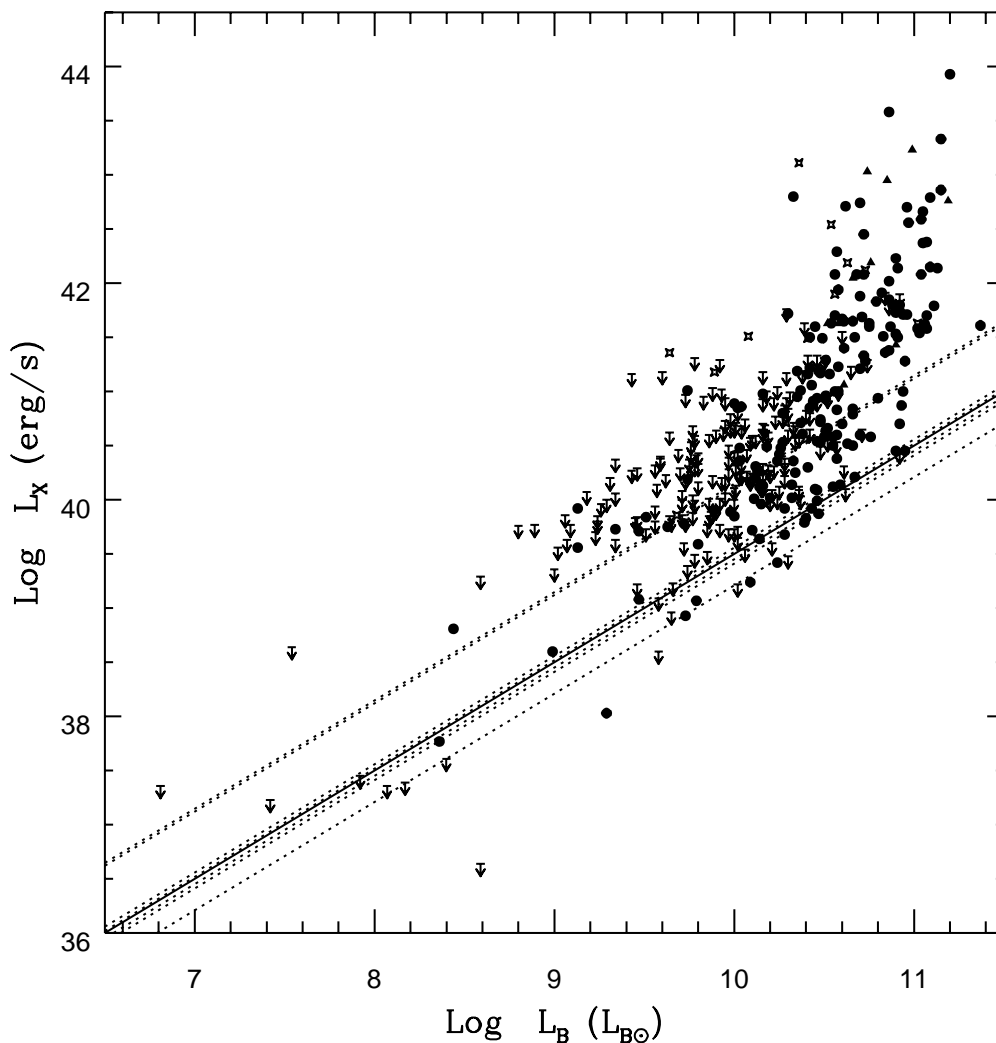


Figure 3.8: Plot of our early-type galaxies with L_{dscr} estimates marked. The dotted lines represent the seven estimates listed in section 3.7.3, and the solid line marks $\text{Log } L_X/L_B = 29.5 \text{ erg s}^{-1} L_{B\odot}^{-1}$. Point symbols are the same as those in Figure 3.3.

number of our data points lie below this line. For dwarf galaxies ($\text{Log } L_B < 9.0 L_{B\odot}$), we may expect to see quite large variations in L_X . Each dwarf needs only a small number of LMXBs to produce the expected luminosity of $10^{36-38} \text{ erg s}^{-1}$, so minor variations in population can produce large changes in integrated luminosity. In larger galaxies this statistical variation is less important, but some degree of scatter in L_X may be expected to result from factors such as different galaxy evolutionary histories. It is also worth noting that, as discussed in Section 3.3, we expect to underestimate the luminosity of galaxies whose X-ray emission is primarily from LMXBs, owing to our assumption of a 1 keV MEKAL model. With the exception of NGC 5102, all our detected non-dwarf galaxies are within a factor of three of our L_{dscr} estimate. All upper

limits are also within this range, although NGC 1375 has a luminosity of almost exactly $L_{dscr}/3$. Given the factor of two expected from underestimation of L_X in these galaxies and the factor of four variation in L_{dscr} found by Kraft et al. (2001), we conclude that our data are consistent with our estimate of L_{dscr} , within the expected errors.

The L_X - L_{dscr} : L_B relation

Using our value of L_{dscr} , we can now examine how removing stellar emission affects our L_X : L_B relation. This should provide us with a more accurate measure of the relation between the luminosity of the galaxies' gaseous halos and their optical luminosity. As we expect a real variation of a factor ~ 4 in L_{dscr} between galaxies, we cannot simply subtract the mean expected L_{dscr} from all values of L_X . To do so would produce extremely low values of L_X for galaxies with total luminosities similar to L_{dscr} , strongly biasing any fits. We have therefore removed all galaxies which have L_X values within a factor of 4 of L_{dscr} , and subtracted the mean expected L_{dscr} from the remainder. Excluding AGN, BCGs and galaxies with $\text{Log } L_B < 9 L_{B\odot}$, this leaves us with a total sample of 257 points, of which 136 are upper limits. Fitting this dataset we find slopes of 2.03 ± 0.1 (EM) and 2.00 ± 0.13 (BJ). The standard deviation about the regression line is 0.58 in both cases. If we further exclude galaxies to form a very conservative sample as described in Section 3.7.1, the slopes of the fits are lowered to 1.63 ± 0.13 (EM) and 1.60 ± 0.14 (BJ). The data and these fits are shown in Figure 3.9.

These fits are very similar to those produced by fitting the L_X : L_B relation to the sample as a whole (see Table 3.6 for a comparison). This is to be expected, as although L_{dscr} is comparable to the L_X/L_B values of some of the galaxies, the majority have luminosities inconsistent with X-ray emission from discrete sources alone. As these galaxies are dominated by gas emission, subtraction of the discrete source contribution has little effect on their overall luminosity. In order to test the robustness of this result, we also fitted samples based on excluding galaxies with X-ray luminosities within factors of 2 and of 6 of L_{dscr} . In the latter case, the slopes are slightly steeper when excluding AGN, BCGs and dwarfs (~ 1.9) and slightly shallower for the more conservative sample (~ 1.5). This is likely to be an effect of the smaller number of data points (136) and larger numbers of upper limits (97). However, when we use a factor of 2 the slopes are less well defined; for the sample excluding AGN, BCGs and dwarfs we find slopes of

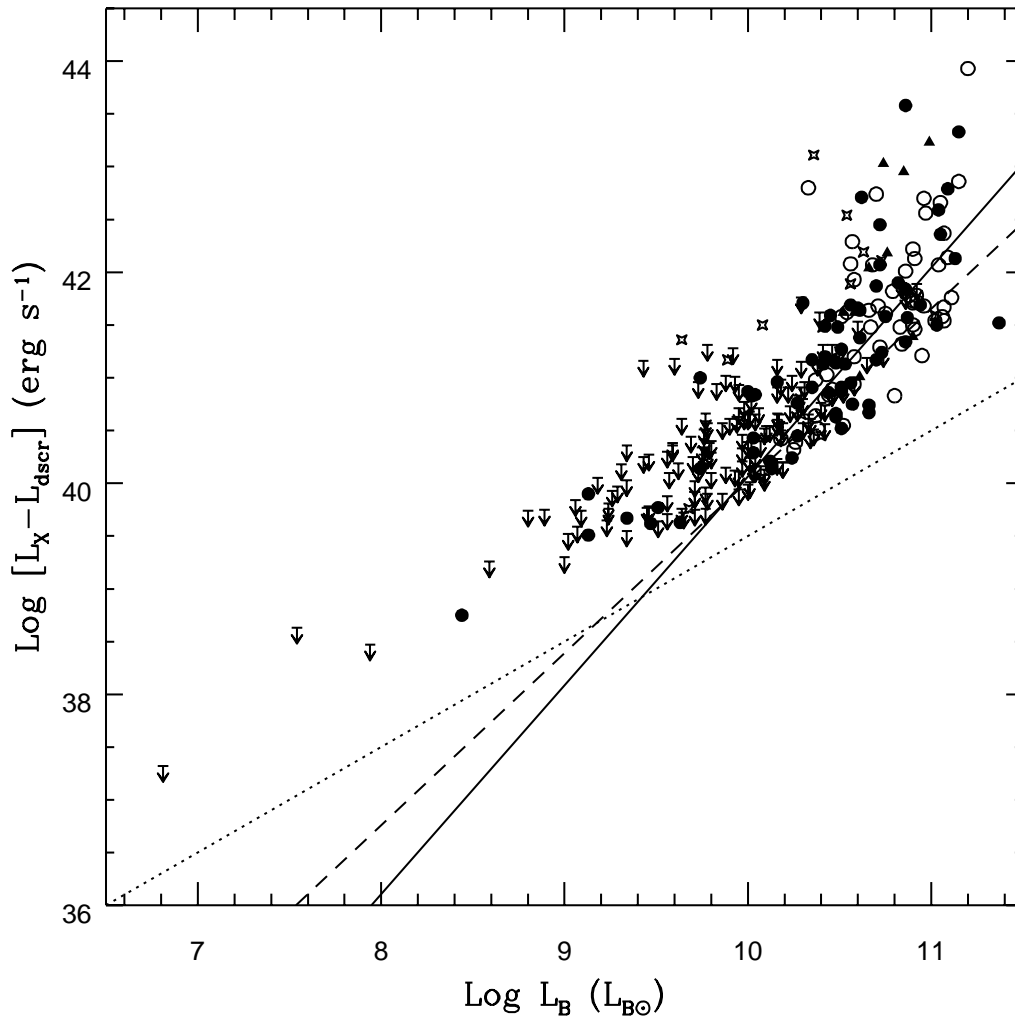


Figure 3.9: $\text{Log} [L_X - L_{dscr}]$ against $\text{Log} L_B$ for all galaxies in our main catalogue with $\text{Log} L_X/L_B > 30.1$ ($4 \times L_{dscr}$). Open circles are BGGs, triangles are BCGs, stars are AGN, filled circles are normal detected galaxies and arrows are upper limits. The Solid line is the best fit to the sample excluding AGN, BCGs and dwarf galaxies. The dashed line is the best fit to a very conservative sample which also excludes BGGs, galaxies at a distance > 70 Mpc, NGC 5102 and NGC 4782. The dotted line shows our estimate of $L_{dscr}/L_B 29.5 \text{ erg s}^{-1} L_{B\odot}^{-1}$.

2.14 ± 0.11 (EM) and 2.31 ± 0.14 (BJ). For the conservative sample, the slopes are again shallower, but still not in good agreement, with values of 1.61 ± 0.14 and 2.08 ± 0.19 . As these datasets are similar in size to the corresponding samples used in fitting the $L_X:L_B$ relation, this scatter is probably a product of the underlying distribution rather than an effect of subtracting L_{dscr} .

Figure 3.4 (Section 3.6) shows that at low L_B the slope of the $L_X:L_B$ relation breaks and becomes shallower. A possible explanation for this is that the observed X-ray luminosities are the result of a combination of emission from discrete sources and hot gas. A break in the slope would

then suggest that the shallower section is dominated by the discrete sources while the steeper section is more influenced by gas emission. Similarly, the lowest binned point in Figure 3.4 will have an X-ray luminosity dominated by discrete source emission, whereas the fit lines will describe the relation for gas emission. If this is the case, then subtracting the mean value of L_{dscr} expected for the lowest bin should move the point downwards, into agreement with the line fits. We calculate that the mean value of L_X^{gas} for the bin is $\text{Log}(L_X - L_{dscr}) = 38.96 \text{ erg s}^{-1}$, which is in marginal agreement, at the high L_B end of the bin, with the EM fit. However, it is important to note that we expect to underestimate the luminosities of galaxies which are dominated by discrete source emission by a factor of ~ 2 , due to our use of an inappropriately soft spectral model. This may mean that the mean L_X value calculated for the bin is also underestimated. It may also be important to take into account the expected variations in L_{dscr} between galaxies. Although we expect a scatter of a factor of ~ 4 , some of the galaxies in this low L_B bin have very low X-ray luminosities, which could be significantly affected by small differences in the number of X-ray binaries they contain. We cannot therefore be certain, on the basis of the data presented here, that the break in the relation is caused by the change from gas dominated to discrete source dominated galaxies.

3.7.4 Environmental Dependence of L_X/L_B

Although there are several suggested mechanisms by which the environment of a galaxy can affect its X-ray properties, the actual role these effects play is unclear. The observational evidence is conflicting and often difficult to interpret.

White & Sarazin (1991) found that for a sample of early-type galaxies studied by *Einstein*, galaxies with $\text{Log } L_X/L_B < 30 \text{ (erg s}^{-1} L_{B\odot}^{-1})$ had $\sim 50\%$ more neighbours than X-ray bright galaxies. They attributed this to ram-pressure stripping, which would be expected to reduce L_X more in higher density environments. An opposite view was presented by Brown & Bregman (2000), who found that L_X/L_B increased with environmental density. Their explanation was that for the majority of galaxies (with the possible exception of those in the densest environments) ram-pressure stripping is a less important effect than the stifling of galactic winds by a surrounding intra-group or -cluster medium. In this model, the IGM/ICM encloses the galaxy, increasing the gas density of its halo and therefore its X-ray luminosity.

Brown & Bregman (1999) claimed an environmental dependence based on a correlation between L_X/L_B and Tully density parameter ρ (Tully 1988) for their 34 galaxies. However, Helsdon et al. (2001) show that group-dominant galaxies, of which there are several in Brown & Bregman's sample, often have X-ray luminosities which are governed by the properties of the group rather than the galaxy. Their high luminosities are more likely to be caused by a group cooling flow than by a large galaxy halo. Once these objects are removed from consideration, the correlation between L_X/L_B and ρ is weakened to a $\sim 1.5\sigma$ effect (Helsdon et al. (2001)).

Our larger sample of galaxies gives us the opportunity to study this correlation over a wide range of L_X , L_B and environmental density. In Figure 3.10 we therefore plot L_X/L_B against ρ for 196 of our galaxies listed in the Tully catalogue.

Galaxies in this plot are subdivided into group, cluster and field samples. Cluster membership was based on the Abell et al. (1989) and Faber et al. (1989) catalogues while group membership was taken from Garcia (1993). In total, this gives 50 cluster galaxies and 113 group galaxies. Brightest Group Galaxies were also taken from Garcia (1993) and it is important to remember that these objects are only brightest optically, not necessarily the dominant galaxy at the centre of the group or group X-ray halo. However, we believe that the majority are actually group-dominant galaxies. The group subset contains 37 BGGs. The remaining 33 galaxies not listed in the cluster or group catalogues were assumed to lie in the field. This is probably the weakest classification and is likely to be contaminated to some extent with galaxies at the edges of clusters and groups.

The plot shows no obvious trend, but to check for weak correlations we used the statistical tests described in section 3.5. No trend was found in the sample as a whole, nor in any of the subsamples. We also calculated mean L_X/L_B values for each of the subsamples, excluding all AGN, BCGs and dwarf galaxies. These values are shown in table 3.5. The field, group and cluster subsamples have similar mean values, while the BGG subsample has a slightly larger mean L_X/L_B , as might be expected from the previous results.

The lack of a general correlation is surprising, as the previous studies suggest we should find at least a weak trend. As we are using the same method as Brown & Bregman, we decided to check for a correlation in their sample of galaxies using our own X-ray luminosities. These data (excluding galaxies identified as BGGs in Helsdon *et al.*) are plotted in Figure 3.11.

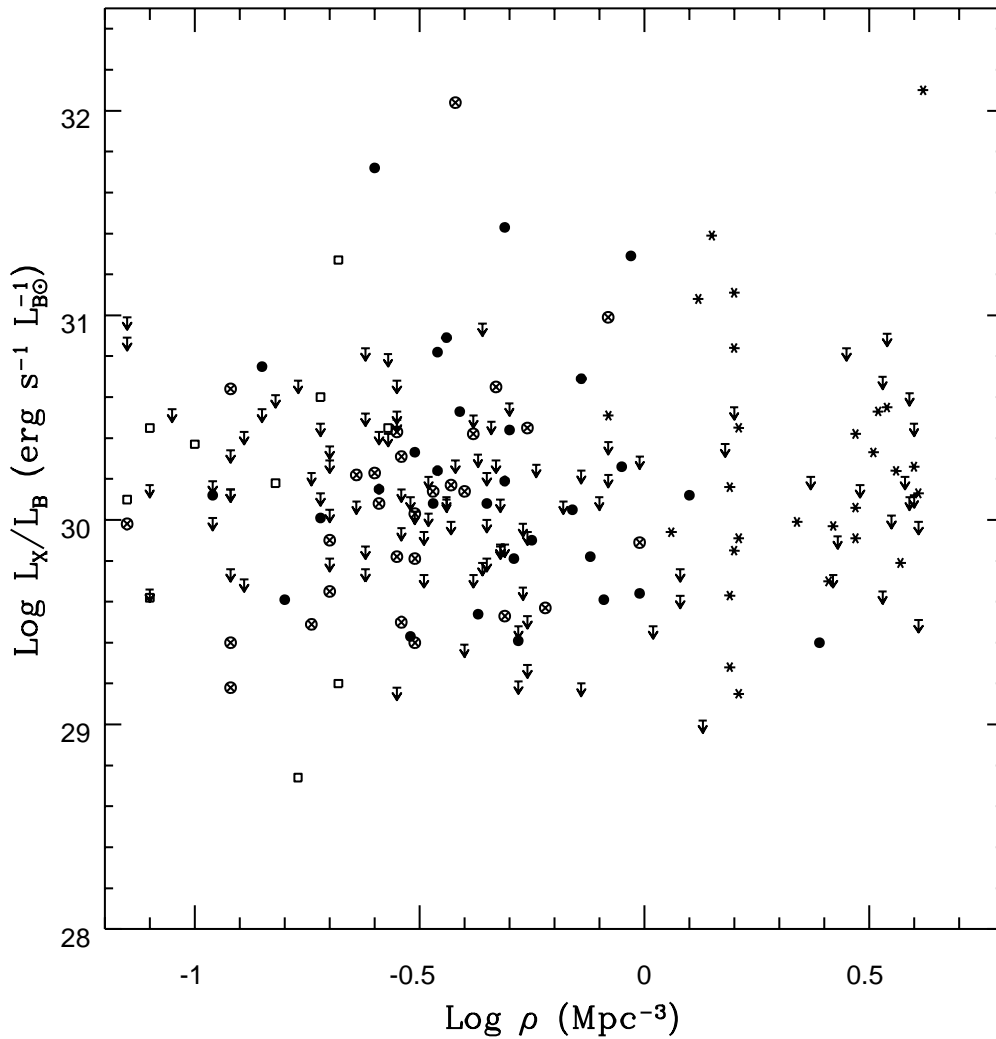


Figure 3.10: Plot of normalised X-ray luminosity against environmental density. Open squares are field galaxies, filled circles non-central group galaxies, crossed circles BGGs, asterisks cluster galaxies and arrows upper limits of all types.

Although there is more scatter in L_X/L_B than seen in Brown & Bregman's plot, a trend for increasing L_X/L_B with environmental density is clear. Statistical tests show the correlation to be at least 97% (2.5σ) significant, with a best fit slope of 0.78 (EM) or 0.75 (BJ). Binning the data in the same ranges as used by Brown & Bregman and Helsdon *et al.* produces the three large crosses in the plot. These also clearly show a trend, despite the fact that the centre and right hand crosses are likely to be biased downwards as the lowest points in these bins are upper limits.

As the trend is seen in this sample of galaxies but not in our more general catalogue, it seems likely that it is a product of the sample selection process. Brown & Bregman's sample is

Subset	mean L_X/L_B	Error
Cluster	29.733*	± 0.094
Field	29.548	± 0.196
Group (total)	29.908	± 0.066
Group (non-BGG)	29.719*	± 0.065
Group (BGG)	29.977	± 0.096

Table 3.5: Mean L_X/L_B values for the environmental subsamples shown in Figure 3.10. Values marked by an asterisk may be slightly biased as the lowest value in the sample was an upper limit.

composed of the 34 optically brightest galaxies chosen from Faber et al. (1989), excluding AGN and dwarf galaxies. The selection of bright galaxies has one clear effect; more than half of their galaxies are BGGs, likely to have unusually high X-ray luminosities. Of the remaining galaxies, three are found in the field, six are in groups and five in clusters. Of the cluster galaxies, the two most X-ray luminous are NGC 1404, a large E1 galaxy in the Fornax cluster, and NGC 4552 (M89), one of the large ellipticals in the Virgo cluster. The high L_X values of these two galaxies and the low L_X value of NGC 5102 have a strong influence on the fitted slope. Indeed, when using our data, their removal eliminates the correlation altogether. NGC 4552 is known to be a Seyfert 2 (Veron-Cetty & Veron 1996), and therefore its X-ray luminosity is likely to be misleading. NGC 1404 may also be an unusual case, as it lies within the X-ray envelope of NGC 1399 and may be interacting with it (Forbes et al. 1998). As mentioned in Section 3.7, NGC 5102 is a recent (~ 400 Myr) post-starburst galaxy and has a population of young blue stars (Bica & Alloin 1987) which may have ‘artificially’ raised its B band luminosity.

3.7.5 The $L_X:L_B$ relation in different Environments

In order to gain another viewpoint on the relation between environment and X-ray luminosity, we decided to examine the $L_X:L_B$ relation in field, group and cluster environments. We split the sample as described above, but no longer limited ourselves to galaxies listed in the Tully catalogue. The sample therefore included all galaxies within $5,500 \text{ km s}^{-1}$ (the limit of the Garcia (1993) group catalogue). The resultant fits are shown in Table 3.6, along with the fits to the field, group and cluster sets. In each case we have removed cluster central galaxies, AGN, dwarf galaxies and galaxies at distances >70 Mpc before fitting. The cluster sample contains

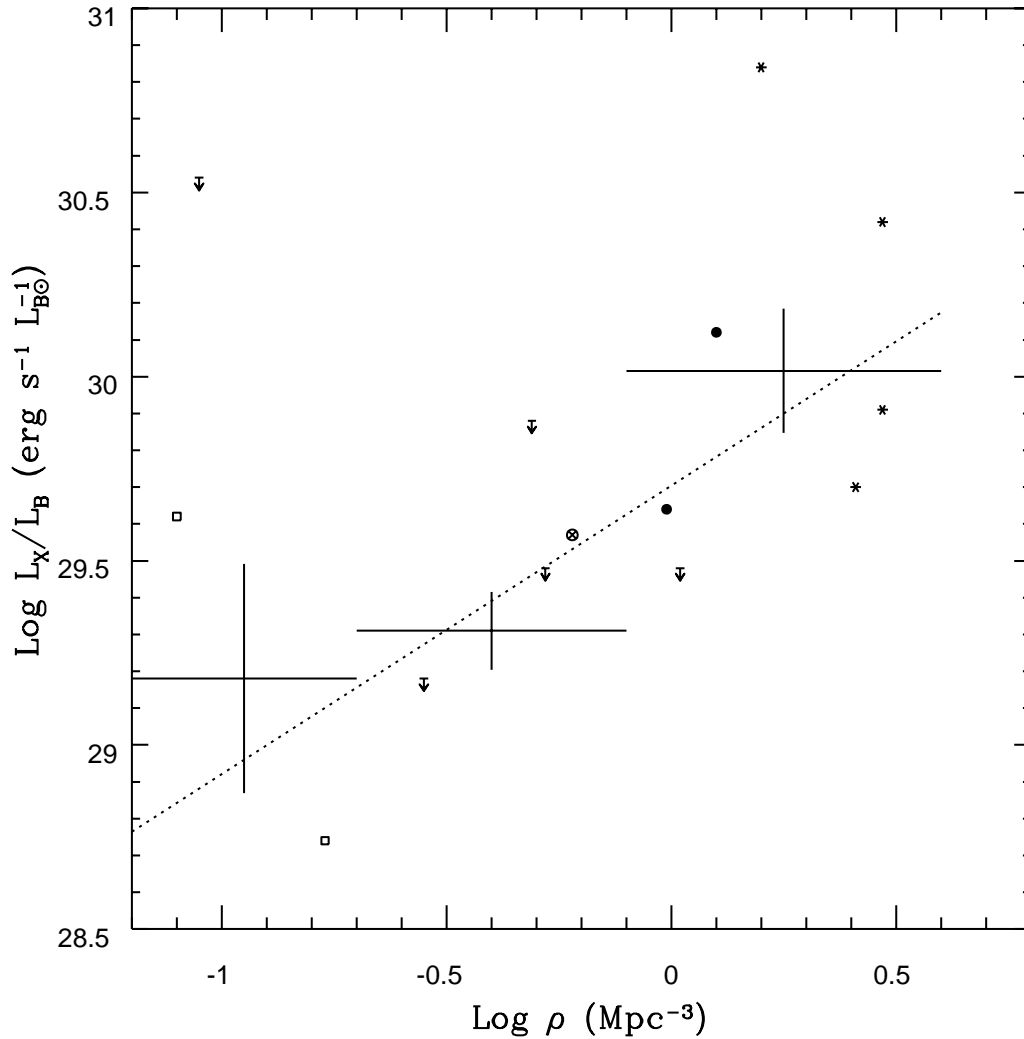


Figure 3.11: Plot of L_X/L_B against ρ for non-BGG galaxies from the sample of Brown & Bregman (1999). L_X/L_B values are from our catalogue, ρ values are from Tully (1988). The dotted line is the best fit to the data, and the large crosses are mean values for the three bins described in the text. Other symbols are the same as in Figure 3.10.

57 objects (of which 36 are upper limits), the field sample 76 objects (55 upper limits) and the group sample 185 objects (85 upper limits). Separating BGGs from the group sample gives a non-BGG sample of 116 objects (69 upper limits) and a BGG sample of 69 objects (16 upper limits).

Figure 3.12 shows plots of the cluster, field and group data with best fit lines. In terms of L_B , it is notable that although the field and group sets cover a similar range, there are very few optically faint cluster galaxies. This is likely to be caused by the difficulty of observing small, X-ray faint galaxies in an X-ray bright ICM. In the field no such problem occurs, and many groups are faint enough to allow such small objects to be observed. Both group and cluster data

Subset	Fit	Slope (Error)	Intercept (Error)
Combined	EM	1.63 (± 0.14)	23.38 (± 1.41)
	BJ	1.94 (± 0.17)	20.13
L_X - L_{dscr}	EM	1.63 (± 0.13)	23.70 (± 1.36)
	BJ	1.60 (± 0.14)	24.11
Cluster	EM	1.77 (± 0.27)	21.91 (± 2.71)
	BJ	1.77 (± 0.29)	21.93
Field	EM	1.62 (± 0.23)	23.58 (± 2.40)
	BJ	1.61 (± 0.26)	23.61
Group (total)	EM	1.92 (± 0.13)	20.56 (± 1.39)
	BJ	1.90 (± 0.16)	20.73
Group (non-BGG)	EM	1.62 (± 0.14)	23.57 (± 1.39)
	BJ	1.59 (± 0.16)	23.85
Group (BGG)	EM	2.58 (± 0.36)	13.60 (± 3.76)
	BJ	2.57 (± 0.40)	13.71

Table 3.6: Best fit $L_X:L_B$ lines for galaxies in field, group and cluster environments. All subsets exclude AGN, BCGs, dwarf galaxies and galaxies at distances > 70 Mpc. The Combined values for the complete sample *excluding BGGs*, and the best fits to the L_X - $L_{dscr}:L_B$ relation are shown for comparison.

Subset	Slope = 1.63	Slope = 1.94
	Intercept (Error)	Intercept (Error)
Combined	23.446 (± 0.048)	20.252 (± 0.054)
Cluster	23.384 (± 0.091)	20.253 (± 0.096)
Field	23.446 (± 0.109)	20.247 (± 0.126)
Group (total)	23.457 (± 0.049)	20.323 (± 0.051)
Group (non-BGG)	23.473 (± 0.062)	20.266 (± 0.069)
Group (BGG)	23.667 (± 0.083)	20.401 (± 0.081)

Table 3.7: Best fit intercepts to $L_X:L_B$ relations with fixed slopes as shown in the table. All values are calculated using the Kaplan-Meier estimator. All subsamples exclude AGN, BCGs, dwarf galaxies and galaxies at distances > 70 Mpc. The Combined subset also excludes BGGs.

show a number of highly X-ray luminous objects, probably giant ellipticals and group or cluster dominant galaxies at the centres of large X-ray halos. In the field, only one galaxy (NGC 6482) has $\text{Log } L_X > 42 \text{ erg s}^{-1}$ and the high end of the $L_X:L_B$ line is sparsely populated. Comparing $L_X:L_B$ slopes shows a similar trend, with the BGG sample producing the steepest slope, then cluster galaxies, non-BGGs and lastly field galaxies with the shallowest relation. The slope of the BGG sample is similar, within errors, to that of the best fit line to the Brown & Bregman sample.

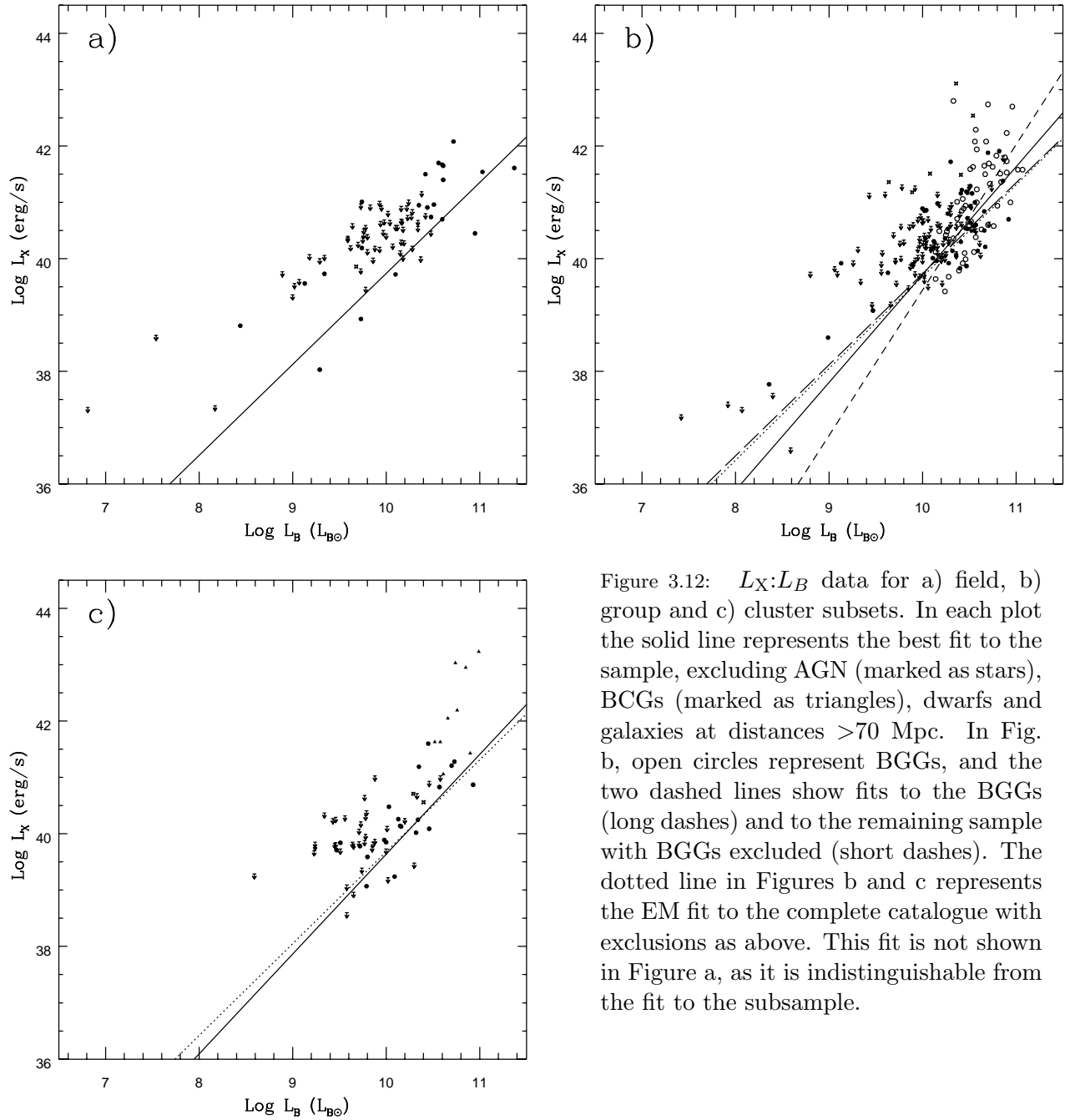


Figure 3.12: $L_X:L_B$ data for a) field, b) group and c) cluster subsets. In each plot the solid line represents the best fit to the sample, excluding AGN (marked as stars), BCGs (marked as triangles), dwarfs and galaxies at distances >70 Mpc. In Fig. b, open circles represent BGGs, and the two dashed lines show fits to the BGGs (long dashes) and to the remaining sample with BGGs excluded (short dashes). The dotted line in Figures b and c represents the EM fit to the complete catalogue with exclusions as above. This fit is not shown in Figure a, as it is indistinguishable from the fit to the subsample.

It is interesting to note that the slopes for the field, cluster and non-BGG group samples are all similar, within errors. Table 3.6 also shows the fits to the catalogue as a whole, excluding AGN, BCGs, BGGs, dwarfs and galaxies at distances >70 Mpc. The EM fit to this supersample agrees with the fits to the three subsamples, and the BJ fit has overlapping errors with the field and cluster subsamples. This suggests that the $L_X:L_B$ relation may be similar for the different environmental subsets when biasing objects are excluded. To further investigate this similarity,

we have fitted fixed slope lines to the field, group, cluster and combined subsets described above. As the EM and BJ algorithms find slopes of 1.63 and 1.94 for the combined subset, we use these values. Table 3.7 shows the resulting intercepts and errors, calculated using the Kaplan-Meier estimator. In both cases, the intercepts for the field, cluster and non-BGG group subsets agree within errors, and also agree with the intercept of the combined subset, whilst the BGG intercept is markedly higher. Our results suggest, then, that with the exception of BGGs, early-type galaxies have a universal mean $L_X:L_B$ relation which is unaffected by environment.

3.8 Discussion and Conclusions

3.8.1 The $L_X:L_B$ Relation for Early-type Galaxies

The slope of the $L_X:L_B$ relation has been the subject of debate for some time. As an indicator of how gas properties change with galaxy mass (and therefore probably with time) it is an important relation to measure precisely. The difficulties associated with accurately measuring a large sample of galaxies and avoiding contamination from other X-ray sources has made this difficult. Our sample has some advantages; we are able to remove some group/cluster contamination from our luminosities, and we have a large enough sample to allow us to exclude problem galaxies without making fitting impossible. We are also able to remove BGGs as well as BCGs, which in principle allows us to define a sample of galaxies unbiased by emission from cluster- or group-scale cooling flows.

Our initial fits agree fairly well with previous estimates of the $L_X:L_B$ relation (Beuing et al. 1999; Donnelly et al. 1990; White & Sarazin 1991), providing evidence that our catalogue is similar to the samples used for those fits. This is to be expected, as our sample was selected in a similar way, and contains galaxies (and in some cases data) in common with these fits. However, the line fits for our sample excluding BGGs are somewhat shallower, particularly if we adopt the precaution of removing galaxies whose distance makes their surroundings uncertain. This change in slope shows that the BGGs are, as predicted, steepening our fits. The implication of this result is that previous $L_X:L_B$ values have also been influenced by the inclusion of BGGs (and possibly BCGs, AGN, etc).

As our data are drawn from samples of galaxies which have been observed and analysed in

different ways, we have considered potential problems arising from their combination. The basic $L_X:L_B$ relation for the *ROSAT* data we have analysed agrees fairly well with that of Fabbiano et al. (1992), but less well with the relation of Beuing et al. (1999). This appears to be caused by the difference in data quality and analysis strategies employed. In particular, the low numbers of counts in RASS images can make separation of close pairs of sources difficult, and also makes it difficult to distinguish between emission associated with a cluster or group and its central galaxy. These difficulties have led to overestimation of some galaxy luminosities in Beuing *et al.* . The corrections described in Section 3.4 should counteract this effect to some extent, but we cannot expect all data points to be completely accurate.

Testing our methods of line fitting suggests that of the available algorithms we are probably using the most appropriate. However, the $L_X:L_B$ relation does not appear to be well described by a single powerlaw fit, even when we remove objects whose luminosities are likely to be dominated by AGN, cooling flows or stellar emission. It seems more likely that it is the product of the combination of discrete source emission, with an $L_X:L_B$ slope of approximately unity, and gas emission with a steeper slope. For the catalogue as a whole, a third, even steeper component is added by the cooling flow enhanced luminosities of group and cluster dominant galaxies. This combination of emission mechanisms may explain the variety of slopes which have been measured in previous studies; the slope will be dependent on the range of L_B used and the number of group/cluster dominant galaxies included. However, the small number of detected galaxies and large expected variations in L_X at $\text{Log } L_B \simeq 9 L_{B\odot}$ make this model difficult to test conclusively with our data.

3.8.2 Environmental Dependence of $L_X:L_B$

The results presented in Sections 3.7.4 and 3.7.5 lead us to three main conclusions:

- There is no strong correlation between L_X/L_B and environmental density (ρ).
- BGGs have a significantly steeper $L_X:L_B$ relation than non-BGG group galaxies.
- Once objects such as BGGs, BCGs, AGN and dwarf galaxies are excluded, the $L_X:L_B$ relation is largely independent of environment.

When considering the first of these points it is important to note that the lack of a trend with ρ does not mean that environment has no effect on the galaxy X-ray properties. There are numerous suggestions of processes which can affect the X-ray halo of a galaxy. Ram-pressure stripping is likely to remove gas from galaxies passing through a dense intra-cluster medium (Gunn & Gott 1972), and turbulent viscous stripping may be as effective in the group environment (Nulsen 1982). It is also likely that the IGM and ICM provide reservoirs of gas which can be captured by slow moving or stationary galaxies. Stifling of galactic winds (Brown & Bregman 2000) may also play an important role in increasing the X-ray luminosity of some galaxies. Our results do not rule out these processes.

The lack of trend does however suggest that, in most environments, none of the processes affecting X-ray halos is dominant. It is possible that the processes interact and counter-balance one another, or that the mechanisms are less efficient than thought and only affect galaxies in the very densest environments. It is also probable that the interactions between group/cluster and galaxy halos are more complex than we have assumed. Observations of one $z \sim 0.83$ cluster (van Dokkum et al. 1999) have provided evidence to support the theory that clusters are products of the merger of previously formed groups of galaxies. The evidence of sub-clumping within local clusters suggests that the halos of these groups can survive the merger process. In this case, ram-pressure stripping of gas from the galaxies within the groups seems unlikely. On the other hand, modeling studies strongly suggest that a field galaxy falling into the dense core of a relaxed cluster is very likely to be ram-pressure stripped of the majority of its gas (*e.g.* Quilis et al. 2000). Whether a galaxy is likely to have been stripped depends not only on its position, but on the state of the cluster when that galaxy entered it, whether it fell in as part of a group and how much of the group halo survived, and probably on many other criteria. A comparison of L_X/L_B with ρ may well be too simple a test to tell us much more about the interactions which take place. It is worth remembering that ρ is a measure of the local density of galaxies, whereas most of the mechanisms mentioned above depend on the gas density encountered by a galaxy over the past few gigayears.

The results of the $L_X:L_B$ fits for galaxies in different environments also suggest that although environment may affect individual galaxies, it cannot change the nature of whole populations. The fact that the $L_X:L_B$ relation is similar in field, group and cluster environments provides

strong evidence that X-ray halos are not radically different in these different environments. It seems more likely that the X-ray properties of early-type galaxies are governed by internal processes, with outside influences in most cases producing scatter rather than a complete change. This fits well with the results of our previous paper (O’Sullivan et al. 2001b) in which we showed a trend in L_X/L_B with galaxy age. This trend appears to be driven by the evolution of galaxy winds which produce a general increase in the size and density of the X-ray halo as the galaxy ages after a major starburst. Galaxy wind models predict that the amount of gas produced and retained by a galaxy depends on its mass and on the way in which supernova heating changes with time. In general they predict that larger galaxies will have larger halos, but as noted in Helsdon et al. (2001), most models have been designed to fit the assumption that the $L_X:L_B$ relation is steep ($L_X \propto L_B^2$). It would be interesting to see what changes in the models are needed to reproduce the flatter relations observed in this work.

Comparison between the slopes found in this work, and those found by Helsdon et al. (2001) show some intriguing differences. Helsdon *et al.*, working with a sample of 33 X-ray bright groups, examined the X-ray properties of the galaxies in those groups. The main result of the study was the strong dissimilarity between group-dominant galaxies and all other early-types. A second important result was that the $L_X:L_B$ relation for the non-dominant galaxies appeared to have a slope of ~ 1 . In contrast, we find that our cleaned sample of non-BGG group galaxies has a slope of ~ 1.6 . There are a number of reasons why we might expect such a difference between the two studies. (i) Our sample of non-BGG group galaxies is drawn from ~ 90 groups, for many of which we only have data on one member. (ii) These groups are optically rather than X-ray selected, and cover a wide range of sizes. (iii) The two samples cover somewhat different ranges in $\text{Log } L_B$; ~ 9.8 – 11.4 for Helsdon *et al.*, ~ 9 – 10.8 in this work. (iv) Our X-ray analysis attempts to remove at least a part of any contamination from a surrounding group halo, but is crude compared to the techniques used in the analysis of Helsdon *et al.*. It seems safe to say that the sample of Helsdon *et al.* covers a narrower range of group properties than ours, but provides a more accurate and in-depth view of X-ray bright groups.

Explaining the difference is difficult. One possibility is that the Helsdon *et al.* sample, selected as a sample of X-ray bright groups, represents a high range of gas densities which our sample does not thoroughly cover. In this case, most early-type galaxies in the groups could

have suffered ram-pressure or viscous stripping, leaving them with minimal amounts of hot gas and producing the slope of unity. However, Helsdon *et al.* also found that the level of the $L_X:L_B$ relation for group galaxies was a factor of ~ 2.5 higher than their estimate of discrete source emission. Their estimate of L_{dscr} is consistent with ours, and we must conclude that galaxies in their sample are not entirely devoid of X-ray emitting gas. Another possibility is that the lack of gas in these objects could be caused by the stripping of their dark matter halos as they entered the group. In this case their lack of mass would make retention of gas difficult. In both cases we must assume that the sample presented in this work does not contain enough galaxies from X-ray bright, massive, relaxed groups for the effects of stripping to be clearly observed.

A similar problem occurs in our identification of BGGs. The Helsdon *et al.* sample selects central dominant galaxies based on their position at the centre of the X-ray halo. This ensures that the galaxy is at the centre of the group potential well, and so the excess emission observed is likely to be produced by a group cooling flow centred on the galaxy. In our sample we assume that the galaxy which is optically brightest is central and dominant, neither of which is necessarily true. Some of the groups in our sample are X-ray faint, in which case any cooling flow is likely to have a low mass deposition rate and therefore a minimal effect on the galaxy at its centre. However, the steepness of the $L_X:L_B$ slope for BGGs indicates how different these galaxies are from the general population. It is apparent that these objects can significantly bias studies which include them, and that to consider them simply as elliptical galaxies like any other may be misleading.

What these considerations make clear is that group galaxies, which constitute the majority, both in our sample and the universe as a whole, require further study before we can understand the processes which shape them. We need to know if the dominant galaxies of X-ray faint groups are as different from their neighbours as those in X-ray bright groups. We also need to know how the slope of the $L_X:L_B$ relation changes with group mass and gas density, in order to be able to determine how the slope of unity observed by Helsdon *et al.* is produced. A detailed study of a wide range of groups appears to be the necessary to answer these questions.

3.8.3 The Discrete Source Contribution

As the collecting area and spectral resolution of X-ray observatories has improved, it has become more important to be able to separate the contribution of discrete sources from that of hot gas. Late-type galaxies are dominated in the X-ray by discrete sources, but as shown in Section 3.7.3, there seems to be a significant hot gas component in earlier-type spirals. Similarly in ellipticals and S0s, the brighter galaxies are dominated by gas emission, but accurate spectral fitting requires a discrete source component.

We have attempted to define the level of this contribution. Fitting lines to morphological or luminosity defined spiral subsamples seems to produce normalisations which are too high. This may be because of the inclusion of emission from other X-ray sources such as hot gas, HMXBs, young supernovae or short lived bright transients in some galaxies. The result of fitting a sample for which some of the emission from these sources has been removed is a lower normalisation, which is in closer agreement with the lower boundary of our catalogue of X-ray luminosities.

Ideally we would wish to derive an average L_{dscr} for early-type galaxies from those galaxies themselves. At present, there are few data sets of sufficient quality to allow accurate spectral fitting of a hard component. The estimate of Matsushita et al. (2000) is probably the best of these and is also in fairly close agreement with our catalogue lower boundary. However, *XMM-Newton* and *Chandra* will be necessary to fix the discrete source contribution more precisely, and allow us to examine the evolution of the gas component more precisely. In the mean time, we believe our value of $\text{Log } L_{dscr}/L_B = 29.5 \text{ erg s}^{-1} L_{B\odot}^{-1}$ to be a reasonable estimate of the mean contribution.

Chapter 4

The X-ray halos of luminous Early-type galaxies

Abstract

We present an analysis of 39 X-ray luminous early-type galaxies observed with the *ROSAT* PSPC. Using multi-component spectral and spatial fits to these data we have measured halo abundances, temperatures, luminosities and surface brightness profiles. We compare these measurements to similar results from galaxy groups and clusters, fitting a number of relations commonly used in the study of these larger objects. In particular, we find that the $\sigma:T_X$ relation for our sample is similar to that reported for clusters, consistent with $\beta_{spec} = 1$, and that the $L_X:T_X$ relation has a steep slope (gradient 4.8 ± 0.7), comparable with that found for galaxy groups. Assuming isothermality, we construct 3-dimensional models of our galaxies, allowing us to measure gas entropy. We find no correlation between gas entropy and system mass, but do find a trend for low temperature systems to have reduced gas fractions. We conclude that the galaxies in our sample are likely to have developed their halos through galaxy winds, influenced by their surrounding environment.

4.1 Introduction

Early-type galaxies have been known to possess large halos of hot gas since the detection by *Einstein* of X-ray emission from the elliptical population in the Virgo cluster (Forman et al., 1979). Successive generations of X-ray observatories have been used to observe these galaxies,

and the advent of *XMM-Newton* and *Chandra* has allowed the complex nature of their emission to be studied in detail. Most of the work in this area has focused on the various sources of emission within early-type galaxies (hot gas, X-ray binaries, AGN) and on the surprisingly complicated relation between optical and X-ray luminosity. However, at a quite fundamental level, early-type galaxies resemble the groups and clusters in which they typically reside. Simulations of dark matter halos suggest that they have similar profiles at all mass scales (Navarro et al., 1997). If we consider clusters, groups and galaxies as potentials containing hot gas, we might expect the properties of the halos to be similar across a wide range of masses.

A comparison between halos on different scales becomes increasingly interesting when considering the importance of entropy changes in governing the behaviour of group and cluster halos. Observations of galaxy groups have demonstrated that these systems do not behave as might be expected from the simple scaling down of clusters, but instead require non-gravitational processes. One of the clearest signs of this is the entropy floor (Ponman et al., 1999). Whereas in more massive systems gas entropy scales with the total mass, in groups it appears to reach a constant minimum level. A number of models have been suggested to explain this behaviour, including raising the entropy through the injection of energy by AGN (Wu et al., 2000) or star formation (Ponman et al., 1999), or through the radiative cooling and removal of low entropy gas (Muanwong et al., 2001). It is notable that regardless of the actual process or combination of processes responsible, the site of this entropy rise would be the galaxies in the system. As early-type galaxies possess their own halos, we might expect to see evidence of these processes in their X-ray properties, and for the effect to be strongest in these systems, owing to their position at the bottom of the mass scale.

There is also evidence from previous studies of early-type galaxies (Helsdon et al., 2001; O’Sullivan et al., 2001a) that galaxies in the centres of X-ray bright groups are affected by their environment. They have a significantly steeper $L_X:L_B$ relation, and are on average considerably more luminous than normal ellipticals. A large fraction of group dominant galaxies in one sample have been shown to have temperature profiles indicative of central cooling (Helsdon et al., 2001), leading to the suggestion that their halos are actually the product of cooling flows associated with the surrounding group. Considering the differences between these dominant galaxies and their more normal counterparts, and the biasing effect their inclusion in samples of early-type

galaxies seems to have, further investigation of the processes which have shaped their halos seems warranted.

We have compiled a sample of 39 large, X-ray luminous early-type galaxies for which there is good quality *ROSAT* PSPC data available. We have analysed these data, and fitted two dimensional, two component surface brightness profiles to them. We have also fitted two component spectral models, temperature, abundance and hardness profiles and produced three dimensional models of the galaxies. These allow us to model out contamination from surrounding cluster or group emission and the discrete source population within the galaxy. We can therefore examine the properties of the halo in detail, for the first time in a sample of this size. We can also compare the behaviour of this sample to that of samples of groups and clusters through relations between parameters such as temperature, optical and X-ray luminosity, velocity dispersion, surface brightness slope and gas entropy. In most cases, this is the first time these relations have been studied for halos at this mass scale.

The paper is organized as follows. In Section 4.2 we describe our sample and the selection criteria used to create it. Section 4.3 gives details of the techniques used in reduction of the *ROSAT* PSPC data, and Section 4.4 describes the spectral and spatial fitting processes. Our results are presented in Section 4.5, with data from clusters and groups of galaxies included for comparison. We discuss the results and their implications in Section 4.6, and give our conclusions in Section 4.7. Throughout the paper we assume $H_0=50 \text{ km s}^{-1} \text{ Mpc}^{-1}$, in order to simplify comparison with previous studies of groups and clusters. Optical luminosities are normalised using the solar luminosity in the *B* band, $L_{B\odot} = 5.2 \times 10^{32} \text{ erg s}^{-1}$.

4.2 Sample Selection

Our sample was selected from the Lyon-Meudon Extragalactic Data Archive (LEDA), specifically the PGC-ROM 1996 (2nd edition). This contains information on $\sim 100,000$ galaxies, of which $\sim 40,000$ have the necessary redshift and morphological data. Galaxies were selected to match the following selection criteria:

- Absolute magnitude $M_B < -19$
- Morphological T-type < -2

- Virgocentric flow corrected recession velocity $V_{rec} < 10,500 \text{ km s}^{-1}$

These criteria were chosen to produce a selection of optically luminous nearby early-type galaxies.

A list of galaxies matching these criteria was then compared to a catalogue of *ROSAT* PSPC pointings, to produce an initial sample of galaxies with X-ray data. Only galaxies lying within the PSPC support structure (*i.e.* within $\sim 30'$ of the pointing) were accepted, so as to ensure that the X-ray data were not strongly affected by vignetting effects or off-axis resolution problems. Pointings of less than 10 ksec were also ignored, as these were unlikely to provide X-ray data of sufficient quality. This initial sample contained 47 galaxies.

We then examined images of the raw X-ray data for each galaxy, to look for potential problems. In some cases we found that the galaxies appeared to be extremely compact or point-like, suggesting that surface brightness fitting would be difficult or impossible. These objects were removed from the sample, as were galaxies in which an AGN or nearby quasar dominated the X-ray emission, to produce a final sample of 39 X-ray luminous early-type galaxies. It is worth noting that as the fraction of galaxies in which the halo was too compact or faint for analysis was small, it appears that the majority of massive early-type galaxies do possess bright, extended X-ray halos. Table 4.1 lists our targets.

4.3 Data Reduction

Data reduction and analysis of the X-ray datasets were carried out using the ASTERIX software package. Before the datasets could be used, various sources of contamination had to be removed. Possible sources include charged particles and solar X-rays scattered into the telescope from the Earth's atmosphere. Onboard instrumentation provides information which allows periods of high background to be identified. The master veto counter records the charged particle flux, and we excluded all time periods during which the master veto rate exceeded 170 count s^{-1} . Solar contamination causes a significant overall increase in the X-ray event rate. To remove this contamination we excluded all times during which the event rate deviated from the mean by more than 2σ . This generally removed no more than a few percent of each dataset.

After this cleaning process each dataset was binned into a 3-dimensional (x, y, energy) data cube. Spectra or images can be extracted from such a cube by collapsing it along the axes. A

Name	RA (2000)	DEC (2000)	σ (km s ⁻¹)	V_{rec} (km s ⁻¹)	D (Mpc)	R_e ($'$)	T	Environment
ESO 443-24	13 01 01.6	-32 26 20	279.9	4970.1	99.4	0.388	-3.1	BGG
IC 1459	22 57 09.5	-36 27 37	321.4	1522.0	28.3	0.644	-4.7	BGG
IC 4296	13 36 38.8	-33 57 59	341.2	3587.9	71.8	0.953	-4.8	BGG
IC 4765	18 47 19.0	-63 19 49	288.4	4344.9	86.9	0.239	-3.9	BGG
NGC 499	01 23 11.5	+33 27 36	264.2	4482.7	82.8	0.346	-2.9	BGG
NGC 507	01 23 40.0	+33 15 22	295.8	5015.7	100.3	1.285	-3.3	BGG
NGC 533	01 25 31.4	+01 45 35	250.0	5411.4	95.5	0.792	-4.7	BGG
NGC 720	01 53 00.4	-13 44 21	237.7	1622.0	31.2	0.659	-4.7	BGG
NGC 741	01 56 20.9	+05 37 44	288.4	5529.9	91.6	0.869	-4.8	BGG
NGC 1332	03 26 17.3	-21 20 09	328.1	1355.8	29.5	0.467	-2.9	Group
NGC 1380	03 36 26.9	-34 58 33	240.4	1617.6	27.2	0.659	-2.3	Cluster
NGC 1395	03 38 29.6	-23 01 40	241.0	1516.1	30.8	0.757	-4.8	BGG
NGC 1399	03 38 28.9	-35 26 58	329.6	1211.2	27.2	0.706	-4.5	BCG
NGC 1404	03 38 51.7	-35 35 36	212.3	1701.9	27.2	0.446	-4.7	Cluster
NGC 1407	03 40 12.3	-18 34 52	279.3	1612.0	30.9	1.199	-4.5	BGG
NGC 1549	04 15 45.0	-55 35 31	203.2	932.5	21.7	0.792	-4.3	Group
NGC 1553	04 16 10.3	-55 46 51	167.5	805.8	21.7	1.094	-2.3	BGG
NGC 2300	07 32 19.6	+85 42 32	263.0	2249.7	41.5	0.524	-3.4	BGG [†]
NGC 2832	09 19 46.5	+33 45 02	341.2	6992.2	128.9	0.426	-4.3	BGG
NGC 3091	10 00 13.8	-19 38 14	303.4	3670.2	76.2	0.512	-4.7	BGG
NGC 3607	11 16 54.1	+18 03 12	216.8	999.6	29.7	1.094	-3.1	BGG
NGC 3923	11 51 02.1	-28 48 23	269.8	1468.0	26.8	0.889	-4.6	BGG
NGC 4073	12 04 26.5	+01 53 48	267.9	5970.6	119.1	0.931	-4.1	BGG
NGC 4125	12 08 07.1	+65 10 22	239.9	1618.6	38.9	0.998	-4.8	BGG
NGC 4261	12 19 22.7	+05 49 36	316.2	2244.0	47.2	0.644	-4.8	Cluster
NGC 4291	12 20 18.1	+75 22 21	287.7	2043.9	36.8	0.245	-4.8	Group
NGC 4365	12 24 27.9	+07 19 06	268.5	1290.4	23.9	0.830	-4.8	Cluster
NGC 4472	12 29 46.5	+07 59 58	304.8	931.8	23.9	1.734	-4.7	BCG
NGC 4552	12 35 39.9	+12 33 25	264.2	372.3	23.9	0.500	-4.6	Cluster/AGN
NGC 4636	12 42 49.8	+02 41 17	211.3	1125.2	23.9	1.694	-4.8	Cluster/BGG
NGC 4649	12 43 40.2	+11 32 58	342.8	1221.9	23.9	1.227	-4.6	Cluster
NGC 4697	12 48 35.9	-05 48 02	173.4	1232.2	22.7	1.256	-4.7	BGG
NGC 5128	13 25 29.0	-43 01 00	142.6	385.6	5.8	0.708	-2.1	BGG/AGN
NGC 5322	13 49 15.5	+60 11 29	239.9	2035.5	41.7	0.587	-4.8	BGG
NGC 5419	14 03 38.6	-33 58 41	329.6	4027.5	80.5	0.723	-4.2	BGG [†]
NGC 5846	15 06 29.3	+01 36 25	250.0	1890.0	34.4	1.377	-4.7	BGG
NGC 6269	16 57 58.4	+27 51 19	224.4	10435.0	208.7	0.574	-4.8	BGG
NGC 6482	17 51 49.0	+23 04 20	302.0	4102.0	82.0	0.132	-4.8	Field ?
NGC 7619	23 20 14.7	+08 12 23	310.5	3825.5	60.0	0.536	-4.7	BCG

Table 4.1: A list of galaxies included in our sample. RA and DEC are taken from the LEDA catalogue, as are morphological type (T), Recession velocity (which is corrected for Virgocentric flow and movement within the local group), and velocity dispersion, σ . Distances are taken from Prugniel & Simien (1996) where possible, or calculated from the recession velocity. $H_0=50$ is assumed in both cases. Optical effective radii, R_e , are taken from Faber et al. (1989) and Prugniel & Heraudeau (1998). Galaxy environment is taken from the group catalogues of Garcia (1993), Zabludoff & Mulchaey (1998) and White et al. (1999). [†] indicates galaxies which are not identified as brightest group galaxies in the group catalogues, but lie at the centre of the X-ray halo of their group.

model of the background was then generated based on an annulus taken from this cube. We used annuli of width 0.1° , and inner radius 0.4° where possible. In cases where this would place the annulus close to the source we moved the inner radius of the annulus, generally to $r = 0.55^\circ$. To ensure that the background model was not biased by sources within the annulus, an iterative process was used to remove point sources of $> 4.5 \sigma$ significance. A number of our galaxies are found within groups and clusters of galaxies, many of which have their own X-ray halos. Our intention was to model these spectrally and spatially in order to accurately remove the effects of their contamination of our target galaxies. We therefore moved the inner radius of the annulus outward to avoid the emission, where possible. In cases where the emission appeared to extend to the edge of the field of view, we used a background annulus at $r=0.9^\circ$. This occurred for a small number of galaxies which lie in the centres of clusters (*e.g.* NGC 1399). The use of a background annulus which lies within the cluster emission means that we are likely to overestimate the true background and hence over-correct for it. However, as we are using the largest annulus possible, we should minimise the degree of overestimation. We can also expect the central galaxy component of the emission to have a much higher surface brightness than the cluster emission, so that oversubtraction will have a negligible effect on it. Surface brightness fits should therefore be accurate for the central component, which is our main interest, and as good as is possible for the cluster component.

The resulting background model was then used to produce a background-subtracted cube. Regions near the *PSPC* window support structure were removed from these images, as objects in those areas would have been partially obscured during the observation. The cube was further corrected for dead time and vignetting effects, and point sources were removed.

Examination of background subtracted images allowed us to locate each galaxy and produce a radial profile of the surrounding region. From these profiles, regions of interest were selected, from which images or spectra for use in fitting could then be extracted. The majority of our galaxies are known to be members of groups or clusters, and as such we expected to see emission from an intergalactic medium (IGM) surrounding them. In cases where the galaxy did not appear to be contaminated with other emission, we defined the region of interest (RoI) as being within the radius at which the emission dropped to the background level. This region was suitable for both spatial and spectral fitting. In cases where contaminating intergalactic

emission was seen, we defined separate regions of interest, one for spectral and one for spatial fits. For spatial fitting, we again define the RoI as being within the radius at which emission drops to the background level. This will contain both the galaxy and the surrounding group or cluster, allowing us to fit models to both and thereby accurately remove contaminating emission. A background annulus for use with this region was selected as described above. A second, inner RoI was also defined, using the radius at which the galaxy emission dropped to the level of the surrounding group/cluster halo. This region was selected for use in spectral fitting, as it excludes most of the contaminating emission from the surrounding system. Spectra extracted from such a region are still contaminated by group/cluster emission along the line of sight so we reprocessed the data, this time selecting a local background annulus centred on and close to the galaxy. This annulus generally had an inner radius 0.05° larger than the spectral region of interest. The background model produced from this annulus should therefore have the spectrum of the cosmological background combined with the contaminating group/cluster emission. As the contaminating emission is likely to follow a King profile, the degree to which the contamination is removed by using this background model will depend how far down the slope of the profile the annulus lies. In cases where the annulus lies at a radius similar to the core radius of the group/cluster emission, the technique is likely to remove the majority of the contamination, but at larger radii an increasing fraction will remain unsubtracted and will influence our spectral fits.

4.4 Spectral and Spatial Analysis

Spectra for each galaxy were obtained by removing all data outside the region of interest and collapsing the data cube along its x and y axes. As with the background annulus, an iterative process was used to remove point sources of $>4.5\sigma$ significance in the region of interest, although any point sources within the D_{25} diameter were assumed to be associated with the galaxy itself and therefore not removed. The spectra could then be fitted with a variety of models. To provide a baseline for later fits and to measure the basic properties of the galaxy halo, each spectrum was fitted with a MEKAL hot plasma model (Kaastra & Mewe 1993; Liedahl et al. 1995). Initially, only normalisation was fitted. Hydrogen absorption column densities were fixed at values determined from radio surveys (Stark et al. 1992), and temperature and metal

abundance were fixed at 1 keV and 1 solar respectively. Parameters were then freed in order (temperature, hydrogen column, metallicity), and only re-frozen at their starting values if they became poorly defined or tended to extreme values. The basic temperature and metallicity values are likely to be representative of the majority of early-type galaxies (Matsushita et al. 2000; Matsushita 2001), but clearly fitted values are preferable.

We then attempted to fit two component spectral models for each galaxy. These generally included a power-law + MEKAL model and bremsstrahlung + MEKAL model in which the bremsstrahlung temperature was fixed at 7 keV. This second component was intended to represent contamination by a high temperature emission component produced by the population of X-ray binaries and other unresolved stellar sources within each galaxy. Recent *Chandra* studies of extragalactic X-ray binary populations suggest that this emission component is best modeled by a power-law of index ~ 1.2 (Sarazin et al. 2001; Blanton et al. 2001), while *ASCA* studies show good fits using a high temperature bremsstrahlung model (Matsushita et al., 2000). All models were fitted using the maximum likelihood Cash statistic (Cash, 1979). As well as overall spectral fits to each galaxy, we also intended to fit radial temperature and metallicity profiles (see below) and expected to have much smaller numbers of counts available in each radial bin of these profiles. Maximum likelihood methods are more successful than χ^2 techniques when fitting data with low numbers of counts per bin (Nousek & Shue, 1989), making it the best choice for the profile fitting. In order to maintain a consistent method for all our spectral fitting we therefore chose to use the Cash statistic for our overall galaxy fits as well. The Cash statistic is defined as $-2\ln L$ where L is the likelihood function. This means that the most likely model has a minimum Cash statistic and that differences in the statistic are chi-squared (χ^2) distributed. Thus confidence intervals can be calculated in the same way as for a conventional χ^2 fit. By comparing the best fit Cash statistic for each model, and visually examining the spectral fit, we selected the best fit model for each galaxy. From this we could extract (in most cases) the X-ray temperature and metallicity of the galaxy halo, as well as the X-ray flux from the galaxy halo and the stellar contribution.

For each galaxy in the sample, we also derived simple projected temperature and hardness profiles. Temperature profiles were produced by splitting the larger, surface brightness region of interest into several annuli, from which spectra were extracted. These spectra were then fitted

using the best fitting spectral model for the galaxy as a whole. Initially the models were fitted with the metallicity and hydrogen column density frozen at their global best fit values. However, if the data quality permitted, we freed these parameters, providing us with crude metallicity profiles for a fraction of our sample. Given the limited spectral range of *ROSAT*, the inability of the PSPC to resolve individual spectral lines, and the small number of counts in each annulus, the abundances fitted should not be taken as accurate measurements. However, in some cases they do show interesting trends when considered in conjunction with the temperature profiles.

Hardness profiles were calculated in a somewhat similar manner. Again the larger region of interest was split in to a number of annuli. From each of these, counts in soft (0.3–1.3 keV) and hard (1.3–2.4 keV) bands were extracted and divided to produce a ratio of hard/soft emission. Simulated spectra suggest that a 0.5 keV MEKAL spectrum produces a value of ~ 0.5 , while a power law of $\Gamma=1.7$ and a 7 keV bremsstrahlung spectrum produce values of ~ 1.1 and 1.2 respectively. These profiles can be used to give a basic idea of changes in emission across the galaxy and in particular to identify AGN.

In order to study the spatial properties of the galaxy X-ray emission, we also performed fits to the 2-dimensional surface brightness profile of each galaxy. Following the initial data reduction described in Section 4.3, we extracted an image in the 0.5–2 keV band and corrected it for vignetting. This was done using an energy-dependent exposure map (see Snowden et al. 1994 for a full description). Point sources were removed as in the spectral analysis, and unrelated extended sources identified and excluded by hand. Use of the energy dependant exposure map results in a constant background level across the image, so a flat background was also determined and subtracted from the data.

As in the case of spectral analysis, we can choose to fit a variety of surface brightness models to our data. The most commonly used in this work was a modified King function (or “ β -profile”) of the form:

$$S(r) = S_0(1 + (r/r_{core})^2)^{-3\beta_{fit}+0.5} \quad (4.1)$$

where $S(r)$ is the surface brightness at a given radius, S_0 is the central surface brightness r_{core} is the core radius and β_{fit} is a measure of the slope of the surface brightness profile. At various stages of the analysis we also fitted point source models and de Vaucouleurs $r^{1/4}$ law

models, using the form:

$$S(r) = S_e \cdot \exp\{-7.67[(r/r_e)^{0.25} - 1]\} \quad (4.2)$$

where S_e is the surface brightness at r_e , the effective radius (the isophotal radius containing half the total luminosity.)

Models were convolved with the PSPC point spread function at an energy determined from the mean photon energy of the emission in the region of interest and then fitted to the data. Both spherical and elliptical fits were possible when using the King and de Vaucouleurs models, with the position angle and major to minor axis ratio measuring the shape and orientation of elliptical fits. When using King models, all parameters (core radius, β_{fit} normalisation, x and y position and the ellipticity parameters) were usually allowed to vary freely, as were the parameters in point source models (x and y position, normalisation). The effective radius parameter of the de Vaucouleurs models was initially set at the optically determined value, and held frozen in most cases. We did allow the effective radius to vary for a small number of galaxies, where the fit was well constrained by the data, in order to investigate differences between the optical and X-ray stellar profiles. However only one galaxy, NGC 4697, was best fit by a model including a de Vaucouleurs component. A *Chandra* observation of this object has shown it to have a relatively small gas halo, with much of its emission contributed by point sources (Sarazin et al., 2001), so the success of the de Vaucouleurs component in this case is unsurprising.

The use of 2-dimensional datasets to fit the surface brightness distribution can result in a low number of counts in many of the data bins. Under these conditions χ^2 fitting performs poorly (Nousek & Shue, 1989) so, as in the spectral analysis, maximum likelihood fitting based on the Cash statistic was used. However, the Cash statistic gives no indication of the absolute quality of the fit, only the quality relative to other fits. In order to gain some estimate of the true fit quality, we used a Monte Carlo approach, in which the best fit 1- and 2-component model was used to generate 1000 images of the groups, to which Poisson noise was added. These were then compared to the original image, the Cash statistic determined, and a Gaussian fitted to the resulting spread of values. By comparing the actual Cash statistic to this distribution of values, we were able to determine the probability that the model could have produced the data. We were therefore able to identify cases where the 1-component fit was more likely to reproduce

the data than the 2-component fit, and discard the 2-component fits for these galaxies.

4.5 Results

4.5.1 Spectral and spatial fits

Table 4.2 shows the results of our spectral fits. As mentioned previously, metal abundances from *ROSAT* PSPC spectra are inherently unreliable, due to the relatively poor spectral resolution of the instrument. This is reflected by the large errors on some of our fitted values, and by the fact that in some cases we had to hold metallicity frozen in order to secure a stable fit. The temperature values are more reliable, and give a mean temperature of 0.67 ± 0.29 keV. Given that we have spectrally fitted the emission from the central regions of our targets whereas we have spatially fitted larger regions, including the galaxies and surrounding emission, it is not entirely clear how we should go about calculating the X-ray luminosity. Ideally we would be able to simultaneously fit spectral and spatial data, giving a true luminosity for each component (*e.g.* Lloyd-Davies et al., 2000). In practice, we calculated several luminosities and tested their correlation with other parameters. The most straightforward are luminosities based only on spectral fitting, a gas luminosity from the MEKAL component and discrete source luminosity from the harder bremsstrahlung component (if any). This has the clear disadvantage that the smaller spectral region of interest may miss a significant part of the outer galaxy halo. Alternatively, we can make use of the surface brightness data to produce galaxy and background luminosities by scaling the total luminosity calculated from the spectral fits to the number of counts found in each spatial component. This will provide a luminosity for the galaxy component, but one which includes discrete source emission. It may even overestimate this component, as the region in which we fit the spectrum contains the optical body of the galaxy, where the discrete source contribution will be high compared to the outer halo. The third option is to scale just the MEKAL component by the relative numbers of counts in the spectrally and spatially fitted region. This allows us to calculate a gas luminosity for the galaxy component, but ignores the contribution from discrete sources. This luminosity will therefore be an overestimate of the true gas luminosity associated with the galaxy. However, we expect large optically luminous galaxies such as our targets to be almost entirely dominated by gas emission. With a small number of

Name	n_{H} ($\times 10^{-21} \text{ cm}^{-2}$)	T_{X} (keV)	Z (Z_{\odot})	$\text{Log } L_{\text{X}}$ (erg s^{-1})	Model	Profile
ESO 443-24	$0.50^{+5.3}_{-0.19}$	$0.69^{+0.07}_{-0.39}$	$1.0^{+1.0}_{-0.7}$	$41.78^{+1.0}_{-0.06}$	MK+BR	I
IC 1459	0.069 ± 0.012	0.51 ± 0.05	1.0	40.3 ± 0.2	MK+BR	H
IC 4296	$0.63^{+0.33}_{-0.24}$	0.72 ± 0.07	0.23 ± 0.92	$41.7^{+0.3}_{-0.8}$	MK+BR	C
IC 4765	$2.6^{+3.8}_{-0.9}$	$0.64^{+0.09}_{-0.37}$	0.17 ± 0.17	$42.4^{+0.7}_{-0.1}$	MK+BR	C
NGC 499	$0.79^{+0.32}_{-0.14}$	$0.70^{+0.02}_{-0.03}$	1.0	42.6 ± 0.3	MK+BR	I
NGC 507	0.59 ± 0.09	1.03 ± 0.05	$0.95^{+2.2}_{-0.33}$	$42.9^{+0.4}_{-0.7}$	MK+BR	C
NGC 533	0.29 ± 0.03	$0.84^{+0.05}_{-0.04}$	1.1 ± 1.1	42.2 ± 0.2	MK+BR	C
NGC 720	0.15 ± 0.15	0.50 ± 0.04	$0.28^{+0.06}_{-0.04}$	41.1 ± 0.3	MK+BR	H
NGC 741	$0.54^{+0.11}_{-0.08}$	0.71 ± 0.07	0.26 ± 0.26	$41.9^{+0.3}_{-0.4}$	MK+BR	C
NGC 1332	$0.16^{+0.04}_{-0.03}$	$0.41^{+0.06}_{-0.05}$	0.59 ± 0.59	40.6 ± 0.2	MK+BR	H
NGC 1380	0.18 ± 0.10	$0.30^{+0.08}_{-0.05}$	$0.11^{+0.44}_{-0.07}$	$40.4^{+0.4}_{-1.0}$	MK+BR	?
NGC 1395	0.069 ± 0.016	$0.65^{+0.04}_{-0.05}$	1.0	40.6 ± 0.2	MK+BR	C
NGC 1399	0.12 ± 0.01	1.21 ± 0.03	$1.1^{+0.3}_{-0.2}$	41.8 ± 0.3	MK+BR	C
NGC 1404	0.18 ± 0.02	0.60 ± 0.01	$0.35^{+0.05}_{-0.04}$	$41.66^{+0.04}_{-0.05}$	MK	C
NGC 1407	$0.72^{+0.22}_{-0.16}$	$0.79^{+0.08}_{-0.07}$	$0.14^{+0.14}_{-0.06}$	$41.5^{+0.2}_{-0.3}$	MK+BR	C
NGC 1549	0.046 ± 0.046	$0.25^{+0.08}_{-0.05}$	$0.14^{+0.27}_{-0.08}$	$39.7^{+0.2}_{-0.4}$	MK+BR	I
NGC 1553	0.045 ± 0.033	0.53 ± 0.15	$0.10^{+0.16}_{-0.05}$	$40.2^{+0.3}_{-0.4}$	MK+BR	?
NGC 2300	$0.97^{+0.97}_{-0.30}$	$0.62^{+0.07}_{-0.14}$	0.23 ± 0.23	$41.43^{+0.2}_{-0.07}$	MK+BR	?
NGC 2832	0.13 ± 0.02	0.82 ± 0.05	1.0	41.9 ± 0.2	MK+BR	?
NGC 3091	$0.38^{+0.08}_{-0.06}$	$0.64^{+0.04}_{-0.05}$	1.0	41.7 ± 0.2	MK+BR	C
NGC 3607	0.015 ± 0.015	0.45 ± 0.06	$0.71^{+0.57}_{-0.21}$	$40.7^{+0.3}_{-0.4}$	MK+BR	I
NGC 3923	0.58 ± 0.22	$0.46^{+0.04}_{-0.05}$	1.0	40.8 ± 0.2	MK+BR	H
NGC 4073	$0.16^{+0.02}_{-0.03}$	1.6 ± 0.2	$1.6^{+1.1}_{-0.4}$	$43.1^{+0.1}_{-0.3}$	MK+BR	C
NGC 4125	0.10 ± 0.04	$0.34^{+0.05}_{-0.04}$	0.34 ± 0.34	41.27 ± 0.07	MK	?
NGC 4261	0.087 ± 0.017	$0.67^{+0.04}_{-0.05}$	1.3 ± 1.3	41.0 ± 0.2	MK+BR	C
NGC 4291	$0.22^{+0.18}_{-0.09}$	$0.59^{+0.06}_{-0.07}$	$0.63^{+4.8}_{-0.13}$	$41.20^{+0.4}_{-0.02}$	MK	I
NGC 4365	$0.11^{+0.06}_{-0.05}$	$1.0^{+0.3}_{-0.2}$	$0.064^{+0.11}_{-0.053}$	40.5 ± 0.1	MK	I
NGC 4472	0.162 ± 0.007	0.88 ± 0.01	1.0	41.5 ± 0.2	MK+BR	C
NGC 4552	0.18 ± 0.03	0.54 ± 0.06	1.0	40.7 ± 0.2	MK+BR	?
NGC 4636	$0.25^{+0.05}_{-0.06}$	0.55 ± 0.03	$0.40^{+0.32}_{-0.13}$	$42.0^{+0.1}_{-0.2}$	MK+BR	C
NGC 4649	$0.24^{+0.06}_{-0.07}$	0.78 ± 0.02	$0.80^{+1.0}_{-0.36}$	$39.3^{+0.3}_{-0.5}$	MK+BR	C
NGC 4697	0.16 ± 0.03	0.24 ± 0.02	0.40 ± 0.40	39.0 ± 0.2	MK+BR	I
NGC 5128	$0.43^{+0.07}_{-0.05}$	$0.35^{+0.04}_{-0.03}$	1.0	40.2 ± 0.2	MK+BR	H
NGC 5322	0.045 ± 0.037	$0.33^{+0.100}_{-0.06}$	0.19 ± 0.19	40.3 ± 0.3	MK+BR	?
NGC 5419	$0.29^{+0.07}_{-0.05}$	0.69 ± 0.26	0.32 ± 0.32	$42.0^{+0.3}_{-0.4}$	MK+BR	?
NGC 5846	0.30 ± 0.03	0.66 ± 0.02	1.0	$40.5^{+0.2}_{-0.3}$	MK+BR	C
NGC 6269	0.53 ± 0.12	1.4 ± 0.2	$0.33^{+0.36}_{-0.17}$	43.4 ± 0.1	MK	C
NGC 6482	$0.68^{+0.72}_{-0.19}$	$0.55^{+0.04}_{-0.07}$	$1.0^{+1.0}_{-0.5}$	$41.2^{+0.5}_{-0.4}$	MK+BR	I
NGC 7619	$0.34^{+0.08}_{-0.06}$	0.81 ± 0.03	1.9 ± 1.9	$42.0^{+0.3}_{-0.8}$	MK+BR	C

Table 4.2: Results of the spectral fits to our sample galaxies. Where possible, an absorbed MEKAL+bremsstrahlung (MK+BR) model was fitted, but in cases where the bremsstrahlung normalisation always tended to zero, this component was removed from the fit. All upper and lower (1σ) errors on fitted parameters were calculated individually, but are shown as a single \pm error when they are identical to two significant figures. Those galaxies for which metallicity could not be successfully fitted are listed with a fixed solar metallicity with no errors. Temperature profiles are classified as isothermal (I), cool core (C), hot core (H), or uncertain (?).

exceptions, the spectral fits confirm this, suggesting that in most cases the overestimation is small. It is also notable that because the bremsstrahlung component peaks at a higher energy than the MEKAL, a given luminosity corresponds to a smaller number of bremsstrahlung counts (in the *ROSAT* band) than it would for a MEKAL model. This means that our overestimate of luminosity is reduced, as the number of counts associated with the bremsstrahlung component, and assumed in the scaling to be part of the MEKAL component, will produce only a small increase in gas luminosity. This last option also produces the strongest correlations with other galaxy parameters such as L_B , σ and temperature, and we use this method throughout the paper.

Temperature profiles for our sample of galaxies are shown in figure 4.1. The extent of the profiles varies, owing to the relative quality of data, length of exposure and galaxy distance. We have classified the galaxy profiles into four groups; cooling cores (*e.g.* NGC 1399), hot cores (*e.g.* NGC 720), isothermal (*e.g.* NGC 4697) and those where the data quality prevents a judgement (*e.g.* NGC 4552, where the errors on the outermost bin are large enough to make it suspect). Cool and hot core galaxies are selected under the requirement that their central bin must be hotter or cooler than an average outer temperature by at least 20%, and that the errors in T_X must be smaller than this amount. It is also possible to see evidence of AGN activity in some of the profiles, particularly in the case of NGC 5128, where the central bin has a temperature of ~ 5 keV and the rest of the galaxy < 1 keV. An interesting feature of some of the better defined profiles which show central cooling (*e.g.* NGC 507, NGC 1399, NGC 4636) is that the temperature rises with radius to a value above the apparent outer mean temperature, and then falls back to that mean, producing a temperature peak at moderate radii. As all of these galaxies are embedded in larger group or cluster halos, this peak may mark the boundary or point of interaction between the galaxy and its environment. The observations available for NGC 1399 and NGC 4636 contain very large numbers of counts, allowing us to include metallicity as a free parameter in the profile fitting. Metallicity profiles of these two galaxies are shown in Figure 4.2. Despite the large errors in some bins, it is notable that both metallicity profiles follow the same structure as seen in temperature; a central trough, rising to a peak at moderate radius, with an outer region of relatively low abundance. The peak temperature and metallicity occur at approximately the same radius in both cases. In order to check that correlations between

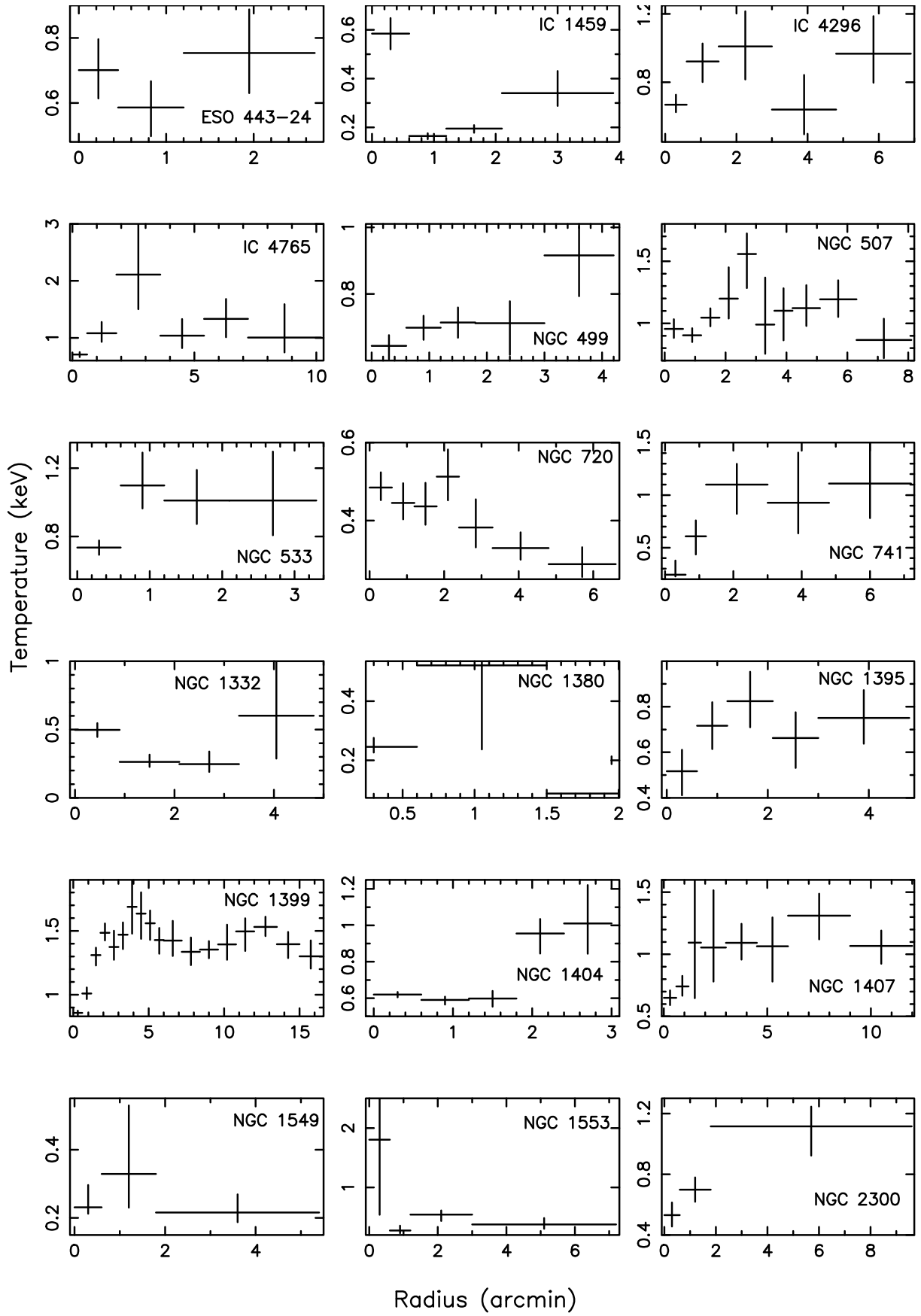


Figure 4.1: Measured temperature profiles for our sample of galaxies

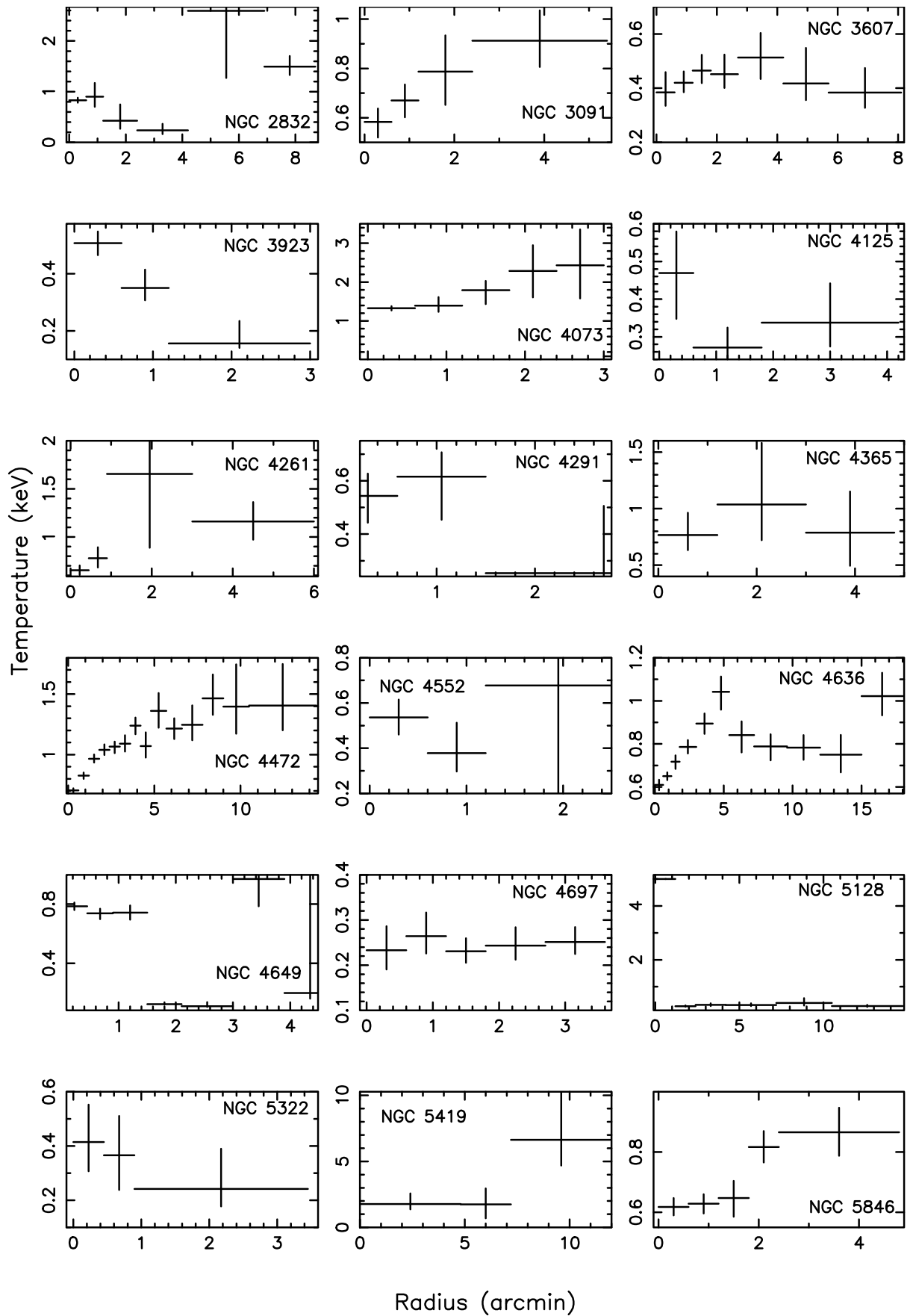


Figure 4.1: Measured temperature profiles for our sample of galaxies

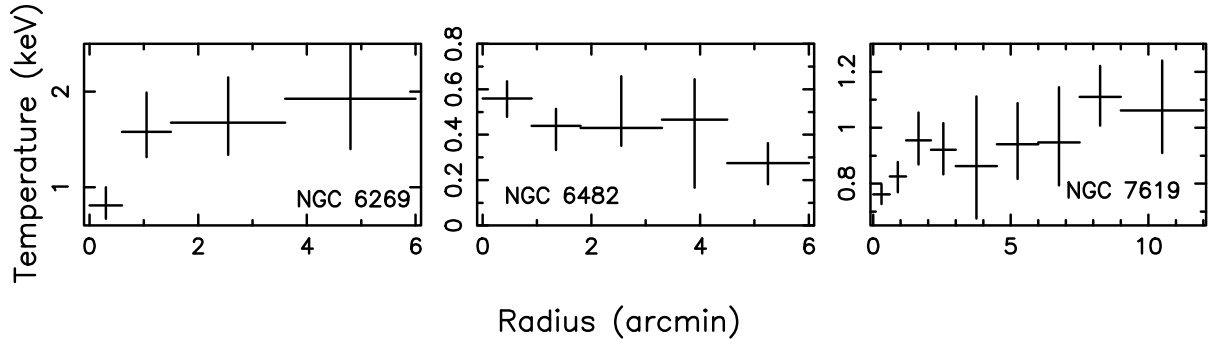


Figure 4.1: Measured temperature profiles for our sample of galaxies

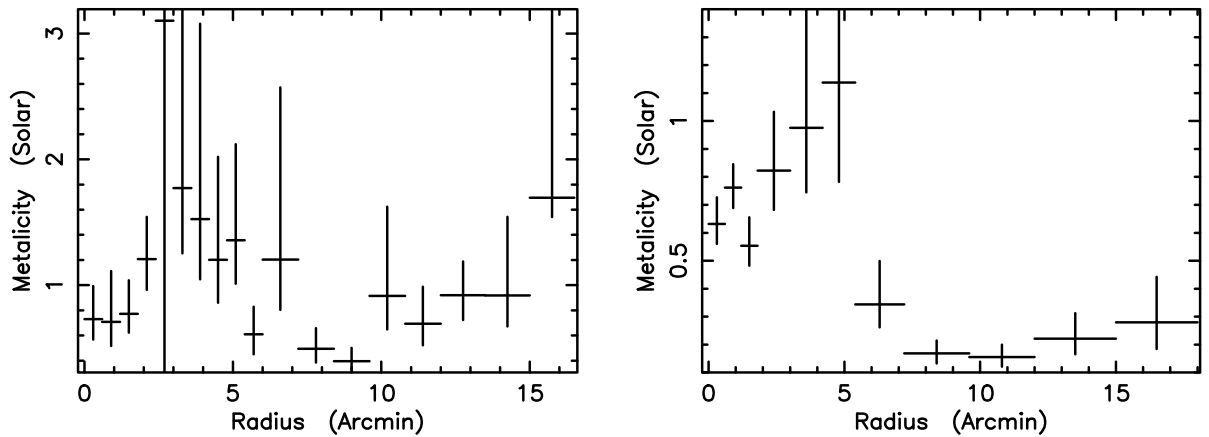


Figure 4.2: Fitted metallicity profiles of NGC 1399 (left panel) and NGC 4636 (right panel)

temperature and abundance in the fits were not biasing the results we modelled the fit space for the two bins on either side of the apparent break in the profiles, calculating fit statistics at a range of temperatures and metallicities. Comparing the confidence regions for the two points shows that they are dissimilar to at least 6σ significance, strongly suggesting the break in the profiles is real.

Table 4.3 lists the results of the surface brightness fitting for the galaxy halos of our target galaxies. In the majority of galaxies we obtain good quality fits, with relatively small errors on the core radius and slope. As we are able to fit elliptical models, we also list the position angle of the major axis and axis ratio of the model fits. For five galaxies, we were unable to determine a reliable position angle, as the model was consistent (within errors) with being spherical. The best fit position angles of these galaxies are listed without errors, and should only be considered

Name	Core Radius (arcmin)	β_{fit}	Axis Ratio	Position Angle (degrees)	RoI Radius (degrees)	Model
ESO 443-24	0.106 ± 0.004	0.55 ± 0.03	$1.7^{+0.3}_{-0.2}$	306 ± 7	0.045	KI
IC 1459	0.17 ± 0.02	$0.89^{+0.36}_{-0.09}$	$1.6^{+1.4}_{-0.2}$	276 ± 7	0.065	KI+KI
IC 4296	0.080 ± 0.004	$0.66^{+0.18}_{-0.02}$	$2.2^{+0.8}_{-0.4}$	29^{+10}_{-8}	0.12	KI+KI
IC 4765	0.39 ± 0.02	$1.24^{+0.6}_{-0.06}$	$1.1^{+0.1}_{-0.7}$	190	0.17	KI+KI
NGC 499	0.85 ± 0.04	0.70 ± 0.03	$1.05^{+0.03}_{-0.04}$	290^{+30}_{-20}	0.25	KI+KI
NGC 507	0.82 ± 0.03	0.54 ± 0.03	$1.05^{+0.04}_{-0.8}$	270	0.14	KI+KI
NGC 533	0.058 ± 0.002	$0.53^{+0.04}_{-0.02}$	1.24 ± 0.06	240 ± 10	0.16	KI+KI
NGC 720	0.15 ± 0.02	$0.483^{+0.010}_{-0.009}$	$1.34^{+0.09}_{-0.08}$	294^{+20}_{-7}	0.11	KI+KI
NGC 741	0.172 ± 0.006	$0.65^{+0.64}_{-0.06}$	$1.41^{+0.08}_{-0.1}$	128^{+10}_{-9}	0.12	KI+KI
NGC 1332	0.010 ± 0.001	$0.548^{+0.009}_{-0.008}$	$1.8^{+0.3}_{-0.2}$	295 ± 4	0.080	KI+KI
NGC 1380	0.090 ± 0.011	$0.51^{+0.04}_{-0.03}$	$1.1^{+0.2}_{-0.3}$	210	0.045	KI
NGC 1395	0.23 ± 0.03	$0.52^{+0.06}_{-0.03}$	1.3 ± 0.1	41^{+9}_{-10}	0.10	KI+KI
NGC 1399	0.11 ± 0.01	0.59 ± 0.02	$1.23^{+0.04}_{-0.03}$	176 ± 3	0.12	KI+KI
NGC 1404	0.32 ± 0.04	$0.770^{+0.005}_{-0.004}$	$1.05^{+0.02}_{-0.01}$	294^{+10}_{-6}	0.20	KI+KI
NGC 1407	0.18 ± 0.02	$0.56^{+0.02}_{-0.01}$	1.20 ± 0.06	91^{+7}_{-8}	0.20	KI+KI
NGC 1549	0.021 ± 0.003	0.509 ± 0.003	$1.56^{+0.10}_{-0.09}$	174^{+7}_{-8}	0.090	KI
NGC 1553	0.43 ± 0.07	$0.66^{+0.06}_{-0.09}$	$1.4^{+0.2}_{-0.1}$	304^{+10}_{-9}	0.17	KI+KI
NGC 2300	0.23 ± 0.02	$0.69^{+0.12}_{-0.06}$	$1.1^{+0.2}_{-0.1}$	330	0.16	KI+KI
NGC 2832	0.0100 ± 0.0003	0.314 ± 0.007	1.4 ± 0.1	357 ± 6	0.15	KI+PS
NGC 3091	1.17 ± 0.05	$1.60^{+0.03}_{-0.04}$	1.31 ± 0.04	325^{+7}_{-6}	0.15	KI+KI
NGC 3607	0.63 ± 0.07	0.48 ± 0.02	$1.17^{+0.07}_{-0.06}$	350 ± 10	0.14	KI
NGC 3923	0.010 ± 0.001	$0.55^{+0.05}_{-0.01}$	$1.8^{+0.4}_{-0.2}$	54^{+6}_{-5}	0.080	KI+KI
NGC 4073	0.072 ± 0.002	$0.46^{+0.02}_{-0.01}$	$1.20^{+0.06}_{-0.05}$	265^{+7}_{-8}	0.10	KI+KI
NGC 4125	0.017 ± 0.001	$0.48^{+0.01}_{-0.08}$	$1.629^{+0.3}_{-0.003}$	269^{+8}_{-9}	0.070	KI+PS
NGC 4261	0.37 ± 0.03	$1.2^{+1.4}_{-0.2}$	$1.8^{+0.3}_{-0.2}$	37 ± 5	0.10	KI+KI
NGC 4291	0.38 ± 0.04	$0.57^{+0.04}_{-0.03}$	1.3 ± 0.1	106^{+9}_{-10}	0.065	KI
NGC 4365	0.54 ± 0.08	$0.60^{+0.04}_{-0.03}$	2.0 ± 0.2	31 ± 4	0.090	KI
NGC 4472	0.25 ± 0.04	$0.597^{+0.009}_{-0.008}$	1.08 ± 0.02	83^{+10}_{-9}	0.24	KI+KI
NGC 4552	0.098 ± 0.014	$0.60^{+0.02}_{-0.03}$	$1.7^{+0.2}_{-0.1}$	164 ± 5	0.045	KI
NGC 4636	0.40 ± 0.06	$0.535^{+0.007}_{-0.006}$	$1.02^{+0.02}_{-0.09}$	24	0.24	KI+KI
NGC 4649	0.13 ± 0.02	0.567 ± 0.008	1.18 ± 0.03	26 ± 6	0.080	KI+PS
NGC 4697	0.99 ± 0.15	$0.46^{+0.13}_{-0.07}$	1.8 ± 0.3	28^{+6}_{-12}	0.045	KI+DV
NGC 5128	0.90 ± 0.53	0.55 ± 0.01	2.21 ± 0.07	52.0 ± 0.9	0.25	KI+KI
NGC 5322	0.0100 ± 0.0008	0.49 ± 0.01	$1.6^{+0.3}_{-0.2}$	57^{+8}_{-9}	0.057	KI
NGC 5419	4.5 ± 0.2	$0.50^{+0.18}_{-0.07}$	1.44 ± 0.06	44 ± 6	0.20	KI+PS
NGC 5846	1.3 ± 0.1	$0.80^{+0.05}_{-0.04}$	1.15 ± 0.03	45^{+7}_{-6}	0.080	KI+PS
NGC 6269	1.21 ± 0.02	$0.40^{+0.04}_{-0.02}$	$1.19^{+0.1}_{-0.08}$	38 ± 15	0.10	KI+PS
NGC 6482	0.162 ± 0.007	$0.524^{+0.009}_{-0.001}$	$1.13^{+0.07}_{-0.05}$	220 ± 10	0.10	KI+PS
NGC 7619	0.031 ± 0.002	$0.447^{+0.006}_{-0.005}$	$1.18^{+0.07}_{-0.06}$	308 ± 10	0.20	KI+KI

Table 4.3: Results of the surface brightness fits to our galaxies, for the components associated with the galaxy halo. Best fit position angle values without errors are given for those galaxies where the angle was essentially unconstrained. All errors are quoted at the 1σ level.

as estimates.

4.5.2 The $L_X:T_X$ relation

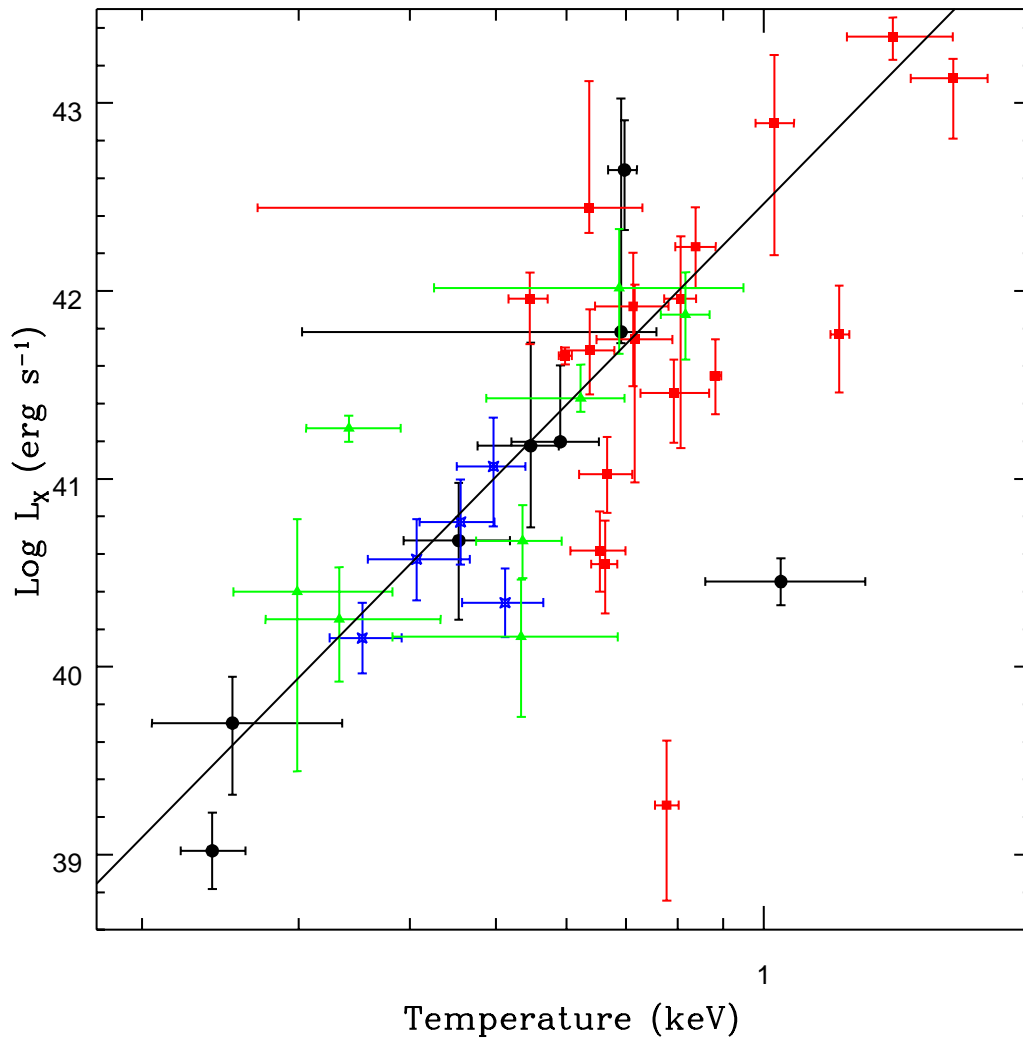


Figure 4.3: $\text{Log } L_X$ plotted against temperature for our sample of galaxies. Galaxies which show signs of central cooling are marked by red squares, those with central heating by blue stars, those which are apparently isothermal with black circles, and those which are unclassified by green triangles. The solid line shows the best fit line for the complete sample

Figure 4.3 shows L_X plotted against temperature for our sample. As can be seen, we find a fairly tight relation between L_X and T_X , with only a small number of outlier points. Using

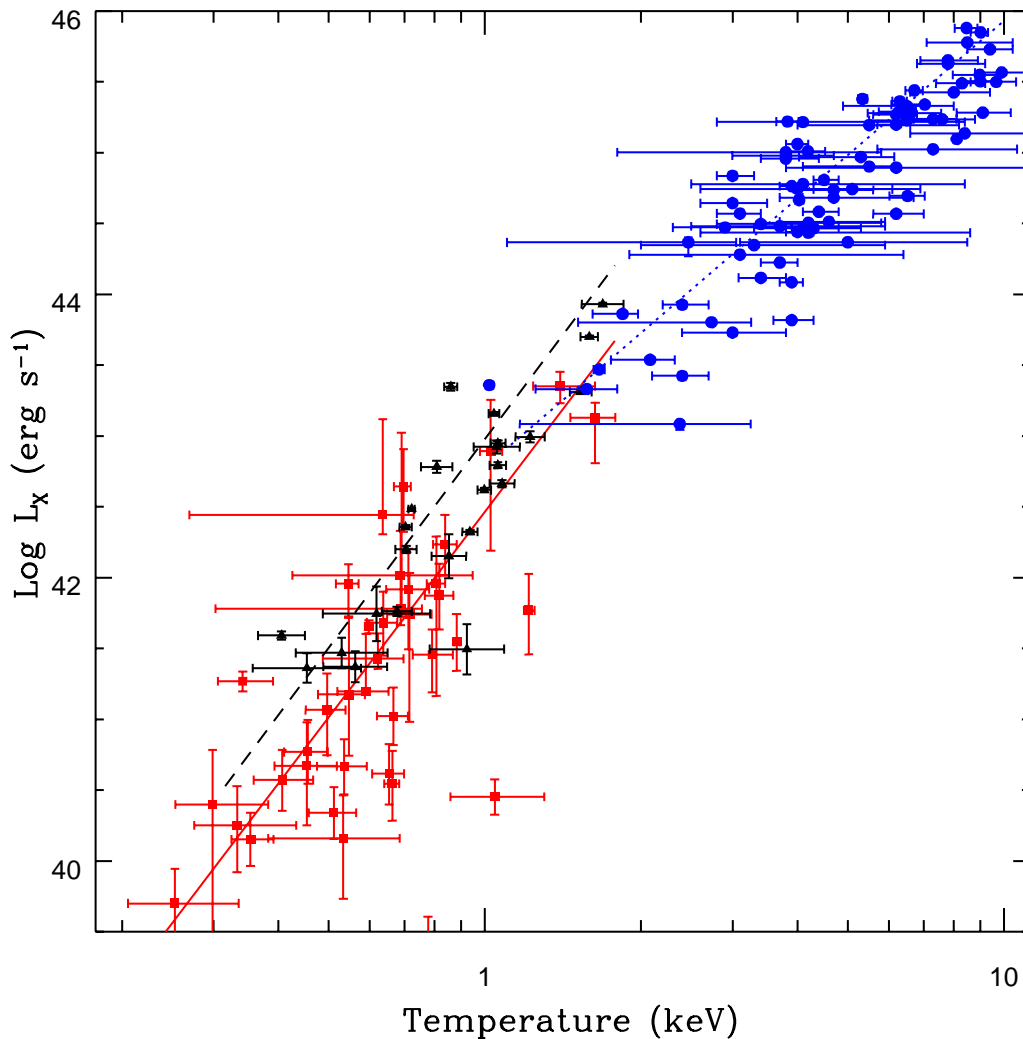


Figure 4.4: The $L_X:T_X$ relation for our sample, with similar relations for groups and clusters. Our galaxy data points are marked by squares, and the relation by a solid line. Group data are taken from Helsdon & Ponman (2000), and are marked by triangular points and a dashed line. Cluster data are drawn from David et al. (1993), Mushotzky & Scharf (1997) and Fairley et al. (2000), and are represented by circles and a dotted line. We find that the galaxy relation has a similar slope to that for groups, but is offset to fainter luminosities by a factor of ~ 3

Kendall's K-statistic (Ponman, 1982) to measure the strength of correlation, we find a significance of $\sim 4.6\sigma$. We fitted the relation using ODRPACK (Boggs et al., 1989) to perform orthogonal least squares regression, and found a slope of 4.8 ± 0.7 . This fitting method uses the errors in x and y for each point, but is unable to take of account of the fact that the errors are asymmetric. The mean of the upper and lower error is used for the error in each axis.

This fitting method should be accurate as long as the points deviate from the mean relation only on account of the statistical errors. In cases where there is a large intrinsic scatter about the relation, the statistical errors do not provide an appropriate basis for the weighting of the data points. An alternate approach is to weight all the points equally, ignoring the statistical errors as misleading. To check our result we also fitted our $L_X:T_X$ relation using the SLOPES package (Isobe et al., 1990) to perform an OLS bisector fit and ignoring statistical errors. The best fit slope for this technique was 5.05 ± 0.44 , very similar to the slope found when using the errors.

From the temperature profiles for each galaxy, we are able to identify which of our targets have strong temperature gradients which could affect the measured mean temperature. Excluding these weakens the relation to $\sim 2.8\sigma$ significance, and gives a best fit slope (fitted using statistical errors) of 5.9 ± 1.3 . We also fit the sample of galaxies with known temperature gradients, and found a $\sim 2.7\sigma$ correlation, with a slope of ~ 3.7 .

The $L_X:T_X$ relation has been used extensively in the study of groups and clusters of galaxies. Figure 4.4 shows our data points plotted alongside those for samples of groups (Helsdon & Ponman, 2000) and clusters (David et al., 1993; Mushotzky & Scharf, 1997; Fairley et al., 2000). Our data follow a relation of similar slope to that of the groups (Helsdon & Ponman find a best fit slope of 4.9 ± 0.8), but offset to a lower luminosity or higher temperature. For a given temperature, our galaxies are a factor of ~ 3 less luminous. Because of the scatter in both samples, there is some overlap between the groups and galaxies, and some of our galaxy data points lie above the group best fit line. Conversely, the best fit relation for clusters is significantly shallower than that for groups or galaxies, though again there is a small region of overlap between the most luminous galaxies and the faintest clusters.

4.5.3 $L_X:L_B$ and $L_B:T_X$ relations

One of the more common relations used in studies of early-type galaxies is the $L_X:L_B$ relation. Figure 4.5 shows the $L_X:L_B$ relation for our galaxies. For the sample as a whole, there is a 3.9σ correlation, with a slope of ~ 2.7 . This is quite a steep relation, comparable to that found for a sample of BGGs in previous work (O’Sullivan et al., 2001a). We have also plotted the best fit relation found for X-ray bright galaxy groups, from Helsdon & Ponman (2002). The slope

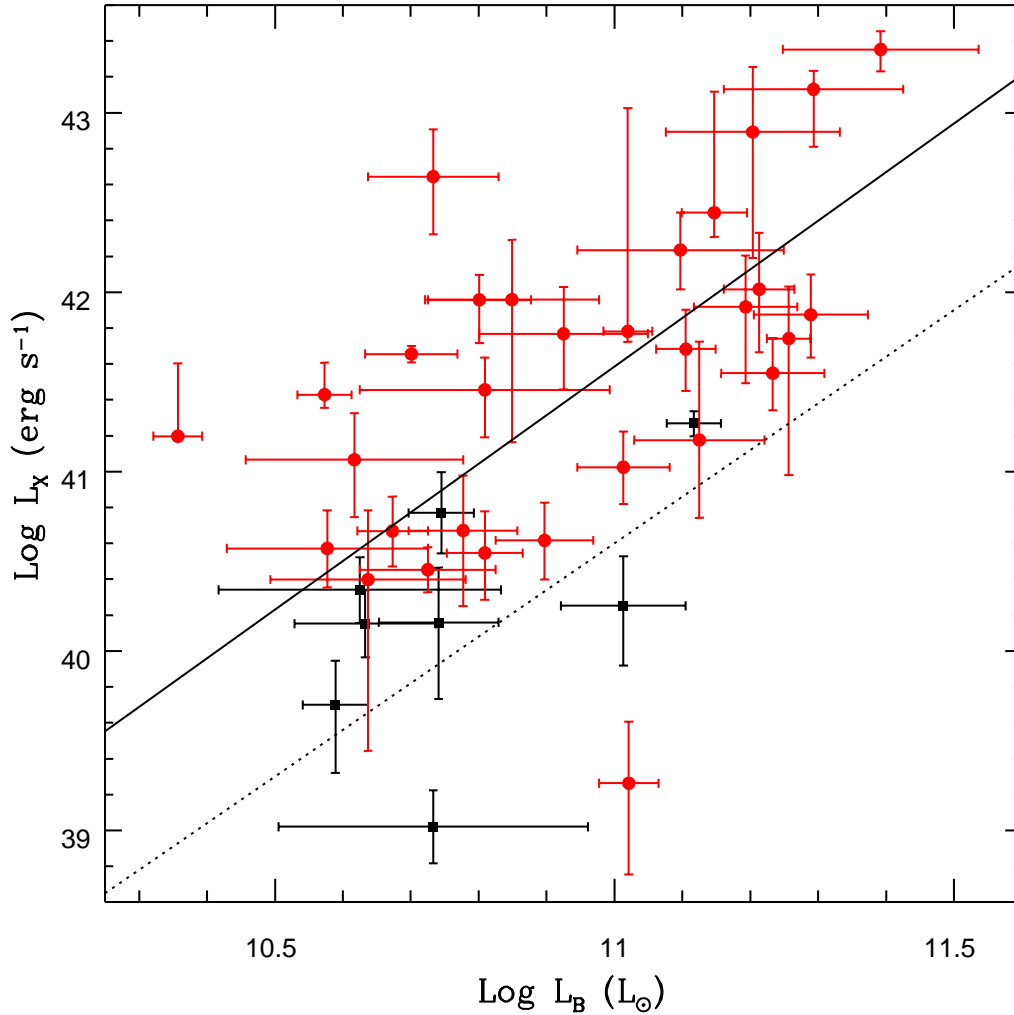


Figure 4.5: L_X plotted against L_B for our sample of galaxies. Although there are some outlying points, a clear trend is visible. Galaxies in X-ray bright groups are marked by red circles, those in X-ray faint groups by black squares. The solid line marks our best fit relation, while the dotted line shows the best fit relation for X-ray bright groups (Helsdon & Ponman, 2002).

of this relation (2.6 ± 0.4) is very similar to that found for our sample of galaxies. However, our relation is offset from that for groups, with galaxies having X-ray luminosities a factor of ~ 9 higher than those of groups with equal optical luminosity, or conversely L_B values ~ 2.3 times lower than groups of similar L_X . This result can be compared to the $L_X:T_X$ relation shown in Section 4.5.2, in which galaxies are offset to lower luminosities at a given temperature, compared to groups.

The $L_B:T_X$ relation for our galaxies is shown in Figure 4.6. Once again, for this relation we find a fairly strong correlation ($\sim 4\sigma$ significance). The slope of the relation is comparable to that found for groups and clusters; 1.91 ± 0.33 for our galaxy sample, 1.64 ± 0.23 for galaxy groups (Helsdon & Ponman, 2002), and ~ 1.5 for galaxy clusters (Lloyd-Davies & Ponman, 2002). However, where the relations for groups and clusters are essentially the same (Helsdon & Ponman, 2002), our relation for galaxies is significantly offset to higher temperatures (by a factor of ~ 2 , compared to groups) or lower L_B (by a factor of ~ 3).

4.5.4 The $\sigma:T_X$ relation

For undisturbed objects with hydrostatic halos, both X-ray temperature and velocity dispersion should be estimators of total system mass. It should be noted that the σ quoted for our galaxies is a stellar velocity dispersion measured in the core of each object, whereas similar relations for groups and clusters use the velocity dispersions of the galaxies within those structures. Figure 4.7 shows the $\sigma:T_X$ relation for our sample, again subdivided by temperature structure. For the sample as a whole, we find a $\sim 3.1\sigma$ correlation, with a relation of the form $\sigma \propto T_X^{0.56 \pm 0.09}$. However, there appears to be a large degree of scatter about this line. Using the errors on the data points to measure the expected statistical scatter, we can estimate the intrinsic scatter of the data. We find that the data points are ~ 1.8 times more scattered than would be expected from the statistical errors alone, hence the statistical scatter accounts for 56% of the variance we see.

Also marked on the plot is the best fit relation for clusters of galaxies, taken from White et al. (1999). Our relation is indistinguishable from this relation in both slope and intercept. The relation for galaxy groups is somewhat steeper; Helsdon & Ponman (2000) find a relation of $\sigma \propto T_X^{1.7 \pm 0.3}$ for their sample. Finally, Figure 4.7 shows a line representing $\beta_{spec}=1$, which is expected for systems where there is equipartition of specific energy between stars and gas. Our relation is consistent with this line, within the errors.

Although there are many previous studies of samples of early-type galaxies, very few have measured temperatures for their targets. Davis & White (1996), one of the few exceptions, fit a $\sigma:T_X$ relation to a sample of 26 galaxies observed using the *ROSAT* PSPC or *Einstein* IPC. They find a slightly steeper relation than ours, with $\sigma \propto T_X^{0.69 \pm 0.1}$. Their slope therefore has an

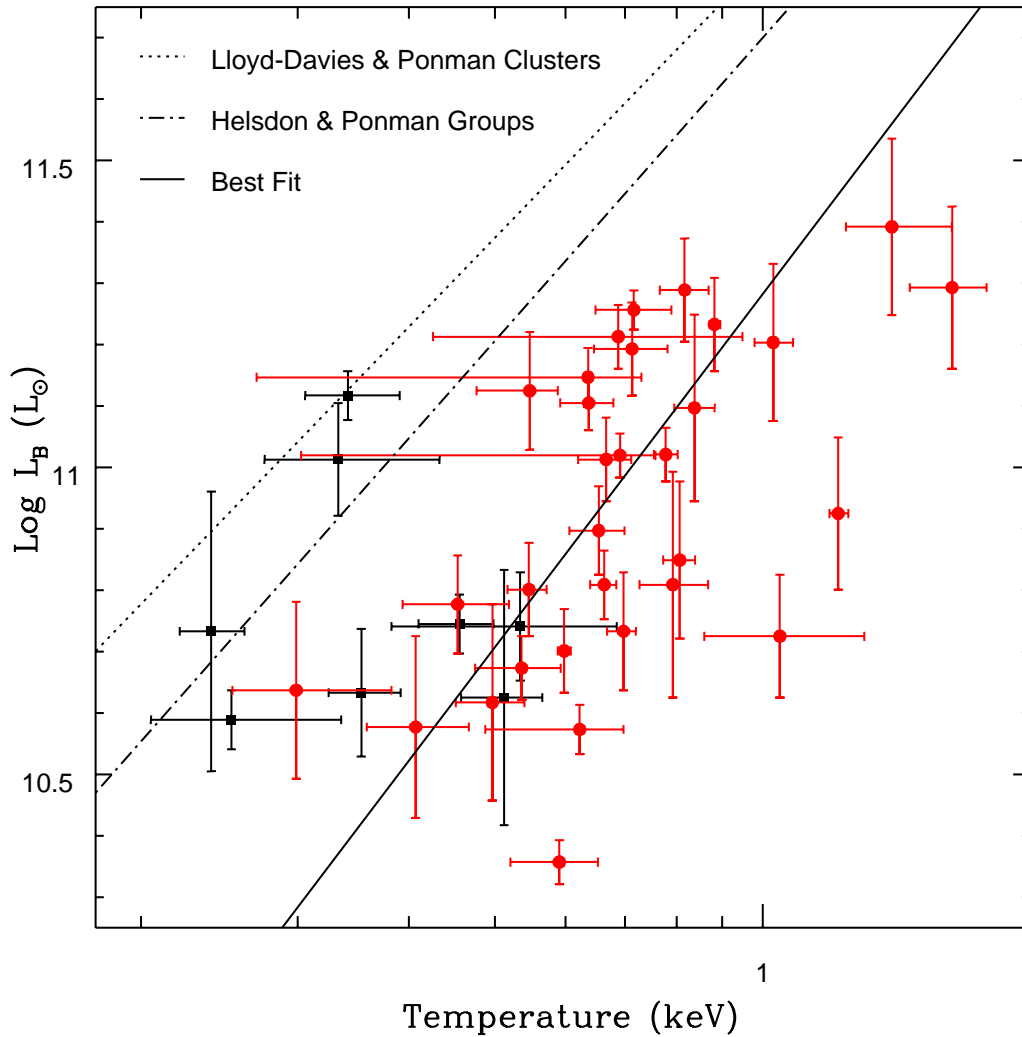


Figure 4.6: L_B plotted against temperature for our sample of galaxies. Red circles mark galaxies which lie in X-ray bright groups or clusters, squares those in X-ray faint groups. The solid line is the best fit relation, while the dotted and dash-dotted lines show the relations for clusters (Lloyd-Davies & Ponman, 2002) and X-ray bright groups (Helsdon & Ponman, 2002) respectively.

overlapping error region with ours, though the best fit line of each does not fall within the errors on the other fit. Their line is also offset to higher temperature. We believe this is probably caused by contamination by surrounding emission or discrete sources, as the spectral fits use a simple single component Raymond-Smith model (Raymond & Smith, 1977). Unless the galaxies in their sample are completely dominated by halo emission, we would expect such contamination to raise the measured temperature of single component models, and we found evidence of such

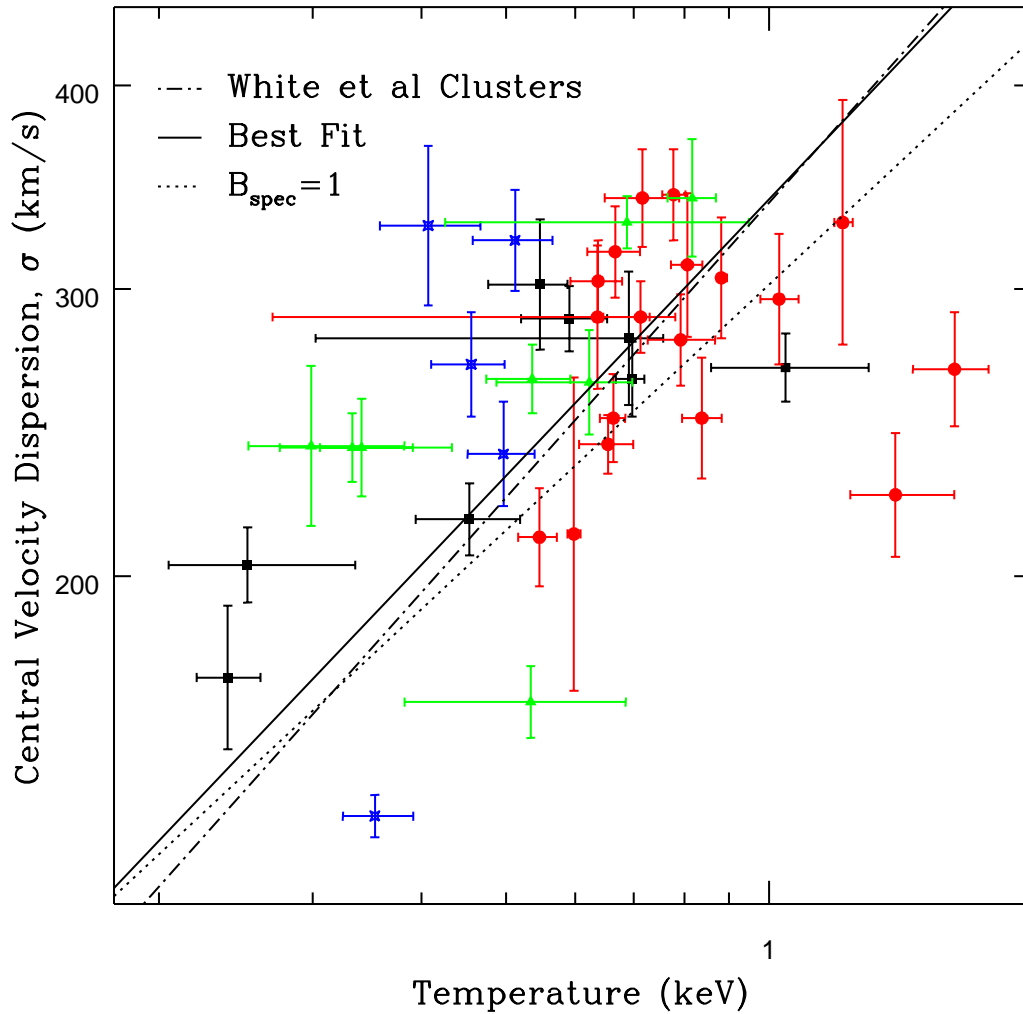


Figure 4.7: Velocity dispersion, σ , plotted against temperature for our sample of galaxies. Galaxies which show signs of central cooling are marked with red circles, those with central heating by blue stars, relatively isothermal galaxies by black squares and those we have been unable to classify by green triangles. The best fit line to the sample as a whole is marked by a solid line, and the fits to the two subsamples are marked by dashed lines. $\beta_{\text{spec}}=1$ is marked by a dotted line, while the best fit relation for galaxy clusters (from White et al., 1999) is marked by a dot-dashed line.

biases when comparing one and two component fits to galaxies in our own sample.

4.5.5 β_{fit} and Entropy

Simple self-similar models of dark matter halos predict that X-ray emission from gas in the halo will always take the same form. Assuming the hot gas in the system is in hydrostatic equilibrium,

the gas density can be represented by a King profile (Cavaliere & Fusco-Femiano, 1976). β_{fit} values for groups and clusters typically lie between 0.4 and 1. Studies of low mass clusters and galaxy groups show that their surface brightness profiles become shallower with decreasing T_X (Ponman et al., 1999). This is usually taken as an indication of additional physical processes affecting the gas, the result of which is that the the gas halo appears more extended and diffuse. Self-similar models also predict that gas entropy will vary linearly with system temperature, as entropy is here defined as $S=T_X/n_e^{2/3}$ (where n_e is the electron density of the plasma), and mean gas density will be constant for all systems which virialised at the same redshift. For high mass clusters, this prediction matches the observed relation, but in lower mass systems the behaviour alters, with the trend flattening so that systems of temperature ~ 1 keV seem to have entropy values (measured at $0.1 R_{virial}$) scattered around a mean value of ~ 140 keV cm² (Lloyd-Davies et al., 2000).

The most common suggested processes which could affect the gas halo are heating, either by galaxy winds (Ponman et al., 1999) or AGN (Wu et al., 2000), or cooling of very low entropy gas (Muanwong et al., 2001). Voit & Bryan (2001) have recently suggested that a combination of cooling and star formation is likely to be a highly efficient way of producing the observed effects, as the heating will be centred in regions containing the lowest entropy gas, giving the maximum entropy increase. The fact that the $S:T_X$ relation approaches a constant entropy “floor” implies that the level of entropy increase is constant over a wide range of systems. In more massive systems, the entropy increase from shock heating is much larger than this amount, so it passes unnoticed. Only in small systems does it become the dominant contribution. Given this, and the fact that the suggested methods of raising the entropy are likely to occur predominantly within galaxies, we might expect that galaxy halos would show the effects of entropy increase very clearly.

The entropy floor observed in low mass systems also has an effect on their surface brightness profiles. Raising the entropy of the intra-cluster medium (ICM) through heating will push gas out to larger radii if it occurs after the system forms, or prevent it from collapsing as far as expected if it occurs beforehand. The halo will therefore be more extended, with a lower central density, presenting a flatter surface brightness profile. We therefore expect β_{fit} to decrease with decreasing temperature, and this is observed across a wide range of systems (Ponman et al.,

1999). Given the likelihood that entropy increase has occurred in galaxy halos, we may also expect to find a relation between β_{fit} and temperature.

Figures 4.8 and 4.9 show the slope parameter β_{fit} plotted against temperature for our sample. There is no obvious trend in the points, and we find no statistically significant correlation. The scatter on the points is quite large, particularly at intermediate temperatures. There is no clear segregation of galaxies by temperature structure, and all classes show comparable amounts of scatter. In Figure 4.9, there is some suggestion that AGN, BGGs and BCGs are more scattered than the more normal ellipticals, particularly if the normal galaxy with the highest value of β_{fit} is excluded. This galaxy is NGC 1404, which is commonly considered to have suffered ram-pressure stripping of its halo (Paolillo et al., 2002). The sharp cut off in its surface brightness profile could conceivably have produced an unusually steep fit. However, the small size of the subsample makes any detailed comparison unreliable. The subsample seems to be centred on $\beta_{fit} \simeq 0.55$, which is similar to the mean value of our sample as a whole.

Assuming that our galaxies are isothermal, we can extrapolate from our 2-dimensional surface brightness models to 3-dimensional density models of our galaxies. Equation 4.1 describes the 2D models, and we can describe the 3D models as shown in Equation 4.3.

$$\rho(r) = \rho_{(0)} [1 + (r/r_{core})^2]^{-\frac{3\beta}{2}} \quad (4.3)$$

The density normalisation, $\rho_{(0)}$, can then be determined from the surface brightness normalisation, assuming the temperature and metallicity determined from spectral fitting. From these 3D models, it is possible to derive gas properties such as density, entropy, cooling time, etc, as a function of radius. In order to be able to compare the resulting profiles fairly, we need to view them on a common scale. This can be done by scaling the profiles by the virial radius of the system, or more usually to a fixed overdensity radius, such as R_{200} . The overdensity is calculated relative to the critical density of the universe at the redshift of formation. This is unknown for most systems, and in the case of clusters and groups is generally taken to be the redshift of observation. For galaxies, such an assumption is very unlikely to be accurate, even taking into account the fact that early-type galaxies will have potentials determined by the density of the universe at the redshift of last major merger rather than that at which the majority of their stellar population formed. In order to calculate R_{200} , we assume a mean redshift of formation for ellipticals of $z_{form}=2$ (Kauffmann et al., 1996; van Dokkum & Franx, 2001). Using this

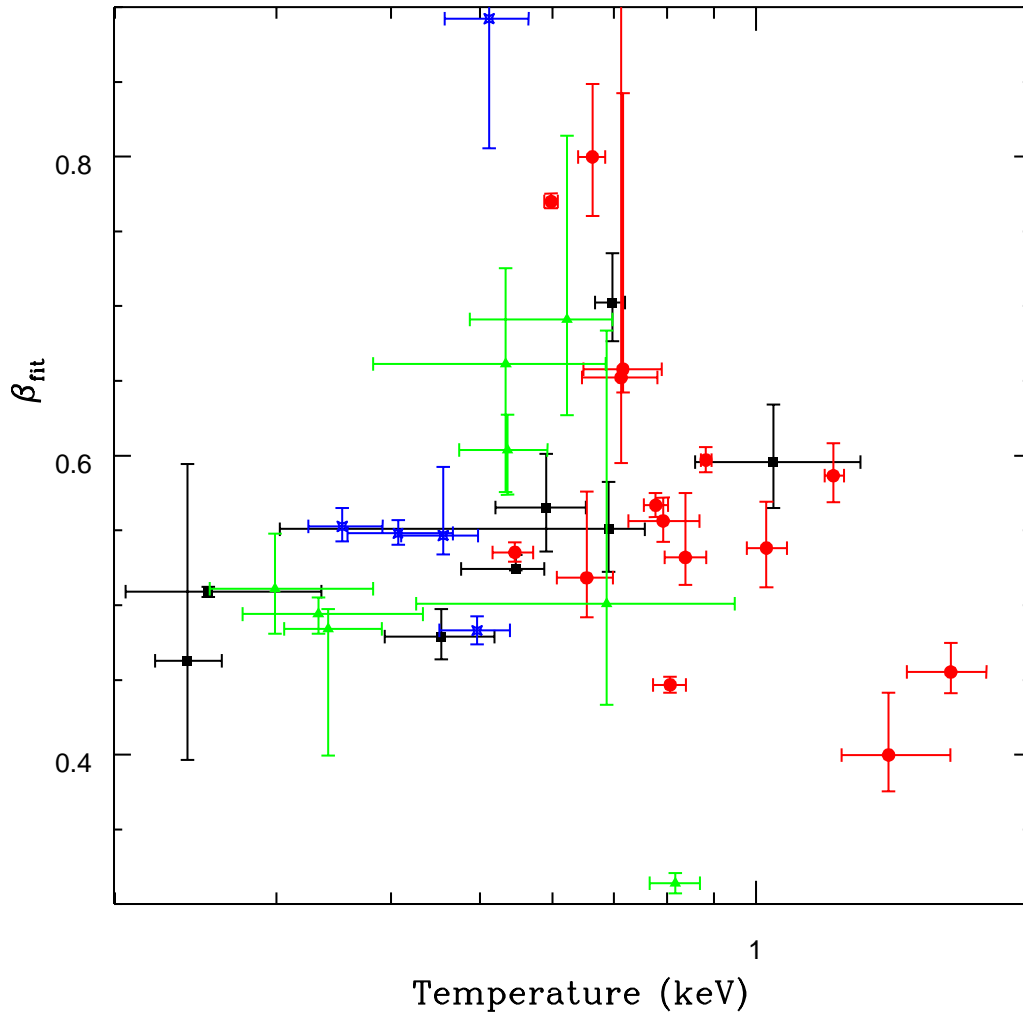


Figure 4.8: Plot of β_{fit} against temperature for our sample of galaxies. Galaxies with cool cores are marked with red circles, those with hot cores by blue stars, those with isothermal profiles by black squares, and those we have been unable to classify by green triangles.

value, we can calculate R_{200} as described in Balogh et al. (1999) and Babul et al. (2002), taking variation of overdensity with redshift from Eke et al. (1996).

Figure 4.10 shows entropy, calculated at one tenth of R_{200} . Once again, galaxies are marked to show their different temperature structures, but while the data shows a large amount of scatter, there is no significant correlation with temperature, or segregation by temperature structure. The galaxy data points do mainly fall at the low temperature end of the $S:T_X$ trend for groups and clusters, but show no evidence of any trend themselves.

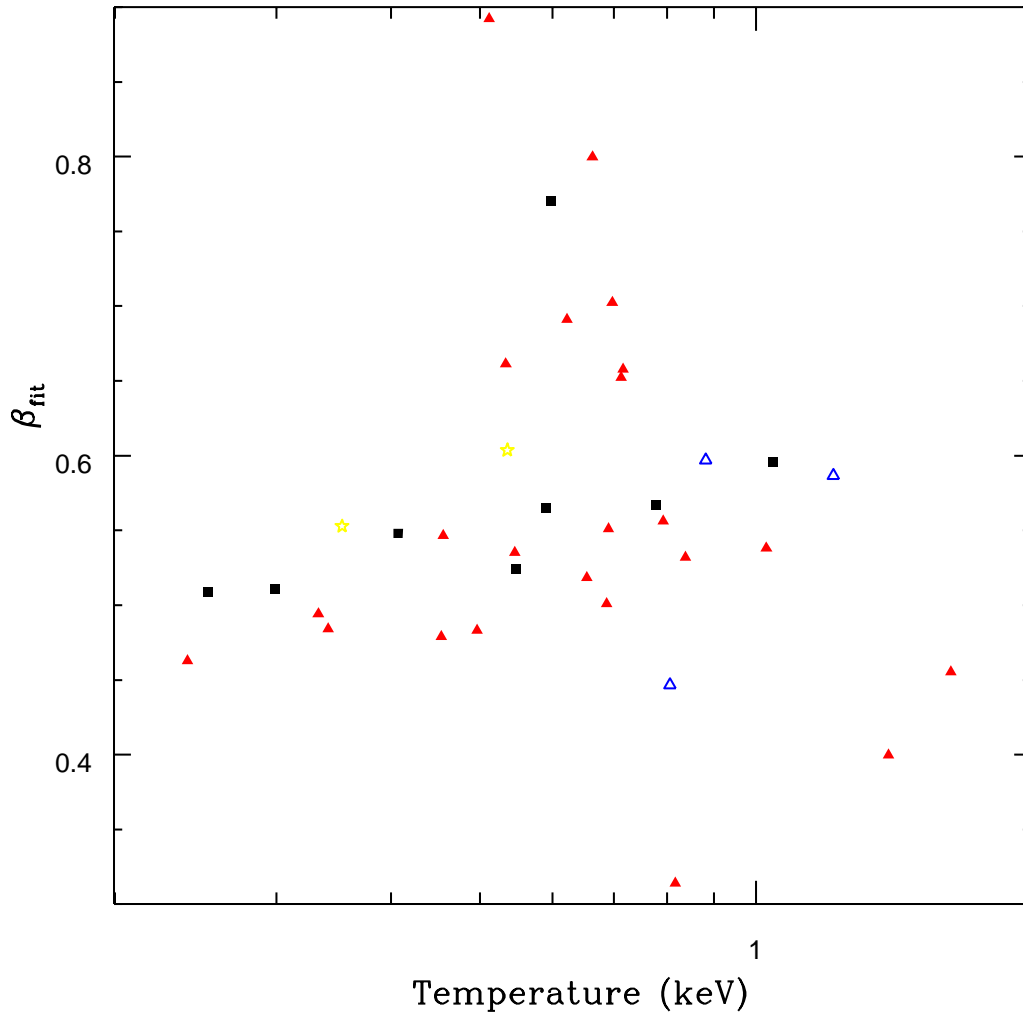


Figure 4.9: Plot of β_{fit} against temperature for our sample of galaxies, as in Figure 4.8. filled triangles represent brightest group galaxies, open triangles brightest cluster galaxies, stars are AGN, and squares are normal early-type galaxies. Error bars are omitted for clarity.

4.6 Discussion

The results presented in the previous section do not lend themselves to a simple explanation. The halos of massive early-type galaxies seem to have some obvious similarities to those of galaxy groups and clusters, but also some intriguing differences. Clearly a number of the relations which hold for groups and clusters also apply to early-type galaxies, the most important examples being the $\sigma:T_X$ and $L_X:T_X$ relations. The $\sigma:T_X$ relation is particularly striking, in that it agrees

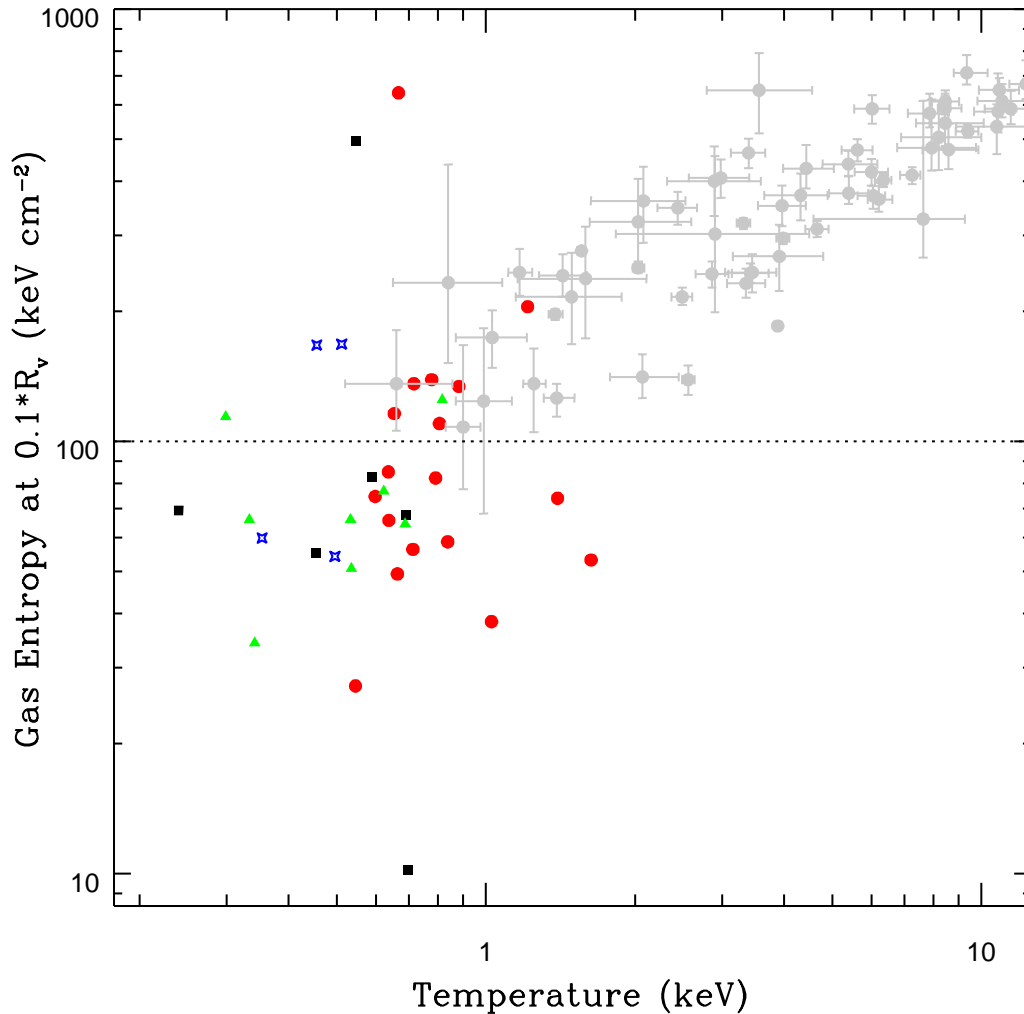


Figure 4.10: Mean gas entropy measured at one tenth of the virial radius plotted against mean halo temperature. Galaxies with cool cores are marked as red circles, galaxies with relatively isothermal halos are represented by black squares, those with hot cores by blue stars and those we were unable to classify by green triangles. Grey points with error bars represent groups and clusters taken from the Birmingham-CfA cluster scaling project (see Sanderson et al., 2002). The approximate level of the entropy floor for groups and clusters is marked by a dotted line.

closely with the relation found for galaxy clusters. The $L_X:T_X$ relation has a similar slope to that of galaxy groups, but is offset to lower luminosities. The $L_B:T_X$ and $L_X:L_B$ relations also show offsets from the cluster and group relations, but to higher X-ray luminosity and temperature. Another important result is the roughly constant value of β_{fit} across a wide range of temperatures. Although there is some suggestion of influence by surrounding groups and

clusters on this parameter, the environment seems to increase scatter rather than producing a trend. Together with the results of our entropy calculations for the sample, the behaviour of β_{fit} suggests that if preheating effects are important in galaxy halos, they produce results quite different to those seen in groups.

4.6.1 Comparison with Groups and Clusters

One of the most important results to arise from studies of galaxy groups and clusters is the demonstration that simple self-similar models do not describe low mass systems well. There is good evidence that galaxy groups differ from higher mass clusters in a number of important ways. The most widely accepted explanation for these differences is that the hot gas in the halos of these systems is affected not only by the processes involved in the formation of the system as a whole, but also by processes such as star formation, AGN heating, and gas cooling. A clear sign of this is seen in the behaviour of gas entropy in systems of different mass. In high mass clusters, entropy can be fairly accurately predicted from simple models in which the gas is heated (and has its entropy profile set) during formation of the system. As the cluster builds up, gas flows into the potential well and is shock heated to a degree dependent on the depth of the potential. This dependence of halo temperature on system mass can be seen in the $\sigma:T_X$ relation for clusters, in which T_X is strongly correlated with σ , with $T_X \propto \sigma^2$, as expected from arguments based on the virial theorem.

However, as system mass (and temperature) drop, the gas entropy begins to depart from the predicted relation, with low mass galaxy groups having higher than expected gas entropies. Lloyd-Davies et al. (2000) have shown that at temperatures below ~ 2 keV, gas entropy appears to remain roughly constant, scattering about a mean value of 140 keV cm^2 . An effect is also seen at around this temperature in the surface brightness profiles of galaxy groups and clusters (Ponman et al., 1999). High temperature systems ($T_X > 4 \text{ keV}$) have profiles which scale self-similarly, but as T_X is lowered, the surface brightness profiles observed are found to be shallower, with lower central densities. This has an obvious effect on the measured X-ray luminosities of these systems, making them fainter than predicted.

Both of these trends are explained through the effects of non-gravitational processes on the gas. To take a simple model, we can imagine a system at the time of formation. As stated

above, we expect the gas falling into the potential of the system to be heated by gravitational processes, but we might also expect heating from other sources. For example, as galaxies form in the system we could expect star formation, galaxy winds, and AGN to affect the gas in the system halo. In a large system, the contribution from these sources will be small compared to that of gravitational heating. However, in smaller systems it will be more important, and will eventually dominate the energy of the gas halo. This additional heating will have a number of effects, such as raising the gas temperature, causing the halo to expand by moving gas to higher radii, raising the entropy of the gas, and so on. In practice, it is possible to achieve these effects through a number of processes, or a combination of several. One promising model is that of Voit & Bryan (2001), in which low entropy gas cools rapidly, providing material for star formation. This star formation then not only removes low entropy gas from the system (raising the mean entropy), but provides heating which is focused in the areas in which low entropy material dominates. From our point of view however, the method is not important; all the suggested processes would occur in galaxies, and might be expected to occur preferentially in large galaxies at the bottom of a group or cluster potential well. For simplicity, we will refer to this as the preheating model.

The $\sigma:T_X$ relation

One of the clearest similarities between the relations for our galaxies and those of larger structures is the correspondence of the $\sigma:T_X$ relation to that of galaxy clusters. As discussed above, the correlation in clusters is expected, and shows that both T_X and σ are good measures of the potential. In galaxy groups, the slope of the relation is observed to be somewhat steeper, $\sim 1.7 \pm 0.3$ (Helsdon & Ponman, 2000). One explanation for this steeper slope is that T_X is raised in low mass systems by the heating and removal of cool gas described above. An alternative is the suggestion that the velocity dispersions measured in groups could be biased. There are a number of groups which, despite apparently possessing extended X-ray halos, have exceptionally low velocity dispersions (Helsdon & Ponman, 2000). If these σ values were accurate, the potential of the group would not only be too shallow to produce the halo luminosity observed, but would be too shallow for the group to have collapsed within the age of the universe. Several reasons for the underestimation of σ can be postulated. It is possible that these low mass

groups form a central core of bright galaxies, with fainter members at higher radii. The brightest galaxies are most likely to be recognised as group members and have measured redshifts, so they will dominate any calculation of σ . Tidal interactions between group members could reduce velocity dispersion by transferring orbital energy from the galaxies to their stars. It has also been suggested that low mass groups may be biased because the groups often have prolate structures. For groups whose major axis lies near the plane of the sky, this particular structure could lead to an underestimation of σ (Tovmassian et al., 2002), biasing samples including such low temperature systems. If σ is biased, correcting the measurements for the lowest temperature groups would probably shift the best fit relation into agreement with that seen in clusters. It is worth noting that the groups with the lowest velocity dispersions listed in Helsdon & Ponman (2000) are also amongst the poorest; all groups in their sample with $\sigma < 150 \text{ km s}^{-1}$ have only 3-5 member galaxies. Calculating velocity dispersion from such small numbers can introduce a bias, producing values which are underestimated by up to 15% (Helsdon, 2002).

The fact that our results agree well with the cluster relation suggests that again, we are looking at systems in which both T_X and σ are good measures of the potential. From a preheating point of view this is surprising. If we expect preheating processes to occur in large galaxies, then we might expect the T_X of their halos to be raised, in much the same way as we see in galaxy groups, producing a steeper relation. We also need an explanation of why the gas in these galaxies has a temperature which is related to the depth of their potential well. As well as additional heating from star formation and AGN activity, we expect large quantities of gas to be lost from the stars in the galaxy. As this gas is produced within the galaxy, we cannot expect shock heating during infall, so we might initially believe its temperature to be entirely determined by supernova heating.

Helsdon et al. (2001) consider a related question, that of the relative importance of different energy sources which contribute to the total X-ray luminosity of early-type galaxies. Their Figure 8 is a plot of L_X/L_B against L_B , showing the contributions to L_X from discrete sources, SNIa and gravity. From our point of view the contribution from discrete sources is irrelevant, as we are interested in energy input to the gas in the galaxy. The gravitational contribution is a combination of two processes, firstly a contribution from the velocity of the stars in the potential (gas lost from these stars will have an added kinetic energy component from their velocity, which

will be thermalized in the surrounding ISM), and secondly a contribution from work done on the gas as gravity causes it to contract and cool. The important result with regards to our situation is that while the SNIa energy input scales with L_B , the gravitational input scales with σ^2 . This means that for low mass systems, the dominant contribution to L_X is from supernova heating, but above $L_B \sim 10^{10} L_\odot$ gravitational work begins to dominate. If we consider these two factors as energy inputs to the gas rather than as contributors to L_X , we can see that the gas temperature is likely to be determined by the supernova rate in low mass systems, and by the depth of the potential in high mass systems. The point at which the two are equal will depend on the details of the model, but if we follow the assumptions made by Helsdon et al. (2001), all our galaxies lie in the high mass, gravitationally dominated region of the plot. **We could therefore expect gas temperature to depend on the depth of the potential, whether the gas has an internal or external origin.**

It seems likely, from this result, that we can draw similar conclusions from the $\sigma:T_X$ relation in galaxies as we would in clusters. T_X and σ are both probably good measures of mass. Preheating, by whatever method, does not appear to have the effect on galaxy halos that is has on those of groups. Like clusters, the galaxy relation is consistent with the systems having $\beta_{spec} = 1$, suggesting that there is equipartition of specific energy between stars and gas. As we will discuss later, this has important implications, in that it suggests that the optical and X-ray density profiles should be similar. One further consideration is the intrinsic scatter in the points. Our data has ~ 1.8 times as much scatter as we would expect from statistical errors alone. For comparison, the galaxy groups studied by Helsdon & Ponman (2000) are less scattered, having only ~ 1.4 times as much as would be expected from the errors. The larger degree of scatter in the galaxy data could have a number of causes. Gas temperature could be affected by many processes, related to the galaxy or the surrounding environment. Velocity dispersion could also be affected by processes associated with the formation or merger history of the galaxy.

The $L_X:T_X$ relation and β_{fit}

Accepting σ and T_X as indicators of the mass of the system, we next consider the $L_X:T_X$ relation. Here, we find that the slope of the relation is steeper than that of clusters, as steep as that of groups. The relation is also offset, so that at a given temperature, galaxies have a

lower luminosity than groups. The steep slope is usually explained as a product of preheating - the additional heating of the gas raises the temperature slightly and moves gas to higher radii, lowering the central density and therefore L_X . If we assume that the steep slope seen in galaxies is caused by the same processes which cause it in groups, then this relation is a strong piece of evidence for the effects of preheating in galaxies.

However, there are other ways in which we might produce such a steep slope. Helsdon et al. (2001) found a strong correlation between the X-ray properties of group dominant galaxies and those of the groups in which they are found. Given the signs of central cooling in many of these groups, they suggested that what had been initially identified as the halos of the dominant galaxies were in fact group scale cooling flows, centred on the dominant galaxy because it lies at the bottom of the group potential. They also found that the L_X of this central galaxy halo/cooling flow was $\sim 25\%$ of the L_X of the group. As 29 of our 39 galaxies are dominant galaxies in groups, clusters or cluster subclumps, we must consider the idea that our relations could be dominated by cooling flows. In that case, we would expect the $L_X:T_X$ relation to have a similar slope to that of groups, but to be offset to lower L_X values by a factor of 4, and also to lower temperatures. Provided the temperature drop is not too large, this could reproduce the relation we see very well. On the other hand, we do not see any segregation in the data between those galaxies which show signs of central cooling and those which do not, nor do we see any difference between galaxies at the centres of groups and those in other environments. This argues against cooling flows as the driver of the relation. We will discuss the evidence for and against cooling flows as the dominant factor in Section 4.6.2.

The lack of a relation between β_{fit} and T_X argues against both cooling flows and preheating as the source of the $L_X:T_X$ relation. In galaxy groups, preheating causes gas to move out to high radii, reducing β_{fit} as the surface brightness profile becomes flatter. As preheating is more effective in smaller mass systems, groups and low mass clusters show a correlation between β_{fit} and T_X with cooler systems having flatter profiles. In galaxies, despite a very large scatter, we see no trend with temperature. Our galaxies lie around a mean value of $\beta_{fit} = 0.55$, which means that even if the group and cluster $\beta_{fit}:T_X$ relation levelled off at low temperature, our sample would not be consistent with it. **This strongly suggests that preheating is not the cause of the steep slope of the $L_X:T_X$ relation.**

If a change in the slope of the surface brightness profile is not responsible for the drop in L_X needed to produce the $L_X:T_X$ relation, then there must be a drop in normalisation. This is demonstrated in Figure 4.11, which shows the surface brightness profiles of our sample, scaled so that if they were behaving self-similarly, they would coincide. To achieve this coincidence, the surface brightness profiles are first scaled by the virial radii of the galaxies, to put them all on a comparable radial scale. To account for self similar scaling with mass and cosmological dimming, we would wish to scale the profiles by $T_X^{1/2}(1+z)^{9/2}\Lambda(T_X)$, where $\Lambda(T_X)$ is the temperature dependence of the plasma emissivity (Ponman et al., 1999). However, as all our galaxies are at low redshifts, we can neglect the $(1+z)$ term. We have scaled each profile by $T_X^{1/2}$, and converted from a surface brightness in counts degree⁻¹ to a surface intensity in erg s⁻¹ degree⁻¹. This conversion to surface intensity, using a counts to flux conversion factor for each galaxy based on its X-ray luminosity and measured count rate, should allow for changes in plasma emissivity with temperature and metallicity ($\Lambda(T_X)$, $\Lambda(Z)$). We can therefore expect galaxies with different halo properties, masses and virial radii to produce similar profiles if they behave self similarly. A comparison between Figure 4.11 and Figure 1 of Ponman et al. (1999) demonstrates the difference between the behaviour of our galaxies and that of groups and clusters. The high temperature clusters in Figure 1 of Ponman et al. (1999) behave self-similarly, having roughly equal surface brightness slopes and scaled normalisations. The lower temperature groups move away from self-similarity, as their slopes flatten and central surface brightness (and density) is lowered. In the galaxies, although there is a large amount of scatter, the slope remains roughly constant across the range of temperatures, but the normalisation of the profiles seems to drop with decreasing temperatures. **This suggests that whereas in galaxy groups the steepening of the $L_X:T_X$ relation is caused by energy injection and movement of gas to higher radii, in galaxies it is caused by changes in normalisation and therefore in the overall gas fraction of the systems.** The processes responsible for this change are not clear, but this result demonstrates how differently galaxies behave compared with groups and clusters.

It is interesting to note that the mean slope of the surface brightness profiles ($\beta_{fit} = 0.55$) is similar to the mean slope of the optical surface brightness profile. Elliptical galaxies are well described in the optical by a de Vaucouleurs profile, which is similar (outside the central regions)

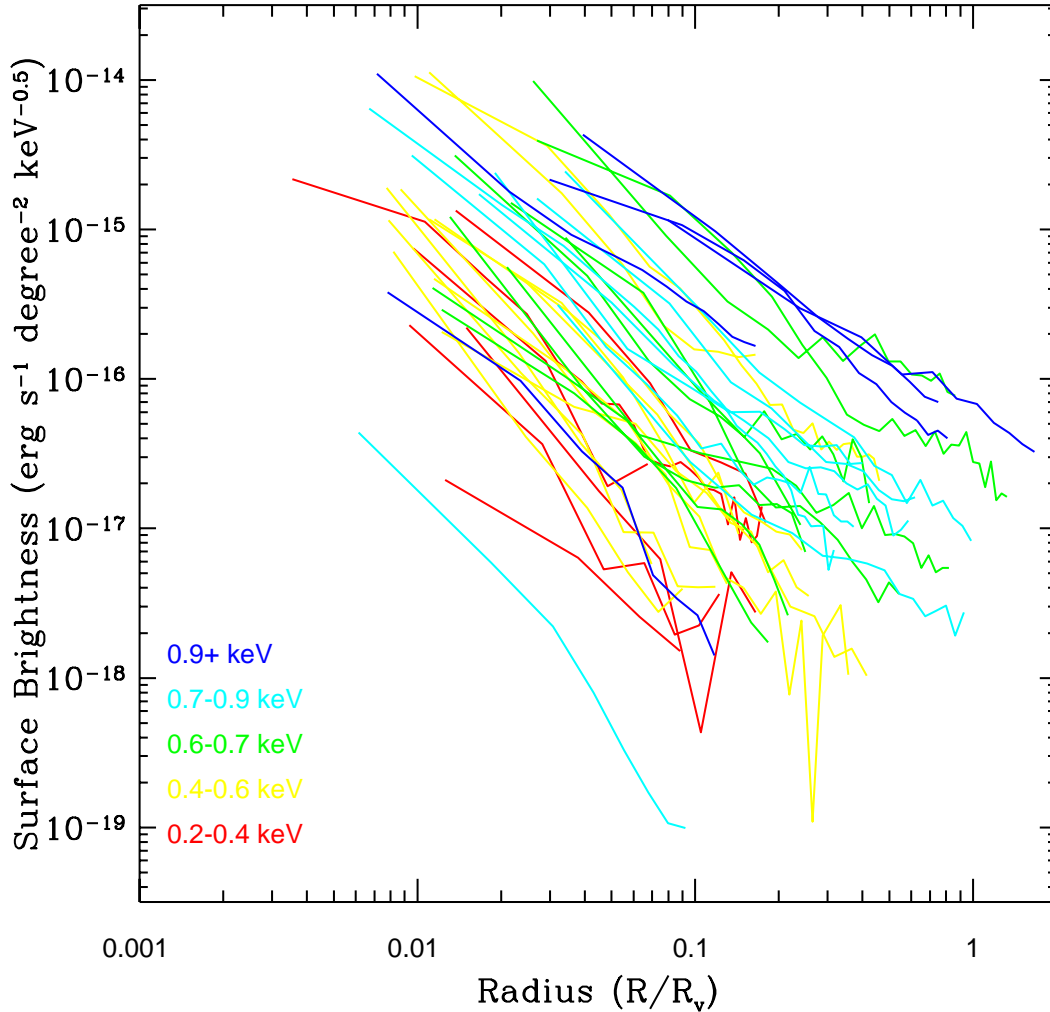


Figure 4.11: Scaled X-ray surface brightness profiles for our galaxies, arranged to show departures from self-similarity. The profiles have been scaled to the virial radii of the galaxies (assuming a redshift of formation $z_{form}=2$), and by $T_X^{1/2}$ to account for self-similar scaling with mass (Ponman et al., 1999). We have also converted from counts to intensity, using the best fit MEKAL component of each galaxy to allow for the temperature and metallicity dependence of the plasma emissivity. As all our galaxies are at low redshift ($z < 0.035$) we ignore cosmological effects as negligible. The profiles are colour coded in temperature bands, and although there is some scatter, it is clear that all have similar slopes and that cooler systems have lower normalisations.

to a King model with $\beta_{fit} = 0.5$. As mentioned in Section 4.6.1, the $\sigma:T_X$ relation is consistent with $\beta_{spec} = 1$, which leads us to expect a similarity between the optical and X-ray density profiles. The similarity in surface brightness profiles is therefore further confirmation of the

$\sigma:T_X$ result. A further interesting note is that galaxy wind models, in which the majority of the gas in the halo is produced by stellar mass loss, predict X-ray surface brightness profiles similar to those in the optical (Pellegrini & Ciotti, 1998). The exact value of β_{fit} would depend on the wind state of the system, with only relatively hydrostatic halos having $\beta_{fit} = 0.5$. Galaxies dominated by supersonic outflows, or those in which inflows are important, would be expected to have steeper profiles owing to their high central gas densities. Galaxies dominated by subsonic outflows would be expected to have slightly flatter profiles ($\beta_{fit} < 0.5$), as the outflowing gas has a higher density at large radii than in a supersonic flow, and less of a central peak. If such models are applicable, it seems likely from the high mass of our galaxies that they would be in the inflow stage, so we would expect $\beta_{fit} > 0.5$, in agreement with our observations.

Entropy

The results of our entropy measurements are in broad agreement with those from the surface brightness profiles. In galaxy clusters and groups we see evidence of similarity breaking and preheating, leading to a trend in entropy which levels off at low temperatures to form the entropy floor. The galaxy data points do not show any sign of a trend, and although they may appear to be consistent with the general trend in higher mass systems, the scatter in the data is very large. Our method of calculating entropy has two important sources of scatter associated with it. Firstly, we must assume that our galaxies are isothermal, despite the fact that we know that many of them have temperature gradients. Secondly, we measure the entropy at one tenth of the virial radius, and when calculating the virial radius we must assume a redshift of formation (or last major merger). Although the assumed value of $z_{form} = 2$ is probably a fairly accurate mean, there will clearly be variation between individual galaxies. Our virial radii will therefore be inaccurate to some degree, meaning that we are actually measuring entropy at a range of radii.

Despite these difficulties, we can draw some important results from the entropy values. A large proportion of the data points lie below 100 keV cm^2 , meaning that they are below the entropy floor observed in galaxy groups. One possible reason for these low values is that the galaxies form earlier than the surrounding groups. The density of systems virialising at a given epoch is related to the critical density of the universe at that time, and so the earlier an object

virialises, the denser we expect it to be. As entropy is inversely proportional to $n_e^{2/3}$, an equal amount of energy injected into a denser system will produce a smaller increase in entropy. Galaxies, forming at $z \sim 2$, might therefore be expected to have higher densities and a lower entropy floor than groups and clusters which have formed more recently. However, we might also expect that as the site of the processes responsible for entropy increase, the amount of energy available to affect entropy in galaxies would be larger than in groups. It is also worth considering that if galaxies had formed with halos of very low entropy gas, it would have cooled on timescales considerably shorter than the Hubble time, probably leading to star formation, heating and a rise in observed entropy (Voit & Bryan, 2001).

An alternative viewpoint is that the majority of the gas in these systems is being produced by stellar mass loss rather than infall, so we should not expect entropy to behave as it does in groups. In this case, galaxy wind models should give a reasonable approximation of the behaviour of the halo, in the absence of significant environmental influences. Several published simulations of galaxy halo development give gas density and temperature profiles (Ciotti et al., 1991; Pellegrini & Ciotti, 1998; Brighenti & Mathews, 1999) for their model galaxies. In models of outflowing winds, both gas density and temperature fall with radius, but density falls more rapidly, so we would expect an entropy profile which increases with radius. In models which have developed gas inflow (cooling flows), temperature may rise with radius throughout most of the model, so again we expect entropy to rise with radius. This matches what we observe in our measured entropy profiles. The entropy predicted at any given radius depends on the details of the model, *e.g.* system mass, age, supernova rate, mass injection rate, *etc.* Entropies ranging from 20-300 keV cm² might be expected for galaxies such as those in our sample. The majority of our galaxies do have entropies within these limits, and considering the expected scatter, the agreement between models and measurements is fairly good.

4.6.2 Cooling Flows

A number of our galaxies have temperature profiles indicative of central cooling. This is not surprising, as they are fairly massive objects, with large halos, and reside within larger structures which are themselves probably capable of producing cooling flows. Among the relations we have examined, several show behaviour which could be explained easily as the product of group cooling

flows. The best example of this is the $L_X:T_X$ relation, where the slope is identical (within errors) with that found for groups, but offset to lower X-ray luminosities. As discussed in Section 4.6.1, this offset (a factor of 3 in L_X) is very similar to that we would predict (a factor of 4), based on studies of X-ray bright groups (Helsdon et al., 2001). We would expect the measured T_X of the cooling flow region to be lower than the group temperature and this could explain the difference between predicted and measured offset. We might also be able to explain the offsets observed in the $L_X:L_B$ and $L_B:T_X$ relation using this model. In both cases we are comparing a parameter which is determined by the galaxy and only weakly influenced by the group (L_B) to a parameter which is determined by the cooling flow and hence by the properties of the group (L_X or T_X). In such a situation, we would have to expect L_X and T_X to appear unusually high for the central galaxy, as they would actually be related to the much larger system of the surrounding group or cluster. Comparing with optical luminosity, we would only expect to find a relation without an offset if we compared them to a value of L_B calculated for all the galaxies in the group, rather than just the central dominant elliptical. We would also expect the galaxies in X-ray faint groups to behave differently, as their halos could not be the product of group scale cooling flows. Unfortunately, the small numbers of such objects in our sample means we cannot test whether they follow a different trend to those in X-ray bright groups, but they do indeed appear to fall at lower L_X and T_X , for a given L_B .

However, there are two powerful arguments against group scale cooling flows as the dominating influence in our sample. Firstly, we find that a significant subset (one third) of our sample do not show signs of central cooling. They are instead approximately isothermal, or have a central rise in temperature. This does not necessarily mean that they have not been at the centre of a group cooling flow in the past, but such a flow would have to have been disrupted, and so would be unlikely to produce the emission we assume to be a halo. Secondly, and most importantly, we see no sign of a difference between those galaxies with or without signs of central cooling. The only segregation we see in any of the relations is a tendency for galaxies which seem to harbour cooling flows to be higher mass systems, and so to have higher values of σ , T_X , L_X , *etc.* We see no other difference between galaxies with differing temperature profiles, and we specifically do not see the galaxies with apparent cooling flows driving the $L_X:T_X$ relation. This strongly suggests that while a number of our galaxies do harbour cooling flows, some of them quite large,

their halos are not simply cooling flows formed by surrounding groups and clusters, unless the properties of the gas halo are independent of whether it arises from stellar winds or group inflow.

4.6.3 Stellar Mass Loss and Galaxy Winds

Large scale cooling flows, in which most of the gas in the galaxy halo has an external origin, do not appear to provide a good model for our galaxy sample. The alternative is a model in which the majority of the gas is produced (and heated) internally, via stellar mass loss. We have already discussed in Section 4.6.1, the relative contributions to the energy of gas produced in a galaxy from supernovae and gravitational processes. Our sample is made up of galaxies with high stellar masses, leading us to believe that the gravitational potential should be the dominant source of energy. This provides an important link between the X-ray properties of the galaxies and their mass, which could explain the correlations we see between optical and X-ray properties in our sample. If gravity is the dominant source of energy in the halos of our galaxies, we would expect them to behave like clusters on many of the relations we have examined. The best example of this is the $\sigma:T_X$ relation, where the galaxies and clusters have best fit lines which are indistinguishable.

However, there are a number of ways in which the relations do not behave like those of galaxy clusters, and we need to find explanations for these differences. The most interesting, and perhaps the most important, is the $L_X:T_X$ relation. This behaves like that of galaxy groups, rather than galaxy clusters. However, instead of a decrease in central gas density in low mass systems, leading to a trend in β_{fit} with temperature, we see a constant value of β_{fit} and a decrease in the normalisation of the surface brightness profiles at low masses. This suggests that the lower mass members of our sample lie progressively further below the cluster $L_X:T_X$ relation because they have a lower gas fraction than their higher mass counterparts. To explain the $L_X:T_X$ relation we observe, we need an explanation of this change in gas fraction with temperature.

A number of possible reasons for this trend in gas fraction (f_{gas}) could be suggested. These include:

- The change in f_{gas} is a natural consequence of halo production by stellar mass loss. Any steady state solution would produce the trend we see.

- The change in f_{gas} is the product of the surrounding environment. Higher mass systems tend to be in higher mass groups and clusters, which have a denser IGM. This prevents the escape of gas, or compresses the halo, or allows accretion of gas, causing the halo to reach higher densities and gas fractions.
- The lower gas fraction in cooler galaxies is an evolutionary effect, related to the age (or time since last major merger) of the galaxy. As the galaxy ages some process causes halo density to rise, and the older systems have the highest density and are therefore the hottest.
- Supernova heating, though not the dominant source of energy in the halos, does have a second order effect on them. Perhaps in lower mass systems, the relatively higher contribution from SNIa causes gas to be lost from the potential, lowering the overall fraction.

Of these suggested models, the last seems the least likely. Although it is plausible that supernova heating could have observable effects on the galaxy halos, particularly in the least massive members of our sample, it seems unlikely that it could affect the gas fraction in the same way at all radii. In the analogous situation of gas heating in galaxy groups, the central gas fraction is lowered, but only by moving gas to higher radii, raising the gas fraction there. There are however some obvious differences which could make this comparison invalid, such as the distributed heating and mass injection expected from the stars in a galaxy. It is also important to remember that we cannot in most cases observe the galaxy halo to high radii. It is possible that gas could be removed to a large fraction of the virial radius, where its low density might make it undetectable, and where it could be easily stripped by any interaction with a surrounding IGM. However, the fact that we see no sign of any trend in β_{fit} is a strong argument against this hypothesis.

There are also problems with the idea that such a trend might be a natural result of galaxy halos forming from gas of stellar origin. Most of our galaxies are large, bright objects which dominate larger surrounding structures. However, previous work on a sample including galaxies found in a variety of environments and with a wide range of luminosities suggests that galaxy winds are the most likely formation method for the halos of early-type galaxies of all sizes (O’Sullivan et al., 2001b,a). The galaxies in our sample could in fact be considered less likely to

conform to such a model because their properties differ from those of the majority of early-type galaxies. The steep trend in the $L_X:T_X$ relation is caused by the drop in f_{gas} and hence L_X . The $L_X:L_B$ relation also has a steep slope compared to that of non-BGG ellipticals (O’Sullivan et al., 2001a), and it seems likely that this is again a product of the trend in f_{gas} with temperature. If so, we cannot argue that the trend in gas fraction is a product of halo formation by galaxy winds, as we would expect all galaxies to show a steep $L_X:L_B$ relation, as seen for this sample.

A change in gas fraction caused by the different formation histories of the galaxies seems a more feasible model. Assuming our galaxies have formed through a number of mergers, we can assume that there is a scatter in the time since the last major merger. While minor mergers can be treated as the accretion of extra matter into the galaxy, major mergers will have more profound effects, including the “resetting” of the potential well through violent relaxation (Salvador-Sole et al., 1998) and the fuelling of bursts of star formation. In a previous paper (O’Sullivan et al., 2001b) we found a relation between the luminosity weighted age of early-type galaxies and their normalised X-ray luminosity, L_X/L_B . Luminosity weighted ages are measured by comparing optical line widths to stellar emission models, from which it is possible to estimate the mean age of the stellar population at the core of the elliptical. Although galaxies are likely to be made up of several populations with ages corresponding to previous mergers, the older populations will be fainter as more massive, luminous stars will have evolved into compact objects. The younger populations will therefore dominate the emission, and as we expect minor mergers to only produce relatively small amounts of star formation, we might expect the line widths to be dominated by the population created during the last major merger. This luminosity weighting means that the age we estimate is likely to be a better estimate of the time since the last major merger, rather than the age of the majority of the stars in the galaxy. Using a sample of 77 galaxies in a range of environments we found that there was a strong correlation between L_X/L_B and luminosity weighted age, indicating that halo luminosity increases as galaxies age. In a stellar wind model, this can be explained by considering the rate of energy injection from SNIa compared to the rate of mass injection from stellar mass loss. The rise in L_X/L_B suggests that the energy injection rate is decreasing more rapidly than the mass injection rate. We would expect this to lead to a slowing of any outflow, a rise in gas density in the halo and hence a rise in halo luminosity.

The question then becomes whether we expect the more massive galaxies in this sample to have had their last major merger earlier, and therefore to have higher halo densities. Hierarchical models of galaxy formation predict that more massive galaxies have longer formation timescales (Kauffmann, 1996), suggesting that this is not the case. However, observational measurements of age for sample of galaxies in clusters and the field suggest that more massive galaxies do indeed form earlier (Thomas et al., 2002). In our previous study of X-ray variations with galaxy age we found no correlation between L_B and age (O’Sullivan et al., 2001b), but in that case our sample included galaxies from a much wider range of environments and with more varied luminosities than is the case in this paper. In the current sample only 16 of our galaxies have measured ages in the catalogue of Terlevich & Forbes (2002), and for this subsample we find only a weak (1.4σ) trend for age to increase with L_B .

Finally there is the possibility that the change in gas fraction we see is related to the environment of the galaxies. The offsets we see in the $L_X:L_B$ and $L_B:T_X$ relations suggest that the presence of a surrounding IGM can increase the X-ray luminosity and temperature of the halo. L_X appears to be more strongly affected, being offset by a factor of ~ 9 , as compared to a factor of ~ 2 in T_X . A surrounding IGM might cause these offsets by containing or stifling galaxy winds, or by accretion of the IGM on to the galaxy halo. If the most massive galaxies were found in the most massive groups and clusters we might expect the density of the surrounding IGM to correlate with galaxy mass. This would mean that more massive systems were more strongly affected, and might produce the trend in gas fraction with temperature. Of the possible processes, containment or stifling would seem the most likely, as accretion of IGM gas might be expected to affect gas fraction differently at different radii. One strong argument for this explanation is the correlation between group and galaxy X-ray luminosity observed by Helsdon et al. (2001). If we assume that this is not caused by group cooling flows then it does indeed suggest that galaxy mass is correlated with group mass.

4.6.4 Environmental Effects and Formation Epoch

Although most of the relations which we have used to investigate our sample of galaxies show no difference between galaxies in different environments, there are three interesting exceptions. These are the $L_B:T_X$, $L_X:L_B$ and $\beta_{fit}:T_X$ relations. The $L_B:T_X$ and $L_X:L_B$ both show similar

behaviour. In each case, we find that the best fit relation has a similar slope to that of groups, but is offset to higher L_X or T_X at a given L_B . However, when we split the sample into galaxies which lie in X-ray bright or X-ray faint groups, we find that those in X-ray faint groups do not appear to be offset to the same degree. We have calculated the residuals about our best fit lines for both relations, and the residuals we would find if the best fit lines for galaxy groups were used. In both cases, the mean residual from our best fit line is considerably higher (by 20-30%) for the galaxies in X-ray faint groups than for those in X-ray bright groups, showing them to be poorly described by the relations. The points are almost all offset toward the group relations, so these large residuals are a measure of that offset. We can also calculate the mean residual from the group relations, which will give us a measure of the offset of the X-ray faint and bright subsets from those relations. The mean residual from the best fit line for groups is smaller (by 40-60%) for galaxies in X-ray faint groups. For the $L_X:L_B$ relation, the mean residual of the galaxies in X-ray faint groups from the *group* relation is actually less than half the mean residual from the *galaxy* best fit line, suggesting that although these galaxies are not well described by either relation, they are closer to the group relation. This supports the idea that the offset is driven by the presence of a surrounding IGM. Alternative subdivisions of the sample, comparing cooling flow and isothermal galaxies, or group dominant galaxies to those in other environments do not show a similar segregation, leading us to the conclusion that this difference is not a product of group cooling flows.

There are a number of ways in which a surrounding IGM could increase the luminosity and temperature of a galaxy halo. If we consider a galaxy in an early wind phase, the rapidly out-flowing gas might expand until stopped by the pressure of the surrounding gas. The IGM could contain the galaxy wind, raising its density and preventing the dispersion of high temperature gas to large radii. We might therefore expect such an object, even if it had now (as is likely) progressed to a later wind phase, to have a higher temperature and luminosity. Similarly, if we consider a galaxy in which there is a global inflow (within the galaxy halo rather than a group cooling flow initially sourced in the surrounding IGM), we might expect gas from the IGM to move into the galaxy potential. This gas would add to the galaxy luminosity, particularly as the galaxy potential would concentrate it. We might also expect it to have a higher temperature than gas produced within the galaxy, though cooling would be likely in such a situation. In

both cases we might also see an increased amount of gas in the galaxy at all radii. If the trend in gas mass fraction discussed in Section 4.6.1 is caused by an increase in halo density for high temperature systems (rather than a density decrease in low T_X galaxies), these models might give us an explanation of the trend. More massive galaxies would produce larger amounts of gas and would be more able to accrete and concentrate a surrounding IGM, so we would expect the trend with temperature.

The other sign of environmental influence on our galaxies is shown in Figure 4.9. If we exclude NGC 1404 (where β_{fit} is likely to be biased by the effects of ram-pressure stripping), we find that galaxies in the centres of groups, clusters and cluster sub-clumps show a larger degree of scatter in β_{fit} than those elsewhere. In this case the trend seems to be related to the position of the galaxy at the centre of the potential well rather than a surrounding or confining IGM. All the non-BGG/BCG galaxies in our sample are found in groups or clusters, so their halos are likely to interact with surrounding gas. A possibility is that the halos of galaxies at the centres of larger structures are affected by the group potential, rather than the IGM. A recent study of NGC 1399 (Paolillo et al., 2002) shows that in the central regions of that galaxy (the dominant elliptical of the Fornax cluster), the mass profile is dominated by the stellar mass of the galaxy. However, the cluster potential does play some part at larger radii, and although we have removed the surface brightness components associated with larger structures, we cannot rule out some level of influence. Another possibility is that the merger history of these central galaxies has an effect on their halo structure. Dynamical friction is thought to cause galaxies in groups and clusters to lose orbital energy and fall toward the centre of the potential. We might therefore expect to find that group and cluster central galaxies undergo many more mergers than galaxies elsewhere, though presumably most of these will be with galaxies considerably smaller than themselves. The associated disturbance, influx of gas, and star formation might produce effects which can change the state of the galaxy halo, inducing the scatter we observe.

Although environmental influences seem likely, and provide an explanation for the offsets seen in the $L_B:T_X$ and $L_X:L_B$ relations, this model raises further questions, when compared to the other relations. There is a discrepancy between the $\sigma:T_X$ and $L_B:T_X$ relations. In the $\sigma:T_X$ relation, temperature appears to be a good measure of mass, with a behaviour similar to that seen in galaxy clusters. In the $L_B:T_X$ relation we see an offset, suggesting that while T_X may be

a good measure of mass, either galaxies have higher temperatures than clusters at a given mass, or that they have lower optical luminosities. If we accept the $\sigma:T_X$ relation, we must assume that the offset is in L_B , and at first glance this suggests that galaxies have a higher mass-to-light ratio than clusters. This is rather unexpected, as cosmological simulations suggest that mass-to-light ratio is correlated with dark halo mass, with galaxy clusters having considerably higher mass per unit L_B than individual galaxies (Somerville et al., 2001). A similar discrepancy is seen between the $L_X:T_X$ and $L_X:L_B$ relations, in which the former has an offset to lower L_X (or higher T_X), while the latter has an offset to higher L_X (or lower L_B). Once again, if we assume temperature behaves as it does in clusters, then the $L_X:T_X$ relation suggests that L_X is reduced, relative to larger structures. The offset in the $L_X:L_B$ relation would in this case again imply a large reduction in L_B , compared to groups and clusters. It is not clear what is causing these offsets, but we can speculate to some extent.

One possibility to be considered is the difference in formation epoch between galaxies, groups and clusters. Although properties such as σ and X-ray temperature can be considered as measures of system mass, they are actually related to the depth of the potential well ($T_X \propto M/R$). We expect systems to have densities related to the critical density of the universe at the time at which they virialise (or undergo their last major merger), so systems of a given mass which form at earlier epochs should have deeper potentials than their more modern counterparts. This suggests that older systems will have higher velocity dispersions, X-ray temperatures and luminosities than younger ones. A comparison of systems of different ages should show these differences, and relations involving these parameters would be affected by them. Relations involving optical luminosity might show them particularly well, if the total stellar luminosity is related to system mass rather than the depth of the potential well.

As we are considering similar systems at different redshifts, we take the total mass, M_{tot} to be constant, but the radius of the system is reduced at higher redshift, $R \propto (1+z)^{-1}$. Therefore, density scales as

$$\rho_{tot} \propto \frac{M_{tot}}{R^3} \propto (1+z)^3, \quad (4.4)$$

as expected. We also know that for bremsstrahlung radiation, the luminosity can be written

$$L_X \propto \rho_{tot}^2 R^3 \sqrt{T_X}. \quad (4.5)$$

Since $\rho_{tot}R^3$ is the mass of gas in the system, we can rewrite this as

$$L_X \propto (1+z)^3 M_{tot} f_{gas} \sqrt{T_X}, \quad (4.6)$$

where f_{gas} is the gas fraction.

T_X is proportional to M/R , so rearranging Equation 4.4, we can say that

$$T_X \propto M_{tot}^{\frac{2}{3}} (1+z), \quad (4.7)$$

and substituting into Equation 4.6 will therefore give

$$L_X \propto (1+z)^{\frac{3}{2}} f_{gas} T_X^2. \quad (4.8)$$

We therefore expect galaxies formed at a redshift $z_{form} = 2$ to have a similar $L_X:T_X$ relation to that of clusters, offset to higher luminosities at a given T_X by a factor of $3^{\frac{3}{2}}$, and modified by the behaviour of f_{gas} . As we in fact see a steeper slope and an offset to lower than expected luminosities, this suggests that f_{gas} is both dependent on the T_X of the system (as we have demonstrated elsewhere, *c.f.* Figure 4.11) and in general lower than is the case in groups and clusters, countering the expected offset to higher luminosities.

Other relations can also be considered in the same way. Velocity dispersion scales with mass and radius in a similar way to temperature, $\sigma^2 \propto M/R$. This means that we expect σ^2 and T_X to scale with redshift by the same factor, so regardless of formation epoch the $\sigma:T_X$ relation should remain constant. This agrees well with our findings. Optical luminosity is assumed to scale with total mass regardless of formation epoch, in which case we can substitute it into Equation 4.7. Rearranging the equation shows that we would expect a relation of the form $L_B \propto T_X^{1.5}$, like that of clusters, but offset to lower luminosities by a factor of $3^{\frac{3}{2}}$. This prediction agrees less well with our results, as we find a slope somewhat steeper than that of clusters, with an offset of a factor ~ 3 . We can also substitute this predicted relation for $L_B:T_X$ into Equation 4.8 to find a prediction for the $L_X:L_B$ relation. This again predicts a relation unlike that we observe, of the form $L_X \propto L_B^{\frac{4}{3}}$ with a large offset to high X-ray luminosities. However, this relation contains an f_{gas} term which is likely to steepen the relation (as f_{gas} is dependent on T_X) and partially counter the offset to high L_X .

Gas fraction is clearly an important quantity for our galaxies. We can use the three dimensional models of our galaxies (see Section 4.5.5) to measure properties such as gas mass and

Mean	Within	
	R_{virial}	$R_{virial}/3$
Total mass (M_{\odot})	1.31×10^{13}	4.25×10^{12}
Gas mass (M_{\odot})	2.39×10^{11}	4.60×10^{10}
Stellar mass (M_{\odot})	4.75×10^{11}	4.75×10^{11}
Gas fraction	0.019	0.012
Stellar fraction	0.050	0.16
Baryon fraction	0.069	0.17
Star Formation Efficiency	0.77	0.92
Mass-to-Light ratio (M_{\odot}/L_B)	166.7	54.8

Table 4.4: Mean masses and other derived quantities for our sample of galaxies.

total halo mass within a range of radii, in much the same way as we calculate gas entropy at a tenth of the virial radius. However it is important to emphasize that these models are by necessity inaccurate. We expect errors in the virial radii of the galaxies, as we do not know the true redshift of formation of each object. We also expect errors associated with temperature structure in the galaxy halos, as we assume all the halos to be isothermal. The values we find are therefore of more interest as representing trends rather than as exact measures. Table 4.4 lists mean values for our sample, excluding four galaxies which we find to have extreme values of gas fraction. In one case (NGC 4073) we find that the gas mass exceeds the mass of the dark halo at all radii, suggesting that the spatial fit is contaminated by group emission. The other three galaxies (NGC 1332, NGC 1549, NGC 4261) all have gas fractions of $<10^{-5}$, considerably lower than most galaxies in the sample. We have also derived the mean gas fraction, stellar mass fraction and total baryon fraction for the galaxies, assuming a stellar mass-to-light ratio of $5 M_{\odot}/L_B$ (Pizzella et al., 1997). We also assume that the stellar component of the galaxy is contained within $R_{virial}/3$.

The gas masses shown in Table 4.4 are quite large, as we would expect given that most of our sample is made up of groups and cluster dominant giant ellipticals. Bregman et al. (1992) find X-ray gas masses for their sample of elliptical galaxies in the range $\sim 10^8-11 M_{\odot}$. Our values are comparable with the upper end of this range particularly if we take in to account the effect of extrapolation out to the virial radius. The mean mass-to-light ratio for the sample may be somewhat high. Lloyd-Davies & Ponman (2002) find the mean mass-to-light ratio of a sample of 20 galaxy groups and clusters to be $120 \pm 20 M_{\odot}/L_B$, and other comparable estimates include

$88 \pm 33 M_{\odot}/L_B$ (Edge & Stewart, 1991) and $100 M_{\odot}/L_B$ for the Perseus cluster (Eyles et al., 1991). However, some estimates suggest that both elliptical galaxies and galaxy clusters may have mass-to-light ratios as high as $200 M_{\odot}/L_B$ (Bahcall et al., 1995). Taking a conservative view, we assume that the total halo masses may be overestimated to some degree, possibly owing to the influence of a surrounding group or cluster halo on the galaxies. The mean gas, stellar and baryon fractions will all be influenced by any overestimate of total mass, so we expect our measured values to be lower than is really the case. However, even given such a bias, it is clear that the gas fraction is considerably lower than is usual in galaxy groups and clusters; $\sim 1\text{-}2\%$, as compared to $\sim 20\%$ in clusters (Lloyd-Davies & Ponman, 2002; Markevitch & Vikhlinin, 1997). This is exactly the kind of difference we expected to see, given the offsets to low luminosity in the $L_X:T_X$ and $L_X:L_B$ relations. The mean star formation efficiency ($M_*/[M_* + M_{gas}]$) is also very high compared to larger structures, which typically have efficiencies of $\sim 0.2\text{-}0.3$ (Lloyd-Davies & Ponman, 2002; Cirimele et al., 1997; Arnaud et al., 1992; David et al., 1990). This could suggest that galaxies convert much more of their gas into stars than is the case in groups or clusters, an unsurprising result considering the extent and temperature of a typical cluster halo. This result is also consistent with theoretical modelling which suggests that galaxy sized halos are likely to contain much more cool gas than larger systems (Baugh et al., 1999). In ellipticals, cool gas is likely to have been formed into stars during the merging process, leading to the high star formation efficiencies we measure. However, high star formation efficiencies would also be found if much of the gas has been removed from the systems via processes such as galaxy winds. The mean baryon fraction for our sample is quite low compared to measured values for galaxy clusters, which range from 0.11-0.3 (Lloyd-Davies & Ponman, 2002; Zaroubi et al., 2001; Hradecky et al., 2000; David et al., 1995). The low end of this scale could be comparable with our value, given the large uncertainties we expect in our result. However, for larger values of baryon fraction in clusters we would have to conclude that up to $\sim 75\%$ of the baryons originally in galaxies have been removed, probably being blown out into the surrounding IGM. Once again, we note that the values listed in Table 4.4 cannot be taken as precise measurements. However, this is the first time that such values have been calculated for a sample of galaxies, and they appear to agree fairly well with the general trend of our results.

4.7 Summary and Conclusions

We have compiled a sample of 39 massive X-ray luminous early-type galaxies for which there are long *ROSAT* PSPC exposures archived. When analysing these data we have carried out detailed spatial and spectral fits, and extrapolated from these to approximate three dimensional models of the galaxies. The properties measured from these fits and models allow us to compare our sample to galaxy groups and clusters. Galaxies may be comparable to these larger systems because at the simplest level they can be considered as dark matter halos containing hot gas, much like the more massive structures in which they reside. If the dark matter profile does not vary significantly with system mass, we might expect the gas properties to be similar as well. To compare our galaxies with larger galaxy systems we fit a number of relations which are commonly used for groups and clusters, including the $L_X:T_X$, $\sigma:T_X$, $\beta_{fit}:T_X$, $L_B:T_X$ and $L_X:L_B$ relations. We are also able to subdivide our sample depending on environment (galaxies in the centres of groups/clusters, galaxies surrounded by a dense IGM) and temperature structure (galaxies with isothermal halos, central cooling or heating). As we have specifically chosen our sample to include the most massive galaxies available, it is unsurprising that most of them are found to lie in the centres of larger systems and that a majority show signs of central cooling.

Most of the relations we fit show similarities to those found for groups and clusters. The best example of this is the $\sigma:T_X$ relation, which is identical (within errors) with that found for galaxy clusters. The scatter about the relation is large and we find that there is a considerably greater degree of scatter than might be expected from the statistical errors on the data. This suggests that the properties of the galaxies have a degree of intrinsic scatter, presumably as a product of their differing formation histories. The similarity of the galaxy relation to that of galaxy clusters suggests that both velocity dispersion and temperature are good measures of the system mass. Temperature is believed to be correlated with mass in clusters because the gas is heated by shocks whose strength depends on the depth of the potential well. This may also be the case in our galaxies, but it is possible that the halo gas may have an internal source. For high mass galaxies, the energy available to heat gas produced through stellar mass loss is dominated by gravitational work rather than supernovae. All of our galaxies have suitably high masses, so the production (or partial production) of the halo through stellar mass loss seems viable.

The $L_X:T_X$ relation shows very different behaviour, with our sample having a best fit slope similar to that of galaxy groups, and significantly steeper than that of clusters. The relation is also offset to lower X-ray luminosities than the group relation. The difference in the slope of the relation between groups and clusters is usually explained through preheating; Whereas in clusters shock heating is the main source of energy in the gas, in groups other energy sources such as galaxy winds and AGN become important. A rise in gas energy and entropy causes a small increase in temperature and a movement of gas outwards from the centres of the groups, lowering central density and measured luminosity. This is most effective in low mass systems where shock heating is weakest, so that low temperature groups have very low luminosities, steepening the $L_X:T_X$ relation. The relation for our galaxies initially suggests either that they are affected by the same processes, or that their halos are in fact group scale cooling flows centred on the galaxies. Temperature profiles of our targets do show signs of central cooling in some cases, but there is no obvious difference between this subset and the rest of the sample, so it seems unlikely that the galaxy halos are in fact cooling flows. We also find that the surface brightness profiles of our galaxies do not behave like those of groups. They are not flattened in low temperature systems, instead having similar gradients but lower normalisations at lower T_X . This suggests that in galaxies the steep $L_X:T_X$ relation is caused not by preheating and movement of gas to higher radii, but by a lowering of the gas fraction. A number of possible reasons for this low gas fraction could be suggested, including environmental or aging effects, heating by supernovae or the consequences of formation by stellar mass loss. Of these, the effect of environment (stifling or compression of the halo, or accretion of gas) or the differing formation histories (higher gas fractions in galaxies which have had more time to build denser halos) seem the most likely explanations.

The $L_B:T_X$ and $L_X:L_B$ relations both show similar behaviour. In both cases we find the slope of the relation to be similar to that of galaxy groups, and to clusters in the case of the $L_B:T_X$ relation. However, the normalisations of the relations differ from those of larger systems, with offsets to lower L_B and higher L_X respectively. These offsets may be a sign of the difference in formation epoch between systems of different mass. We expect galaxies to form earlier than groups or clusters, and as system density is dependant on the critical density of the universe at the epoch of formation, to be denser. Self-similar arguments lead to the conclusion that X-ray

luminosity will be higher and optical luminosity lower (at a given temperature) than in younger systems, as we see. The $\sigma:T_X$ relation would be unaffected by the difference in age, but we would expect a large offset to higher L_X in the $L_X:T_X$ relation. The low gas fractions and trend in f_{gas} with T_X found for our sample would affect these results to some extent, steepening the relations involving L_X and countering the offset to higher luminosity to some extent. However, there is evidence to suggest that the offsets in the relations may actually be the product of environmental influences. In both cases, we find that galaxies which are found in X-ray faint groups (those without a significant IGM) have smaller offsets from the group relations than those found in X-ray bright environments. This could suggest that a surrounding IGM confines the galaxy halo or allows gas accretion, increasing the halo luminosity and temperature. This hypothesis conflicts with the good correlation found for the $\sigma:T_X$ relation, and neither model describes these relations perfectly.

We have also examined the $\beta_{fit}:T_X$ and $S:T_X$ relations, and find no correlations for either. As discussed above, this is indicative of the difference in density profiles between groups and galaxies. The lack of correlation between surface brightness gradient and temperature shows that gas is not being moved to higher radii by preheating processes, but instead has a roughly constant β_{fit} . Only the normalisation of the profiles varies with mass. The lack of correlation between S and T_X may be an indicator that galaxy halos do not form in the same way as those of groups and clusters. Formation by infall and shock heating would produce a trend, and preheating could produce an entropy floor. Without either of these features it seems more likely that a large part of the galaxy halos is produced through stellar mass loss, influenced by the surrounding environment. The low baryon fraction and high mass-to-light ratios of our systems support this conclusion, suggesting that significant quantities of gas have actually been removed from these systems, probably through galaxy winds, rather than gas moving in from outside.

This study has used the best *ROSAT* data available for galaxies, and probably the best available fitting techniques. We have found a number of important similarities to (and differences from) larger systems, and this is the first time that much of the analysis has been attempted for any but the largest cluster dominant galaxies. However, the advent of *Chandra* and *XMM-Newton* mean that almost every section of this work could be greatly improved upon. A large number of observations of X-ray bright early-type galaxies by these observatories are already

archived, and it seems likely that it will shortly be possible to recreate the sample used here with much improved data quality.

Chapter 5

Summary and Future Plans

5.1 Summary of main results

The work presented in this thesis represents one of the most extensive and detailed studies of the X-ray properties of early-type galaxies yet undertaken. We have compiled the largest catalogue of X-ray luminosities available for this class of galaxy, and used it to demonstrate the importance of age and environment in the development of hot gas halos. We have also examined the properties of these halos, and compared them to theoretical models and observational studies of galaxy groups and clusters. This comparison makes clear the similarities between gas halos on all scales, but also shows that galaxy halos are distinctly different from those found in larger structures, probably as a result of their formation history.

The results shown in Chapter 2 make clear the important correlation between galaxy age and X-ray halo luminosity. Normalised X-ray luminosity (L_X/L_B) varies over three decades within the sample we studied, and it seems likely that an increase of L_X/L_B with age can account for at least one third of this range. Changes in the population of X-ray binaries are likely to contribute to this increase, as the population of stellar mass compact objects grows, but the majority of the effect appears to be caused by the growth of the X-ray halo. The trend for increase is long term, with L_X/L_B rising steadily over at least 10 Gyrs. Although a number of models of halo production have been proposed, only those involving galaxy winds come close to predicting such a long period of growth. It seems likely, therefore, that in most normal elliptical and lenticular galaxies, the development of the halo is largely governed by the outflow of gas, produced through stellar mass loss, from within the galaxy. A slow evolution from an initial supersonic wind, to a subsonic outflow and finally to a quasi-hydrostatic halo seems the most feasible model, and we conclude that this is an accurate description of most normal early-type galaxies.

The wide range of X-ray luminosities measured for early-type galaxies is again the subject of our investigation in Chapter 3. The most important results from this section of the thesis deal with the influence of environment. Interactions with other galaxies and the gas and dark matter associated with groups and clusters have been suggested as explanations for the scatter in the $L_X:L_B$ relation, and some evidence exists to support these speculations. In particular, a small number of nearby galaxies show morphologies suggestive of ram-pressure stripping (Paolillo et al., 2002; Forman et al., 1985) and at least one study of galaxies in a rich cluster has found them to have reduced halos (Sakelliou & Merrifield, 1998). However, the two best previous studies find conflicting evidence, and suggest different interactions as being most likely to be the dominant factor in producing the $L_X:L_B$ scatter. Our study is the first to cover a wide range of environments in the X-ray, from the field to moderately dense group and cluster cores. We find no trend with environment, using a sample considerably larger and more representative than those used in previous examinations.

The only case where we do see evidence for environmental influence on galaxy properties is for Brightest Group Galaxies. These objects, which in most cases are found at the bottom of the group potential well, have a higher average L_X/L_B and also a significantly steeper $L_X:L_B$ relation. This indicates an increased mass of hot gas associated with the galaxies and possibly their increased ability to retain gas. Accretion from the surrounding environment, or the superposition of a group scale cooling flow seem the most likely candidates for the source of the gas. As well as confirming the previous work by Helsdon et al. (2001), we are also able to demonstrate how inclusion of these galaxies can bias the measured slope of the $L_X:L_B$ relation, leading to the steep slopes reported by a number of previous studies. Excluding these galaxies (and others likely to bias the relation) we find the gradient of the relation to be much shallower, but still find the extensive scatter traditionally associated with this correlation.

We move on to look at the properties of the X-ray halo in more depth in Chapter 4. As well as improving the quality of the spectral fitting of the halos, we also use two dimensional surface brightness fits to examine the morphology, and construct 3-dimensional models in order to measure parameters such as entropy, mass and gas fraction. In order to perform these analyses, we require high signal-to-noise data, and so our sample is smaller, limited to the brightest early-type galaxies observed by *ROSAT*. All the galaxies in this sample are found to lie in groups and

clusters (with the possible exception of NGC 6482 which may itself be a fossil group) and many of them are the brightest galaxy in their group or cluster. A small number are found in X-ray faint groups, but most appear to be surrounded by a hot IGM which might have influenced their development. Having fitted spectral and spatial models to the targets we plot a number of standard relations in order to allow a comparison of our galaxy halos to the more extensively studied halos of groups and clusters.

Of the relations we examine, only one (the $\sigma:T_X$ relation) has previously been applied to galaxy halos. We find considerable scatter in the data about all of the relations, more than would be expected from the statistical errors alone. The relations suggest that galaxy halo properties are related closely to the depth of the potential well, as is the case in galaxy clusters. However, the halo gas does not seem to be largely primordial, as is the case in clusters. Although the $\sigma:T_X$ relation for galaxies is almost identical to that of clusters, it seems likely that much of the gas in these galaxies is produced through supernovae and stellar mass loss, with the dependence of T_X on potential well depth only apparent because our galaxies are relatively high mass objects. We also find evidence for a change in gas fraction with galaxy mass, with low T_X objects having lower gas fractions and surface brightness normalisations. This trend produces a steepening in the $L_X:T_X$ relation similar to that seen in galaxy groups. Whereas in galaxy groups the $L_X:T_X$ relation is steep because gas has been moved to higher radii by preheating processes, in our galaxies it seems that gas is actually lost to the system, as the overall gas fractions are lower than those in groups and clusters.

There is also some evidence that the environment in which the galaxies are found has an effect on their properties, as galaxies in X-ray faint groups tend to have lower X-ray temperatures and luminosities. Again, this could indicate that galaxies surrounded by a dense IGM can accrete gas from it, or that group dominant galaxies are likely to be the focus of group scale cooling flows. However, it also seems possible that a surrounding IGM would prevent or reduce loss of gas from a galaxy during any wind phase, raising both the gas fraction and gas temperature. Further work using higher quality data is clearly needed to resolve the issue of the origin of the gas in the halos of the most massive ellipticals and the effect of a surrounding IGM. Fortunately the advent of *Chandra* and *XMM-Newton* has begun to provide the necessary high resolution, high signal-to-noise data for such work, and it should soon be possible to recreate our sample

of massive ellipticals using observations from these satellites.

5.2 Future Work

The work presented in this thesis has been based almost entirely upon data from *ROSAT*, and in certain areas we have now reached the limits of the available data from this observatory. The large *ROSAT* field of view means that archived data from this satellite will remain useful for environmental studies, but it seems unlikely that we will be able to improve significantly on either of our main samples without using *XMM-Newton* and *Chandra*. Both of these observatories have superior bandpass, collecting area, spatial and spectral resolution compared to any previous observatory, and are in some ways particularly suited to the study of galaxies. The excellent spatial resolution of *Chandra* means that a large percentage of the point sources in galaxies are resolved out, allowing studies of extragalactic stellar populations and reducing confusion in the study of diffuse emission. The huge collecting area of *XMM-Newton* (more than ten times that of *ROSAT*) means that we will be able to detect much fainter galaxies, and trace diffuse emission out to much higher radii, as well as improving spectral characterisation enormously. Many galaxies have already been the targets of observations by these two satellites, and as more data enter the archives it will become possible to look at samples as well as individual objects. We have already begun (or begun planning for) a number of projects to utilise *XMM-Newton* and *Chandra*, and some of these are described below.

5.2.1 Isolated Elliptical Galaxies

One of the major difficulties associated with the study of early-type galaxies is that they are predominantly found in groups and clusters, and are often surrounded by a hot intergalactic medium. X-ray emission from this IGM contaminates observations of the galaxies, and interactions between the galaxy halo and surrounding gas are possible. As discussed in Chapter 3, although a number of environmental processes can affect the X-ray properties of galaxies, no trend in L_X/L_B is found. However, the scatter in Figure 3.10 suggests that individual galaxies are affected by these environmental interactions, altering the halo size and state. This means that observations of galaxies in groups and clusters are unlikely to provide us with a clear picture of the development of galaxy halos.

The most obvious solution to this problem is to observe truly isolated galaxies, which are not part of a group or cluster. These objects will never have been surrounded by a dense IGM, and will not have interacted with other galaxies, at least since their formation. Field galaxies are usually not isolated enough for such a study, as many are found in pairs or on the borders of groups and clusters, where they may have been disturbed in the past. We have therefore compiled a sample of optically identified isolated early-type galaxies. A small subset of these have X-ray data available, but owing to the lack of observations of low density regions, most of the sample has yet to be detected in the X-ray. Of those which have been observed, one is thought to be a fossil group (Mulchaey & Zabludoff, 1998), one shows signs of a recent merger and one is a Seyfert galaxy. The remainder are apparently normal ellipticals and S0s with no obvious signs of disturbance, but which are found in very low density environments.

The sample was drawn from the Lyon-Meudon Extragalactic Data Archive (LEDA). The version of this catalogue used contains information on $\sim 100,000$ galaxies, of which $\sim 40,000$ have enough information recorded to be of use in this work. From this sample, galaxies were selected which satisfied the following criteria:

- Morphological type $T \leq -3$
- Virgo corrected recession velocity $V_{vir} \leq 9000 \text{ km s}^{-1}$
- Apparent Magnitude $B_T \leq 14.0$
- Galaxy not listed as a member of a Lyon Galaxy Group (Garcia, 1993)

The restrictions on apparent magnitude and recession velocity were imposed to minimise the effect of incompleteness in the catalogue. The LEDA catalogue is known to be 90% complete at $B_T = 14.5$ (Amendola et al., 1997), so this sample should be close to being statistically complete.

The selection process produced 330 galaxies which could be considered as potential targets. These were compared to the rest of the catalogue and accepted as being isolated if they had no neighbours which were:

- within 700 km s^{-1} in recession velocity,
- within 0.67 Mpc in the plane of the sky (assuming $H_0 = 75 \text{ km s}^{-1} \text{ Mpc}^{-1}$), and
- less than 2 magnitudes fainter in B_T .

These criteria were imposed to ensure that the galaxies did not lie in groups or clusters and to ensure that any neighbouring galaxies were too small to have had any significant effect on their evolution and properties.

To check the results of this process, all galaxies were compared to the NASA/IPAC Extragalactic Database (NED) and the Digitized Sky Survey (DSS). A NED search in the area within 0.67 Mpc of the galaxy identifies galaxies which are not listed in LEDA, and examination of the DSS plates reveals galaxies of similar brightness to the target which are not listed in either catalogue. These measures should ensure that the isolation of each galaxy is real, and not produced by errors or omissions in the catalogue. This process produced the list of 36 galaxies shown in Table 5.1.

Only eight of these galaxies have X-ray data available. Three have been detected in the *ROSAT* All-Sky Survey, but only have low numbers of counts available, owing to the short exposures used in the RASS. The remaining five have been observed (or are scheduled to be) with *Chandra* ACIS-S or *XMM-Newton*, three of them as a result of successful proposals associated with Birmingham. *Chandra* data for NGC 1132 and NGC 2110 are available in the archive, but these galaxies are the probable fossil group and Seyfert galaxy mentioned above. We are also collecting optical data for these galaxies, in particular spectra of their central regions and wide field imaging of the galaxies and their environment. As yet eighteen galaxies have wide field imaging (ten in two bands), and five have spectra, but we hope to complete the sample in the near future.

The optical data will allow us to look at two areas of interest. Firstly, we will be able to confirm the isolation of the galaxies, or measure the properties of any neighbour galaxies to determine whether they are likely to have had any significant influence on our targets. Secondly, we will be able to determine the optical properties of the galaxies in much more detail than is currently possible. This will allow us to compare them to samples from other environments, and to relations such as the fundamental plane. Segregation or deviation from such a relation could tell us about the effects of environment on the stellar bodies of galaxies in clusters and groups. Spectra will allow us to look at the luminosity weighted ages of the galaxies. It is not entirely clear what we might expect to find, as early-type galaxies can be expected to form in low density environments at any redshift. However, measured ages can be compared to the

X-ray properties, and for a sufficiently large sample we could study the development of galaxy X-ray halos with age.

With *Chandra* and *XMM-Newton* observations, we will be able to study these galaxies in detail. As well as multi-component spectral fits we will be able to study the discrete source population, the halo size and morphology, and signs of disturbance from internal processes such as star formation and AGN activity. The important factor is that we would expect these galaxies to have been undisturbed by external forces since their formation. We would therefore expect their X-ray properties to be purely the product of their internal structure and formation history, so they would act as a baseline against which we could compare all other early-type galaxies. Their behaviour on the various relations discussed throughout this thesis would be of great interest, particularly if they are found to have significantly different best fit lines, or (as is likely) reduced scatter about the relation. However, further observing proposals must be submitted to extend the sample, and analysis of the currently available data is necessary.

Fossil Groups

We expect a subset of the isolated ellipticals in our sample to be fossil groups. Only a small number of candidates have yet been identified in the literature and all are quite distant, making detailed X-ray studies difficult. Our targets would be at low redshift, allowing much more detailed observations and shorter exposures. Fossil groups are more difficult to identify from optical catalogues than isolated ellipticals. We expect them to have only small, faint neighbour galaxies, which may not be included or may not have measured redshifts, and without identifying these neighbours we cannot distinguish them from isolated ellipticals. However, the optical wide field imaging we are carrying out for our sample will be deep enough to detect all neighbour galaxies within a few magnitudes of the dominant elliptical, in a region extending out to ~ 0.75 Mpc (assuming $H_0 = 50 \text{ km s}^{-1} \text{ Mpc}^{-1}$). We will therefore be able to study the population of any groups found, and produce a luminosity function. Fossil groups have a characteristic luminosity function, with small galaxies appearing in the numbers expected, but a lack of objects at L_* and above. The only galaxy at the high mass end of the function is the dominant elliptical, which lies well above the predicted line, due to its unusually high mass and luminosity. Finding such a luminosity function is as yet the only certain confirmation of a fossil group.

The highly luminous and extended emission we expect to see for such objects should allow detailed spatial modelling of the halo. As well as comparisons with more normal groups and galaxies, we can consider the halo properties with regard to the age of the system. Fossil groups are thought likely to have formed at high redshift, through a process of rapid merging after the virialisation of the group. We would therefore expect the system to have a high density compared to more recently formed objects, to harbour a cooling flow (or show signs of past cooling), and perhaps to contain unusually low entropy gas, owing to the increased halo density. We could also place the systems on the $L_X:T_X$ plot and derive a mass-to-light ratio for them. Although studies of distant fossil groups suggest they have anomalous properties, it is not yet clear whether they lie unusually high on one or both of these measures (Vikhlinin et al., 1999; Jones et al., 2000). Spectral information would allow mapping of the abundance distribution through the halo. Formation through rapid merging at high redshift would lead to suppressed star formation, compared to more normal groups. We would therefore expect the ratio of Iron to alpha-elements to be high, as the number of type-II supernovae will be lower.

As well as looking for fossil groups in the isolated galaxy sample, we have identified a small number of candidates which already have X-ray data available. One of these galaxies has been the subject of a successful *Chandra* proposal, but the other two only have *ROSAT* All-Sky Survey data available. The *Chandra* observation will provide detailed information on the central 90 kpc of the galaxy, but the limited field of view means that we will not be able to trace the halo further out toward the virial radius. *XMM-Newton* observations of a small sample of these objects would be the ideal method of studying the properties of these objects in detail.

5.2.2 X-ray Faint Early-type Galaxies

In Chapter 3 we discussed the mean contribution to L_X from discrete sources. Although the scatter in the $L_X:L_B$ relation is large, many early-type galaxies have luminosities comparable to that expected from discrete sources alone, and some lie significantly below the minimum expected for objects of their optical luminosity. In small galaxies, this might be expected as their low mass makes them less likely to be able to retain a gaseous halo and small variations in the discrete source population could have a sizable effect on the total X-ray luminosity. However, studying more massive, optically luminous but X-ray faint galaxies would allow us to answer

two important questions. Why do these large galaxies have such faint halos? And what are the properties of their discrete source population?

These questions put conflicting constraints on the data required. In order to study the discrete source population we require the high resolution of *Chandra*. On the other hand, detection of low surface brightness diffuse emission calls for the large collecting area of *XMM-Newton*. Owing to the difficulties associated with analysing diffuse emission, most of the *Chandra* studies published as yet have focused on discrete sources, and a body of information on these populations is beginning to build up. One of the most commonly used methods has been to plot the luminosity function of the sources in individual galaxies, but comparisons are hampered by factors such as variable absorption, uncertain galaxy distances, differing detection thresholds and errors caused by assumptions about source spectra. More detailed studies, analysing statistical samples of galaxies in a consistent manner are necessary, and these are becoming viable as the *Chandra* archive expands. Given spectral characterisation of the sources in a reasonable number of early and late-type galaxies, it should be possible to find links between galaxy star formation history and current discrete source population. For example, we might expect the presence of relatively short lived sources such as high mass X-ray binaries to be a sign of recent star formation (Kilgard et al., 2002).

The halos of low luminosity ellipticals have yet to be studied in any great detail. Previous work has used data from *ROSAT*, *Einstein* and *BeppoSAX*, which were unable to resolve any but the brightest point sources, but did identify hard and soft spectral components associated with them (Trinchieri et al., 2000; Pellegrini, 1999a; Pellegrini, 1994). The further characterisation of the spectral properties of the discrete source population by *Chandra* should make removal of contamination easier, and the superior properties of *XMM-Newton* mean that it will be possible to look at the spatial distribution of the halo in these objects for the first time. One explanation of their low X-ray luminosity is that their halos are in a supersonic outflow phase (Ciotti et al., 1991; Pellegrini & Ciotti, 1998). If this is the case we would expect to see only a low surface brightness halo away from the core of the galaxy. Alternatively, environmental effects such as ram-pressure or viscous stripping could be responsible, in which case we might expect to see signs of disturbance or a truncated halo. We successfully proposed observation of a small sample of these galaxies in *XMM* cycle 1 and will begin the analysis of the data in the near future.

5.2.3 Galaxies in Clusters and Groups

Another possibility which the high spatial resolutions and collecting areas of *Chandra* and *XMM-Newton* make possible is the detailed study of galaxies in groups and clusters. Prior to these two observatories, the best examples of work in this area are studies of cluster galaxies using the *ROSAT* HRI (Drake et al., 2000; Sakelliou & Merrifield, 1998), and of group galaxies using the PSPC (Helsdon & Ponman, 2002; Helsdon et al., 2001). In both cases, despite the efforts of the observers, the limitations of the instruments made accurate measurements of all but the brightest galaxies very difficult. Background subtraction was the main problem, making the luminosities and extensions measured questionable in some cases. This means that although the conclusions drawn from samples of group and cluster galaxies stand, the properties of individual galaxies are not well defined.

The larger numbers of source counts and lower background expected from *Chandra* or *XMM-Newton* observations will make the task of accurate background subtraction somewhat easier. Other difficulties, such as the differences in background between CCDs (or indeed within CCDs) are likely to cause some problems, but in general reliable identification of extended emission should be simpler. For relaxed systems, where the emission of the cluster or group is reasonably regular, it should be possible to model the IGM and subtract it, leaving galaxy and point source emission only. Systems with large amounts of substructure will require the use of local background subtraction, but this should still be more accurate than that available using *ROSAT*. In particular, selection of the local background region should be improved, as the extent of the galaxy emission will in most cases be much clearer than was previously the case.

Given this improvement, it should be possible to consider a number of interesting questions regarding galaxies in these relatively dense environments. It will certainly be possible to look for signs of ram-pressure or viscous stripping of galaxy halos, such as galaxy wakes. Similarly, comparisons of the surface brightness and temperature profiles of galaxies will provide information on the fraction of galaxies whose halos have been reduced by such processes in the past. Modeling of ram-pressure stripping in cluster environments suggests that while L_X/L_B is only changed by relatively small amounts the extent and gradient of the surface brightness profile may change much more dramatically (D. Acreman, private communication). Similarly, the temperature profile can be strongly affected by stripping, shocks and accretion. Information on

the densities at which stripping is effective and the time taken to rebuild the halo would be of great use in constraining models. It will also be possible to characterise the $L_X:L_B$ relation for galaxies in these dense environments. Our own examination of this relation across a range of environments (see Chapter 3) finds similar best fit lines for normal galaxies, but some indication of a slightly steeper slope for galaxies in clusters. However, Helsdon et al. (2001) find that normal galaxies in groups have an $L_X:L_B$ relation with a slope of unity, indicating a direct scaling of X-ray to optical luminosity. If this is the case, it could be seen as an indication that gas stripping is the dominant environmental process in these systems. This would be an important result, with implications for the formation of the IGM in groups and clusters.

Another area of interest in such a study would be the properties of the central dominant galaxies. The sample described in Chapter 4 is mainly composed of such galaxies, and such a study would allow the expansion of the sample with improved data quality. Central dominant galaxies are likely to have large X-ray halos, so it would be possible to carry out quite detailed analysis of their properties, perhaps including 3-dimensional modelling and accurate measurement of mass, entropy and gas fraction profiles. There is also the question of cooling flows in groups and clusters. Although there is a great deal of interest at present in the field of cooling flows, most of this is focused on high mass clusters. Our results confirm those of previous studies of groups (Helsdon & Ponman, 2000; Mulchaey & Zabludoff, 1998) which found central cool components in the group halo. With good quality data we would be able to calculate the cooling time at various radii, determining whether these components are actually cooling flows and whether they are fueled by the group or galaxy halos. We would expect the properties of such flows to vary with the environment and perhaps the properties of the central galaxy. However, with good quality *Chandra* and *XMM-Newton* observations it should be possible to disentangle the group, galaxy and cooling flow emission, and determine the mass dropout rate as well as looking for any central AGN powered by the flow.

In the short term, the simplest way to proceed would be to select small samples of nearby groups and clusters with a range of masses. We would expect the effectiveness of interactions between galaxies and cluster gas to scale with mass, so would hope to see stronger evidence of such interactions in the more massive clusters and groups. We would also hope to see evidence of galaxy interactions, such as starbursts, AGN and galactic outflows, in the denser group cores. In

the longer term, these samples could be expanded to give more statistically reliable information. The effects of substructure on the galaxies might also be an interesting area to investigate, again with regard to the formation and enrichment of the group and cluster IGM.

Name	V_{vir} (km s ⁻¹)	M_B (mag)	Hubble Type	B_T (mag)
NGC 682	5473	-21.26	-3	13.42
NGC 821	1747	-20.41	-4.8	11.74
NGC 1041	6994	-21.44	-3	13.82
NGC 1045	4529	-21.59	-3	12.69
NGC 1132	6904	-21.99	-4.9	13.26
NGC 1162	3838	-20.77	-4.9	13.14
NGC 2110	2091	-19.71	-3	13.40
NGC 2128	3331	-20.27	-3	13.78
NGC 2271	2412	-20.42	-3.2	13.24
NGC 2865	2451	-20.71	-4.1	12.41
NGC 3562	7000	-22.11	-4.9	13.17
NGC 4240	1864	-19.49	-4	12.78
NGC 4271	4976	-20.85	-3	13.60
NGC 4555	6775	-21.82	-4.8	13.31
NGC 6172	5028	-21.01	-4.4	13.72
NGC 6411	3967	-21.24	-4.9	12.80
NGC 6653	4934	-21.30	-4.8	13.48
NGC 6702	4978	-21.45	-4.8	13.24
NGC 6776	5281	-21.86	-4.1	13.01
NGC 6799	4845	-21.32	-3.9	13.36
NGC 6849	5924	-22.08	-3.1	13.01
NGC 7330	5520	-21.59	-4.8	13.52
NGC 7796	3145	-21.05	-3.9	12.42
IC 1211	5873	-21.02	-4.9	13.81
UGC 1735	8160	-21.76	-3.3	13.94
UGC 2328	5125	-21.06	-4.8	13.72
ESO 107-G004	2917	-20.55	-4	12.87
ESO 153-G003	6268	-21.27	-3.9	13.73
ESO 194-G021	3051	-20.09	-3	13.30
ESO 218-G002	4055	-21.51	-3.9	13.53
ESO 318-G021	4621	-21.16	-4	13.55
ESO 462-G015	5748	-22.07	-4.8	12.94
MCG -01-27-013	8943	-21.98	-3	13.81
MCG -01-03-018	5792	-20.96	-3	13.82
MCG -02-13-009	5512	-21.26	-4	13.53
MCG -03-26-030	8921	-22.56	-3	13.28

Table 5.1: Basic properties of our sample of isolated early-type galaxies. The galaxies in the table above are selected to be isolated as described in the text. V_{vir} is a Virgo-corrected recession velocity. All values are taken from the LEDA catalogue.

References

- Abell G. O., Corwin H. G., Olowin R. P., 1989, *ApJS*, 70, 1
- Adami C., Mazure A., Katgert P., Biviano A., 1998, *A&A*, 336, 63
- Allen S. W., Di Matteo T., Fabian A. C., 2000, *MNRAS*, 311, 493
- Allen S. W., Fabian A. C., 1998, *MNRAS*, 297, L57
- Amendola L., Di Nella H., Montuori M., Sylos Labini F., 1997, *Fractals*, 5, 635
- Angelini L., Loewenstein M., Mushotzky R. F., 2001, *ApJ*, 557, L35
- Arnaud M., Rothenflug R., Boulade O., Vigroux L., Vangioni-Flam E., 1992, *A&A*, 254, 49
- Ashman K. M., Zepf S. E., 1992, *ApJ*, 384, 50
- Böhringer H., Matsushita K., Churazov E., Ikebe Y., Chen Y., 2002, *A&A*, 382, 804
- Babul A., Balogh M. L., Lewis G. F., Poole G. B., 2002, *MNRAS*, 330, 329
- Bahcall N. A., Lubin L. M., Dorman V., 1995, *ApJ*, 447, L81
- Balogh M. L., Babul A., Patton D. R., 1999, *MNRAS*, 307, 463
- Bauer F. E., Brandt W. N., Sambruna R. M., Chartas G., Garmire G. P., Kaspi S., Netzer H., 2001, *AJ*, 122, 182
- Baugh C. M., Cole S., Frenk C. S., Benson A. J., Lacey C. G., 1999, in *ASP Conf. Ser. 163: Star Formation in Early Type Galaxies Early-Type Galaxies in the Hierarchical Universe*. p. 227
- Bender R., Surma P., Döbereiner S., Mollenhoff C., Madejsky R., 1989, *A&A*, 217, 35
- Benson A., Bower R., Frenk C., White S., 1999, *MNRAS*, 314, 557
- Beuing J., Döbereiner S., Böhringer H., Bender R., 1999, *MNRAS*, 302, 209

- Bhavsar S. P., Barrow J. D., 1985, MNRAS, 213, 857
- Bhavsar S. P., Cohen J. P., 1990, MNRAS, 247, 462
- Bica E., Alloin D., 1987, A&AS, 70
- Blanton E. L., Sarazin C. L., Irwin J. A., 2001, ApJ, 552, 106
- Blanton E. L., Sarazin C. L., McNamara B. R., Wise M. W., 2001, ApJ, 558, L15
- Blumenthal G., Faber S., Primack J., Rees M., 1984, Nature, 311, 517
- Boggs P. T., Donaldson J. R., Byrd R. H., Schnabel R. B., 1989, ACM Transactions on Mathematical Software, 15, 348
- Borne K., Bushouse H., Colina L., Lucas R., Baker A., Clements D., Lawrence A., Oliver S., Rowan-Robinson M., 1999, preprint, astro-ph/9902293
- Bradt H., Mayer W., Naranan S., Rappaport S., Spada G., 1967, ApJ, 150, L199
- Bregman J. N., Hogg D. E., Roberts M. S., 1992, ApJ, 387, 484
- Brighenti F., Mathews W. G., 1998, ApJ, 495, 239
- Brighenti F., Mathews W. G., 1999, ApJ, 512, 65
- Brinks E., Bajaja E., 1986, A&A, 169, 14
- Brown B., Bregman J., 1998, ApJ, 495, L75
- Brown B. A., Bregman J. N., 2000, ApJ, 539, 592
- Brown B. A., Bregman J. N., 2001, ApJ, 547, 154
- Bruzual A. G., Charlot S., 1993, ApJ, 405, 538
- Burstein D., Jones C., Forman W., Marston A. P., Marzke R. O., 1997, ApJS, 111, 163
- Buzzoni A., Gariboldi G., Mantegazza L., 1992, AJ, 103, 1814
- Buzzoni A., Mantegazza L., Gariboldi G., 1994, AJ, 107, 513
- Canizares C. R., Fabbiano G., Trinchieri G., 1987, ApJ, 312, 503

- Cappellaro E., Evans R., Turatto M., 1999, *A&A*, 351, 459
- Carlberg R. G., Yee H. K. C., Ellingson E., 1997, *ApJ*, 478, 462
- Carollo C., Franx M., Illingworth G., Forbes D., 1997, *ApJ*, 481, 710
- Carollo C. M., Danziger I. J., Buson L., 1993, *MNRAS*, 265, 553
- Cash W., 1979, *ApJ*, 228, 939
- Cavaliere A., Fusco-Femiano R., 1976, *A&A*, 49, 137
- Ciotti L., D'Ercole A., Pelegri S., Renzini A., 1991, *ApJ*, 376, 380
- Cirimele G., Nesci R., Trevese D., 1997, *ApJ*, 475, 11
- Coles P., Lucchin F., 1995, *Cosmology. The origin and evolution of cosmic structure*. Chichester: Wiley
- David L. P., Arnaud K. A., Forman W., Jones C., 1990, *ApJ*, 356, 32
- David L. P., Forman W., Jones C., 1991, *ApJ*, 369, 121
- David L. P., Jones C., Forman W., 1995, *ApJ*, 445, 578
- David L. P., Slyz A., Jones C., Forman W., Vrtilik S. D., Arnaud K. A., 1993, *apj*, 412, 479
- Davis C. S., Stephens M. A., 1989, *Appl. Stat.*, 38, 535
- Davis D. S., White R. E. I., 1996, *ApJ*, 470, L35
- D'Ercole A., Ciotti L., 1998, *ApJ*, 494, 535
- D'Ercole A., Recchi S., Ciotti L., 2000, *ApJ*, 533, 799
- D'Ercole A., Renzini A., Ciotti L., Pelegri S., 1989, *ApJ*, 341, 9
- Djorgovski S., Davis M., 1987, *ApJ*, 313, 59
- Donnelly R. H., Faber S. M., O'Connell R. M., 1990, *ApJ*, 354, 52
- Drake N., Merrifield M. R., Sakelliou I., Pinkney J. C., 2000, *MNRAS*, 314, 768

- Dressler A., 1980, *ApJ*, 236, 351
- Dressler A., Lynden-Bell D., Burstein D., Davies R. J., Faber S. M., Terlevich R. J., Wegner G., 1987, *ApJ*, 313, 42
- Dreyer J. L. E., 1888, *Mem. R. Astron. Soc.*, 49, 1
- Dubinski J., 1998, *ApJ*, 502, 141
- Ebeling H., Jones L. R., Perlman E., Scharf C., Horner D., Wegner G., Malkan M., Fairley B. W., Mullis C. R., 2000, *ApJ*, 534, 133
- Edge A. C., Stewart G. C., 1991, *MNRAS*, 252, 428
- Ehle M., Pietsch W., Beck R., Klein U., 1998, *A&A*, 329, 39
- Eke V. R., Cole S., Frenk C. S., 1996, *MNRAS*, 282, 263
- Elmegreen B. G., Efremov Y. N., 1997, *ApJ*, 480, 235
- Eskridge P. B., Fabbiano G., Kim D., 1995, *ApJ*, 442, 523
- Eskridge P. B., Fabbiano G., Kim D.-W., 1995, *ApJS*, 97, 141
- Eyles C. J., Watt M. P., Bertram D., Church M. J., Ponman T. J., Skinner G. K., Willmore A. P., 1991, *ApJ*, 376, 23
- Fabbiano G., Kim D. W., Trinchieri G., 1992, *ApJS*, 80, 531
- Fabbiano G., Kim D.-W., Trinchieri G., 1994, *ApJ*, 429, 94
- Fabbiano G., Schweizer F., 1995, *ApJ*, 447, 572
- Fabbiano G., Trinchieri G., 1985, *ApJ*, 296, 430
- Fabbiano G., Trinchieri G., 1987, *ApJ*, 315, 46
- Fabbiano G., Zezas A., Murray S. S., 2001, *ApJ*, 554, 1035
- Faber S., 1972, *A&A*, 20, 361
- Faber S., 1973, *ApJ*, 179, 731

- Faber S., Tremaine S., Ajhar E., Byun Y.-I., Dressler A., Gebhard K., Grillmair C., J. K., Lauer T., D. R., 1997, *AJ*, 114, 1771
- Faber S. M., Burstein D., 1988, *Motions of galaxies in the neighborhood of the local group. Large-Scale Motions in the Universe: A Vatican study Week*, p. 115
- Faber S. M., Gallagher J. S., 1976, *ApJ*, 204, 365
- Faber S. M., Jackson R. E., 1976, *ApJ*, 204, 668
- Faber S. M., Wegner G., Burstein D., Davies R. L., Dressler A., Lynden-Bell D., Terlevich R. J., 1989, *ApJS*, 69
- Fabian A. C., Crawford C. S., Edge A. C., Mushotzky R. F., 1994, *MNRAS*, 267, 779
- Fairley B. W., Jones L. R., Scharf C., Ebeling H., Perlman E., Horner D., Wegner G., Malkan M., 2000, *MNRAS*, 315, 669
- Feigelson E. D., Nelson P. I., 1985, *ApJ*, 293, 192
- Ferrari F., Pastoriza M. G., Macchetto F., Caon N., 1999, *A&AS*, 136, 269
- Forbes D., Ponman T., Brown R., 1998, *ApJ*, 508, L43
- Forbes D. A., Brodie J. P., Grillmair C. J., 1997, *AJ*, 113, 1652
- Forbes D. A., Brodie J. P., Huchra J., 1997, *AJ*, 113, 887
- Forbes D. A., Forte J. C., 2001, *MNRAS*, 322, 257
- Forbes D. A., Grillmair C. J., Williger G. M., Elson R. A. W., Brodie J. P., 1998, *MNRAS*, 293, 325
- Forman W., Jones C., Tucker W., 1985, *ApJ*, 293, 102
- Forman W., Schwarz J., Jones C., Liller W., Fabian A. C., 1979, *ApJ*, 234, L27
- Forte J. C., Martinez R. E., Muzzio J. C., 1982, *AJ*, 87, 1465
- Frenk C., Ellis R., Shanks T., Heavens A., J.A. P., 1988, *Epoch of Galaxy Formation*. Kluwer, Dordrecht

- Fritze-von Alvensleben U., Burkert A., 1995, *A&A*, 300, 58
- Fukugita M., Peebles P. J. E., 1999, *ApJ*, 524, L31
- Garcia A. M., 1993, *A&AS*, 100, 47
- Gebhardt K., Bender R., Bower G., Dressler A., Faber S. M., Filippenko A. V., Green R., Grillmair C., Ho L. C., Kormendy J., Lauer T. R., Magorrian J., Pinkney J., Richstone D., Tremaine S., 2000, *ApJ*, 539, L13
- Georgakakis A., Forbes D. A., Norris R. P., 2000, *MNRAS*, 318, 124
- Giacconi R., Branduardi G., Briel U., Epstein A., et al. 1979, *ApJ*, 230, 540
- González J. J., 1993, PhD thesis, University of California, Santa Cruz
- Goudfrooij P., de Jong T., Hansen L., Norgaard-Nielsen H. U., 1994, *MNRAS*, 271, 833
- Gunn J. E., Gott J. R. I., 1972, *ApJ*, 176, 1
- Helsdon S. F., 2002, PhD thesis, University of Birmingham
- Helsdon S. F., Ponman T. J., 2000, *MNRAS*, 319, 933
- Helsdon S. F., Ponman T. J., 2000, *MNRAS*, 315, 356
- Helsdon S. F., Ponman T. J., 2002, *MNRAS*, submitted
- Helsdon S. F., Ponman T. J., O'Sullivan E., Forbes D. A., 2001, *MNRAS*, 325, 693
- Hernquist L., Mihos J., 1995, *ApJ*, 448, 41
- Hertz P., Grindlay J. E., 1983, *ApJ*, 275, 105
- Heyl J. S., Hernquist L., Spergel D. N., 1994, *ApJ*, 427, 165
- Hibbard J. E., Guhathakurta P., van Gorkom J. H., Schweizer F., 1994, *AJ*, 107, 67
- Hibbard J. E., van Gorkom J. H., 1996, *AJ*, 111, 655
- Hickson P., 1982, *ApJ*, 255, 382

- Hradecky V., Jones C., Donnelly R. H., Djorgovski S. G., Gal R. R., Odewahn S. C., 2000, *ApJ*, 543, 521
- Hubble E., 1936, *The Realm of the Nebulae*. New Haven: Yale University Press
- Huchra J. P., Geller M. J., 1982, *ApJ*, 257, 423
- Huchtmeier W. K., Richter O.-G., 1988, *A&A*, 203, 237
- Huchtmeier W. K., Richter O.-G., 1989, *A&A*, 210, 1
- Irwin J., Sarazin C., 1998a, *ApJ*, 494, L33
- Irwin J. A., Sarazin C. L., 1998b, *ApJ*, 499, 650
- Irwin J. A., Sarazin C. L., Bregman J. N., 2000, *ApJ*, 544, 293
- Irwin J. A., Sarazin C. L., Bregman J. N., 2002, *ApJ*, 570, 152
- Isobe T., Feigelson E. D., Akritas M. G., Babu G. J., 1990, *apj*, 364, 104
- Isobe T., Feigelson E. D., Nelson P. I., 1986, *ApJ*, 306, 490
- Jones C., Forman W., 1984, *ApJ*, 276, 38
- Jones C., Stern C., Forman W., Breen J., David L., Tucker W., Franx M., 1997, *apj*, 482, 143
- Jones L., Ponman T., Forbes D., 2000, *MNRAS*, 312, 139
- Kaastra J., Mewe R., 1993, *A&AS*, 97, 443
- Kauffmann G., 1996, *MNRAS*, 281, 487
- Kauffmann G., Charlot S., White S. D. M., 1996, *MNRAS*, 283, L117
- Kellogg E., Baldwin J. R., Koch D., 1975, *ApJ*, 199, 299
- Kilgard R. E., Kaaret P., Krauss M. I., Prestwich A. H., Raley M. T., Zezas A., 2002, preprint, astro-ph/0203190
- Killeen N. E. B., Bicknell G. V., 1988, *ApJ*, 325, 165
- Kim D. W., Fabbiano G., Trinchieri G., 1992, *ApJ*, 393, 134

- King I., 1962, *AJ*, 67, 471
- Kissler-Patig M., Grillmair C. J., Meylan G., Brodie J. P., Minniti D., Goudfrooij P., 1999, *AJ*, 117, 1206
- Knapp G. R., Turner E. L., Cunniffe P. E., 1985, *AJ*, 90, 454
- Kormendy J., Richstone D., 1995, *ARA&A*, 33, 581
- Kraft R. P., Kregenow J. M., Forman W. R., Jones C., Murray S. S., 2001, *ApJ*, 560, 675
- Kuntschner H., Davies R., 1998a, *MNRAS*, 295, 29
- Kuntschner H., Davies R., 1998b, *MNRAS*, 295, L29
- Larson R. B., 1975, *MNRAS*, 173, 671
- Lee M. G., Geisler D., 1993, *AJ*, 106, 493
- Lees J. F., Knapp G. R., Rupen M. P., Phillips T. G., 1991, *ApJ*, 379, 177
- Lewis A. D., Ellingson E., Stocke J. T., 2002, *ApJ*, 566, 771
- Liedahl D. A., Osterheld A. L., Goldstein W. H., 1995, *ApJ*, 438, L115
- Lloyd-Davies E., Ponman T. J., 2002, *MNRAS*, in prep.
- Lloyd-Davies E. J., Bower R. G., Ponman T. J., 2002, *MNRAS*, submitted
- Lloyd-Davies E. J., Ponman T. J., Cannon D. B., 2000, *MNRAS*, 315, 689
- Loewenstein M., Mathews W. G., 1987, *ApJ*, 319, 614
- Loewenstein M., White R. E., 1999, *ApJ*, 518, 50
- Mackie G., Fabbiano G., 1997, in Arnaboldi M., Da Costa G. S., Saha P., eds, *ASP Conf. Ser.* 116: *The Nature of Elliptical Galaxies; 2nd Stromlo Symposium Environmental and internal optical properties and the x-ray content of e and sos.* p. 401
- Magorrian J., Tremaine S., Richstone D., Bender R., Bower G., Dressler A., Faber S. M., Gebhardt K., Green R., Grillmair C., Kormendy J., Lauer T., 1998, *AJ*, 115, 2285

- Mahtessian A. P., 1998, *Astrofizika*, 41, 255
- Markevitch M., 1998, *ApJ*, 504, 27
- Markevitch M., Vikhlinin A., 1997, *ApJ*, 491, 467
- Materne J., 1978, *A&A*, 63, 401
- Mathews W., Brighenti F., 1998a, *ApJ*, 503, L15
- Mathews W. G., Brighenti F., 1997, *ApJ*, 493, L9
- Mathews W. G., Brighenti F., 1998b, in Zaritsky D., ed., *ASP Conf. Ser. 136: Galactic Halos*
Hot gas and halos in elliptical galaxies. p. 277
- Mathews W. G., Brighenti F., 1999, *ApJ*, 526, 114
- Matsumoto H., Koyama K., Awaki H., Tsuru T., Loewenstein M., Matsushita K., 1997, *ApJ*,
482, 133
- Matsushita K., 2001, *ApJ*, 547, 693
- Matsushita K., Makishima K., Awaki H., Canizares C. R., Fabian A. C., Fukazawa Y., Loewen-
stein M., Matsumoto H., Mihara T., Mushotzky R. F., Ohashi T., Ricker G. R., Serlemitsos
P. J., Tsuru T., Tsusaka Y., Yamazaki T., 1994, *ApJ*, 436, L41
- Matsushita K., Ohashi T., Makishima K., 2000, *PASJ*, 52, 685
- Melnick J., Sargent W. L. W., 1977, *ApJ*, 215, 401
- Moore B., Governato F., Quinn T., Stadel J., Lake G., 1998, *ApJ*, 499, L5
- Moore B., Katz N., Lake G., Dressler A., Oemler A., 1996, *Nature*, 379, 613
- Muanwong O., Thomas P. A., Kay S. T., Pearce F. R., Couchman H. M. P., 2001, *ApJ*, 552,
L27
- Mulchaey J. S., 2000, *ARA&A*, 38, 289
- Mulchaey J. S., Zabludoff A. I., 1998, *ApJ*, 514, 133

- Mulchaey J. S., Zabludoff A. I., 1998, *ApJ*, 496, 73
- Mushotzky R. F., Scharf C. A., 1997, *ApJ*, 482, L13
- Navarro J. F., Frenk C. S., White S. D. M., 1997, *ApJ*, 490, 493
- Nieto J.-L., Bender R., 1989, *A&A*, 215, 266
- Nolan L. A., Dunlop J. S., Jimenez R., Heavens A. F., 2001, preprint, astro-ph/0103450
- Nousek J. A., Shue D. R., 1989, *ApJ*, 342, 1207
- Nulsen P. E. J., 1982, *MNRAS*, 198, 1007
- O'Connell R., 1980, *ApJ*, 236, 430
- Oemler A. J., 1974, *ApJ*, 194, 1
- Oosterloo T., Morganti R., Sadler E., 1999, *Publications of the Astronomical Society of Australia*, 16, 28
- Ostriker J. P., Tremaine S. D., 1975, *ApJ*, 202, L113
- O'Sullivan E., Forbes D. A., Ponman T. J., 2001a, *MNRAS*, 328, 461
- O'Sullivan E., Forbes D. A., Ponman T. J., 2001b, *MNRAS*, 324, 420
- Paolillo M., Fabbiano G., Peres G., Kim D.-W., 2002, *ApJ*, 565, 883
- Pedlar A., Ghataure H. S., Davies R. D., Harrison B. A., Perley R., Crane P. C., Unger S. W., 1990, *MNRAS*, 246, 477
- Pellegrini S., 1994, *A&A*, 292, 395
- Pellegrini S., 1999a, *A&A*, 343, 23
- Pellegrini S., 1999b, *A&A*, 351, 487
- Pellegrini S., Ciotti L., 1998, *A&A*, 333, 433
- Pence W. D., Snowden S. L., Mukai K., Kuntz K. D., 2001, *ApJ*, 561, 189

- Pizzella A., Amico P., Bertola F., Buson L. M., Danziger I. J., Dejonghe H., Sadler E. M., Saglia R. P., de Zeeuw P. T., Zeilinger W. W., 1997, *A&A*, 323, 349
- Ponman T., 1982, *MNRAS*, 201, 769
- Ponman T. J., Allan D. J., Jones L. R., Merrifield M., McHardy I. M., Lehto H. J., Luppino G. A., 1994, *Nature*, 369, 462
- Ponman T. J., Bertram D., 1993, *Nature*, 363, 51
- Ponman T. J., Cannon D. B., Navarro J. F., 1999, *Nature*, 397, 135
- Prandoni I., Iovino A., MacGillivray H. T., 1994, *AJ*, 107, 1235
- Prugniel P., Heraudeau P., 1998, *A&AS*, 128, 299
- Prugniel P., Simien F., 1996, *A&A*, 309, 749
- Quilis V., Moore B., Bower R., 2000, *Science*, 288, 1617
- Raymond J., Smith B., 1977, *ApJS*, 35, 419
- Read A., Ponman T., Strickland D., 1997, *MNRAS*, 286, 626
- Read A. M., Ponman T. J., 1998, *MNRAS*, 297, 143
- Read A. M., Ponman T. J., 2001, *MNRAS*, 328, 127
- Richstone D. O., 1976, *ApJ*, 204, 642
- Roberts M. S., Hogg D. E., Bregman J. N., Forman W. R., Jones C., 1991, *ApJS*, 75, 751
- Sakelliou I., Merrifield M. R., 1998, *MNRAS*, 293, 489
- Salvador-Sole E., Solanes J. M., Manrique A., 1998, *ApJ*, 499, 542
- Sanderson A. J. R., Ponman T. J., Finoguenov A., Lloyd-Davies E. J., Markevitch M., 2002, *MNRAS*, in prep
- Sansom A. E., Hibbard J., Schweizer F., 2000, *AJ*, 120, 1946
- Sarazin C. L., Ashe G. A., 1989, *ApJ*, 345, 22

- Sarazin C. L., Irwin J. A., Bregman J. N., 2000, *ApJ*, 544, L101
- Sarazin C. L., Irwin J. A., Bregman J. N., 2001, *ApJ*, 556, 533
- Schmitt J. H. M. M., 1985, *ApJ*, 293, 178
- Schweizer F., 1980, *ApJ*, 237, 303
- Schweizer F., 1987, in *Nearly Normal Galaxies. From the Planck Time to the Present Star formation in colliding and merging galaxies.* p. 18
- Schweizer F., Seitzer P., 1992a, *AJ*, 104, 1039
- Schweizer F., Seitzer P., 1992b, *AJ*, 104, 1039
- Schweizer F., Seitzer P., Faber S., Burstein D., Dalle Ore C., Gonzalez J., 1990, *ApJ*, 364, L33
- Searle L., Zinn R., 1978, *ApJ*, 225, 357
- Shapley A., Fabbiano G., Eskridge P. B., 2001, *ApJS*, 137, 139
- Shapley H., Ames A., 1932, *A survey of the external galaxies brighter than the thirteenth magnitude.* *Annals of Harvard College Observatory, Cambridge, Mass.: Astronomical Observatory of Harvard College, 1932*
- Slezak E., Bijaoui A., Mars G., 1990, *A&A*, 227, 301
- Snowden S. L., McCammon D., Burrows D. N., Mendenhall J. A., 1994, *ApJ*, 424, 714
- Somerville R. S., Lemson G., Sigad Y., Dekel A., Kauffmann G., White S. D. M., 2001, *MNRAS*, 320, 289
- Stark A. A., Gammie C. F., Wilson R. W., Bally J., Linke R. A., Heiles C., Hurwitz M., 1992, *ApJS*, 79, 77
- Stephens M. A., 1974, *J. Am. Stat. Assoc.*, 69, 730
- Stevens I. R., Acreman D. M., Ponman T. J., 1999, *MNRAS*, 310, 663
- Tammann G. A., 1982, in Rees M., Stoneham R., eds, *Supernovae: A Survey of Current Research.* Dordrecht: Reidel, p. 371

- Terlevich A. I., Forbes D. A., 2002, MNRAS, 330, 547
- Thomas D., Maraston C., Bender R., 2002, preprint, astro-ph/0202166
- Toomre A., Toomre J., 1972, ApJ, 178, 623
- Tovmassian H. M., Yam O., Tiersch H., 2002, ApJ, 567, L33
- Trinchieri G., Fabbiano G., 1985, ApJ, 296, 447
- Trinchieri G., Pellegrini S., Wolter A., Fabbiano G., Fiore F., 2000, A&A, 364, 53
- Tully R., Fisher J., 1977, A&A, 54, 661
- Tully R. B., 1980, ApJ, 237, 390
- Tully R. B., 1988, Nearby Galaxies Catalog. Cambridge University Press
- Tully R. B., Verheijen M. A. W., Pierce M. J., Huang J., Wainscoat R. J., 1996, AJ, 112, 2471
- Turner M. S., 1999, PASP, 111, 264
- Turner T., George I., Mushotzky R., Nandra K., 1997, ApJ, 475, 118
- van Dokkum P. G., Franx M., 1995, AJ, 110, 2027
- van Dokkum P. G., Franx M., 2001, ApJ, 553, 90
- van Dokkum P. G., Franx M., Fabricant D., Kelson D. D., Illingworth G. D., 1999, ApJ, 520, L95
- van Driel W., Rots A. H., van Woerden H., 1988, A&A, 204, 39
- Veron-Cetty M., Veron P., 1996, ESO Scientific Report No.17, A Catalogue of Quasars and Active Nuclei. 7th Edn.
- Vikhlinin A., McNamara B. R., Hornstrup A., Quintana H., Forman W., Jones C., Way M., 1999, ApJ, 520, L1
- Voges W., Aschenbach B., Boller T., Bräuninger H., Briel U., Burkert W., Dennerl K., Engenhauser J., et al. 1999, A&A, 349, 389

- Voit G. M., Bryan G. L., 2001, *Nature*, 414, 425
- Weinberger R., Tempurin S., Kerber F., 1999, *ApJ*, 522, L17
- White D. A., Fabian A. C., 1995, *MNRAS*, 273, 72
- White R. A., Bliton M., Bhavsar S. P., Bornmann P., Burns J. O., Ledlow M. J., Loken C., 1999, *AJ*, 118, 2014
- White R. E., Davis D. S., 1998, *PASP Conf. Series*, 136, 299
- White R. E. I., Sarazin C. L., 1991, *ApJ*, 367, 476
- Worthey G., 1994, *ApJS*, 95, 107
- Worthey G., Ottaviani D. L., 1997, *ApJS*, 111, 377
- Wu K. K. S., Fabian A. C., Nulsen P. E. J., 2000, *MNRAS*, 318, 889
- Xu H., Kahn S. M., Peterson J. R., Behar E., Paerels F. S. B., Mushotzky R. F., Jernigan J. G., Makishima K., 2001, preprint, astro-ph/0110013
- Zabludoff A. I., Mulchaey J. S., 1998, *ApJ*, 496, 39
- Zaroubi S., Squires G., de Gasperis G., Evrard A. E., Hoffman Y., Silk J., 2001, *ApJ*, 561, 600

Appendix

A

Catalogue of X-ray luminosities

This appendix contains the catalogue of X-ray luminosities for 401 early-type and 24 late-type galaxies discussed in Chapter 3.

Name	D (Mpc)	Log L_B ($L_{B\odot}$)		Log L_X (erg s^{-1})	Source	T
ESO101-14	30.12	9.93*	<	41.02	B	-3.0
ESO107-4	38.89	10.22	<	40.94	B	-4.0
ESO137-6	69.75	10.56		42.08	N	-4.8
ESO137-8	47.95	10.42*		41.22	N	-3.9
ESO137-10	42.27	10.46*		40.94	N	-3.0
ESO138-5	35.39	10.16*	<	41.18	B	-3.0
ESO148-17	38.36	10.04	<	40.68	B	-4.8
ESO183-30	33.59	10.18	<	41.00	B	-3.2
ESO185-54	56.36	10.84*		41.36	N	-4.8
ESO208-21	10.36	9.34		39.73	B	-3.1
ESO243-45	100.91	10.84*	<	41.91	N	-3.0
ESO273-2	3.20	7.54	<	38.64	B	-3.2
ESO286-50	33.31	9.76	<	40.53	B	-3.2
ESO306-17	139.95	11.15*		43.33	B	-3.9
ESO322-60	32.85	9.86*	<	40.60	B	-2.1
ESO351-30	1.99	8.59	<	36.64	N	-4.8

Name	D (Mpc)	Log L_B ($L_{B\odot}$)		Log L_X (erg s^{-1})	Source	T
ESO356-4	0.63	8.17	<	37.39	B	-4.8
ESO381-29	32.65	9.78	<	40.59	B	-3.8
ESO400-30	30.17	9.76	<	40.45	B	-4.0
ESO425-19	89.40	10.75*		41.60	B	-3.0
ESO428-11	10.49	9.07	<	39.63	B	-2.9
ESO443-24	65.97	10.67		41.50	N	-3.2
ESO495-21	9.16	9.13*		39.56	N	-2.6
ESO507-21	40.23	10.51*		40.93	B	-2.8
ESO552-20	123.49	11.04*		42.59	B	-3.9
ESO553-2	61.88	10.42		41.50	B	-2.2
ESO565-30	132.99	11.05*		42.37	B	-3.1
E1090221	37.43	10.46	<	40.52	B	0.0
E920130	19.79	9.70	<	40.29	B	-3.8
IC310	63.39	10.54		42.54	B	-2.0
IC989	101.33	10.60	<	41.55	F	-4.9
IC1024	21.68	9.31*	<	40.20	F	-2.0
IC1459	18.88	10.37		40.71	N	-4.7
IC1531	100.69	10.87*		41.60	B	-2.7
IC1625	86.20	10.90		41.75	B	-3.2
IC1633	93.81	11.09		42.79	N	-3.9
IC1729	18.09	9.29	<	40.00	B	-4.0
IC1860	90.15	10.62		42.71	B	-4.7
IC2006	18.11	9.88	<	41.03	B	-4.3
IC2035	16.52	9.64	<	40.62	B	-2.3
IC2311	22.11	9.88	<	40.22	B	-4.6
IC2533	31.45	10.00	<	40.44	B	-3.0
IC2552	38.37	10.00*	<	40.69	B	-3.0
IC2597	58.34	10.58	<	41.03	B	-3.9

Name	D (Mpc)	Log L_B ($L_{B\odot}$)		Log L_X (erg s^{-1})	Source	T
IC3896	25.29	9.97*	<	40.50	B	-4.8
IC3986	59.49	10.41*		40.30	N	-4.0
IC4197	38.63	9.95	<	40.73	B	-3.1
IC4296	47.56	10.90		41.53	N	-4.8
IC4329	58.83	10.86*	<	41.82	F	-3.0
IC4765	58.20	10.79*		41.83	N	-3.9
IC4797	33.31	10.31	<	40.99	B	-3.9
IC4889	29.51	10.42	<	40.80	B	-4.4
IC4943	34.67	9.90	<	40.64	B	-4.9
IC5181	24.63	9.97	<	40.28	B	-2.1
IC5250	41.53	10.59		40.14	N	-2.4
IC5269	24.52	9.69*	<	40.46	R	-1.8
IC5358	113.09	10.86		43.58	B	-3.9
NGC57	55.21	10.61		41.65	B	-4.9
NGC127	48.53	9.43	<	41.16	F	-2.0
NGC128	48.53	10.50	<	41.15	F	5.0
NGC130	48.53	9.60	<	41.18	F	-3.0
NGC147	0.65	7.92	<	37.45	B	-4.8
NGC185	0.62	8.07	<	37.36	B	-4.8
NGC205	0.72	8.40	<	37.61	B	-4.8
NGC221(M32)	0.72	8.36		37.77	N	-4.7
NGC227	71.01	10.65	<	41.23	R	-3.6
NGC315	58.88	11.07		41.58	N	-4.0
NGC383	56.49	10.86		41.38	N	-2.9
NGC404	0.72	7.42	<	37.23	B	-2.8
NGC410	56.75	10.82		41.91	B	-4.3
NGC439	74.60	10.94*		41.71	B	-3.2
NGC499	55.21	10.57		42.29	N	-2.8

Name	D (Mpc)	Log L_B ($L_{B\odot}$)		Log L_X (erg s^{-1})	Source	T
NGC507	67.19	10.96		42.70	N	-3.2
NGC529	65.96	10.57		40.60	N	-3.0
NGC533	63.68	10.90		42.23	N	-4.8
NGC541	63.39	10.66		40.84	N	-3.8
NGC545	63.39	10.51		41.29	N	-2.9
NGC547	63.39	10.92		40.70	N	-4.7
NGC568	73.24	10.49		41.49	B	-3.0
NGC584	22.18	10.36	<	40.09	B	-4.6
NGC596	22.28	10.21	<	39.60	N	-4.3
NGC636	22.28	10.00	<	40.11	B	-4.8
NGC708	55.21	10.74		43.03	B	-4.8
NGC720	20.80	10.38		40.61	N	-4.8
NGC741	61.09	10.90		41.73	N	-4.8
NGC777	55.21	10.68		42.08	B	-4.8
NGC821	20.99	10.16	<	40.33	B	-4.8
NGC855	9.33	8.89	<	39.77	B	-4.8
NGC984	59.08	10.21	<	41.37	F	-1.3
NGC1016	73.79	10.95		41.28	N	-4.9
NGC1044	85.67	10.29	<	41.17	F	-3.0
NGC1052	17.70	10.12		40.31	N	-4.7
NGC1167	67.67	10.50*	<	41.31	F	-2.4
NGC1172	28.71	10.10	<	40.59	B	-3.9
NGC1199	28.71	10.24		39.42	N	-4.7
NGC1201	20.67	10.16*	<	40.26	B	-2.5
NGC1209	28.71	10.19	<	40.62	B	-4.8
NGC1265	102.45	10.92	<	40.45	N	-4.0
NGC1316	18.11	10.93		40.87	N	-1.7
NGC1332	19.68	10.27		40.53	N	-2.9

Name	D (Mpc)	Log L_B ($L_{B\odot}$)		Log L_X (erg s^{-1})	Source	T
NGC1336	18.11	9.46	<	40.29	B	-3.0
NGC1339	18.11	9.73	<	40.21	B	-4.2
NGC1340	18.11	10.20	<	40.27	B	-3.9
NGC1344	18.11	10.30	<	39.48	N	-3.9
NGC1351	18.11	9.78	<	40.33	B	-3.1
NGC1366	18.11	9.56	<	40.32	B	-2.3
NGC1374	18.11	9.98		39.89	N	-4.5
NGC1375	18.11	9.58	<	38.60	N	-2.0
NGC1379	18.11	10.09		39.24	N	-4.8
NGC1380	18.11	10.46		40.09	N	-2.3
NGC1380A	18.11	9.65	<	38.96	N	-1.9
NGC1381	18.11	9.79		39.07	N	-2.0
NGC1387	18.11	10.03		40.48	F	-2.9
NGC1389	18.11	9.71*	<	40.08	F	-2.9
NGC1399	18.11	10.52		41.63	N	-4.5
NGC1395	20.51	10.44		40.89	N	-4.8
NGC1400	20.51	10.14		40.12	N	-3.7
NGC1404	18.11	10.35		41.19	N	-4.7
NGC1407	20.61	10.58		41.00	N	-4.6
NGC1411	10.56	9.34	<	39.63	B	-3.0
NGC1419	18.11	9.34	<	40.37	B	-4.8
NGC1426	20.61	9.92	<	40.01	B	-4.6
NGC1427	18.11	10.00		39.85	N	-4.0
NGC1439	20.61	10.00	<	40.00	B	-4.7
NGC1497	84.12	10.41*	<	41.33	F	-2.0
NGC1510	10.01	8.80	<	39.76	F	-2.0
NGC1537	16.44	10.02	<	39.75	B	-3.3
NGC1549	14.45	10.28		39.92	N	-4.3

Name	D (Mpc)	Log L_B ($L_{B\odot}$)		Log L_X (erg s^{-1})	Source	T
NGC1550	48.49	10.33		42.80	B	-3.9
NGC1553	14.45	10.63		40.52	N	-2.3
NGC1573	51.52	10.72		41.33	B	-4.9
NGC1574	14.45	10.01	<	40.32	F	-2.9
NGC1581	14.45	9.06	<	39.86	B	-3.0
NGC1587	44.87	10.51		40.64	N	-4.8
NGC1600	59.98	11.03		41.54	B	-4.8
NGC1705	4.87	8.44*		38.81	N	-3.0
NGC1947	13.43	10.18	<	40.05	F	-3.2
NGC2089	38.07	10.18*	<	40.56	B	-3.0
NGC2271	32.16	9.94*	<	40.66	B	-3.2
NGC2272	0.72	6.81	<	37.36	B	-3.0
NGC2292	28.33	10.36*	<	40.60	B	-2.1
NGC2293	23.92	10.03	<	40.21	B	-1.1
NGC2300	27.67	10.41		41.16	N	-3.5
NGC2305	45.92	10.60		41.67	B	-4.8
NGC2314	48.53	10.44		40.91	R	-4.7
NGC2325	29.79	10.60		40.70	B	-4.6
NGC2328	12.20	9.02	<	39.56	B	-2.9
NGC2329	71.12	10.73		42.12	B	-3.0
NGC2340	73.79	11.04		42.08	B	-4.9
NGC2380	21.11	9.93	<	40.20	B	-2.2
NGC2434	14.06	9.89		39.90	B	-4.8
NGC2444	50.82	9.92	<	41.29	F	-2.0
NGC2488	117.12	10.97		42.56	B	-3.0
NGC2502	11.07	9.00	<	39.36	B	-2.1
NGC2562	59.43	10.18	<	41.20	F	-0.1
NGC2563	59.43	10.54		41.63	N	-2.0

Name	D (Mpc)	Log L_B ($L_{B\odot}$)		Log L_X (erg s^{-1})	Source	T
NGC2577	28.68	9.74		40.19	N	-3.0
NGC2629	52.13	10.29	<	40.94	F	-3.2
NGC2634	33.49	10.07	<	40.46	B	-4.8
NGC2663	27.42	10.95		40.45	B	-4.6
NGC2685	15.85	9.80	<	40.10	F	-1.1
NGC2693	62.81	10.74	<	41.29	F	-4.8
NGC2694	62.81	9.78	<	41.31	F	-4.9
NGC2695	27.42	9.97	<	40.39	B	-2.1
NGC2716	46.44	10.44	<	40.67	F	-1.2
NGC2768	20.89	10.57		40.38	N	-4.4
NGC2778	29.24	9.80	<	40.33	B	-4.8
NGC2832	85.90	11.06		41.62	N	-4.3
NGC2859	23.92	10.21	<	39.98	F	-1.2
NGC2865	36.48	10.48	<	40.49	B	-4.1
NGC2880	23.55	9.95	<	40.06	B	-2.6
NGC2887	35.01	10.17	<	40.69	B	-3.2
NGC2888	27.12	9.62	<	40.23	B	-4.0
NGC2904	29.35	9.75	<	40.37	B	-3.2
NGC2911	41.30	10.52	<	40.96	F	-2.1
NGC2974	28.31	10.50		40.58	F	-4.8
NGC2986	30.34	10.51		40.96	B	-4.6
NGC3065	30.04	9.74		41.01	F	-2.0
NGC3073	18.49	9.09	<	39.77	B	-2.8
NGC3078	33.42	10.48		40.72	B	-4.8
NGC3087	34.67	10.52	<	40.56	B	-4.2
NGC3091	50.82	10.75		41.63	N	-4.5
NGC3115	8.83	10.10		39.72	N	-2.8
NGC3136	19.11	10.07	<	40.26	B	-4.8

Name	D (Mpc)	Log L_B ($L_{B\odot}$)		Log L_X (erg s^{-1})	Source	T
NGC3156	19.95	9.71	<	40.00	B	-2.5
NGC3158	86.30	10.96		41.71	B	-4.8
NGC3193	21.58	10.15		39.96	N	-4.7
NGC3222	75.09	10.46	<	41.33	F	-2.1
NGC3224	38.55	10.16	<	40.65	B	-3.7
NGC3226	21.58	10.12		40.20	N	-4.8
NGC3250	37.67	10.71	<	40.65	B	-4.8
NGC3258	38.37	10.48		41.17	F	-4.3
NGC3268	38.37	10.48		40.53	N	-4.3
NGC3271	47.81	10.43*		41.06	N	-1.8
NGC3311	58.34	10.76		42.19	N	-3.4
NGC3375	30.92	9.80	<	40.43	B	-2.0
NGC3377	10.00	9.72	<	39.60	B	-4.8
NGC3379	10.00	10.06	<	39.54	B	-4.8
NGC3384	10.00	9.85	<	39.52	B	-2.6
NGC3458	27.03	9.77*	<	40.61	F	-2.0
NGC3516	38.37	10.36		43.11	N	-2.0
NGC3557	32.21	10.76		40.58	N	-4.8
NGC3585	16.07	10.39		39.79	N	-4.5
NGC3599	19.77	9.66	<	39.23	N	-2.0
NGC3605	19.77	9.47		39.08	N	-4.7
NGC3606	37.75	9.98*	<	40.69	B	-4.9
NGC3607	19.77	10.46		40.54	F	-3.1
NGC3608	19.77	10.11		40.01	N	-4.8
NGC3610	27.29	10.40		39.83	N	-4.2
NGC3613	27.29	10.36	<	40.12	B	-4.7
NGC3617	27.39	9.59	<	40.40	B	-3.9
NGC3640	22.91	10.43		39.92	N	-4.8

Name	D (Mpc)	Log L_B ($L_{B\odot}$)		Log L_X (erg s^{-1})	Source	T
NGC3656	41.00	10.10	<	40.61	B	0.0
NGC3658	30.76	9.92	<	39.77	N	-2.2
NGC3665	30.76	10.70		40.60	N	-2.1
NGC3706	37.21	10.38	<	41.19	B	-3.3
NGC3818	21.48	9.80	<	40.16	B	-4.8
NGC3842	82.04	10.92		41.80	N	-4.9
NGC3862	82.04	10.56		41.90	B	-4.9
NGC3894	46.37	10.47		41.19	F	-4.1
NGC3904	17.86	10.06	<	40.74	B	-4.6
NGC3923	17.86	10.52		40.66	N	-4.5
NGC3962	21.68	10.28	<	40.22	B	-4.8
NGC3990	12.16	8.99		38.60	N	-2.7
NGC3998	17.46	10.08		41.51	N	-2.1
NGC4024	20.84	9.77	<	40.04	B	-3.2
NGC4033	19.25	9.71	<	40.00	B	-4.5
NGC4036	21.73	10.24	<	40.03	B	-2.5
NGC4073	79.43	11.07		42.38	N	-4.1
NGC4104	111.87	11.05*		42.66	N	-2.0
NGC4105	22.85	10.25*		40.42	F	-4.6
NGC4125	25.94	10.80		40.94	N	-4.8
NGC4168	33.73	10.40		40.56	F	-4.8
NGC4203	16.22	9.89		41.18	N	-2.7
NGC4215	31.48	9.98	<	40.46	F	-0.8
NGC4233	31.48	10.02	<	39.22	N	-2.0
NGC4239	16.75	9.24	<	39.85	B	-4.7
NGC4251	16.22	10.02	<	39.65	F	-1.9
NGC4261	31.48	10.70		41.21	N	-4.8
NGC4262	15.92	9.65	<	39.82	B	-2.7

Name	D (Mpc)	Log L_B ($L_{B\odot}$)		Log L_X (erg s^{-1})	Source	T
NGC4267	15.92	9.88	<	39.90	B	-2.7
NGC4278	16.22	10.24		40.36	N	-4.8
NGC4283	16.22	9.46	<	39.22	N	-4.8
NGC4291	24.55	10.00		40.89	N	-4.8
NGC4339	15.92	9.71	<	39.86	B	-4.7
NGC4340	15.92	9.84		39.75	R	-1.2
NGC4350	15.92	9.85	<	39.77	F	-1.8
NGC4365	15.92	10.34		40.25	N	-4.8
NGC4374(M84)	15.92	10.57		40.83	N	-4.0
NGC4382	15.92	10.64		40.33	F	-1.3
NGC4386	24.55	9.90	<	39.93	F	-2.1
NGC4387	15.92	9.47		39.71	N	-4.8
NGC4406(M86)	15.92	10.66		42.05	N	-4.7
NGC4417	15.92	9.77	<	40.68	F	-1.9
NGC4425	15.92	9.64	<	39.86	F	-0.7
NGC4434	15.92	9.45	<	39.83	B	-4.8
NGC4435	15.92	10.01	<	40.13	F	-2.1
NGC4458	16.14	9.51		39.84	F	-4.8
NGC4459	15.92	10.20		40.17	R	-1.4
NGC4464	15.92	9.20	<	39.81	B	1.7
NGC4467	15.92	8.59	<	39.29	F	-4.9
NGC4472(M49)	15.92	10.90		41.43	N	-4.7
NGC4473	16.14	10.15		40.14	F	-4.8
NGC4474	15.92	9.64	<	39.85	F	-2.0
NGC4476	15.92	9.43	<	40.27	R	-3.0
NGC4477	15.92	10.13		40.26	N	-1.9
NGC4478	15.92	9.79	<	40.41	R	-4.8
NGC4479	15.92	9.23	<	39.70	F	-1.9

Name	D	Log L_B		Log L_X	Source	T
	(Mpc)	($L_{B\odot}$)		(erg s^{-1})		
NGC4486(M87)	15.92	10.85		42.95	B	-4.3
NGC4489	15.92	9.46	<	39.84	B	-4.8
NGC4494	21.28	10.62	<	40.10	B	-4.8
NGC4503	15.92	9.77	<	39.88	B	-2.0
NGC4507	45.24	10.33	<	41.40	F	1.9
NGC4515	15.92	9.24	<	39.80	B	-3.0
NGC4526	15.92	10.47		39.87	N	-1.9
NGC4550	15.92	9.72		39.78	N	-2.1
NGC4551	15.92	9.58	<	39.09	N	-4.8
NGC4552(M89)	15.92	10.29		40.71	N	-4.6
NGC4555	90.33	10.86*		41.85	N	-4.8
NGC4564	15.92	9.86	<	39.85	B	-4.7
NGC4578	15.92	9.78	<	39.99	F	-2.0
NGC4581	15.92	9.26	<	39.96	B	-4.4
NGC4589	24.55	10.33		40.36	R	-4.8
NGC4621	15.92	10.32		40.02	R	-4.8
NGC4627	12.13	9.13		39.92	B	-4.7
NGC4636	15.92	10.51		41.59	N	-4.8
NGC4638	15.92	9.80		39.59	N	-2.7
NGC4645	32.03	10.09*	<	40.57	B	-3.9
NGC4648	24.55	9.87	<	39.89	B	-4.9
NGC4649(M60)	15.92	10.73		41.28	N	-4.6
NGC4660	15.92	9.74	<	39.39	N	-4.7
NGC4697	15.14	10.55		40.12	N	-4.8
NGC4696	37.01	10.99*		43.23	N	-3.9
NGC4709	59.31	10.94		41.00	N	-4.5
NGC4733	15.92	9.51	<	39.73	B	-3.9
NGC4742	12.42	9.56	<	39.80	B	-4.8

Name	D (Mpc)	Log L_B ($L_{B\odot}$)		Log L_X (erg s^{-1})	Source	T
NGC4751	23.97	9.76*	<	40.31	B	-2.9
NGC4753	20.23	10.46		39.99	F	-1.6
NGC4754	15.92	10.00	<	39.73	B	-2.5
NGC4756	53.93	10.30		41.72	F	-2.9
NGC4760	63.39	11.02		41.58	B	-4.8
NGC4762	15.92	10.16		40.13	F	-1.8
NGC4767	37.39	10.33	<	40.71	B	-4.0
NGC4782	63.39	11.37		41.61	F	-4.8
NGC4880	20.28	9.83	<	40.20	F	-1.5
NGC4839	87.90	10.90		40.45	N	-4.0
NGC4889	88.31	11.19		42.76	N	-4.3
NGC4915	43.85	10.28	<	40.87	B	-4.7
NGC4936	41.07	10.71*		41.69	B	-4.6
NGC4946	38.53	9.98	<	40.79	B	-4.1
NGC4976	11.43	9.97	<	39.73	B	-4.4
NGC4993	37.49	10.01*	<	40.71	B	-3.0
NGC5011	38.76	10.40	<	40.82	B	-4.8
NGC5018	30.20	10.57	<	40.53	B	-4.5
NGC5044	30.20	10.70		42.74	N	-4.8
NGC5061	18.28	10.28		39.68	N	-4.3
NGC5077	30.20	10.26		40.48	F	-4.8
NGC5084	16.90	10.18		40.49	F	-1.6
NGC5087	18.71	10.03		40.36	B	-3.0
NGC5090	42.23	10.41		41.49	B	-4.9
NGC5102	4.16	9.29		38.03	N	-3.0
NGC5128	3.89	10.45		40.10	N	-2.3
NGC5129	91.20	10.91		42.14	N	-4.9
NGC5153	55.65	10.55		40.50	N	-4.8

Name	D (Mpc)	Log L_B ($L_{B\odot}$)		Log L_X (erg s^{-1})	Source	T
NGC5173	34.99	10.04	<	40.36	B	-4.9
NGC5193	47.41	10.55		40.58	N	-4.2
NGC5195	9.12	9.93		39.42	F	0.1
NGC5198	34.99	10.28	<	40.38	B	-4.8
NGC5216	42.33	10.02*		40.85	B	-4.9
NGC5253	3.64	8.96	<	38.77	B	7.7
NGC5273	17.09	9.68		39.86	N	-1.9
NGC5306	96.41	10.91		41.50	N	-2.1
NGC5308	27.80	10.20	<	40.01	B	-2.0
NGC5318	59.49	10.24	<	41.04	F	-2.0
NGC5322	27.80	10.67		40.21	N	-4.8
NGC5328	61.40	10.70		41.88	B	-4.8
NGC5353	34.67	10.56		41.00	F	-2.1
NGC5354	33.32	10.30	<	40.84	F	-2.0
NGC5363	15.79	10.17		40.14	F	0.0
NGC5382	58.19	10.32		40.14	N	-2.0
NGC5419	53.44	10.88		41.80	N	-4.4
NGC5473	28.18	10.21	<	40.09	B	-2.7
NGC5485	28.18	10.25	<	40.12	B	-2.0
NGC5507	25.85	9.63		39.75	N	-2.1
NGC5532	98.13	11.02		41.63	F	-2.0
NGC5546	98.53	10.86		42.02	B	-4.9
NGC5574	21.68	9.57	<	40.14	B	-2.8
NGC5576	21.68	10.16	<	40.14	B	-4.8
NGC5582	18.40	9.73	<	39.82	B	-4.9
NGC5638	21.68	10.09	<	40.20	B	-4.8
NGC5687	31.49	10.15	<	40.14	B	-3.0
NGC5812	24.55	10.19	<	40.32	B	-4.8

Name	D (Mpc)	Log L_B ($L_{B\odot}$)		Log L_X (erg s^{-1})	Source	T
NGC5831	22.91	10.03	<	40.25	B	-4.8
NGC5838	22.91	10.20		40.02	F	-2.7
NGC5845	22.91	9.56	<	39.94	N	-4.9
NGC5846	22.91	10.66		41.65	N	-4.7
NGC5866	13.18	10.32		39.69	F	-1.3
NGC5898	23.88	10.22	<	40.31	B	-4.2
NGC5903	23.88	10.28	<	40.33	B	-4.6
NGC5982	37.50	10.53		41.16	B	-4.8
NGC6027	60.88	9.63	<	41.39	F	-1.4
NGC6034	137.28	10.63		42.19	F	-4.0
NGC6127	65.01	10.61		41.40	B	-4.9
NGC6137	112.72	11.13		42.14	B	-4.8
NGC6146	107.65	10.92	<	41.90	F	-4.7
NGC6160	127.65	10.72*		42.45	B	-4.9
NGC6166	108.64	11.20		43.93	B	-4.3
NGC6173	107.65	11.09		42.15	B	-4.9
NGC6269	139.68	11.15		42.86	B	-4.8
NGC6305	33.72	9.95	<	40.94	B	-3.0
NGC6407	58.67	10.58*		41.94	B	-2.0
NGC6482	54.69	10.72		42.08	N	-4.8
NGC6487	105.39	11.07		41.70	B	-4.9
NGC6673	12.29	9.34	<	40.06	B	-3.9
NGC6684	8.47	9.73		38.93	N	-1.8
NGC6703	29.92	10.37	<	40.03	B	-2.8
NGC6776	70.41	10.66		40.79	N	-4.1
NGC6841	0.15	5.01	<	36.06	B	-3.9
NGC6851	34.67	10.30	<	40.64	B	-4.8
NGC6861	34.67	10.42	<	40.65	B	-2.7

Name	D (Mpc)	Log L_B ($L_{B\odot}$)		Log L_X (erg s^{-1})	Source	T
NGC6868	34.67	10.58*		41.23	N	-4.4
NGC6876	48.56	10.83*		41.51	F	-4.9
NGC6880	50.77	10.33	<	41.10	F	-1.0
NGC6909	34.67	10.27	<	40.78	B	-4.1
NGC6920	34.13	9.83	<	40.95	B	-2.0
NGC6958	34.79	10.34	<	40.68	B	-3.5
NGC6963	58.93	9.73	<	40.97	F	-2.3
NGC6964	51.83	10.02	<	40.84	F	-4.4
NGC7007	37.39	10.16	<	40.70	B	-2.9
NGC7029	34.97	10.34	<	40.57	B	-4.4
NGC7041	23.39	10.09	<	40.24	B	-3.0
NGC7049	27.27	10.37		41.01	B	-2.1
NGC7097	29.24	10.13		40.28	N	-4.8
NGC7144	21.38	10.14		39.64	N	-4.8
NGC7145	21.38	10.04	<	40.25	B	-4.8
NGC7166	30.43	10.02	<	40.45	B	-2.9
NGC7168	34.57	10.12	<	40.59	B	-4.7
NGC7173	32.65	10.04		40.86	N	-4.1
NGC7176	32.39	10.27		40.80	N	-4.6
NGC7180	16.05	9.18	<	40.07	B	-2.4
NGC7185	24.04	9.59	<	40.38	B	-3.0
NGC7192	35.77	10.42		40.85	B	-3.9
NGC7196	36.51	10.35		40.95	B	-4.8
NGC7236	105.60	10.39	<	41.63	F	-3.0
NGC7237	105.31	10.29	<	41.76	F	-3.0
NGC7252	52.48	10.66		40.50	N	-2.0
NGC7265	68.17	10.56		41.70	B	-2.7
NGC7332	15.28	9.86	<	40.01	F	-1.9

Name	D	Log L_B		Log L_X	Source	T
	(Mpc)	($L_{B\odot}$)		(erg s^{-1})		
NGC7385	105.75	11.11		41.79	B	-4.8
NGC7454	24.32	9.95	<	40.20	B	-4.8
NGC7457	10.67	9.78	<	39.49	B	-2.7
NGC7465	24.32	9.64		41.36	N	-1.9
NGC7484	34.69	10.16*	<	40.93	B	-4.8
NGC7507	17.78	10.23	<	40.77	B	-4.8
NGC7550	69.64	10.61	<	40.31	N	-3.0
NGC7562	39.99	10.46	<	40.93	F	-4.8
NGC7619	39.99	10.58		41.63	N	-4.8
NGC7626	39.99	10.61		41.06	N	-4.8
NGC7768	92.04	10.92		41.74	B	-4.9
NGC7796	39.45	10.48		40.74	N	-3.9
UGC34(Maff I)	82.45	10.39	<	41.29	B	2.0
UGC1308	55.21	10.16*		40.98	N	-4.9
UGC4956	67.63	10.45		41.60	B	-4.9
UGC5470(Leo I)	2.33	8.60	<	38.52	B	-4.8
UGC6253(Leo II)	2.17	7.94	<	38.51	B	-4.8

Table A.1: Combined catalogue of X-ray luminosities. The catalogue contains 401 early-type galaxies and 24 late-type objects which were included in previous catalogues. L_B values are based on B_T magnitudes, except those marked *, which are based on m_B magnitudes (see Section 3.4). L_X values are bolometric and T-type is taken from LEDA. The source of each L_X value is shown, B signifying Beuing *et al.* (1999), F = Fabbiano, Kim & Trinchieri (1992), R = Roberts *et al.* (1991) and N = new values calculated by the authors as described in Section 3.3.